SEDIMENTOLOGY, STRATIGRAPHY, ARCHITECTURE AND ORIGIN OF DEEP-WATER, BASIN-FLOOR DEPOSITS: MIDDLE AND UPPER KAZA GROUP, WINDERMERE SUPERGROUP, B.C., CANADA

Viktor Terlaky

Thesis submitted to the

Faculty of Graduate and Postdoctoral Studies

in partial fulfillment of the requirements

for the Ph.D. degree in Earth Sciences

Ottawa-Carleton Geoscience Centre

Faculty of Science

University of Ottawa

Abstract

Ancient basin-floor strata are exceptionally well exposed in the Neoproterozoic Windermere Supergroup in the southern Canadian Cordillera. Data from the Castle Creek outcrop, where strata of the upper Kaza Group crop out, and the Mt. Quanstrom outcrop, where the middle Kaza is exposed, form the main dataset for this study. The aim of this study is to describe and interpret the strata starting at the bed scale, followed by stratal element scale, lobe scale and ultimately fan scale.

Strata of the Kaza Group comprise six sedimentary facies representing deposition from a variety of fluid and cohesive sediment gravity flows. These, in turn, populate seven stratal elements that are defined by their basal contact, cross-sectional geometry and internal facies distribution. The lithological characteristics of stratal elements vary little from proximal to more distal settings, but their relative abundance and stacking pattern do, which, then, forms the basis for modeling the internal architecture of lobes.

Lobes typically comprise an assemblage of stratal elements, which then are systematically and predictably arranged in both space (along a single depositional transect) and time (stratigraphically upward). Lobes typically became initiated by channel avulsion. In the proximal part of the system scours up to several meters deep, several tens of meters wide are interpreted to have formed by erosion downflow of the avulsion node. Erosion also charged the flow with fine-grained sediment and on the lateral margins and downflow avulsion splays were deposited. Later flows then exploited the basin-floor topography and on the proximal basin-floor carved a feeder channel, which then fed a downflow depositional lobe. At the mouths of feeder channels flows became dispersed through a network of distributary channels that further downflow shallow and widen until eventually merging laterally in sandstone-rich terminal splays. During the lifespan of a single lobe the feeder channel remains fixed, but the distributary channel network and its associated terminal splays wander, causing them to stack and be intercalated laterally and vertically. Eventually an upstream avulsion terminates local sediment supply, causing a new lobe to be initiated elsewhere on the fan, and the process repeats.

Résumé

La stratification d'un ancien système de dépôts de plancher de bassin océanique du Néoprotérozoïque est exceptionnellement bien exposée dans la partie sud de la cordillère canadienne. Cette étude porte sur les dépôts du groupe Kaza, une des constituantes du supergroupe Windermere, et plus particulièrement, sur le Kaza supérieur (affleurement de Castle Creek) et sur le Kaza moyen (affleurement du Mont Quanstrom). L'objectif de cette étude est de décrire et d'interpréter la suite dépositionnelle de petite à grande échelle, soit de l'échelle du lit, à celle de l'élément architectural, puis du lobe dépositionnel, puis, ultimement, à l'échelle de l'éventail sous-marin profond.

Le dépôt du groupe Kaza est constitué de six faciès sédimentaires représentant la déposition par des courants de gravité de divers niveaux de fluidité et de cohésion. Ces faciès composent sept éléments architecturaux définis en fonction de leur contact basal, de leur géométrie en coupe et de leur distribution interne de faciès. Les caractéristiques lithologiques des éléments architecturaux varient peu d'une position proximale à distale (vs l'embouchure du système). Par contre, l'abondance relative et les patrons d'empilement, eux, varient et servent de base à la modélisation de l'architecture interne des lobes dépositionnels.

Les lobes sont généralement constitués d'un assemblage d'éléments architecturaux. Ces derniers sont organisés de manière systématique et prévisible en fonction des dimensions espace (le long d'une surface dépositionnelle) et temps (vers le haut de la succession stratigraphique). La formation de lobes semble habituellement être initiée par l'avulsion du chenal. Dans la partie proximale du système, des marques d'affouillements allant jusqu'à une dizaine de mètres de profond et quelques dizaines de mètres de large sont possiblement attribuables à l'érosion en aval du node d'avulsion. Cette érosion sature le courant de fines particules qui forment des dépôts d'épandage d'avulsion sur les marges latérales du chenal et en aval du système. Les courants subséquents ont exploité la topographie du fond marin et ainsi creusé un chenal d'alimentation dans la partie proximale du fond marin (ou en amont), lequel a ensuite alimenté un lobe dépositionnel en aval. À la source des chenaux d'alimentation le courant se disperse à travers un réseau de chenaux distributeurs devenant moins profonds et plus larges en aval du système, jusqu'à éventuellement converger pour former des dépôts d'épandage terminaux riches en sable. Au cours de la période d'activité d'un lobe, le chenal d'alimentation demeure fixe, mais le réseau de chenaux distributeurs et les dépôts d'épandage terminaux leur étant associés, eux, se déplacent, ceux-ci se retrouvant ainsi empilés et intercalés latéralement et (aussi bien que) verticalement. Éventuellement, une avulsion en amont coupe l'alimentation en sédiment et cause l'initiation d'un nouveau lobe ailleurs dans le système de l'éventail sous-marin profond et le processus se répète.

Dedication

To the memory of Dr. Sue Vajoczki

professor, mentor, inspiration and friend

who started me on this wonderful journey called geology.

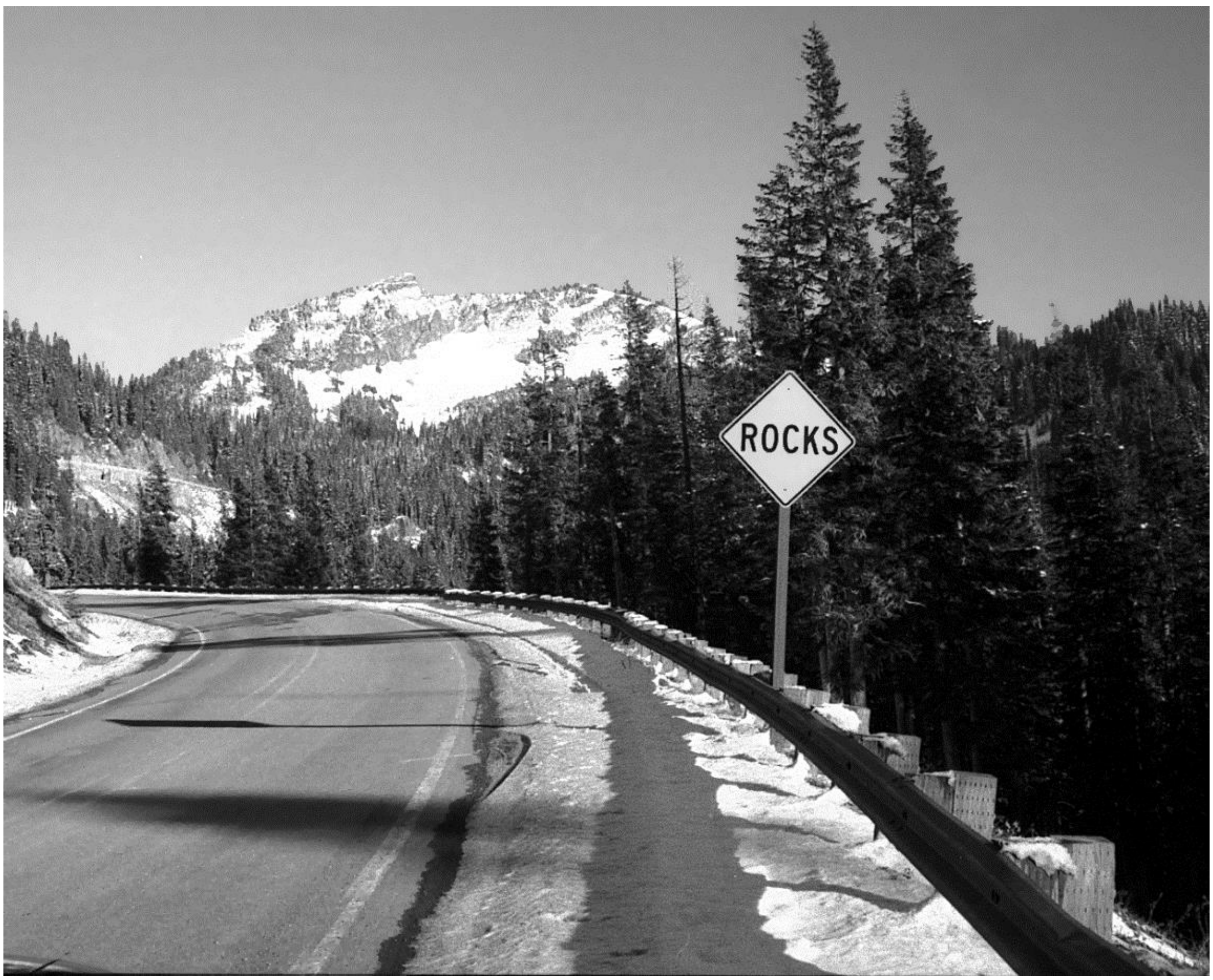

Acknowledgements

As with any academic work, this thesis too could not have been completed without the support of many individuals that are not present on the authors' list. Fist and foremost, I thank my supervisor Bill Arnott, who not only supported the thesis project academically and financially, but also allowed me the freedom to explore new areas of interest beyond the scope of the original project (and thus allowed me to expand the temoporal scope of the thesis too). I would like to thank Drs. David Pyles, André Desrochers, Don Cummings and Quentin Gall who agreed to read and referee this thesis and serve on my defense committee. You all made the defense a stress-free and enjoyable occasion – thank you!

Many thanks also to the partners of the Windermere Consortium. The consortium provides the financial backing for all Windermere projects, and allows many graduate students a wonderful opportunity to study ancient deep-water rocks. I also enjoyed the discussions with colleagues at the annual partners' meetings, which always provided me with new and interesting things to think about.

Two support staff in the Earth Sciences department in particular have my gratitude for their help during my tenure at the university: George Mrazek for preparation of thin sections and Hélène De Gouffe for all the administrative support.

A large component of this project is based on field work conducted in the beautiful backcountry of the Cariboo Mountains. The McKirdy family was essential in providing smooth infrastructure and support in the field. This project truly could not have been completed without your dedicated support. Also a huge thanks to Yellowhead Helicopters and their skilled pilots for always getting us in and out of the field safely – and let's not forget the many food and mail drops during field season! I am also very grateful for my many field assistants over the years: Greg, Pierce, Adam, Jordan, Jonathan, Jenni, Omar and Michelle, you all made my life so much easier in the field.

Thanks go out to all the undergrads, grads, post-docs and Drs. that were part of my journey over the years at Ottawa. Many of you have contributed to this work through our many lengthy conversations about deep-water sedimentology, geology in general, or just life… In no particular order: Ernesto, Hugues, Paul, Mark, Shann, Mike, Lilian, Simon, John, Jonathan, Martha, Leena, Dave L., Natasa, Lindsay, Gerry, Irving, Kelsey, Kim, Katrina, Joel, Dave A., Adam, Greg, Michelle, Omar, Jordan, Pierce, Jenni, Claude, Simone, Ben, Dave S., Glenn, and many others that I've forgotten to name.

Many thanks to the Schembris for being my family in Ottawa.

A huge thanks to my parents, who have always believed in me, supported and encouraged me in life to strive to always be my best. I could not have made it this far without you!

Last, but certainly not least, I'd like to thank Amanda for loving me and always being there to support me through thick and thin.

Thank you.

Table of Contents

List of Figures

List of Tables

Chapter 1: Thesis introduction

1.1 Thesis rationale

Deep-water basin-floor fans are the most distal and final repository for clastic and pelagic sediment, and volumetrically form the largest sedimentary bodies on earth. These fans host some of the world's largest hydrocarbon reserves (Talling *et al*., 2012), and in spite of a limited understanding of these systems (compared to other sedimentary environments/systems), oil and gas exploration and development continues to be successful in these plays. Fuelled by both economic and academic interests the study of deep-marine systems has increased significantly in the past few decades. Nevertheless, despite this intensified research effort, basin-floor lobes, in particular, remain poorly understood. To illustrate, Mulder and Etienne (2010) stated that "Because of the difficulty related to the water depth under which they usually lie, [basin-floor lobes] have been understudied.". Similarly, Jegou *et al*. (2008) noted that "The architecture of these channel-mouth lobes is still poorly understood … More analysis of the controls on their development is required for a better understanding of deep-sea fans deposits.".

Studies of modern deep-water systems typically rely on seismic and/or side-scan sonar to image a 2-D slice or 3-D volume at varying levels of vertical resolution, and/or surface topography and surface sediment cover, respectively. The globally growing 3-D seismic data bank has contributed immensely to an increasingly detailed understanding of the internal architecture of basin-floor fan deposits, but due to vertical resolution limitations the finely detailed (cm to Dm scale) internal sedimentology and architecture of deep-marine basin-floor "channelized-lobe" strata remain poorly known. In modern systems core data are also commonly available, either as a stand-alone data set or as a supplement to geophysical data sets. Although core provides a detailed 1-D stratigraphic perspective, it is typically hampered by the wide spacing of drill cores and their typically short length.

Another key aspect of deep-water sedimentary research is the study of ancient outcrop analogues. Earlier studies focused on more proximal base-of-slope channel-levee systems, and comparatively fewer studies have focused on more distal lobe deposits. To date, the arguably best studied examples of ancient basin-floor fan deposits include parts of the Ross Formation in Ireland (e.g. Elliott 2000; Sullivan *et al.* 2000; Martinsen *et al.* 2000, 2003; Pyles 2007, 2008; Pyles and Jennette, 2009) and Karoo Basin in South Africa (e.g. Sullivan *et al*. 2000; Johnson *et al*. 2001; Sixsmith *et al.* 2004; Hodgson *et al*. 2006; Prélat *et al.* 2009; Groenenberg *et al*. 2010; Flint *et al*. 2011). Less well documented ancient examples also include the Brushy Canyon Formation in Texas (Beaubouef *et al*. 1999; Carr and Gardner 2000; Gardner and Borer 2000; Gardner *et al*. 2003) and the Punta Barrosa and Cerro Toro formations in southern Chile (Fildani *et al.* 2007, 2009; Hubbard *et al.* 2008; Bernhardt *et al.* 2011; Romans *et al*. 2011). Collectively these studies on seismic-scale outcrops have helped bridge the gap between large-scale seismic data and small-scale outcrop data, but still a number of important spatial disconnects remain.

Basin-floor lobe deposits in the Kaza Group, Windermere Supergroup are exposed in several km-scale outcrops in east-central British Columbia, Canada. The objective of this thesis is to provide detailed descriptions and interpretations of these "sheet-like" deposits and thereby contribute to the ever-expanding literature on similar deep-marine deposits. Starting with small (grain to bed) scale sedimentological description of these strata flow and depositional processes are interpreted. Beds are, then used to populate larger (meso) scale stratal elements, which in turn are placed in a larger scale stratigraphic context to formulate a depositional model for the entire basin-floor fan.

1.2 Geological setting and regional stratigraphy

1.2.1 Overview

The Neoproterozoic Windermere Supergroup (WSG) comprises an extensive outcrop belt that extends from northern Mexico to the Alaska-Yukon border (Figure 1.1; Ross *et al*. 1989; Ross, 1991). The most southern exposures of the WSG in northern Mexico and southwestern United States are discontinuous and comprise continental and shallow-marine sedimentary rocks (Link *et al*., 1993). Further north the WSG outcrops form a continuous belt stretching from southeastern British Columbia to northwestern Yukon (Figure 1.1). Deep-marine siliciclastic rocks of the WSG crop out superbly in the southern Canadian Cordillera (Campbell *et al.* 1973; Ross *et al.* 1995), whereas further north in the Mackenzie Mountains shelf and upper-slope facies are exposed (Ross *et al*., 1995). The WSG is interpreted to represent deposition along the paleo-Laurentian passive continental margin into the paleo-Pacific miogeocline (Figure 1.2; Bell *et al*., 1987; Ross, 1991; Ross *et al*., 1995; Karlstrom *et al*., 2001; Ross and Arnott, 2007).

This thesis focuses on deep-water rocks in the Cariboo Mountains in the southern Canadian Cordillera (Figure 1.1 and Figure 1.3). These rocks are part of the Foreland Fold and Thurst and Omineca belts (Figure 1.4) and are exposed over an area of about 35,000 km^2

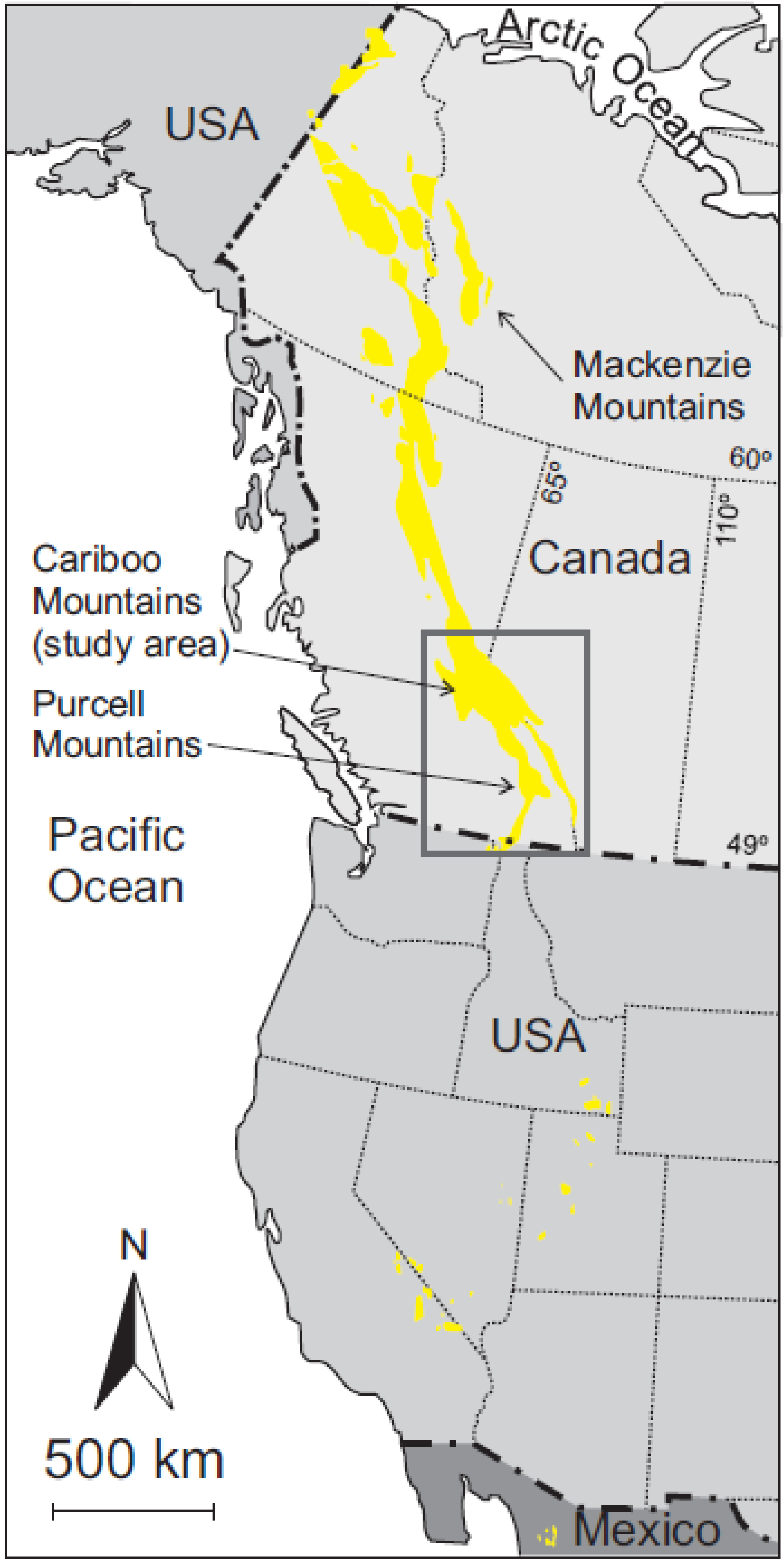

Figure 1.1: Location of Windermere Supergroup outcrops (yellow) in western North America. The grey rectangle shows the location of generally well-exposed deep-water rocks in the southern Canadian Cordillera (after Ross, 1991).

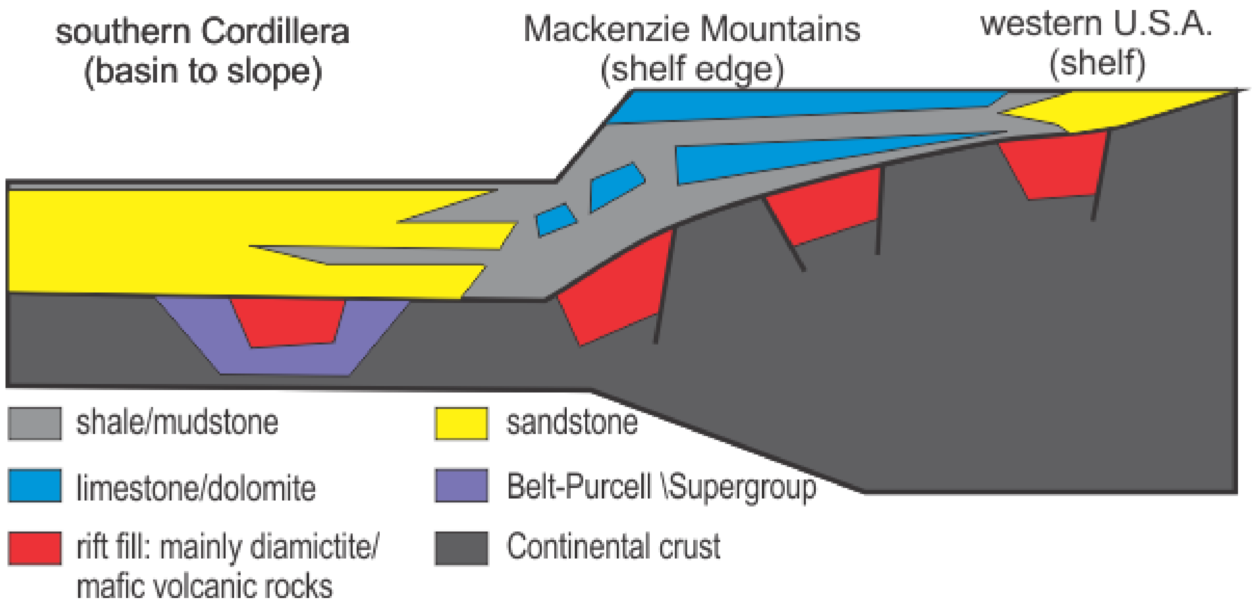

Figure 1.2: Schematic cross-section of western North America ca. 600 Ma (redrawn by Khan, 2011; from Ross, 1991). The correlation of shelf strata in the southwestern USA with deep-water rocks in the Canadian Cordillera are unknown, but age and continuity of major stratigraphic elements (e.g. glaciogenic diamictites and mafic volcanic rocks) suggest a once continuous basin (Eisbacher, 1985; Ross, 1991). Sub-Cambrian erosion has removed shallow-water strata in the southern Canadian Cordillera (Ross, 1988).

(up to 80,000 km^2 palinspastically reconstructed; Ross and Arnott, 2007) and form an up to 9 km thick upward-shoaling succession (Figure 1.5).

Accretion and mountain building have led to pervasive deformation and metamorphism in Mesozoic and older rocks of the southern Canadian Cordillera (Reid *et al*., 2002), although east of the Southern Rocky Mountain Trench levels of deformation and metamorphism are relatively low (Ross and Arnott, 2007). West of the Southern Rocky Mountain Trench, however, rocks of the Omineca Belt typically are at a higher metamorphic grade and in many places are complexly structurally deformed. Locally several areas within the Omineca Belt exhibit lower grades of metamorphism and less complex tectonic deformation (Ross and Arnott, 2007).

Primary sedimentary textures and structures are preserved here, allowing for detailed sedimentological field data to be recorded.

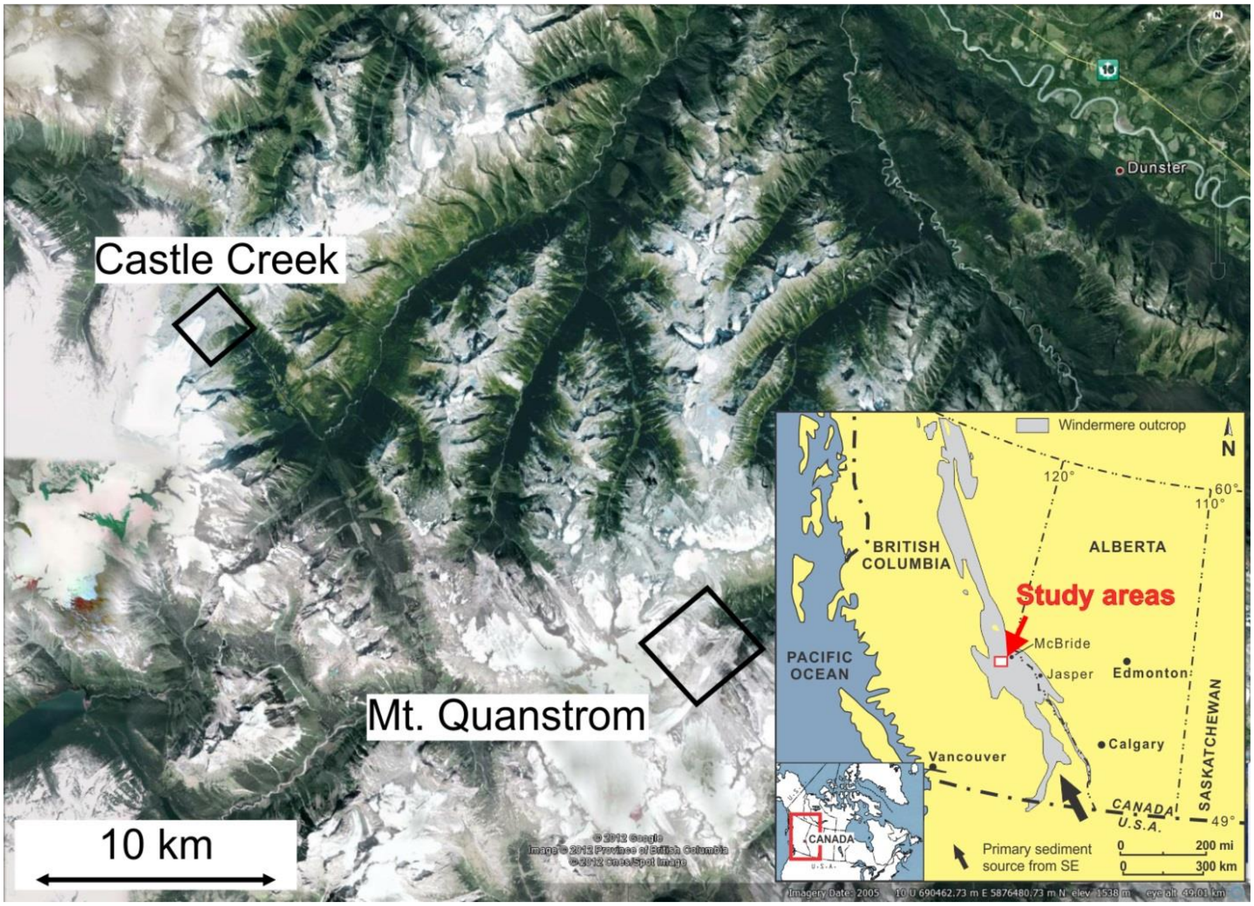

Figure 1.3: Location of the two periglacial exposures of the WSG near McBride, British Columbia, Canada (black boxes). Both outcrops comprise superbly exposed vertically dipping beds. The upper Kaza Group is exposed at Castle Creek and the middle Kaza Group is exposed at Mt. Quanstrom (background image © Cnes/Spot 2012, © Province of British Columbia 2010, © Google 2012; inset image modified from Ross, 1991).

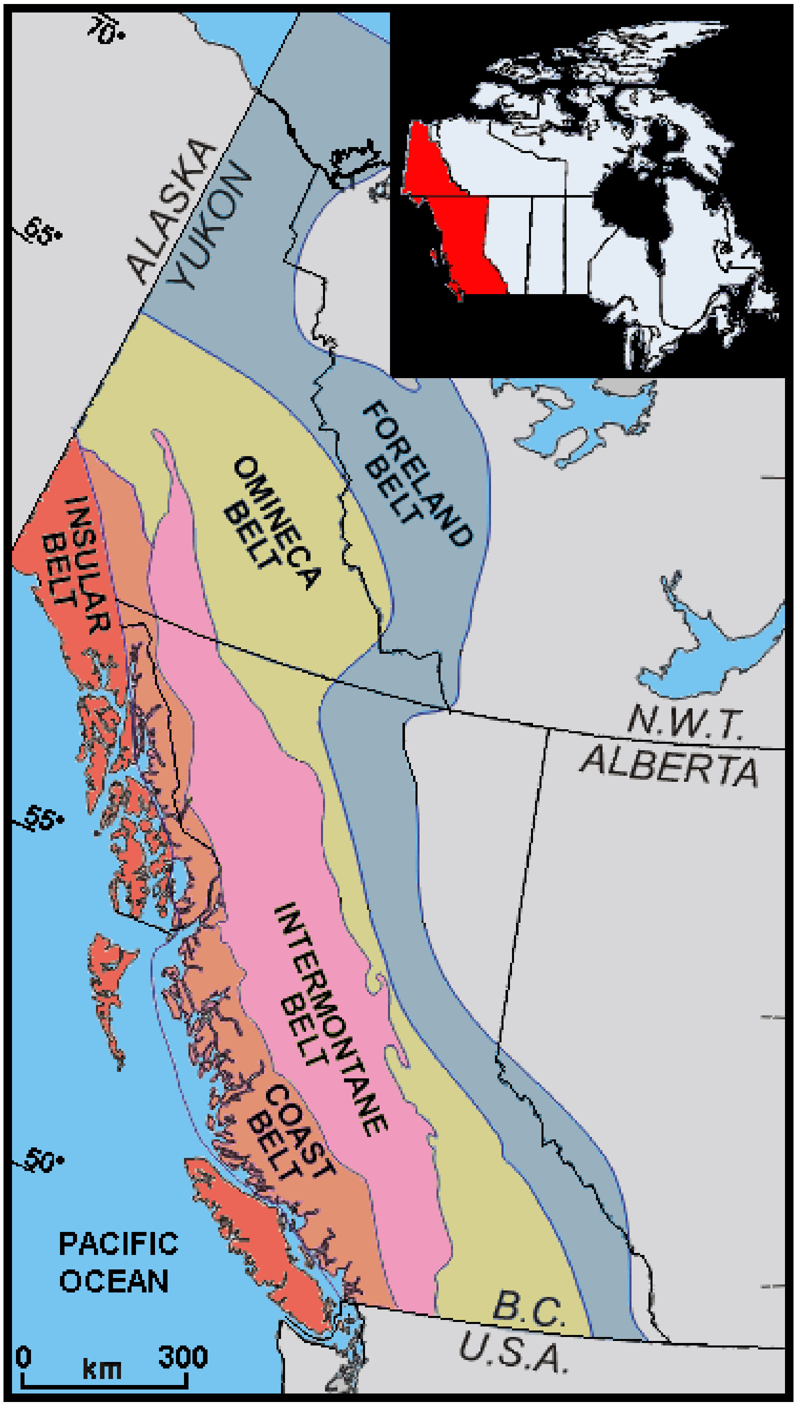

Figure 1.4: The Western Canadian Cordillera comprises five morpho-tectonic belts. From east to west they include the: Foreland Belt, Omineca Belt, Intermontane Belt, Coast Belt and Insular Belt. The northwest-southeast trending belts reflect mountain building processes related to collisional tectonism and accretion of allochtonous terranes along the western margin of Laurentia between the Mid-Jurassic (185 Ma) and Early Cenozoic (50 Ma; Price, 2000). Map after Wheeler and McFeely, 1991.

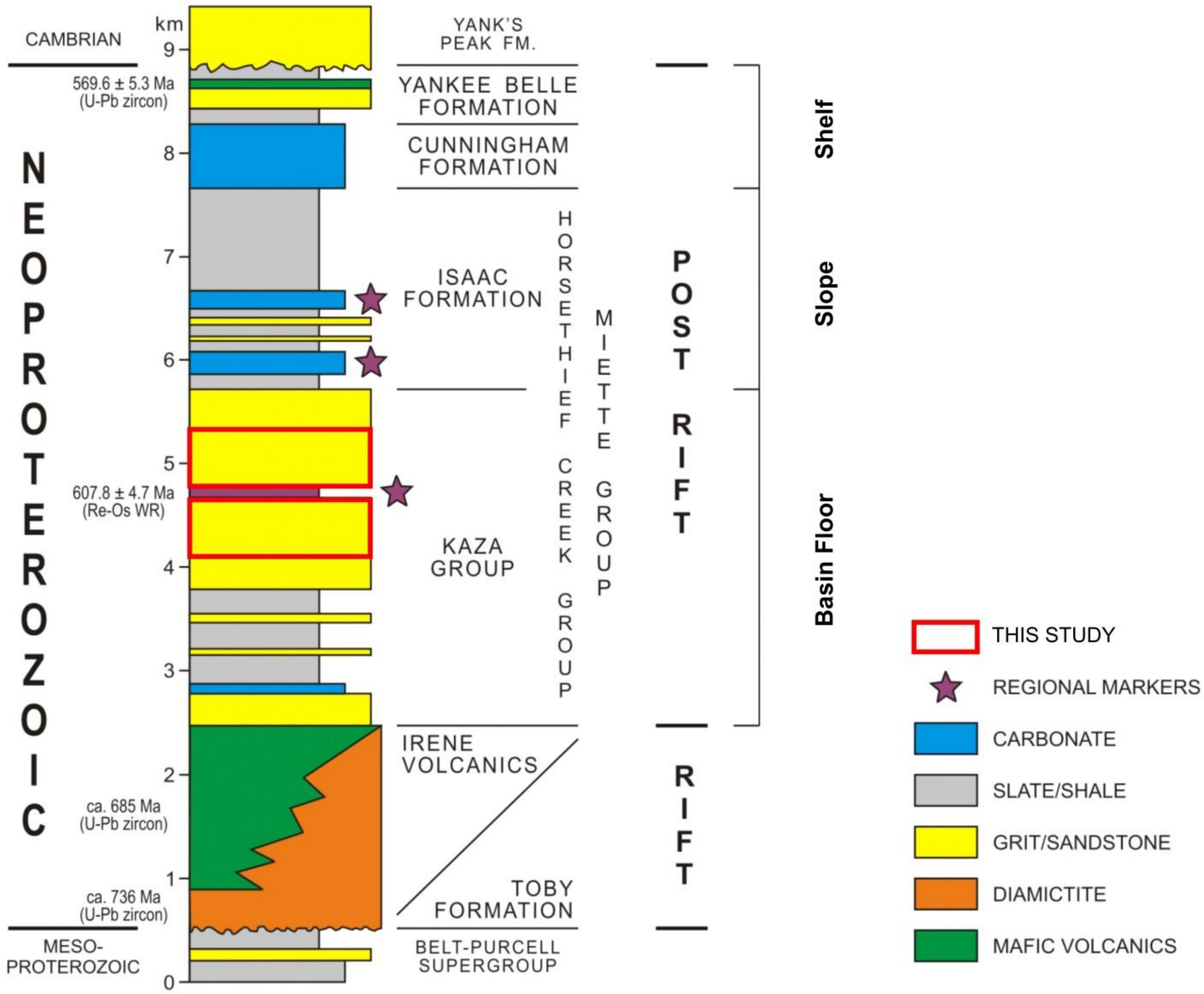

Figure 1.5: Regional stratigraphy of the Windermere Supergroup in the Southern Canadian Cordillera. This study focuses on the middle and upper Kaza Group, which are highlighted by the red rectangles (modified from Ross and Arnott 2007). Geochronological dates from Ross *et al*. (1995), Lund *et al*. (2003), Kendall *et al*. (2004) and Colpron *et al*. (2002).

1.2.2 Stratigraphic framework and depositional interpretation of the WSG in the southern Canadian Cordillera

At ca. 750 Ma (middle Neoproterozoic) break-up of the supercontinent Rodinia began (Bell *et al*., 1987; Ross, 1991; Ross *et al*., 1995; Karlstrom *et al*., 2001), creating a deep-water ocean basin (proto-Pacific Ocean) and an extensive passive margin on the northern (now western) margin of Laurentia (Ross *et al*., 1995). In the southern Canadian Cordillera the oldest rocks of the Windermere Supergroup comprise coarse-grained siliciclastic strata of the Toby Formation and mafic volcanic rocks of the Irene Formation (see Figure 1.5; Aalto, 1971; Ross *et al*., 1995), interpreted to be syn-rift deposits. This interpretation is supported by rift-correlative rocks in northern British Columbia and Idaho with ages of varying precision that range from 762-684 Ma (Devlin *et al*., 1998; Ferri *et al*., 1999; Lund *et al*., 2003; Fanning and Link, 2004).

The Toby and Irene formations are overlain by an up to 5 km thick succession of predominantly deep-water siliciclastic rocks with subordinate carbonate rocks (Figure 1.5). These rocks are known regionally by several names: Miette Group in the western Rocky Mountains (Charlesworth *et al*., 1967; Mounjoy, 1980), Horsethief Creek Group in the Purcell Mountains (Reesor, 1973), and the Kaza Group and Isaac Formation in the Cariboo Mountains (Campbell *et al*., 1973) (Figure 1.6). The topmost rocks of the Windermere Supergroup are the Cunningham and Yankee Belle formations, interpreted to be upper slope and shelf deposits (Figure 1.5). Collectively these rocks are interpreted to form a km-scale, upward-shoaling succession of basin-floor to outer shelf deposits (Ross *et al*., 1989; 1995; Ross and Arnott, 2007), and represent the basinward progradation of the Laurentian continental margin into the proto-Pacific miogeocline (Bell *et al*. 1987; Ross 1991; Ross *et al*. 1995; Karlstrom *et al*. 2001; Ross and Arnott 2007).

The minimum and maximum age of WSG deposition is constrained by ages obtained from rocks below and above the WSG sedimentary succession. Crystalline basement rocks that unconformably underlie the WSG were U-Pb dated and have an age range of 740-728 Ma (Parrish and Armstrong, 1983; Evenchick *et al*., 1984; Parrish *et al*., 1988) and provide a maximum age of WSG deposition. A minimum age was obtained from rhyolites in the Gog

Group that unconformably overlie the WSG; U-Pb dating yielded an age of 569.6 ± 5.3 Ma (Colpron *et al*., 2002). The only age constraint within the WSG sedimentary pile was obtained from black shales in the Old Fort Point Formation (Kendall *et al*., 2004) that provide an age of 607.8 ± 4.7 Ma (Figure 1.5).

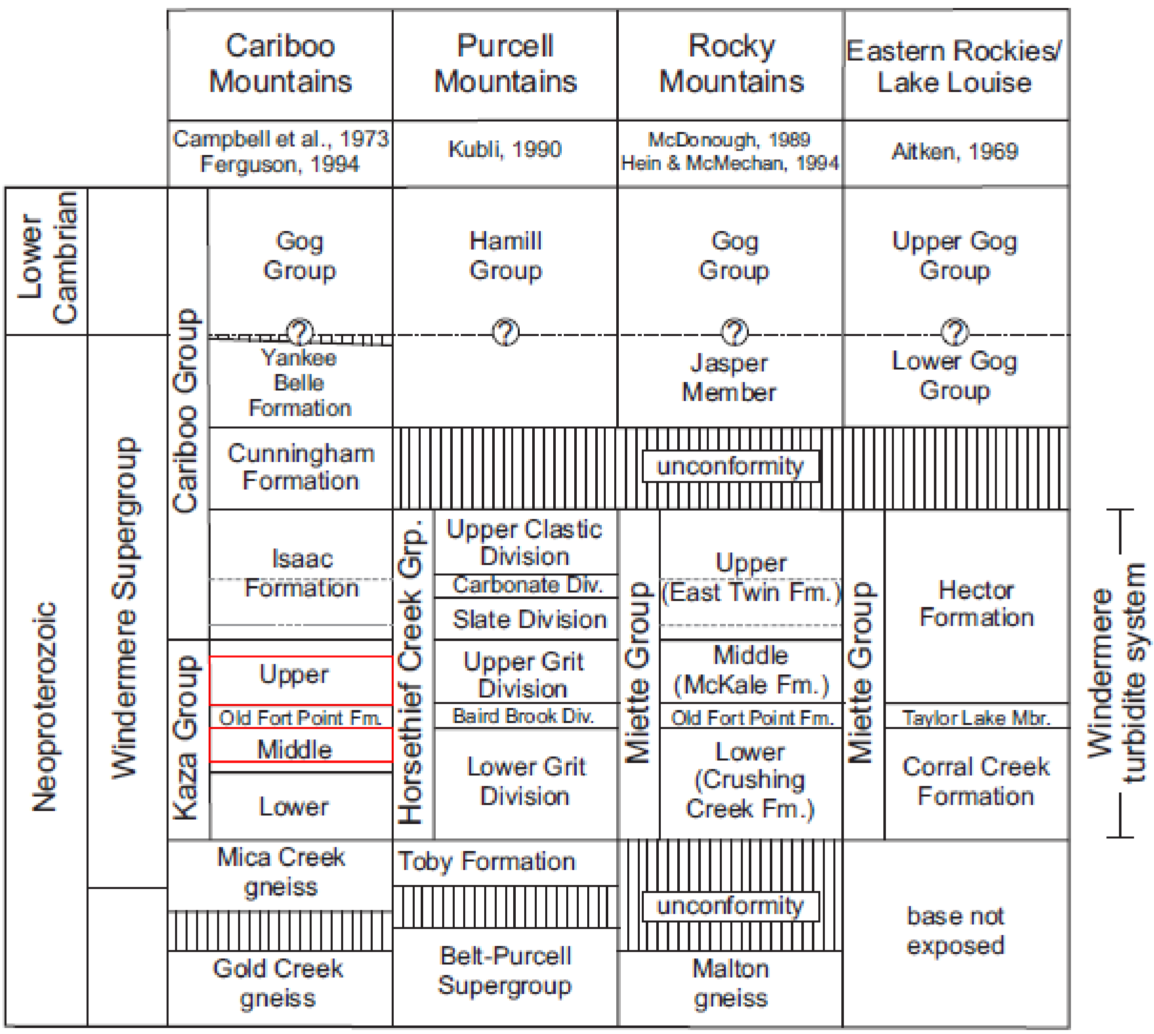

Figure 1.6: Regional terminology for rocks of the Windermere Supergroup in different parts of western Canada. The red rectangles indicate the strata that are the focus of this study. Chart modified from Ross and Arnott, 2007.

Although biostratigraphic markers are absent in the WSG, regional correlations are made possible by several regionally extensive lithostratigraphic marker units. The first regional marker is the Old Fort Point Formation (OFP), which crops out across the entire deep-marine Windermere outcrop belt, and forms an up to 450 m thick, geochemically distinct deep-marine succession of locally green, purple and black slate with lesser carbonate and sandstone (Figure 1.5; Smith 2009; Smith *et al*. 2012). In the Isaac Formation two less areally extensive carbonate marker units are recognized (Figure 1.5), informally termed the first and second Isaac carbonates. The Isaac carbonates consist of interstratified thin- to medium-bedded calciturbidites and subordinate conglomerate, breccia and slump blocks. These units range from 10-250 m thick and are interpreted to have been deposited during periods of sea level highstand with attendant carbonate production on the continental shelf and consequent shedding into deep water (Ross *et al*., 1995; Ross and Arnott, 2007).

Sediment provenance using detrital zircon grains indicates a bimodal age distribution: older than 2.6 Ga and around 1.9-1.75 Ga (Ross and Bowring, 1990; Ross and Parrish, 1991). These ages suggest the WSG sediments were derived from the Canadian Shield and northwestern United States (Ross *et al*., 1995; Ross and Arnott, 2007). The sediments were likely transported by a major continental fluvial system to the marine realm, and then fed by a canyon system (Arnott and Hein, 1986) into deeper water parts of the basin. Regional palaeocurrent data suggest transport in a general west-northwest direction (Ross *et al*., 1995; Ross and Arnott, 2007), although local variations exist (Arnott and Hein, 1986; Schwarz and Arnott, 2007; Khan and Arnott, 2011).

Collectively these data suggest that deep-water rocks of the WSG were deposited in a single, continental scale turbidite system that was fed for a prolonged period of time by a single continental sediment source.

1.3 Study areas and previous work

This study focuses on two exposures of the Kaza Group in the Cariboo Mountains, southern Canadian Cordillera (Figure 1.3): the Mt. Quanstrom study area where rocks of the middle Kaza Group crop out and the Castle Creek study area where the upper Kaza Group is exposed. Geologic work in the region was first conducted by Campbell *et al*. (1973) who completed a regional (1:250,000) map and described the regional stratigraphy, deformation and metamorphism. Subsequently a 1:50,000 map, which includes the Castle Creek study area, was published by Ross and Ferguson (2003) (Figure 1.7), but neither this map, nor any subsequent map include the Mt. Quanstrom area. In addition, several studies that focused on the regional geology and structure of this area in the Cariboo Mountains have been published, including Murphy and Rees (1983); Murphy (1987a, b); Ross and Murphy (1988); Aitken and McDonough (1990); Ross (1991, 2000); Gabrielse and Campbell (1991); Hein and McMechan (1994); Ross *et al*. (1995); Reid *et al*. (2002); Reid (2003).

The Mt. Quanstrom and Castle Creek study areas (referred collectively hereafter as "study area") were affected by at least four phases of Mesozoic tectonic deformation (Murphy and Rees, 1983; Murphy, 1987a; Reid *et al*., 2002). The oldest (D_1) phase of deformation is

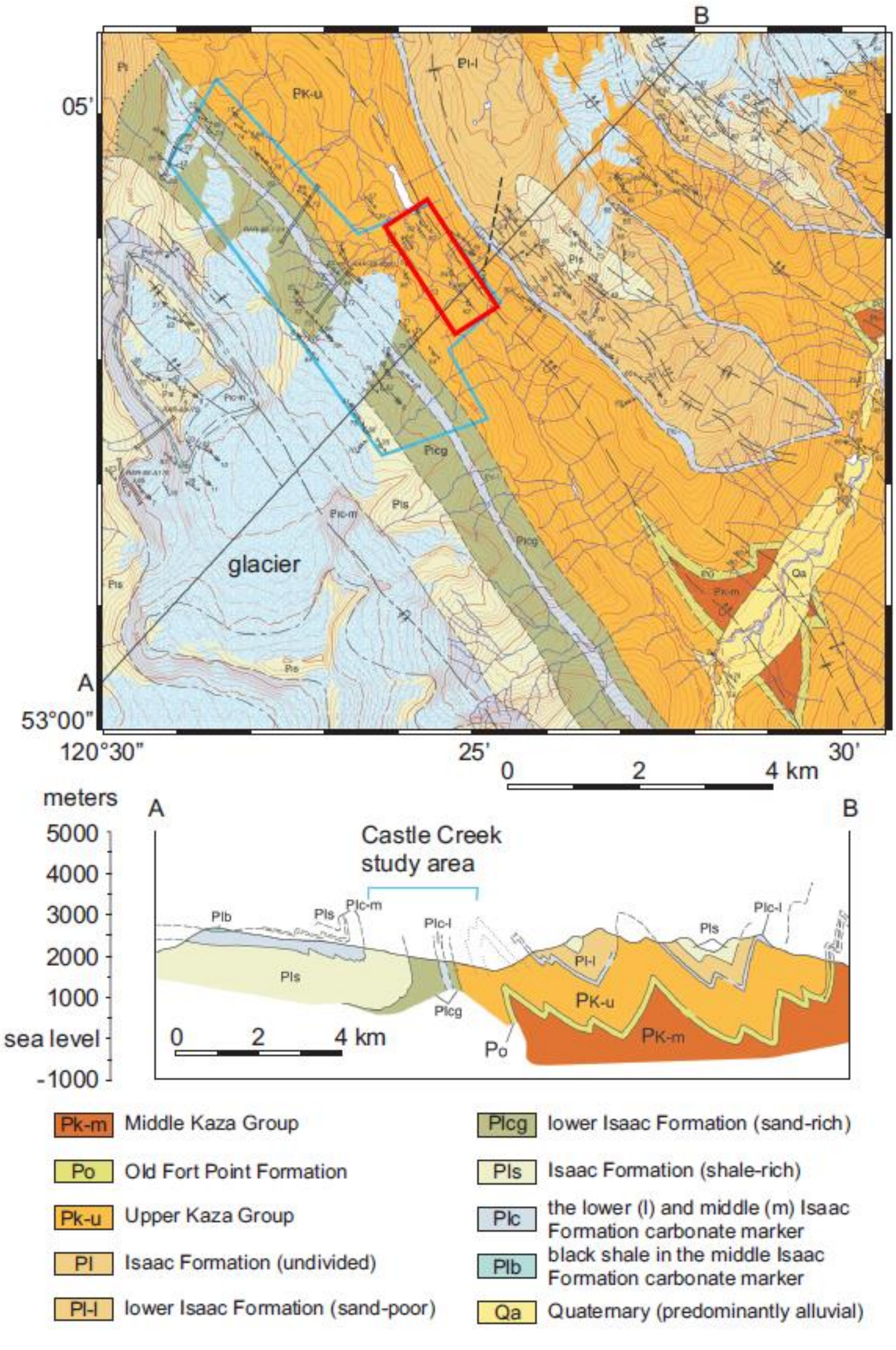

Figure 1.7: Regional geology of the Castle Creek area (excerpt from the Eddy 1:50,000 map area: Ross and Ferguson, 2003). The larger Castle Creek field area is highlighted by the blue polygon; this study focuses on the area in the red rectangle.

expressed in east-verging, meter-scale folds and sub-parallel-to-bedding cleavage (S_1). Regionally dominant, kilometer-scale, southwest-verging folds are related to the second (D_2) phase of deformation that resulted also in an axial planar cleavage (S_2) and a prevalent crenulation cleavage in the study area (Murphy, 1987a). These two deformation phases are cross-cut by igneous intrusions dated at 174 Ma, thus providing a minimum age for the D_1 and D_2 events (Pigage, 1977; Gerasimoff, 1988). The third phase of deformation, D_3, resulted in dextral strike-slip faults, northeast-verging kilometer-scale folds, and an axial planar cleavage that crenulates S_2 cleavage (Reid *et al*., 2002). The fourth (D_4) and final deformation phase resulted in local meter-scale kink folds (Reid *et al*., 2002).

Regional metamorphism in the study area is interpreted to have started after D_1, and peaked between D_2 and D_3 (Murphy, 1987a), altering the rocks to sub-greenschist and greenschist facies. Although both deformation and metamorphism have affected the study area, primary sedimentary structures, as small as mm-scale laminae, are well preserved (see also, for example, Ross and Arnott, 2007). It is this remarkable preservation that allows detailed sedimentological analyses to be conducted, and also why terminology for sedimentary rather than metamorphic rocks is used.

The stratigraphy at Castle Creek comprises the upper Kaza Group (stratigraphic thickness of ~800 m exposed at the base of the outcrop; Figure 1.8) overlain conformably by the Isaac Formation (~1.6 km section exposed; Figure 1.8). The upper Kaza Group comprises predominantly coarse-grained sandstone beds that form laterally continuous “sheet-like” elements (Meyer, 2004; Meyer and Ross, 2007a, b; Rocheleau, 2011). Towards the top of the Kaza Group sandstone filled channels and debrites become more common (Rocheleau, 2011; Navarro, pers. comm.). The Isaac Formation comprises several decameter-thick, several 100 m to few km wide, coarse-grained sandstone filled channels that are encased on all sides by finer-grained turbidites (Navarro, 2006; Arnott, 2007a, b; Barton *et al*., 2007; Gammon *et al*., 2007; Navarro *et al*., 2007a, b; O'Byrne *et al*., 2007a, b; Ross and Arnott, 2007; Schwarz and Arnott, 2007a, b, c; Mussa-Caleca, 2008, Khan, 2011; Khan and Arnott, 2011; Khan *et al*., 2011). Debrites, slump and slide deposits are also common in the Isaac Formation, which in one instance form a 110 m-thick mass-transport deposit (Arnott *et al*., 2011).

The stratigraphy at Mt. Quanstrom comprises a well-exposed succession of the middle Kaza Group about 1.5 km thick. The middle Kaza Group is conformably overlain by the Old Fort Point Formation, a regional marker (Figure 1.5) that crops out at the top of the Mt. Quanstrom section. This marker unit provides stratigraphic control for the otherwise monotonous stratigraphy of the middle Kaza Group at Mt. Quanstrom.

Both the Castle Creek and Mt. Quanstrom field areas (Figure 1.3) occur on the overturned limb of a major southwest-verging fold in the Isaac synclinorium (Campbell *et al*., 1973; Ross and Arnott, 2007), resulting in near-vertical bedding at both locations. Both study areas are adjacent to rapidly retreating glaciers, resulting in recently deglaciated, well-polished outcrops that are largely devoid of vegetation or soil cover. Glacial debris and moraines are present locally at both field sites. At Castle Creek, WSG rocks crop out in a 7 km wide (parallel to bedding) and 2.5 km thick (perpendicular to bedding) exposure; this study focuses only on the upper Kaza Group (Figure 1.5) at Castle Creek, which is exposed in the lower ~500 m thick and ~ 1 km wide part of the outcrop (Figure 1.8). The Castle Creek field site has a gentle topography, and the part of the outcrop studied in this thesis is continuously exposed (Figure 1.8). At Mt. Quanstrom the topography is more rugged and additionally is broken up into several exposures bounded by a glacial outflow stream, a forested cliff and a glacier (Figure 1.9).

1.3.1 Previous work by the Windermere Consortium

This study is funded by the Windermere Consortium, an industry and government supported research program based at the University of Ottawa. Research documenting the sedimentology, stratigraphy and architecture of deep-water strata at Castle Creek area has intensified significantly since the inception of the program (Arnott and Ross, 2007; Ross and Arnott, 2007). Basin-floor deposits (upper Kaza Group, Figure 1.7) were originally described by Meyer (2004) and Meyer and Ross (2007a, b). Later Rocheleau (2011) conducted a highly detailed sedimentological analysis of a smaller area within the upper Kaza Group. Work in the overlying Isaac Formation includes study of base-of-slope channel-levee complexes (Navarro, 2006; Arnott, 2007a, b; Barton *et al*., 2007; Gammon *et al*., 2007; Navarro *et al*., 2007a, b; O'Byrne *et al*., 2007a, b; Ross and Arnott, 2007; Schwarz and Arnott, 2007a, b, c; Mussa-Caleca, 2008, Khan, 2011; Khan and Arnott, 2011; Khan *et al*., 2011), overbank deposits (Arnott, 2007c, d; Davis, 2011, Khan, 2011; Khan and Arnott, 2011; Khan *et al*., 2011), and mass transport deposits (Laurin *et al*., 2007; Arnott *et al*., 2011). Architectural attributes of Castle Creek have also been used to develop analogue reservoir models (Buckley *et al*., 2010) in order to provide insight into many hydrocarbon charged, subsurface deep-water leveed-channel systems.

Previously no detailed work has been conducted on the Mt. Quanstrom outcrop except for the regional mapping of Campbell *et al*. (1973) and reconnaissance exploration by Schwarz, Smith and Altosaar (pers. comm.). These researchers report that the stratigraphy of the middle Kaza Group consists of alternating decameter-thick, fine-grained and coarse-grained sandstone units that are laterally continuous across the outcrop (sheet-like deposits).

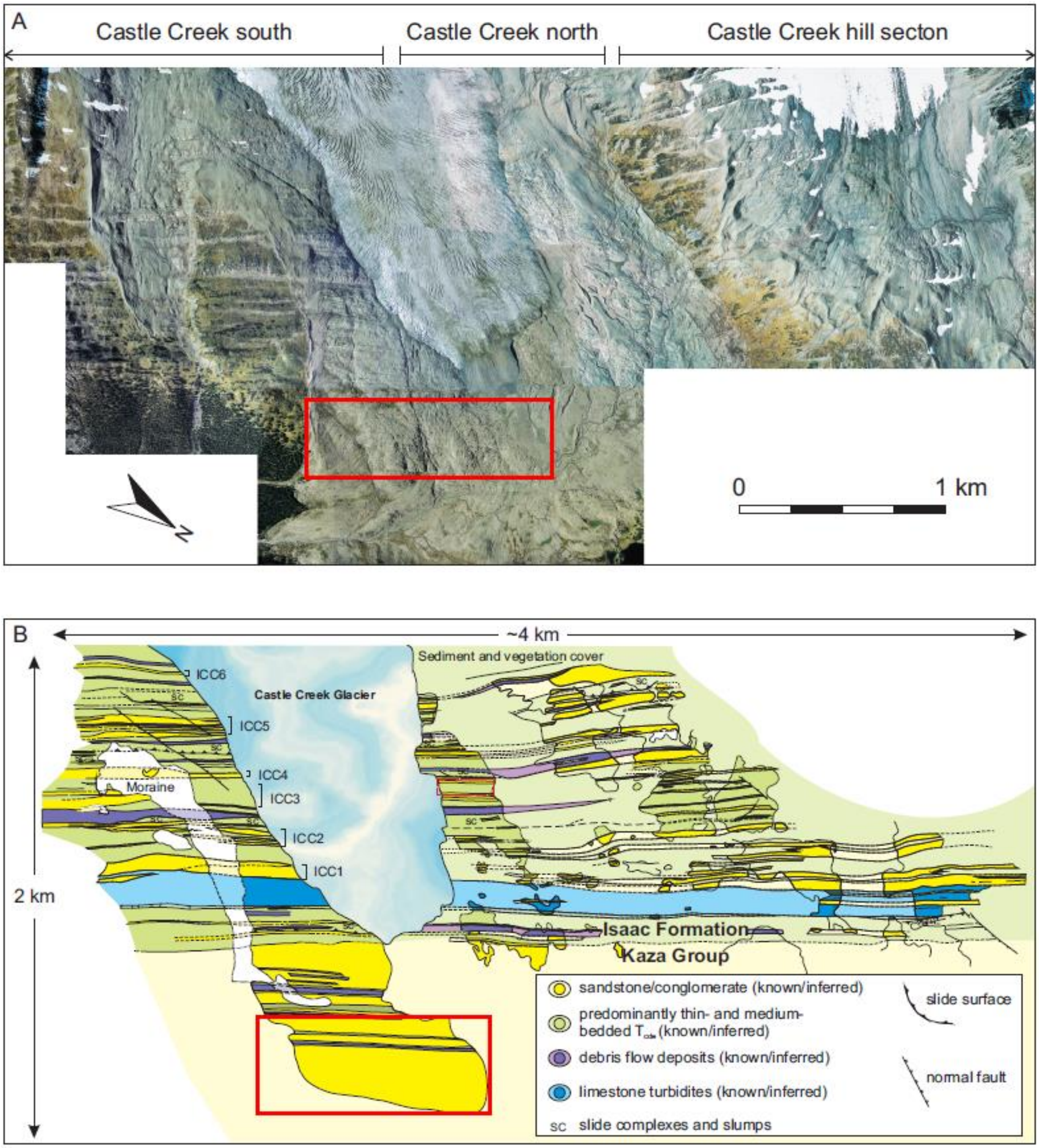

Figure 1.8: A) Photomosaic of the Castle Creek study area. B) Interpreted geologic map of the Castle Creek study area. This study focuses on the areas highlighted by the red rectangles. For location of previous studies conducted at Castle Creek see figure 5B in Ross and Arnott, 2007. Figure modified from Ross and Arnott, 2007.

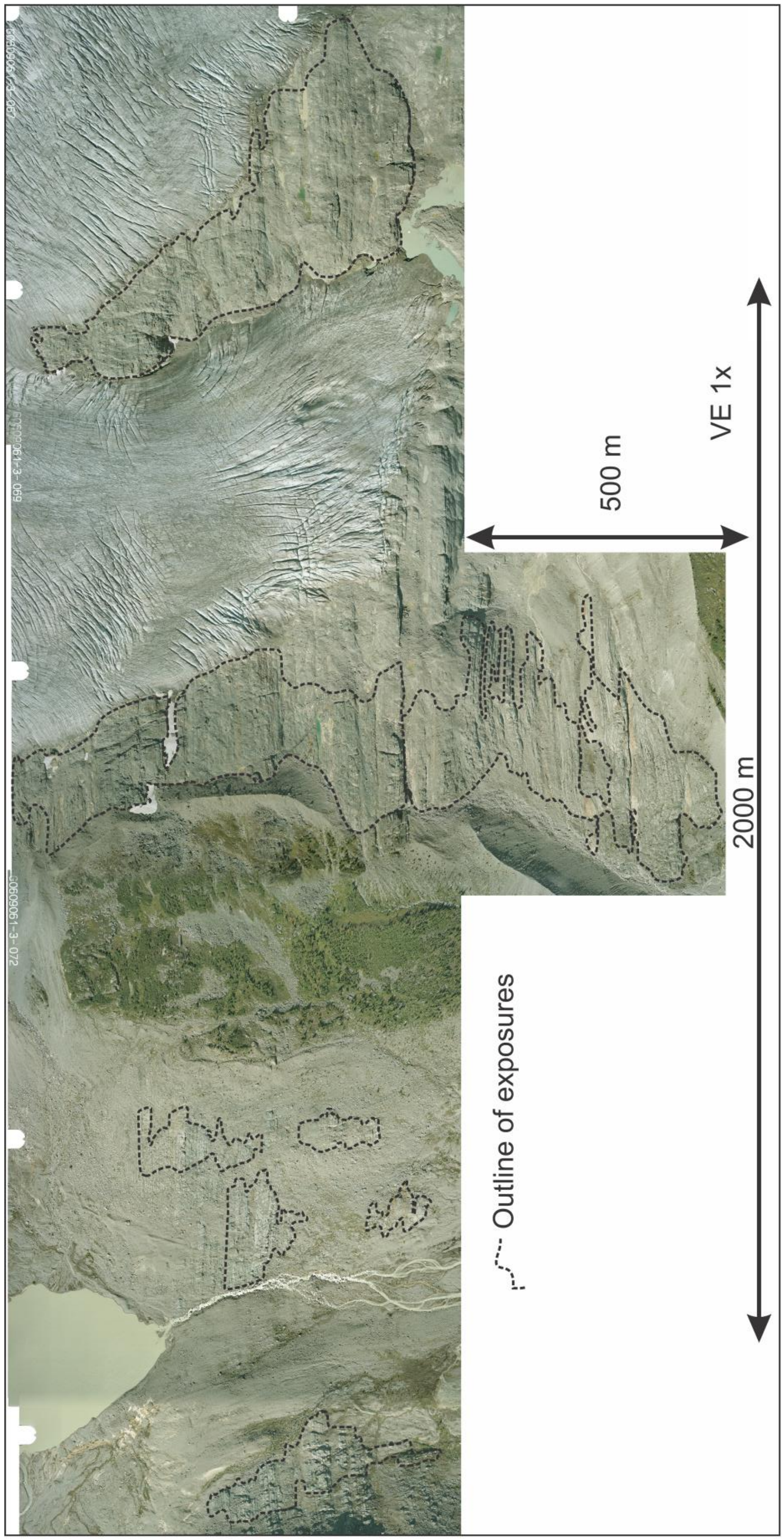

Figure 1.9: Photomosaic of the Mt. Quanstrom field area. Dashed lines indicate the margins of exposures.

1.4 Terminology

Despite the metamorphic alteration of the rocks, in this study sedimentary terminology is used to describe them (see above). The original clay mineral constituents of the rock have been altered to chlorite and muscovite during metamorphism. Moreover, due to recrystallization the grain size of the original clay mineral constituents is unknown, and as a consequence matrix is defined in part by its mineralogy. Collectively, chlorite and muscovite, regardless of crystal size, in addition to minor unaltered siliciclastic silt (grain size < ~65 μm), constitute the 'matrix' in matrix-rich sandstones.

Strata are classified in a hierarchical basis in this study, starting from smallest to largest: lamina, bed, unit, stratal element (Figure 1.10). The term lamina is used in its classical sense: a sedimentary layer <1 cm thick (e.g. McKee and Weir, 1953). The term 'bed' refers exclusively to an event bed, which encompasses the full thickness and lateral extent of a sedimentary layer deposited by a single flow event. A 'unit' is a stratal package comprising two or more event beds, and in which >50% of the beds are composed of a single sedimentary facies. Moreover, a unit is independent of the nature of its lower and upper bounding surfaces, or any lateral change in facies. For example a "unit of matrix-rich sandstone" refers to a stratal package comprising two or more matrix-rich beds that make up at least >50% of the local stratal succession. A stratal element, in turn, is defined by the nature of its bounding surfaces and the vertical and lateral arrangement of its constituent beds and/or units.

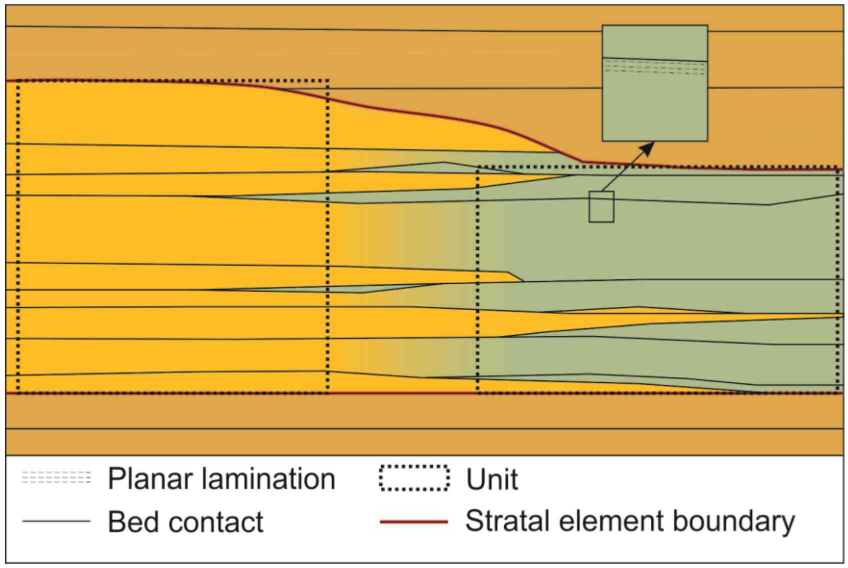

Figure 1.10: Line diagram illustrating the terminology for strata in a hypothetical cross-section. Colours are arbitrary and indicate three different sedimentary facies. A lamina is the thinnest (<1 cm) layer within (event) beds. Beds comprise the total volume of sediment deposited by a single flow event, or following post-depositional erosion, the remnants thereof. Facies may change laterally. Units are local stratal packages comprising >50% of one sedimentary facies; lateral facies changes nor the nature of bounding surfaces are considered. Stratal elements are made up of one or more units and are defined by their bounding surfaces and the lateral and vertical arrangement of their component units.

In this example three stratal elements are shown. The lower stratal element comprises beds of the brown facies. The middle stratal element has a planar basal surface and comprises two units. The left unit is dominated by beds of the orange facies whereas the right unit consists mostly of beds of the grey-green facies. Beds of the grey-green facies are capped by planar laminated sandstone. Note that several beds show a lateral facies change from orange to grey facies. The upper stratal element has an erosional basal surface and consists entirely of the brown facies.

1.5 Thesis objectives and structure

This thesis aims to describe and interpret deep-water basin-floor strata of the Windermere Supergroup at three different observational scales: grain to bed scale, stratal element scale and outcrop scale. To achieve this, a detailed field study of the middle Kaza Group at Mt. Quanstrom and the upper Kaza Group at Castle Creek (Cariboo Mountains, B.C., Canada) was performed.

1. Grain- to bed-scale observations include detailed field-based sedimentological descriptions of WSG strata and thin section analysis, which then were used to:
    a. Provide a detailed facies description of each of the observed facies;
    b. Interpret flow processes operating on the basin-floor during WSG deposition;
    c. Interpret how these flows developed through space and time.

2. Seven stratal elements making up the basin-floor deposits of the WSG are recognized. These were mapped on aerial photographs and identified on stratigraphic correlation panels in order to:
    a. Describe the internal facies distribution within each stratal element;
    b. Describe the overall cross-sectional shape and size of each stratal element;
    c. Interpret the formative evolution of each element;
    d. Propose an idealized model for the formation of each element.

3. Mapping and logging of both field sites provide data that was used to:
    a. Describe the long-term evolution of the sedimentary succession based on upward stratal changes;
    b. Describe the spatial arrangement of stratal elements;
    c. Based on the vertical and horizontal arrangement of stratal elements, propose a basin-floor fan model of the WSG;
    d. Based on the vertical arrangement of stratal elements in the upper Kaza Group, create a predictive model for 1D stratigraphic logs.

This thesis is a compilation of articles describing basin-floor rocks of the Windermere Supergroup, although each article has been greatly expanded with additional background information and detail from the submitted journal version. The chapters follow a logical dimensional order, starting with observations of small-scale sedimentary structures, which then are used to populate a comprehensive large-scale model of a basin floor turbidite system. Chapter 2 starts with a review of sediment gravity flows, which sets the stage for detailed facies descriptions and interpretations. Chapter 3, then, places these facies into meso-scale (few metres to several 100 m) stratal elements, which in turn are interpreted individually based on their shapes, sizes, internal distribution of facies and stratigraphy. Chapter 4 focuses on two stratal elements, scours and avulsion splays, by providing a more detailed description and elaborating on their origin. These elements have been increasingly recognized in deep-water strata around the world, and have particular (and timely) interest in the geologic community due to their potential impact on reservoir quality. In the final chapter, Chapter 5, a large-scale model of basin-floor strata in the WSG is developed.

1.6 Statement of contributions

Chapters 2 and 3 are expanded versions of a manuscript in preparation for submission:

Terlaky, V., Rocheleau, J., and Arnott, R.W.C., in preparation, Stratal composition and component stratal elements of an ancient deep-marine basin-floor succession, Neoproterozoic Windermere Supergroup, British Columbia, Canada.

This paper is based principally on fieldwork carried out by Viktor Terlaky (VT), with assistance in the field from Jonathan Rocheleau (JR), Greg van Hees, Pierce Grogan, Dave Anthony, Gilian Cramm, Adam Tudor, Amanda Schembri, Jordan Clarke, Jenni Morris, Michelle English, Omar Al-Mufti and Dr. Bill Arnott. Lori Meyer and Hugues Longuepeé conducted preliminary field work in the upper Kaza Group, but except for general observations none of their data was used in this thesis. JR was the first worker to recognize and describe in detail scours and feeder channels in the upper Kaza Group. The interpretation of scours in this thesis is similar to that of JR. The description of the feeder channel originally described by JR (Rocheleau, 2011) has been expanded with three additional stratigraphic logs, and interpretation of the channel modified in this thesis. All figures are those of VT, except where indicated. The initial manuscript was written by VT and later revised through discussion with Dr. Arnott.

Chapter 4 in large part reproduces a manuscript accepted for publication in the journal *Sedimentology*:

Terlaky, V., and Arnott, R.W.C., accepted, Matrix-rich and associated matrix-poor sandstones: avulsion splays in slope and basin-floor strata. Sedimentology. DOI: 10.1111/sed.12096

The original idea for this paper developed gradually through many years of field observation and discussion between students and professors in the Windermere Consortium. Field work for this paper was carried out mainly by VT and Adam Tudor, with assistance from JR, Jenni Morris, Michelle English, Omar Al-Mufti and Dr. Arnott. This paper also benefitted greatly from discussion with Mike Tilston regarding preliminary results of his Ph.D. thesis on subaqueous sediment gravity flow behaviour. All figures were prepared by VT, unless otherwise indicated. The manuscript was written by VT and later revised through discussion with Dr. Arnott. The manuscript was submitted to Sedimentology on the 25th of February, 2013 and accepted pending revisions on May 17th, 2013. The revised manuscript was accepted for publication on Novermber 12th, 2013.

Chapter 5 is an expanded version of a manuscript in preparation for submission:

Terlaky, V., and Arnott, R.W.C., in preparation, Spatial organization and temporal evolution of the stratal elements that make-up deep-marine, basin-floor lobes – insights from the Neoproterozoic Kaza Group, Windermere Supergroup, southern Canadian Cordillera.

This paper is based on the same field work as chapters 2, 3 and 4, and has benefitted from assistance by JR, Greg van Hees, Pierce Grogan, Dave Anthony, Gilian Cramm, Adam Tudor, Amanda Schembri, Jordan Clarke, Jenni Morris, Michelle English, Omar Al-Mufti and Dr. Bill Arnott. Figures were prepared by VT, unless original sources are referenced. The manuscript was written by VT and later revised through discussion with Dr. Arnott.

Appendix E is a reproduction of the paper:

Buckley, S.J., Schwarz, E., Terlaky, V., Howell, J., Arnott, R.W.C., 2010., Combining aerial photogrammetry and terrestrial Lidar for reservoir analog modeling: Photogrammetric Engineering & Remote Sensing, V. 76, No. 8, p. 953-963.

This paper combines several datasets collected at the Castle Creek outcrop to create a virtual 3D outcrop and a geocellular reservoir model of Isaac Channel 3 (a channel and levee complex in the base-of-sope Isaac Formation). Data for the virtual outcrop was collected by Simon Buckley, Ernesto Schwarz and VT and includes ground-based laser scanning and photography of the outcrops. Lithologic and stratigraphic data of Isaac Channel 3 was collected by Lilian Navarro and Shann Khan (see Navarro, 2006; Navarro *et al*., 2007; Khan and Arnott, 2011). Processing of laser and image data and creation of the virtual outcrops was done by VT with assistance from Simon Buckley. The geocellular model was created by Ernesto Schwarz with assistance from Simon Buckley, John Howell and VT. The manuscript was written by Simon Buckley and Ernesto Schwarz with editorial input from all authors.

Chapter 2: Sedimentary facies in the middle and upper Kaza Group

2.1 Introduction

The aim of Chapter 2 is to present a detailed sedimentological description of the rocks that make up the middle and upper Kaza Group, and to interpret the depositional origin of each facies. To aid in the interpretation of these facies a short overview of submarine sediment gravity flow types, their processes and resultant deposits is first presented.

2.2 Sediment gravity flows

Sediment gravity flows are mixtures of fluid and sediment, where gravity acts on the sediment to propel the flow. These flows are the main mechanism that deliver sediment into deep-marine environments, and are volumetrically the most important flow process operating on Earth (Talling *et al*., 2012). Flows are initiated commonly along the continental shelf edge (Shanmugam, 2006) as a result of one or a combination of: high slope gradients (e.g. near the mouth of the Magdalena River, Colombia; Heezen, 1956), high rates of sedimentation (e.g. the Mississippi delta front, Gulf of Mexico; Coleman and Prior, 1982), earthquake disruption (e.g. 1929 Grand Banks tremors, east coast Canada; Heezen and Ewing, 1952), salt movement (e.g. intraslope basins, Gulf of Mexico; Tripsanas *et al*., 2004), glacial loading (e.g. the Scotian margin, North Atlantic; Mosher *et al*., 2004), tsunamis (e.g. Gutenberg, 1939), storm waves (e.g. Henkel, 1970), biological erosion (e.g. along submarine canyon walls; Warme *et al*., 1978), and gas generation due to organic decay (e.g. Scripps submarine canyon head, west coast U.S.A; Dill, 1964). Single submarine flows can transport over 100 km^3 of sediment (Rothwell *et al*., 1998; Piper *et al*., 1999; Talling *et al*., 2007), travel at speeds up to between 60-100 km/h as measured by submarine cable breaks (Heezen and Ewing, 1952; Piper *et al*., 1999a; Hsu *et al*., 2008) and have run-out distances in excess of 1500 km across the ocean floor (Wynn *et al*., 2002b; Talling *et al*., 2007; Frenz *et al*., 2008). Submarine sediment movements can broadly be divided into mass movements (coherent material, i.e. slides and slumps) and sediment flows (incoherent sediment and water mixture, i.e. debris flows and turbidity currents). Slides and slumps commonly occur in the most proximal parts of the sedimentary system (continental slopes and submarine canyon heads; Shanmugam, 2006), but regardless of setting require a slope to initiate and maintain motion. Slides and slumps travelling down a steep slope accelerate and disintegrate, and eventually form a sediment flow ("ignite"; Shanmugam, 2006) (Figure 2.1). Rocks of the middle Kaza Group contain no coherent mass movement deposits and only a minor portion of the upper Kaza Group consists of mass movement deposits. The remainder of the chapter, therefore, focuses on the description and physical basis of sediment gravity flows.

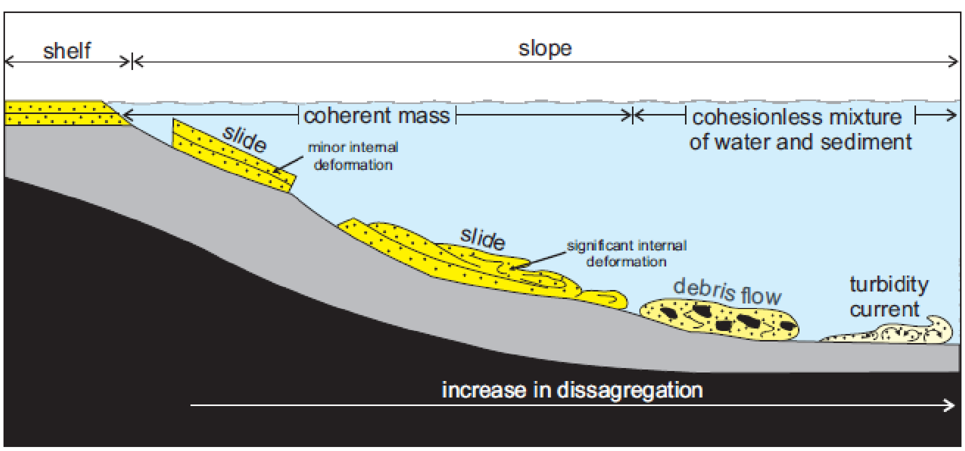

Figure 2.1: Downslope evolution of sediment gravity flows. Initially sediment failure at the shelf edge forms coherent slides and slumps, which downflow transform into debris flows and ultimately turbidity currents. Modified from Shanmugam *et al*., 1994.

2.2.1 Classification

Subaqueous gravity flows are traditionally classified into two end-member kinds: frictional flows (or turbidity currents) and cohesive flows or debris flows (e.g. Middleton & Hampton, 1976; Lowe, 1979, 1982; Mulder and Alexander, 2001; Talling *et al*., 2012). Large submarine debris flows have not been observed or monitored in nature, and few studies have succeeded in directly monitoring turbidity currents, in part due to their inaccessibility in deep water settings, their unpredictable occurrence, but mostly their destructive nature (Khripounoff *et al*., 2003; Xu *et al*., 2004, 2010). One large tubidity current in a submarine valley offshore Zaire was measured at 4000 m water depth with current meters, turbidimeter and a sediment trap located in the axis of a channel (Khripounoff *et al*., 2003). The velocity of the current at 150 m above the channel floor was 121 cm s^{-1} and the sediment trap deployed 40 m above the channel floor collected coarse sand and plant debris. A sediment trap moored on the distal part of the channel levee, 13 km to the south of the channel axis, collected quartz silt and plant material, indicating that the current overflowed the valley and flowed for a considerable distance beyond its confinement.

In theoretical and laboratory research flow characteristics are measured directly (e.g. Best *et al.*, 2001; Tilston, 2012) and flows are commonly classified based on flow rheology and sediment concentration. In field studies, however, flow characteristics and flow type is inferred from lithological characteristics observed in the rock record, which has resulted in a plethora of classification schemes (e.g. Pickering *et al.*, 1989; Guibaudo, 1992; Stow and Johansson, 2000; Mulder and Alexander 2001; Talling *et al.*, 2012 and references within). The resulting discrepancies and confusion in terminology encouraged Mulder and Alexander (2001) to propose a simplified classification scheme based on particle cohesion, flow duration, sediment concentration and particle-support mechanisms (Figure 2.2). Continued research on turbidites in the past decade has recognized several deposit types that could not easily be classified based on previous schemes, and in response Talling *et al.* (2012) proposed an expanded classification that is heavily influenced by field observations of debrites, turbidites and intermediate flow types. Interpretations in this thesis, however, are based mostly on the classification of Mulder and Alexander, but, where appropriate, other classification schemes are used as indicated.

Mulder and Alexander's classification differentiates between cohesive flows, hyperconcentrated and contentrated density flows and turbidity flows (Mulder and Alexander, 2001). Cohesive flows are unique in the classification scheme, and are the only flow type with a plastic rheology and laminar flow character. These flows are interpreted to be debris flows, and in the rock record termed debrites. Hyperconcentrated and concentrated density flows and turbidity flows are all non-cohesive, and are differentiated based on grain support mechanism. Concentrated and hyperconcentrated density flows span from 9%, at which grain to grain interaction starts to occur, to up to 50% sediment concentration. Grains are supported largely by grain-to-grain interactions, matrix-strength, hindered settling, buoyancy and dispersive pressure; in more dilute flows the upward component of turbulence can be a major grain support mechanism. In hyperconcentrated flows matrix strength and buoyancy play a more important role. The main difference between these two flow types in terms of the deposits they produce is that in the former differential grain settling results in graded beds (e.g. Lowe sequences, Figure 2.3; Lowe, 1982), whereas in the latter differential grain settling is suppressed, resulting in ungraded beds. Turbidity flows are defined by the Bagnold limit of 9% volume sediment concentration (Bagnold, 1962); the grains in the flow are fully supported by the upward component of turbulence and result in graded beds (e.g. Bouma sequences, Figure 2.4; Bouma, 1962). Based on flow characteristics, grain size and sorting in the flow, a full range of flow types

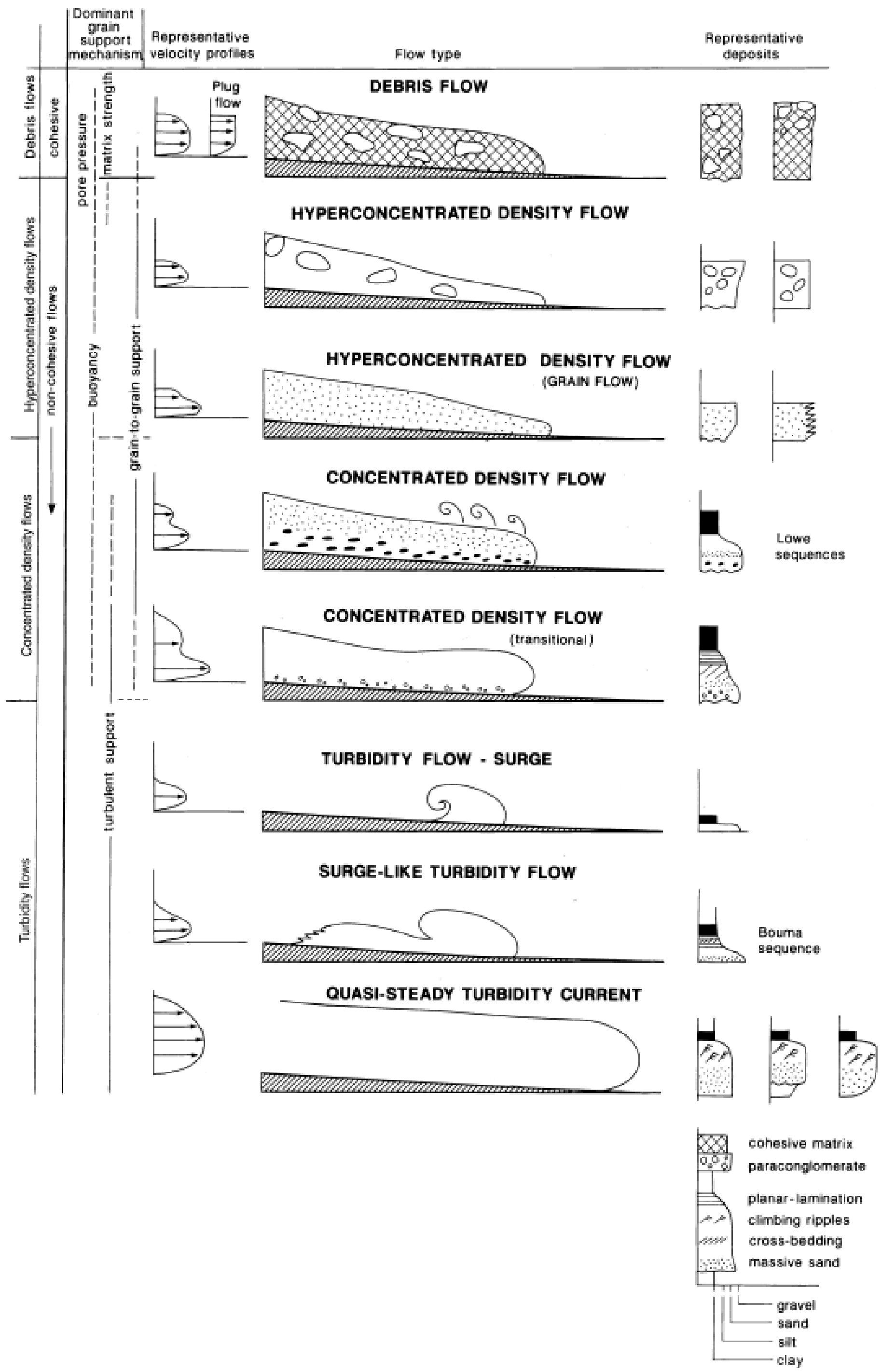

Figure 2.2: Sediment gravity flow types (from Mulder and Alexander, 2001).

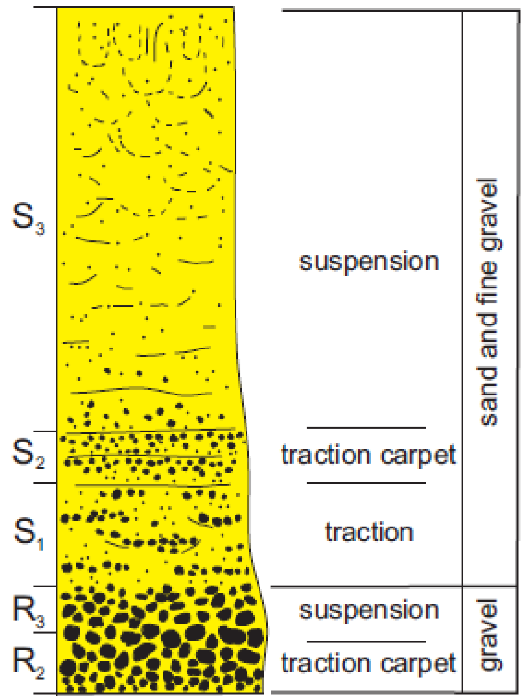

Figure 2.3: Ideal deposit of a sandy high-density turbidity current proposed by Lowe. Redrawn from Lowe (1982).

are possible between these end members. Despite major efforts in the scientific community to develop an all-encompassing classification scheme, interpretations based on observable characteristics in the ancient sedimentary record remains problematic and often controversial, especially in flows interpreted to have contained high amounts of suspended fine-grained sediment (e.g. Lowe and Guy, 2000; Mulder and Alexander, 2001; Haughton *et al.*, 2009; Baas *et al.*, 2011; Talling *et al.*, 2012).

Flows with high sediment concentration, especially flows with a high fine-grained component, show transitional character between laminar, quasi-laminar and fully turbulent (e.g. Mulder and Alexander, 2001; Baas *et al.*, 2009, 2011; Talling *et al.*, 2012; Talling, 2013). To

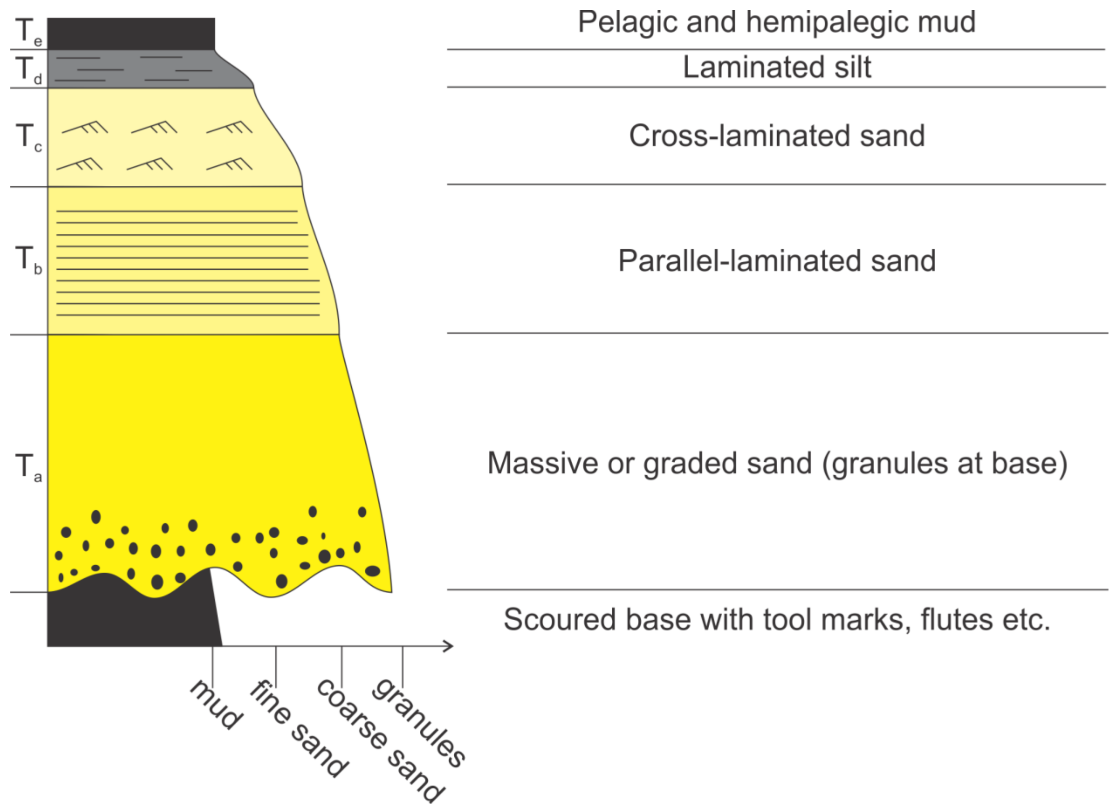

Figure 2.4: Idealized sequence of sedimentary textures and structures formed by a decelerating, dilute turbidity current (after Bouma, 1962).

date only a small number of laboratory experiments have been carried out on such flows (Baas and Best, 2002; 2008; Baas *et al*., 2009, 2011), and as a result they remain enigmatic, More studies need to be conducted to fully understand the interaction of cohesive and turbulent forces in these flows, and how grain size distribution, concentration and the nature of the grains influence flow characteristics and, ultimately, deposit attributes. Nevertheless, Baas *et al.* (2009) and Sumner *et al*. (2009) presented a quantitative analysis of deposits formed by decelerating laboratory flows with a range of grain and flow conditions, which provides an initial framework for devising future experiments (Figure 2.5) and also a basis for interpreting the fluid and sediment conditions in flows that deposited sandy mud-rich strata in the stratigraphic record.

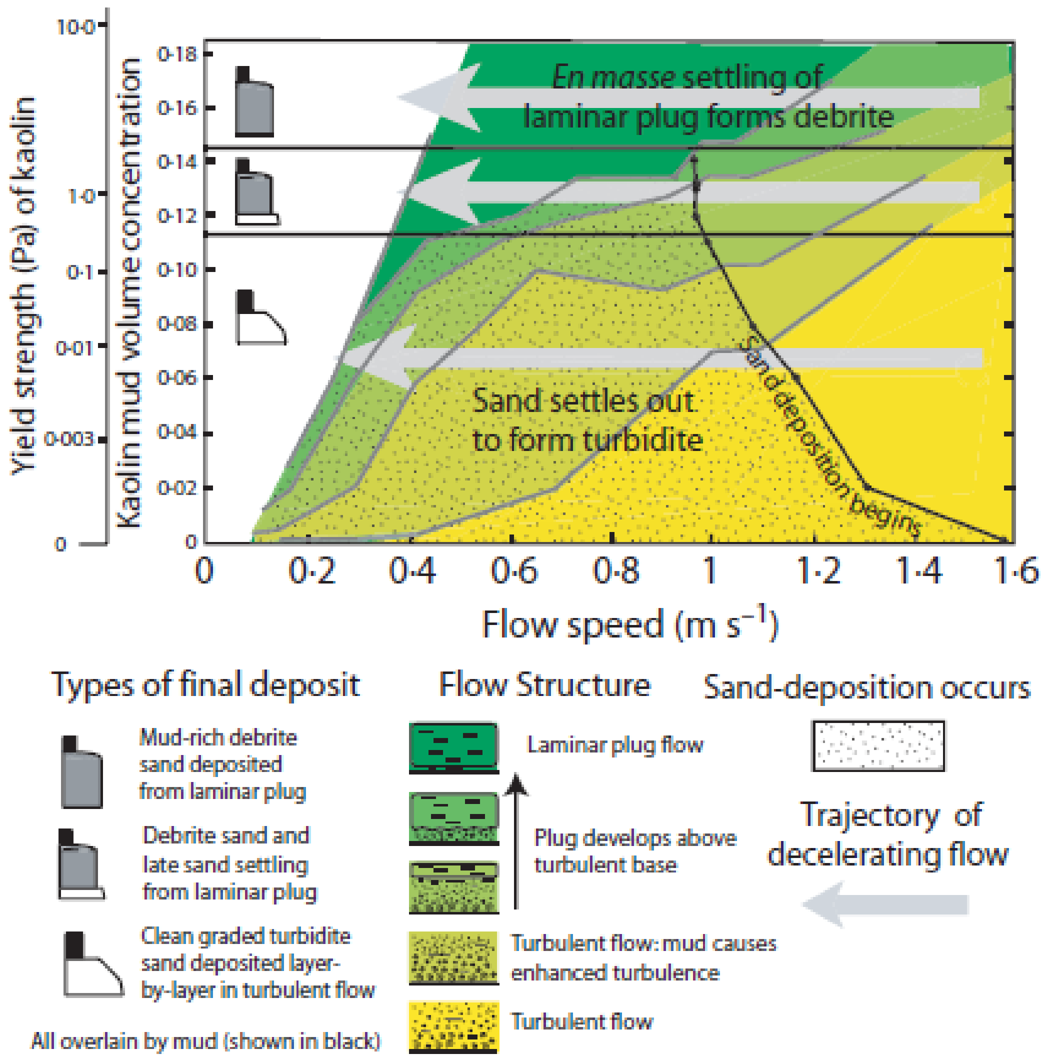

Figure 2.5: Phase diagram showing the relationship between flow speed and volume concentration cohesive mud in an initially fully turbulent sediment suspension which then decelerates (indicated by the thick grey arrows) (after Sumner et al., 2009). The figure combines results from the recirculating flume experiments of Baas et al. (2009), which described characteristics of vertical flow structure, and annular flume experiments by Sumner et al., 2009 that documented the lithological character of the deposits. Both sets of experiments involved mixtures of kaolin and water, with sand being added to the Sumner et al. experiments. Depending on mud content flow deceleration can lead to development of a non-shearing laminar plug, which in turn controls which of the three different types of deposit form. At low mud content, sand settles through the turbulent suspension and gradually builds up a clean, graded sandy turbidite. At high mud contents (>14.25% kaolin clay), en masse consolidation of a laminar plug that extends from the top to the base of the flow forms an ungraded, mud-rich sandy debrite. At intermediate concentrations, late-stage settling of sand from the laminar plug results in a thin, sand-rich basal layer beneath a sandy, mud-rich plug deposit. Sufficiently high mud fractions will support small mud clasts, and at even higher sediment concentrations large mud clasts can become buoyant. From Talling et al. (2012).

In the rock record matrix-rich sandstones are interpreted to have been formed from such flows. Flow types inferred from the rock record range from laminar debris flows, and where mud-rich sandstones are associated with an underlying clean sandstone unit are termed linked debrites, through hyperconcentrated and concentrated gravity flows (termed slurry flows when turbulence is inferred to be significantly suppressed), to turbulent gravity flows (Lowe and Guy, 2000; Lowe *et al.*, 2003; Haughton *et al*., 2003, 2009; Sylvester and Lowe, 2004; Talling *et al*., 2004, 2007, 2012; Amy and Talling, 2006). An expanded review of specifically marix-rich sandstones is presented in Chapter 4.

2.3 Data set and methodology

This study focuses on the middle and upper Kaza Group (Figure 1.5) combining data from two exposures (Figure 1.3) located in the Cariboo Mountains near McBride, British Columbia. Both exposures comprise well-exposed vertically-dipping periglacial strata. Due to the relatively recent deglaciation of these strata overburden cover is limited to localized till and outwash. Vegetation, such as grass or lichen, is generally absent, even on fine-grained rocks. In conjunction with the superb exposure, the vertical dip of the rocks allows beds to be physically walked-out in the field, resulting in highly accurate stratigraphic correlations and detailed documentation of lateral changes in facies, bed thickness and contacts. Due to the two-dimensional nature of the outcrop, however, paleoflow directions are limited to a small number of measurements that indicate transport generally toward the northwest, although local variation exists.

At Mt. Quanstrom the middle Kaza Group exposure comprises five outcrops that allow for correlation of strata over more than 2 km laterally and exposes a total stratigraphic thickness of over 1 km (Figure 1.9). Across the outcrops a total of over 2.3 km of section was logged at centimeter-scale (Figure 2.6) and triplicate gamma-ray measurements taken every 75 cm. Major lithofacies boundaries were mapped on high-resolution aerial photographs for all outcrops. In addition, the two best sandstone exposures (each ~150 m wide and 30-35 m thick) were mapped bed-by-bed on the aerial photos (Appendix A).

The upper Kaza Group crops out well at Castle Creek and consists of a single ~1 km wide outcrop with a vertical exposure of ~600 m. Most of the data discussed here were collected from the lower ~150 m of the outcrop where a total of ~1500 m of section was measured and mapped in detail on aerial photos (Figure 2.7). The upper ~450 m of the upper Kaza Group stratigraphy was surveyed and key attributes (facies, stratal elements and their stacking patterns) were noted and mapped. In addition, type examples of three stratal elements were logged and mapped in detail in the upper part of the upper Kaza Group.

2.4 Facies descriptions and interpretations

2.4.1 Introduction

Fieldwork investigating strata of the middle Kaza Group at Mt. Quanstrom and the upper Kaza Group at Castle Creek identified six lithofacies. In addition to field-based lithological

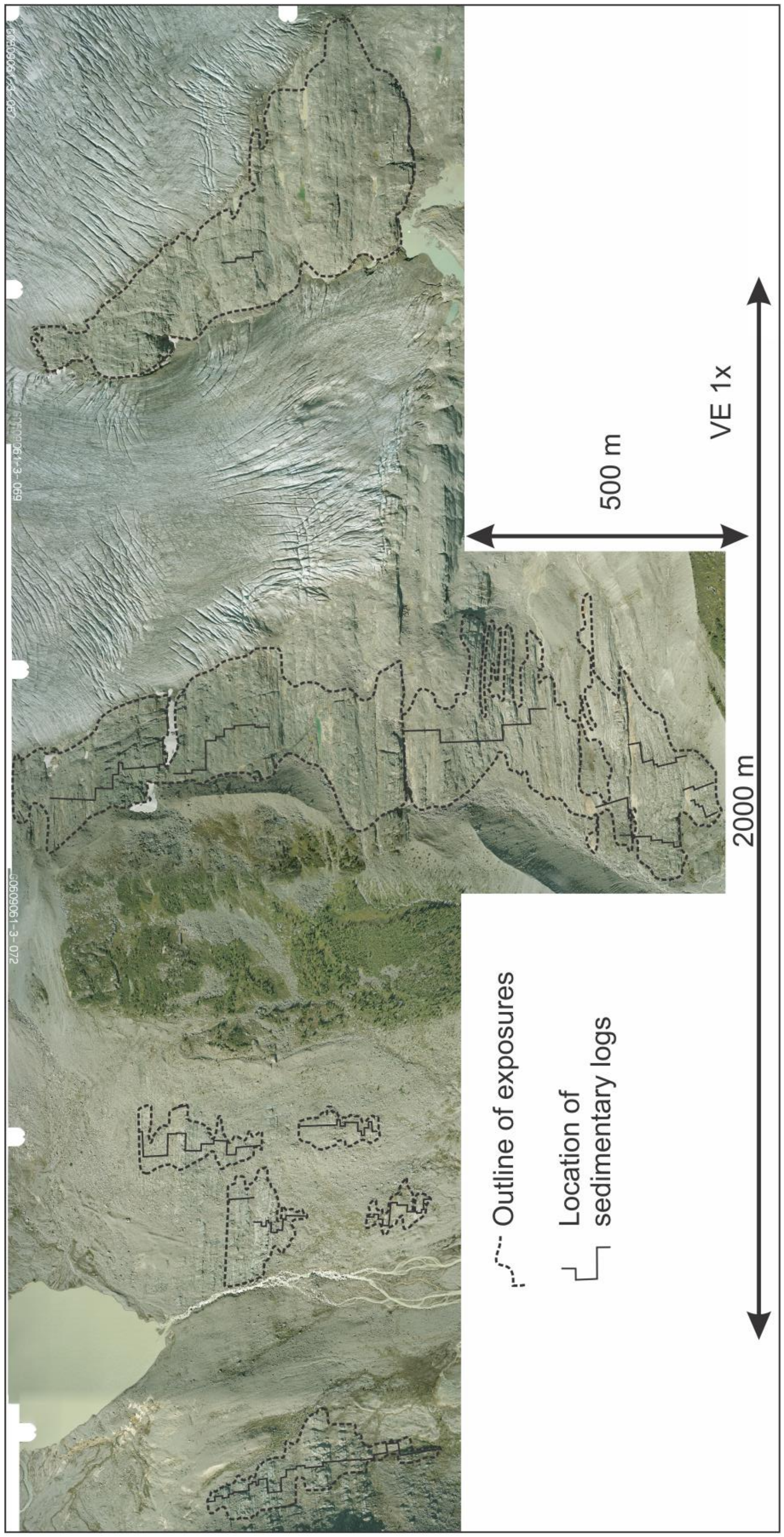

Figure 2.6: Photomosaic of the Mt. Quanstrom field area. Dashed lines indicate the margins of exposures and solid lines indicate the location of sedimentary logs.

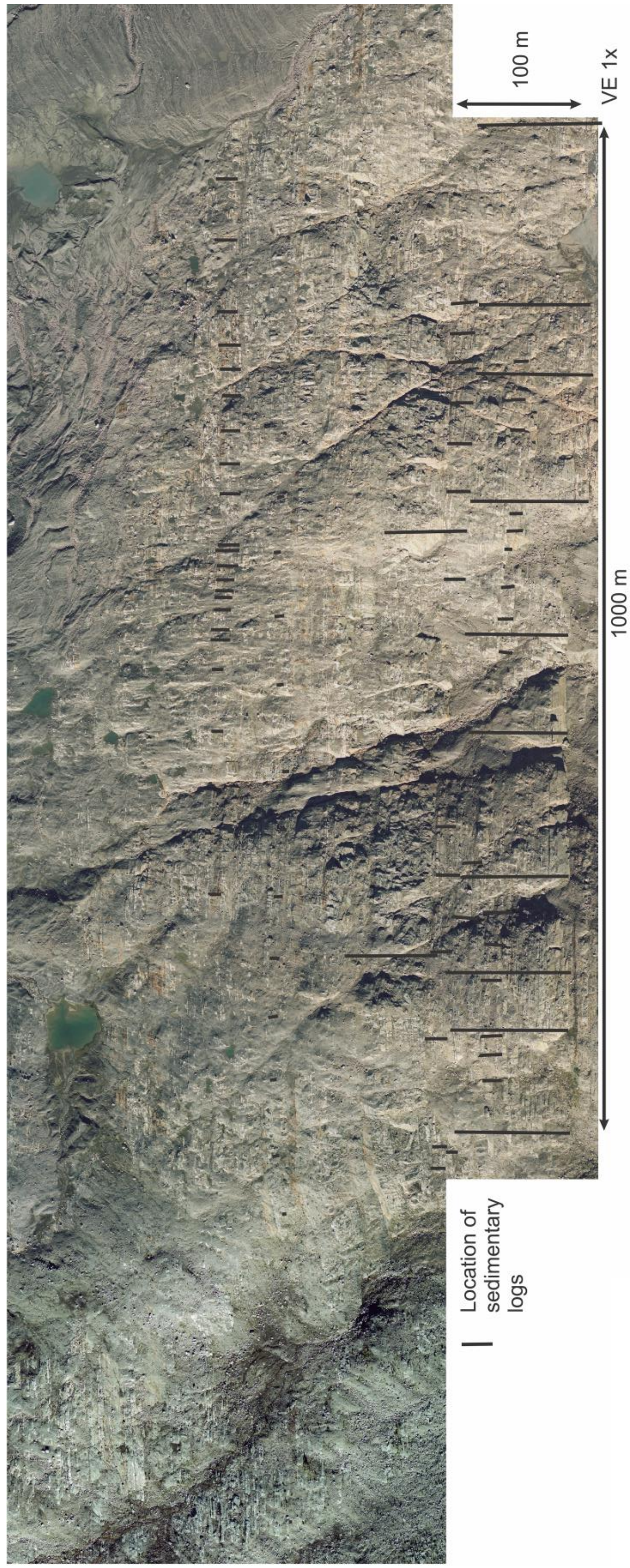

Figure 2.7: Photomosaic of the Castle Creek field area. Solid lines indicate the location of sedimentary logs.

descriptions, thin section analysis and gamma-ray profiles measured with a hand-held scintillometer were used to characterize each facies. The six facies include:

1. Massive to coarse-tail graded, coarse-grained, amalgamated sandstone
2. Coarse-tail graded sandstone with traction transport structures
3. Graded sandstone beds with locally well-stratified fine-grained tops
4. Massive and coarse-tail graded, medium-grained, matrix-rich sandstone
5. Thin to medium-bedded siltstone and mudstone
6. Mud-rich chaotic conglomerate

A summary of facies descriptions and interpretations are presented in Appendix B. All facies, except Facies 6, are present throughout the middle and upper Kaza Group; Facies 6 is notably absent in the middle Kaza Group. It should be noted that these six facies are end-members, and a continuum of gradational facies between the end-member kinds can be identified. Facies may also grade laterally into another over distances of several 10's of meters to 100's of meters through intermediate facies.

2.4.2 Facies 1: Massive to coarse-tail graded, coarse-grained, amalgamated sandstone

Facies 1 comprises massive to graded sub-arkose sandstone. Grain size grades upward from upper very coarse sandstone at the base of the bed to lower very coarse sandstone at the top. Sub-angular granules and pebbles up to 8 mm in diameter are commonly dispersed throughout the bed (Figure 2.8). Matrix content is ~20-30%, and consists of silt, with minor chlorite and muscovite. Beds range from several decimeters to >3 m thick, and vary laterally

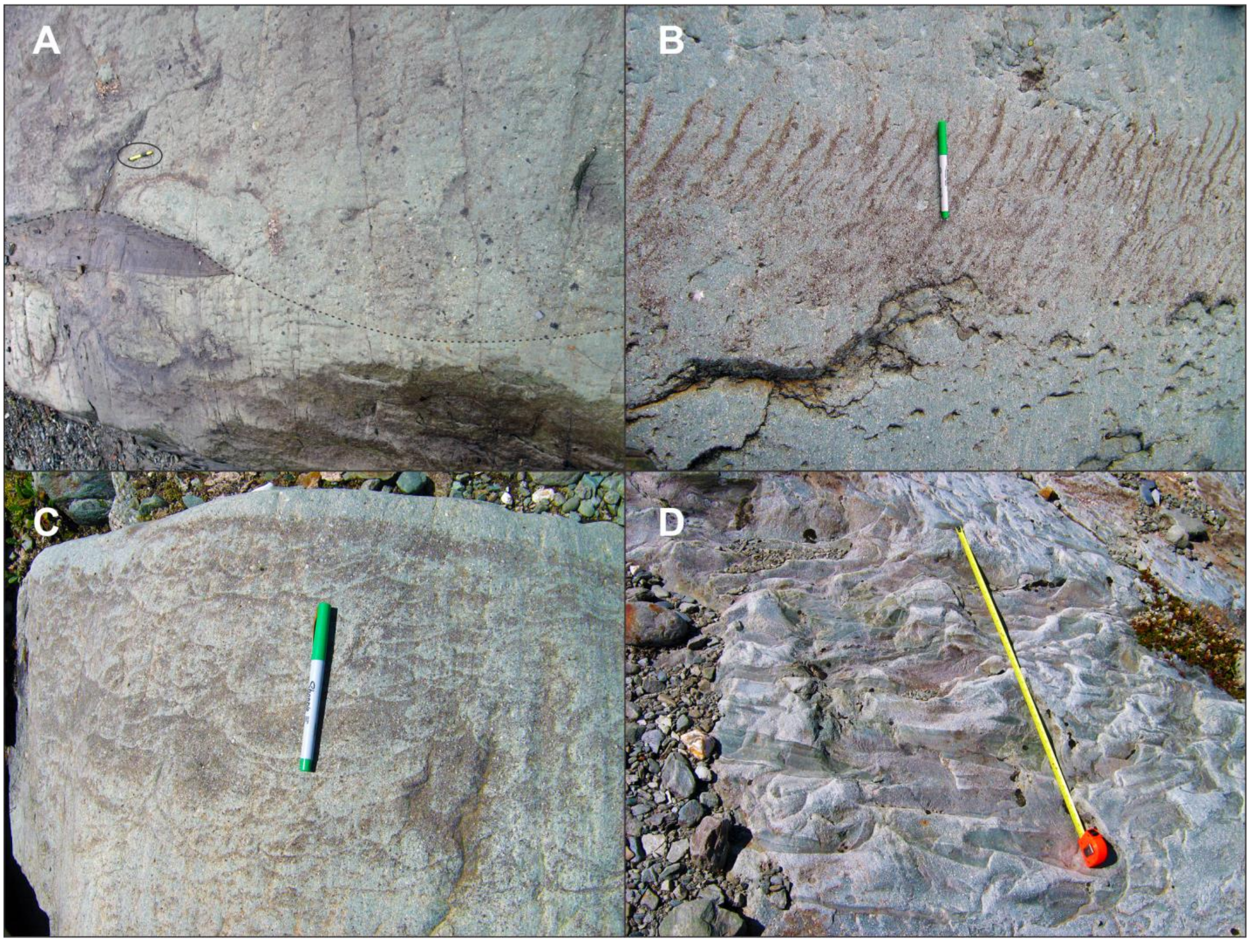

Figure 2.8: Examples of Facies 1. A) Dispersed granules and pebbles are commonly distributed throughout the thickness of beds of Facies 1. In this photograph a bed consisting of coarse-tail graded sandstone and pebbly conglomerate erodes the underlying planar laminated sandstone (dashed line). Note pencil for scale. Pipe (B) and dish (C) structures are locally abundant in beds of Facies 1. D) In beds of Facies 1 several dm long elongated mudstone clasts are abundant locally.

in thickness because of post-depositional scouring. Basal contacts commonly undulate with scours up to 30-40 cm deep. In most cases however, beds are amalgamated and bed contacts are typically difficult to demarcate. Pipe, dish, ball-and-pillow and flame structures are abundant locally (Figure 2.8b and c). Mudstone clasts vary from absent to abundant and in some cases make up about 30% of the total volume in some beds. Mudstone clasts vary from small round clasts several centimeters in diameter to elongated clasts up to ~20 cm thick and up to several meters long. In beds with abundant mudstone clasts the clasts tend to be small and distributed uniformly through the thickness of the bed, and range up to several dm in length (Figure 2.8d). In contrast, large mudstone clasts, with sizes up to several meters in length, occur mostly near and at the tops of the bed. Scintillometer measurements in strata of Facies 1 range from 40-60 counts per second (cps).

2.4.3 Facies 1: Interpretation

Grains in a non-cohesive gravity flow are typically supported by buoyancy, turbulence, hindered settling and grain-to-grain interaction generating dispersive pressure (Bagnold, 1954, 1962; Middleton and Hampton, 1973; Jaeger *et al*., 1996). The relative importance of each support mechanism cannot be measured directly based on sedimentary deposits, but generalizations can be made. The occurrence of granules and pebbles in strata of Facies 1 indicates that the upward directed component of turbulence alone is insufficient, and therefore some combination of other support mechanisms are also required (Jaeger *et al*., 1996; Mulder and Alexander, 2001). Flows that deposited strata of Facies 1 are interpretedto be concentrated density flows (Mulder and Alexander, 2001), also known as “high density” turbidity currents (Lowe, 1982). These flows allow for differential grain settling, which considering all things equal, improves with distance of transport. Near the bed and front of the sediment-charged turbidity current grain-to-grain interaction and hindered settling are probably the primary support mechanisms, but near the top and towards the tail where the flow is less dense and grain size smaller, turbulence most probably dominates. Scours at bed contacts indicate that prior to deposition flows were fast flowing and at least locally, or initially, highly turbulent.

Massive or graded beds are thought to have been deposited from the base of the flow by gradual although rapid aggradation (Arnott and Hand, 1989; Stow and Johansson, 2000, Sumner *et al.*, 2008; Cantero *et al*., 2012). In these areas of the flow sediment concentration exceeded flow capacity (Allen, 1991) and sediment was rapidly deposited from collapsing laminar sheared layers, preventing the initiation of traction current bedforms (Arnott and Hand, 1989, Kneller and Branney, 1995; Sumner *et al.*, 2008). As the flow progressed sediment was replenished by downward settling from areas higher in the flow (Kneller and Branney, 1995; Stow and Johansson, 2000; Sumner *et al.*, 2008). Alternatively, Cantero *et al*. (2012) propose that sediment in flows traversing areas of low slope stratify the flow and dampen turbulence near the bed. This dampened turbulence prohibits the reentrainment of sediment into the flow, resulting in the deposition of graded or massive beds, depending on the longitudinal sorting of grains within the flow.

The absence of grading, abundance of mudstone clasts, and absence of traction current structures suggest that flows were not well stratified in their lower part compared to flows depositing well-graded beds (e.g. see basal part of bed in Facies 2). Sedimentation conditions are interpreted to have varied little with time as grains settled from the base of the flow and were replenished from higher in the flow. Ungraded beds may originate when grains higher and further back in the flow are of similar size to those lower and towards the head of the flow (Stow and Johansson, 2000; Cantero *et al*., 2012), meaning that these flows had undergone negligible vertical and longitudinal grain size sorting prior to deposition. A lower grain size gradient indicates that internal grain mobility was restricted and that at best flows were poorly stratified. Turbulence was probably dampened because of high particle concentration, and the main sediment support mechanism was grain-to-grain interaction and hindered settling (Lowe, 1982;

Mulder and Alexander, 2001). Moreover, the common occurrence of mudstone clasts, commonly of meter scale, also suggests that turbulence was damped, preventing break-up of these clasts. The largest of the mudclasts may have been transported in such flows along a density interface separating the lower, dense and unstratified part of the current from the upper, more dilute part (Postma *et al.*, 1988). The absence of a long-lived dilute and fully turbulent tail of the flow may explain the absence of traction bedforms at the tops of beds. Alternatively traction bedforms may be absent in this Facies 1 due to erosion and bed amalgamation by subsequent flows.

Although present in other facies, pipes, dishes, ball-and-pillow and flame structures are most common in strata of Facies 1. Pipes and dishes are created by escaping pore fluids when a significantly high pore water pressure gradient exists. This gradient can be achieved by rapid loading of loosely packed, water-saturated sediment (Lowe, 1975; Stow and Johansson, 2000), which in turn can generate Rayleigh-Taylor instability at the sediment interface, resulting in load structures, such as ball-and-pillow and flame structures at bed contacts. The presence of these dewatering and loading structures in coarse sandstone indicates rapid deposition of sand and a short recurrence interval between depositional events (Lowe, 1975; Stow and Johansson, 2000).

2.4.4 Facies 2: Coarse-tail graded sandstone with traction transport features

Facies 2 comprises coarse-tail graded sandstone capped commonly with medium- to large-scale (5 cm to ~1 meter) cross-stratified or planar-laminated sandstone (Figure 2.9). Beds are typically ~1-2 m thick and form bed-sets up to 10 m thick. Bed bases are commonly erosional with shallow (< 20 cm deep) scours. Load and flame structures are uncommon.

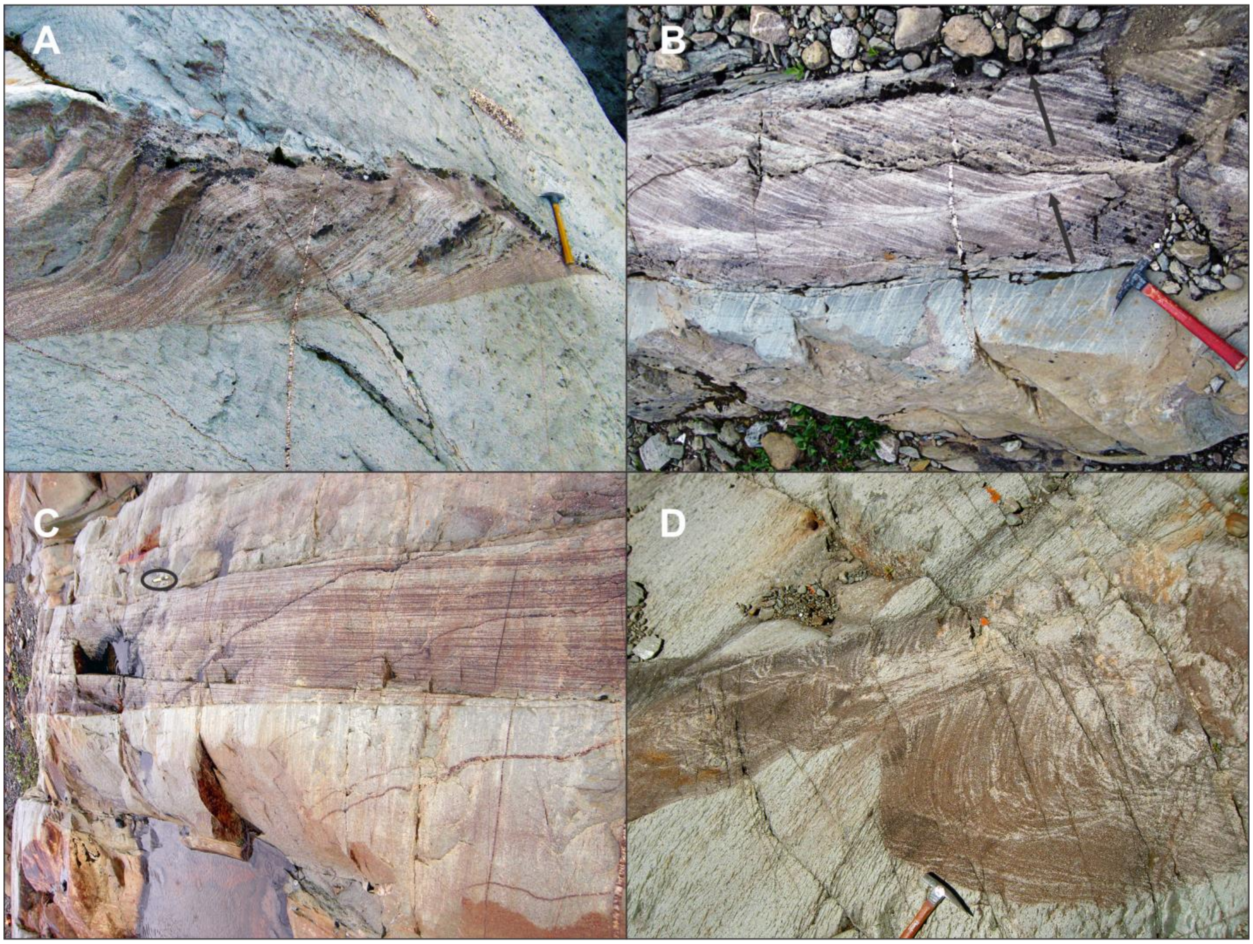

Figure 2.9: Examples of Facies 2. A) Well-sorted, 40 cm thick, over-steepened dune cross-stratified sandstone on top of a poorly-sorted coarse-grained sandstone bed. B) Rare example of stacked dune sets (arrows mark the set bases). C) Well-sorted, coarse-grained, red-brown coloured, planar-laminated sandstone. D) Syndepositionally deformed cross-stratified or planar-laminated sandstone is commonly observed. This picture shows foundered dune cross-stratified sandstone (note deformed, but preserved lamination).

Elongated mudstone clasts up to several decimeters long and 20 cm thick are present in some beds. Strata are subarkosic in composition, with a matrix of silt and less common chlorite and muscovite in the lower, graded part of the bed. Beds typically grade from upper very coarse and upper coarse sandstone with dispersed granules upward to upper coarse and upper medium grained sandstone. These strata are commonly overlain abruptly by well-sorted, upper coarse-grained, dune cross-stratified or planar-laminated sandstone. Matrix is generally absent in this part of the bed and pores are filled with ferroan calcite cement that imparts a distinctive red-brown colour to these strata. Centimeter-scale dewatering pillars and dishes have been observed in several beds, and although conspicuous in the field due to their red-brown coloured carbonate cement, are not common. Scintillometer measurements in Facies 2 range from 30-50 cps in the lower, graded sandstone part of the bed, and decrease to 20-30 cps in the well-sorted layer at the top.

The most distinctive feature of Facies 2 is the common occurrence of well-sorted, coarse-grained, planar or medium- to large-scale cross-stratified sandstone at the top of beds. Characteristically these strata have high primary porosity, which was filled by an early and pervasive ferroan calcite cement (Meyer, 2004), making these strata conspicuously rusty red-brown coloured. Cross-stratification occurs as single 5-40 cm thick sets (Figure 2.9a) that are commonly over-steepened and deformed. Set bases are sharp and locally deformed. In addition, sets typically are isolated along the top of beds, but multiple single set "trains" have also been observed locally. Formsets are rarely preserved, presumably due to local erosion. Rarely, units comprising three stacked sets are observed (Figure 2.9b). Some beds, however, are capped instead by planar-laminated, coarse-grained sandstone up to tens of cm thick (Figure 2.9c). Both planar- and cross-stratified structures are commonly syndepositionally deformed, and in some cases have partially to completely foundered into the underlying part of the bed (Figure 2.9d).

2.4.5 Facies 2: Interpretation

The graded basal part of Facies 2 has similar characteristics, including grain size, mean bed thickness and shallow scours along bed contacts, as strata of Facies 1, and this is reflected in a similar depositional interpretation. The relatively coarse grain size and the presence of scours indicate that beds of Facies 2 were deposited from fast-flowing energetic concentrated density flows, similar to Facies 1 beds (see above; Mulder and Alexander, 2001). The main difference is the presence of traction transport structures at the top of beds in Facies 2, which in turn must relate to differences in flow characteristics.

Medium- and large-scale cross-stratification at the tops of beds is interpreted to be dunes whereas planar stratified sandstone is interpreted to be upper-regime plane bed. Traction structures at the tops of beds are the same grain size as the sediment in the upper part of the graded or massive part of the bed they cap, but are distinctively better sorted. Foundering and syndepositional deformation of these strata indicates that when the dunes and plane bed were active the underlying substrate had not sufficiently dewatered and strengthened to support their weight. This suggests that the traction structures at the top of beds were most probably formed by the same flow that deposited the underlying part of the bed. Moreover, the similarity in grain size between the upper part of the underlying bed and the overlying cross-stratified and/or planar laminated features suggests that the dunes and plane bed formed from sediment reworked from the upper part of the underlying bed, in turn indicating that flow speeds in the dilute tail part of the current are maintained for prolonged periods of time. Moreover, the occurrence of angular bedforms (dunes) indicates that sediment concentration, at least in the tail part of the flow, was sufficiently low to have permitted the initiation, amplification and development of dune bedforms (Arnott, 2012). Where the flows were faster and/or the sediment concentration too high, traction-transported sediment formed plane bed (Arnott, 2012).

2.4.6 Facies 3: Graded sandstone beds with common well-stratified fine-grained tops

Beds of Facies 3 are generally ~1 m thick and are made up of a thick basal part, comprising coarse-grained, coarse-tail graded structureless sandstone overlain abruptly by a thinner succession comprising graded fine-grained sandstone to siltstone with common traction sedimentary structures. Framework grains have a subarkosic composition with a silt, chlorite and muscovite matrix. Bed bases are commonly flat, but undulating contacts with shallow scours up to about 15 cm deep occur. Grain size in the lower part of the bed ranges from upper coarse to very coarse sandstone with dispersed pebbles (< 1 cm) near the base of beds to upper coarse and upper medium sandstone near the top of the structureless interval. In a small number of beds elongated mudstone clasts up to several decimeters long and up to 20 cm thick are locally abundant, and commonly occur at the interface between the basal structureless sandstone and the overlying planar-laminated sandstone. Centimeter-scale pipe and dish structures occur in the lowermost massive part of some beds, and although conspicuous in the field because of their red-coloured carbonate cement, are not common. Loading and flame structures although uncommon, are observed.

The structureless basal part of the bed is abruptly overlain by fine and very fine sandstone that has a distinctly darker grey colour (Figure 2.10). This upper part of the bed comprises a unit of planar-laminated sandstone overlain by cross-stratified sandstone, and commonly is about 10 cm thick, although thicknesses up to several decimeters have been observed. The basal planar-laminated sandstone is typically subtly normally graded, and commonly is the thickest part of the tractional unit, being up to about 25 cm thick in many beds. This unit is rich in interstitial muscovite and chlorite. Overlying it is an up to 5 cm thick cross-

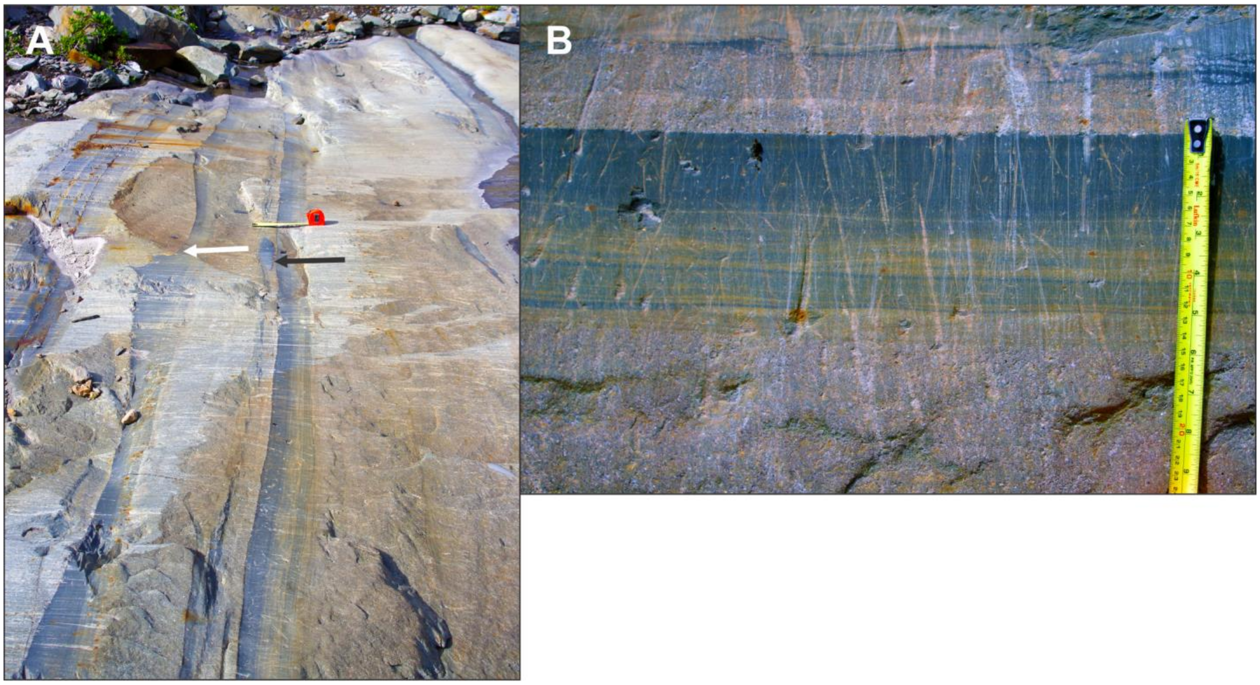

Figure 2.10: Examples of Facies 3. A) Beds of Facies 3 capped sharply by dark-grey fine-grained sandstone grading upward to siltstone. Tape measure is 20 cm long. Note the rare mudclasts in the lower, coarse-grained part of beds (black arrow) and the undulating and loaded basal contact (white arrow). Stratigraphic up is towards the left. B) Close-up of a bed-top. Here lower coarse sandstone is overlain abruptly by planar-laminated and then ripple-cross-stratified fine sandstone capped by faintly laminated siltstone.

stratified sandstone unit that is typically one set thick with no angle of climb, and which commonly scours the underlying planar-laminated unit up to several centimeters deep locally. In thin section these strata consist of well-sorted, fine and very fine sandstone with sharp grain-size changes demarcating adjacent cross-laminae. The topmost unit is commonly a few centimeters thick and comprises faintly planar-laminated to massive fine-silt with a chlorite and muscovite matrix (Figure 2.10b).

Scintillometer readings in this Facies 3 change rapidly from the base to the top of each bed. In the basal structureless part readings are generally between 40-60 cps whereas in the upper stratified part readings increase upward from 60 to 75 cps at the top.

2.4.7 Facies 3: Interpretation

Facies 3 is interpreted to be deposited from fully turbulent flows where the upward component of turbulence was the principal sediment support mechanism (Mulder and Alexander, 2001). Relatively lower relief basal scours suggest that flows were less concentrated and/or had less energetic turbulence compared to Facies 1 and 2. Graded structureless sandstone at the base of beds is analogous to the Bouma T_a division (Bouma, 1962), or Lowe (1982)'s S3 division. These units are interpreted to have been deposited by a continuously high fallout rate from the flow (Stow and Johansson, 2000, Sumner *et al.*, 2008). Normal grading indicates the progressive waning of depositional energy from a longitudinally stratified flow. The abrupt grain size change from the lower graded and structureless part of the bed to the overlying planar and/or ripple cross-laminated unit indicates a hiatus during deposition. This suggests that following deposition of the basal structureless part of the bed flows bypassed before resuming deposition.

As the flow continued to decelerate planar laminated sand was typically deposited first. Scouring at the base of this unit is absent and matrix content is high, which contrasts the relatively matrix-poor character of the overlying cross-stratified unit. Due to its high matrix content deposition of the planar-laminated sandstone is interpreted to be capacity driven. High near-bed sediment concentration and fall-out rates prevented bed defect formation and amplification, and thus sustained plane bed formation even though flow speeds may have been below upper-stage plane bed (Leclair and Arnott, 2005; Sumner *et al.*, 2008; Arnott, 2012).

The planar laminated unit is capped by an erosion surface, overlain by a thin layer of small-scale cross-stratification. At this time the flow is interpreted to have had lower sediment concentration and deposition was competence driven. Cross-stratification is interpreted to be formed by unidirectional current ripples, analogous to the Bouma T_c division (Bouma, 1962).

Commonly only a single set of non-climbing ripples is present, indicating that suspension fallout rate was negligible (Khan and Arnott, 2010). Where scouring by later events was minimal beds are capped by a fine-grained drape interpreted to have been deposited from the tail parts of flows and are analogous to the Bouma T_d division (Bouma, 1962).

2.4.8 Facies 4: Massive and coarse-tail graded, medium-grained matrix-rich sandstone

Facies 4 comprises massive to graded subarkosic sandstone with a grain size ranging from lower medium to lower coarse sand, and commonly with abundant (30-50%) chlorite and muscovite matrix and minor silt, giving the rocks a distinctive dark grey-green colour (Figure 2.11a). Matrix content is observed to decrease laterally over several 100 meters in several observed bedsets of Facies 4, changing from a high matrix content end-member (30-50%) to a relatively low matrix content end-member (approximately 20-30%). Basal contacts are laterally variable, ranging from non-scoured planar surfaces to undulatory scoured surfaces with scour depths of several centimeters. Bed thickness ranges from 10 cm to 1 m. Small-scale (<5cm thick) cross-stratification is rare, but where present occurs at the top of the bed. Planar lamination overlain by small-scale cross-stratification sharply caps some beds. Facies 4 comprises laterally discontinuous up to several meter thick bedsets, which commonly extend laterally with negligible thickness change for several tens to hundreds of meters before being eroded by overlying strata over distances of several tens of meters. Rounded and elongated sandstone and mudstone clasts are common in Facies 4 strata, and are commonly sheared and highly plastically deformed. Clasts are uniformly distributed through the thickness of beds, but commonly vary in

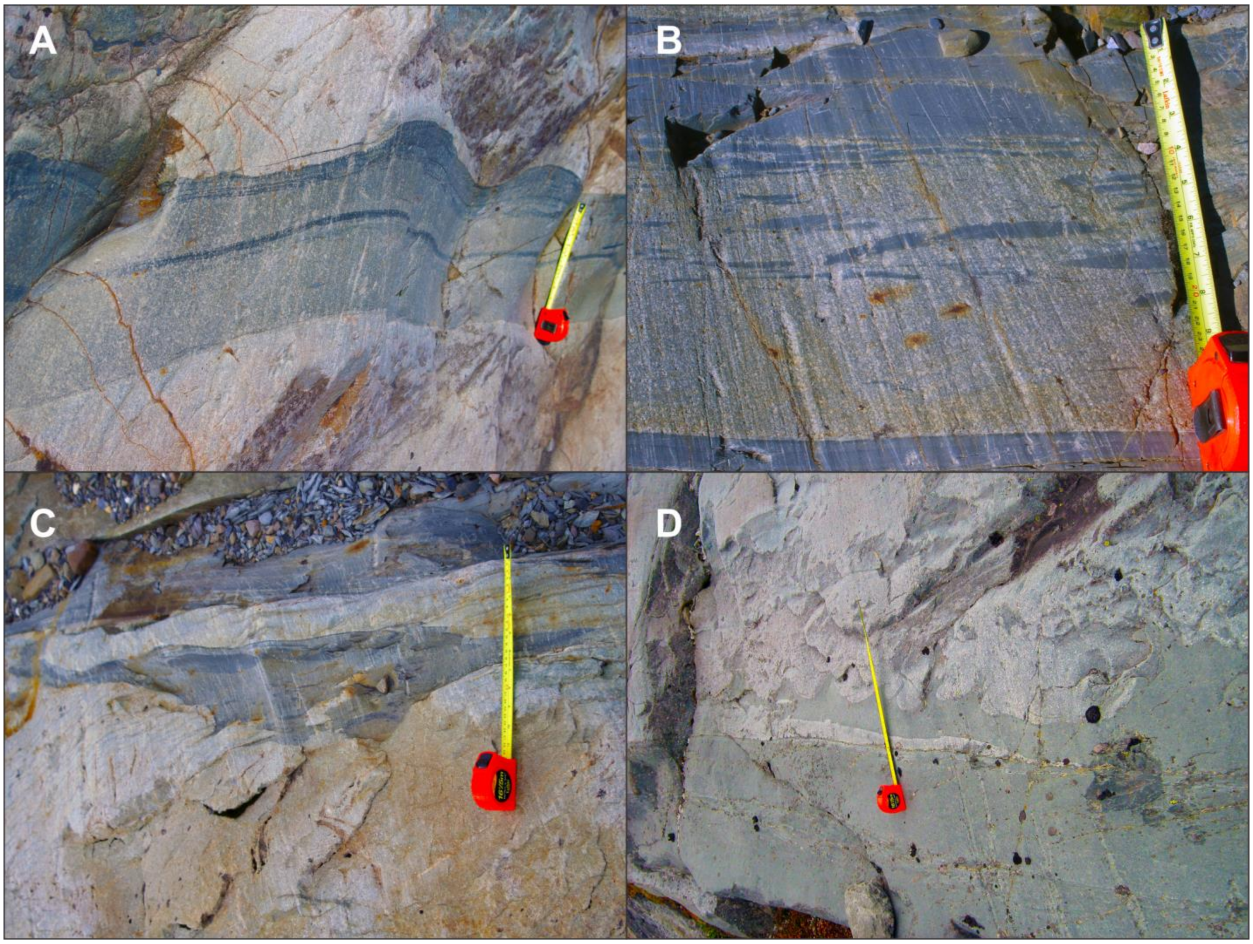

Figure 2.11: Examples of Facies 4. A) Two beds of Facies 4 sandwiched between beds of Facies 1. Strata of Facies 4 have a distinctive dark green-grey colour due to their high matrix content (green colour is related to occurrence of metamorphic chlorite). Tape measure is 25 cm. B) Close-up of a bed of Facies 4 containing small elongate mudclasts. Tape measure is 25 cm. C) Large clast of matrix-rich Facies 4 surrounded by more matrix-poor sandstone end-member of Facies 4 (note the lighter colour). Tape measure is 30 cm. D) Facies 4 strata commonly terminate laterally due to scour and loading by overlying strata. Rip-up, injection and flame structures are shown in this photograph. Tape measure is 50 cm.

abundance laterally over distances of several 10s to 100s of meters. Clasts range in size from several centimeters thick and long to 15 cm thick and ~1 m long, but clasts several dm thick and several meters long have been observed. Smaller clasts are typically observed in relatively more matrix-rich beds, and consist almost exclusively of massive or laminated mudstone (Figure 2.11b). Larger clasts, on the other hand, are more common in the relatively matrix-poor sandstone end-member, and typically comprise laminated thin-bedded turbidites of Facies 5 and, more rarely, clasts of Facies 4 sandstone (Figure 2.11c). At the base of beds flame structures, and in extremely uncommon cases pseudonodules, are present locally, particularly where units of Facies 4 are erosionally truncated by overlying strata of a different facies (commonly coarse grained sandstones of Facies 1-3; Figure 2.11d). Flame structures are up to several decimeters long. Scintillometer readings in this facies range from 45-70 cps.

2.4.9 Facies 4: Interpretation

The coarsest grain size fraction in Facies 4 is lower coarse sand, and therefore most probably supported fully by the upward component of turbulence. Grain-to-grain interaction may have also provided partial support (Mulder and Alexander, 2001). Accordingly, beds may have been deposited from fully turbulent turbidity currents. Although common, scours at the bases of beds are generally only a few centimeters deep, suggesting that scouring was limited to episodic downward energetic sweeping eddies. The distinctive poorly-sorted nature, matrix-rich composition, massive to subtly graded beds, and abundant mudstone clasts suggest that strata of Facies 4 represent capacity-driven deposition from flows undergoing extreme rates of sediment fallout (Hiscott, 1994; Leclair and Arnott, 2005). Such high rates of fallout completely suppressed the development of tractional bedforms (Arnott and Hand, 1989; Leclair and Arnott, 2005; Sumner *et al.*, 2008). As with Facies 3, planar lamination that occurs at the top of some beds is interpreted, to be the result of high sediment-fallout and/or near-bed sediment concentration that suppressed the formation of angular bedforms (Leclair and Arnott, 2005; Sumner *et al.*, 2008; Arnott, 2012). The thin overlying small-scale cross-stratified layer is notably better sorted and finer grained, indicating deposition of new sediment sourced from the low energy, dilute tail part of flows. These structures are interpreted to be ripple cross-stratification (analogous to the Bouma T_c division; Bouma (1962)).

Mudstone clasts are common in strata of Facies 4. Clasts were sourced upstream from erosion of previously deposited and consolidated sediment, and are commonly sheared and highly plastically deformed, suggesting that despite their consolidation, shearing within the flow was sufficient to deform them. Also, clasts are more or less evenly dispersed within beds, and thus are not concentrated along an inferred density interface in the flow like in Facies 1-3. This, therefore, indicates that these flows were likely more poorly stratified, and may have been transitional in nature between cohesive and non-cohesive flow (Talling *et al.*, 2004). The lithology of the clasts directly reflects the composition of the seafloor that was eroded by these flows, indicating that commonly these flows were cannibalizing either previously deposited muddy sediment, but locally also eroded previous deposits of Facies 4 and 5.

Ball-and-pillow, flame, and, in extreme cases of loading, pseudonodules likely formed as a result of loading by sediment deposited by subsequent flows (Ankettel *et al.*, 1970; Mills, 1983). The commonality of these structures in Facies 4 is significant as it implies an insufficient time for the underlying bed to dewater before deposition of the overlying bed. This in turn may indicate a short recurrence interval between sedimentation events, and more significantly that the dewatering rate of beds of Facies 4 was likely reduced because of the matrix-rich nature of these strata. Therefore lowered permeability enhanced loading and the formation of loading structures in these strata.

2.4.10 Facies 5: Thin to Medium-bedded Siltstone and Mudstone

Facies 5 comprises thin- and medium-bedded siltstone and mudstone with common traction current structures. Bedsets of Facies 5 range from <10 cm to 35 meters thick; thicker intervals are commonly, but not always, interstratified with individual sandstone beds of Facies 1-4. This facies is generally dark grey or grey/green in colour, but several intervals up to several meters thick are conspicuously rusty-red stained. Thicker intervals of Facies 5 (meters to tens of meters) are easily identified in the field and on aerial photographs. Beds typically comprise only a single set of ripple cross-stratified siltstone overlain gradationally by diffusely and discontinuously planar-laminated siltstone and mudstone (Figure 2.12). Structureless fine to very-fine sandstone, and planar-laminated very fine sandstone units underlying the cross-stratification are observed also. Scintillometer readings range from 60-65 cps in sandier intervals to over 120 cps in mud rich intervals.

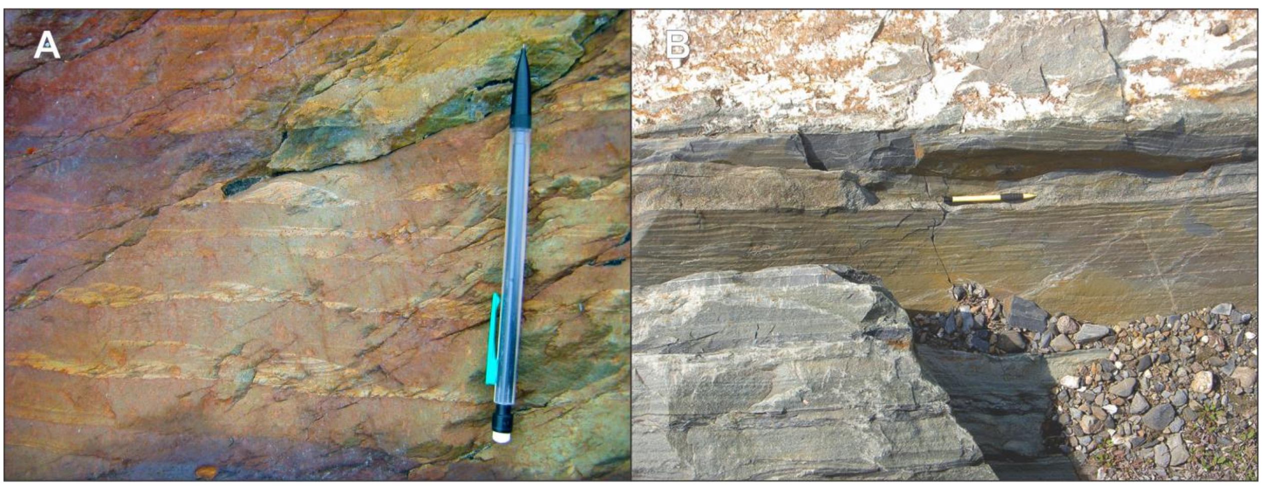

Figure 2.12: Examples of Facies 5. A) Beds of Facies 5 commonly comprise ripple cross-stratified fine-grained sandstone overlain by a several cm thick siltstone cap. B) In the photograph two sets of these beds are shown as dark and light bands, one unit under and one above the pencil. The lower unit of fine-grained beds overlie several matrix-rich beds (Facies 4), the pencil rests on a coarse-grained T_a sandstone (Facies 1) that separates the two fine-grained units, and the upper fine-grained unit is overlain by a thick coarse-grained T_a sandstone (Facies 1).

At the base of some beds is a structureless fine sandstone unit typically a few centimeters thick, although thicker (up to 15 cm) units have been observed. It consists of normally graded, upper and lower medium sandstone that grades upward to fine and very fine sandstone. More commonly the base of beds consists of poorly-sorted, planar-laminated fine-grained sandstone, generally a few centimeters thick. Strata are well sorted fine to very fine sandstone with common granular pyrite, which when weathered gives the rock its distinctive rusty-red colour. Planar-laminated and cross-stratified units may grade into one another laterally. Diffusely planar-laminated units cap virtually all beds, and consist of dark-grey silty mudstone. The thickness varies not only between beds, but also laterally along a single bed, and may vary from < 1 cm to ~ 15 cm. Although rare, scours up to several centimeters deep occur at the base of cross-stratified beds.

2.4.11 Facies 5: Interpretation

The depositional mechanism of Facies 5 is similar to that of Facies 3 (see above). The finer grain size, limited scouring and dominance of higher order Bouma sequences (Ta divisions are commonly missing) in Facies 5, however, implies deposition from relatively more dilute, low energy turbidity currents. The lack of erosion at the base of Facies 5 beds, combined with the paucity of dm- to m-scale coarse-grained interbeds of Facies 1-4 within thicker bedsets of Facies 5, suggests that these strata were not deposited from the low-concentration tails of larger and coarser-grained bypass flows, but instead from flows that had already deposited most of their coarse-grained load either upflow, or laterally.

2.4.12 Facies 6: Mud-rich Chaotic Facies

Facies 6 is a matrix-supported conglomerate, composed of a mud-rich matrix and chaotically dispersed clasts. Beds are ungraded and range from ~1 m to several 10's of meters thick. Clasts composed of sandstone and mudstone are observed, and are commonly intensely sheared and/or folded (Figure 2.13). Clasts are subparallel to the basal contact and are up to several meters in diameter. Clasts that are >10 cm in diameter are commonly internally stratified with thin-bedded, fine-grained, upper division turbidites. Small (several cm long and wide)

Figure 2.13: Clasts are deformed and chaotically dispersed in beds of Facies 6. Tape measure is 1 meter.

mudstone clasts are typically rounded and elongate, and are composed of massive very fine sandstone to mudstone. Dispersed quartz pebbles are locally abundant. Importantly this facies is observed only in the upper Kaza Group where it forms sharp-based laterally extensive units that change little in thickness over the width of the outcrop (~ 1000 m). Owing to the abundance and variable composition of clasts, in addition to the mudstone matrix, scintillometer readings tend to be highly variable, but generally are of the order of 50-70 cps.

2.4.13 Facies 6: Interpretation

Strata of Facies 6 are interpreted to be debris flow deposits. Debris flows are cohesive, commonly laminar flows with high, up to >90% sediment concentration (Leeder, 1982), and in which matrix strength provides the main sediment support. Strata deposited by debris flows comprise ungraded, poorly-sorted, matrix-rich beds, with variously sized and commonly sheared and deformed clasts exhibiting a poor to moderately developed fabric oriented parallel to the base of the bed (e.g. Johnson, 1970; Rodine and Johnson, 1976). Deformed clasts indicate that they were consolidated but not lithified at the time of transport. The occurrence of large meter-scale clasts indicates that turbulence was damped, because large-scale turbulence would most likely have disintegrated unlithified clasts (Postma *et al.*, 1988). The clasts are embedded in a fine-grained matrix, which provides matrix strength through electrostatic forces between fine-grained particles and buoyancy effects. Grain-to-grain interactions and internal shear are of lesser to negligible importance as a sediment support mechanism.

Commonly ambient water is mixed into debris flows as they move downslope (Piper *et al.*, 1985, 1999a), which reduces cohesive and buoyancy forces, and in some cases causes the flow to transform into a non-cohesive flow or even "ignite" (Hampton, 1972; Fisher, 1983). Strata of Facies 6, however, represent deposition from flows that maintained sufficient strength to have moved downslope and then deposited as a single contiguous unit. This indicates that flows had short travel distances, and/or were sufficiently cohesive to damp internal turbulence. The general paucity of Facies 6 indicates that these events were rare punctuations within "normal" sedimentation of the other facies described.

2.5 Conclusions

Chapter 2 introduced sediment gravity flows, then described and interpreted six sedimentary facies in the upper and middle Kaza Group:

Facies 1. Coarse-grained massive and graded sandstone deposited by concentrated and hypercontentrated turbidity currents;

Facies 2. Coarse-grained graded sandstone capped by dune cross-stratified and/or planar stratified sandstone. The basal part of the bed was deposited by concentrated and hyperconcentrated turbidity currents; the tails of the currents reworked the underlying bed to create dunes and/or upper stage plane bed;

Facies 3. Coarse-grained graded sandstone with finer grained Bouma turbidite (T_{b-d}) tops. The basal part of the bed was deposited by concentrated turbidity currents; the upper part of the bed was deposited by the dilute tail part of the flows;

Facies 4. Medium- to coarse-grained, massive to coarse-tail graded, matrix-rich sandstone deposited rapidly by "transitional" flows containing a high concentration of fine-grained sediment.

Facies 5. Fine-grained, thin-bedded turbidites deposited by dilute turbidity currents;

Facies 6. Chaotic fine-grained deposits containing abundant deformed sandstone and mudstone clasts interpreted to be debrites.

Collectively these six facies make up larger, meso-scale stratal elements in the middle and upper Kaza Group, which will be described and interpreted in Chapter 3.

Chapter 3: Stratal elements in the upper and middle Kaza Group

3.1 Introduction

The understanding of “sheet-like deposits” or “channelized lobes” in modern on shallow-subsurface deep-water basin-floor settings has in recent years been greatly improved due insights from high-resolution seismic data and sediment cores (e.g. Normark, 1978; Piper and Normark, 2001; Beaubouef *et al.*, 2003; Posamentier and Kolla, 2003; Deptuck *et al*., 2008; Jegou *et al.*, 2008; Saller *et al.*, 2008). However, modern marine seismic and core typically lack the vertical and lateral resolution, respectively, to effectively identify and characterize small-scale architectural elements. The majority of basin-floor studies, then, describe the dimensions of large-scale features like basin-floor fans, lobe complexes and lobes (for a comprehensive compilation see Prélat *et al.*, 2010). Seismic or side-scan sonar studies that describe the dimensions of smaller, meso scale architectural elements that make up the sedimentary bodies of lobes include: *isolated scours* by Normark *et al*. (1979), Kenyon and Millington (1995), Morris *et al.* (1998), Wynn *et al.* (2002b), and Deptuck *et al*. (2008); *feeder channels* by Twitchell *et al.* (1992), Wynn *et al.* (2002b), Jegou *et al.* (2008) and Saller *et al.* (2008); *distributary channels* by Normark (1978); Normark *et al.* (1979), Twitchell *et al.* (1992), Gardner *et al*. (1996), Piper *et al*. (1999b), Beaubouef *et al.* (2003), Deptuck *et al*. (2008), Jegou *et al.* (2008), Saller *et al.* (2008), and Gervais *et al*. (2010); and *terminal splays* by Piper *et al*. (1999b), Beaubouef *et al.* (2003), Deptuck *et al*. (2008), Saller *et al.* (2008) and Gervais *et al.* (2010). The internal sedimentology and stratigraphy of the elements is typically determined from core, or is inferred based on seismic facies only (e.g. low-intensity backscatter was inferred as distal distributary channels on the Mississippi Fan by Twitchell *et al.* (1992)).

Study of outcrop analogue examples remains integral to the understanding of depositional basin-floor systems. Though many outcrops are compromised by lateral and/or vertical size limitations, studies across a number of ancient turbidite systems have provided an ever growing knowledge base of deep-water deposits, including channels and sheet-like sand bodies of the Brushy Canyon Formation (Beaubouef *et al*., 1999; Carr and Gardner, 2000; Gardner and Borer, 2000; Gardner *et al*., 2003), channels and sheet-like sand bodies of the Punta Barrosa and Cerro Toro formations (Fildani *et al.*, 2007, 2009; Hubbard *et al.*, 2008; Bernhardt *et al.*, 2011; Romans *et al*., 2011), scours, channels, lobe elements (sand sheets), slumps and mudstone sheets of the Ross Formation (Elliott, 2000; Sullivan *et al.*, 2000; Martinsen *et al.*, 2000, 2003; Pyles, 2007, 2008), and channels and sheet-like sandstones of the Karoo Basin (Sullivan *et al*., 2000; Johnson *et al*., 2001; Sixsmith *et al.*, 2004; Hodgson *et al*., 2006; Prélat *et al.*, 2009; Groenenberg *et al*., 2010; Flint *et al*., 2011). The purpose of this chapter is to add to this ever-growing knowledge base of basin-floor strata by providing a detailed sedimentological and stratigraphic description of the internal stratigraphy of stratal elements that make up the deep-marine basin-floor fan system of the Windermere Supergroup, which are interpreted to include isolated scours, avulsion splays, feeder- and distributary channels, terminal splays, debrites, and off-axis fine-grained units. From this study it is clear that, excluding debrites, all basin-floor stratal elements comprise similar facies, but nevertheless can be differentiated by their overall cross-sectional shapes and dimensions, and/or internal organization of facies. In order to provide a widely usable predictive framework, then, the dimensions of the stratal elements described in this study are compared with similar features reported in the literature and shown to be similar.

This finding supports earlier studies (Sullivan *et al.*, 2000); Sinclair and Tomasso, 2002; Pyles, 2008); Pyles *et al*., 2011) that showed a self-similarity in depositional element size and stacking patterns across different tectonic settings and styles of sediment input. This suggests that the reported lithological make up and stratigraphic relationship between elements in this study add to developing a robust predictive framework that can be used in other basin-floor fans, modern or ancient, especially where such data are limited.

3.2 Definition

Architectural element analysis has been common practice since it was first introduced for fluvial strata by Miall (1985). Since its inception the concept of architectural element analysis has been applied successfully to submarine-fan strata and is gaining in popularity (e.g. Pickering and Clark, 1996; Carr and Gardner, 2000; Gardner and Borer, 2000; Sullivan *et al*., 2000; Drinkwater and Pickering, 2001; Johnson *et al*., 2001; Sprague *et al*., 2002; Hodgson *et al*., 2006; Pyles 2007, 2008; Prélat *et al*. 2009, 2010), although due to a lack of common definition and terminology, a plethora of terms has been in use to describe the various building blocks across various hierarchical levels of a submarine fan. In this paper the definition of architectural element (3-D sedimentary body) proposed by Pyles (2007) is adopted for the definition of stratal elements (2-D sedimentary unit in outcrop) in the Kaza Group: an architectural element is defined here as “a mesoscale lithosome (>1 m [>3 ft] thick, >20 m [>66 ft] wide) characterized by its external shape in depositional-strike view that forms the fundamental building block for larger stratigraphic units, including parasequences, systems tracts and sequences”. This definition is expanded to include that stratal elements are also defined by the internal arrangement of sedimentary facies. As such it can be applied usefully to this study, because it limits the size of stratal elements to mesoscale features that are observable and mappable at outcrop scale, and also characterizes stratal elements by their external shape in strike-view and internal facies distribution, which is the view available in the observed 2-D outcrops. Furthermore, this definition of architectural (stratal) elements is useful because it implicitly implies a hierarchical system of elements, and can be merged seamlessly with existing basin-floor lobe models (see Mulder and Etienne (2010) for a review and summary of recent lobe terminology, morphology, geometry and construction). In this study we adapt the hierarchical scheme compiled by Mulder and Etienne, where stratal elements (termed lobe elements in several papers, e.g. Prélat *et al*,. 2009; Mulder and Etienne, 2010) comprise the sedimentary bodies of depositional lobes, which in turn stack to form lobe complexes and ultimately the depositional fan.

3.3 Stratal Elements in Basin-Floor Strata of the WSG

Seven stratal elements were identified in strata of the upper and middle Kaza Group. Each stratal element (SE) comprises one or more of the previously described facies, which vary not only between the different elements, but also spatially within an individual element (e.g. depositional axis, or margin, proximal or distal). The elements include:

1. Isolated scour with coarse-grained sandstone fill (*Isolated scours*, common in the upper Kaza, rare in the middle Kaza)
2. Deep scour and heterolithic channel fill (*Feeder channels*, two examples in the upper Kaza)

3. Shallow scour and heterolithic channel fill (*Distributary channels*, common in the upper Kaza)
4. Sheet-like coarse-grained sandstone (*Terminal splays*, common in both the upper and middle Kaza)
5. Sheet-like medium-grained matrix-rich sandstone (*Avulsion splays*, present in both the upper and middle Kaza, but more common in the upper Kaza)
6. Sheet-like fine-grained turbidites (*Distal and off-axis fine-grained turbidites,* common in both the upper and middle Kaza)
7. Thick-bedded chaotic units (*Debrites*, present only in the upper Kaza)

3.3.1 Stratal Element 1: Isolated Scour with Coarse-grained Sandstone Fill

SE 1 comprises 1 to up to ~5 m deep and several tens to up to 300 m wide scours with massive coarse-grained sandstone fills (Facies 1), interbedded locally with mudstone breccia and sandstones of Facies 2 and 3. These elements are rare in the middle Kaza, and become more common stratigraphically upward in the upper Kaza. The bases of SE 1 are irregular scours reaching a depth of several meters over a distance of several tens of meters (Figure 3.1 and Figure 3.2). In the upper Kaza scour bases typically truncate distributary channels and/or avulsion splays (Figure 3.1; see next sections), but in the middle Kaza terminal splays are eroded (Figure 3.2; see next sections). Regardless of stratigraphic setting the fill of SE 1 shows negligible lateral or vertical facies change and sandstone beds commonly onlap the basal scour surface. Erosion at bed bases is common within SE 1, with scours ranging from several centimeters up to several dm deep.

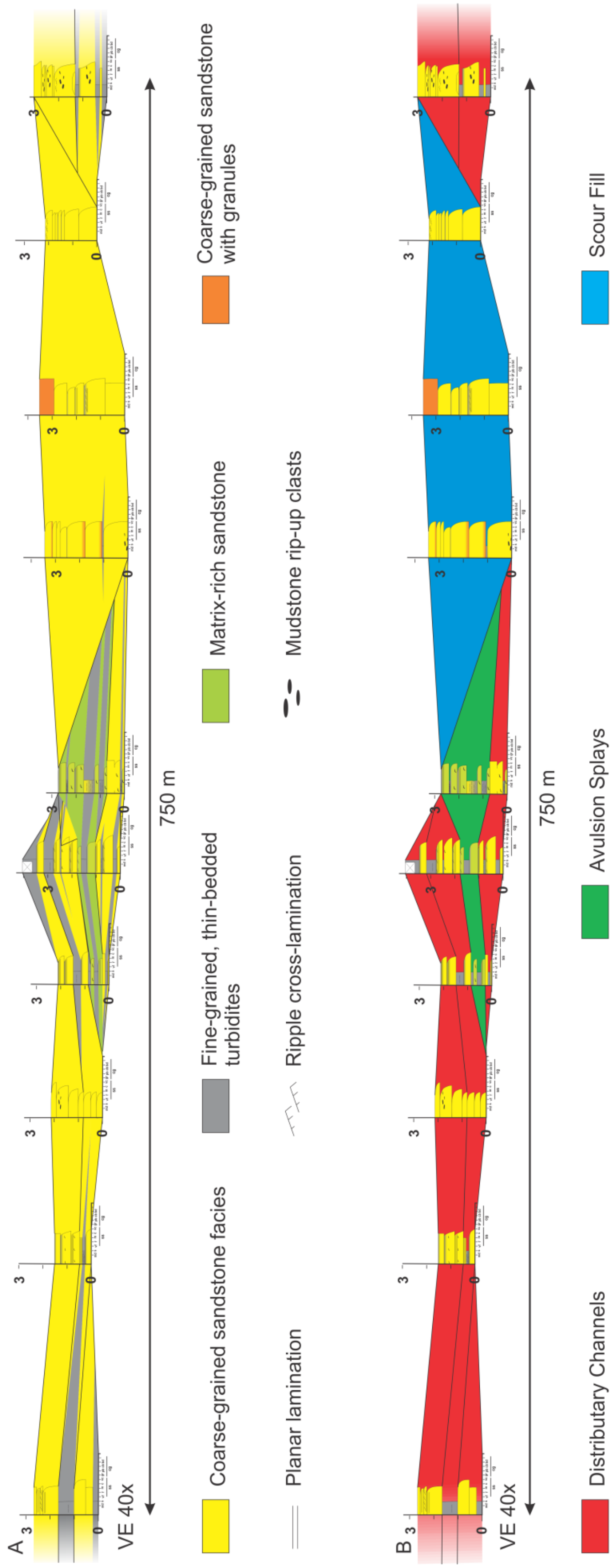

Figure 3.1: Stratigraphic correlation of strata from the upper Kaza showing facies distribution (A) within three different stratal elements (B). Isolated scours (blue) commonly erode distributary channels (red) and avulsion splays (green), and are subsequently filled with amalgamated coarse-grained sandstone. Avulsion splays are commonly observed at the margins of isolated scours and in this instance comprise interbedded matrix-rich sandstone (Facies 4) and thin-bedded, fine-grained turbidites (Facies 5). Distributary channels have low aspect, erosive bases and show a lateral facies change from amalgamated sandstone in their axis to finer-grained, thinner-bedded strata towards the margins. The location of this correlation panel is shown in Appendix C.

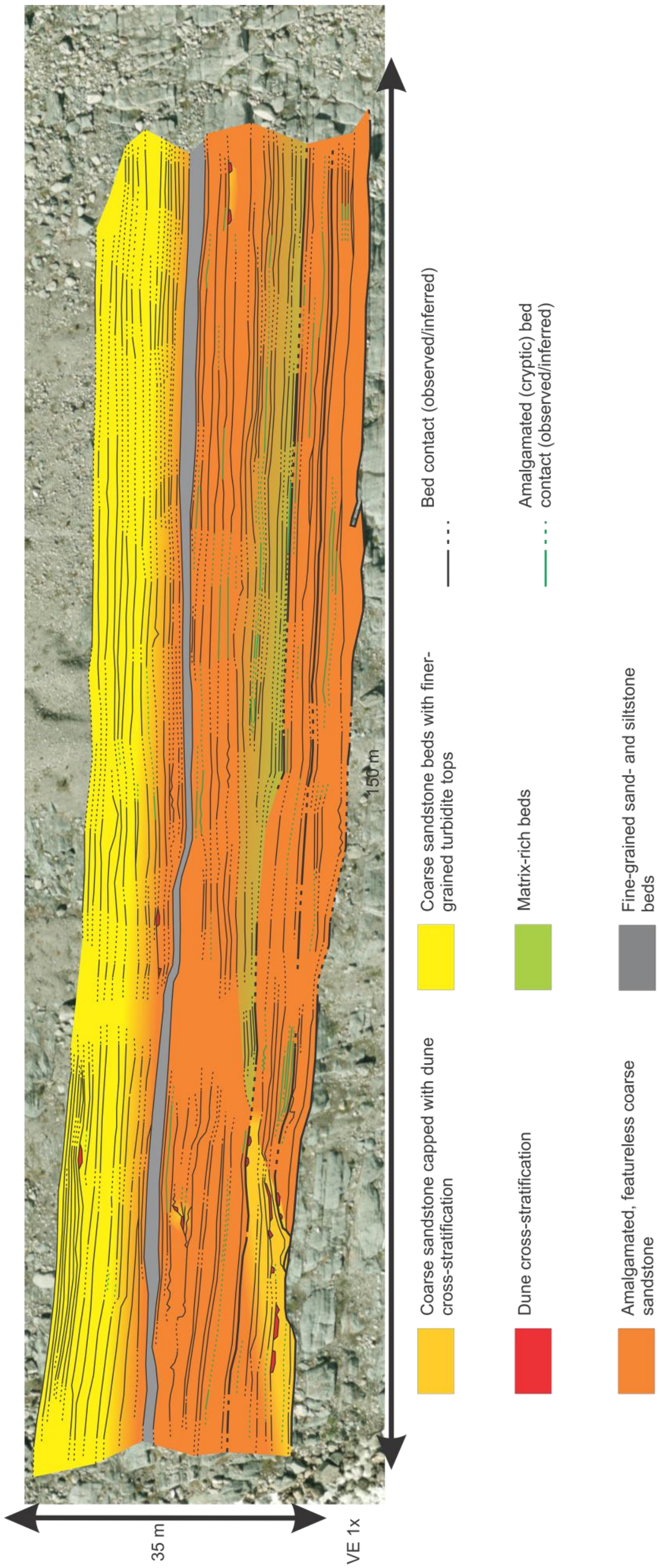

Figure 3.2: Detailed correlation of a sandstone unit (S2) in the middle Kaza. All bed contacts were walked out and mapped directly on the aerial photographs. This 35 m thick sandstone package comprises four stacked terminal splays (SE 4); contacts are highlighted by the thick black lines. The lowermost terminal splay is eroded by a several meter deep scour (SE1) on the lower left of the diagram. Beds near the base of the scour onlap the erosion surface, but beds higher up are laterally continuous and form the second terminal splay. Terminal splays 2 and 3 are locally separated by an avulsion splay (SE 5, green shading), and terminal splays 3 and 4 are separated by a laterally continuous unit comprising fine-grained, thin-bedded turbidites (SE 6). The complete 35 m thick sandstone package is interpreted to be the distal part of two depositional lobes, the lower consisting of three amalgamated terminal splays (1-3), and the upper consisting of a single terminal splay (4).

SE 1 is most common in the upper part of the upper Kaza, or more specifically, in the most proximal part of the basin floor setting. SE 1 is interpreted to be shallow scours created by energetic turbulence in Type C flows of Huang *et al*. (2009), that were then filled by later flows. Type C flows have densiometric Froude numbers less than unity and experience energetic hydraulic jumps at acslope break, resulting in local, but intense erosion of the basin floor (Huang *et al.* 2009). Scours with dimensions similar to those of SE 1 have been described by Wynn *et al.* (2002b) at the slope break (termed channel-lobe transition zone) on the modern Rhone Fan and at the mouths of the Lisbon and Agadir canyons. These scours created local topography on the basin floor, and subsequently were either rapidly filled with coarse sediment by bypassing flows, or were exploited by these flows to create a continuous conduit of sediment transport, a “feeder channel” (see SE 2).

3.3.2 Stratal Element 2: Deep Scour and Heterolithic Channel Fill

Two occurrences of SE 2 are exposed in the upper Kaza Group at Castle Creek, but SE 2 is absent in the middle Kaza Group. In both cases the base is a sharp and terraced erosional surface exposed over the full width of the outcrop (~800 m). Erosion is up to ~15 meters deep. The scour at the base of the lowermost occurrence deepens from the northwest towards the southeast, whereas the surface underlying the uppermost occurrence deepens from the southeast towards the northwest. Assuming a (semi-) symmetrical shape of the scour and an only slightly oblique orientation to the outcrop (palaeocurrent roughly perpendicular to outcrop face), it is evident that only part of this feature is exposed, implying that SE 2 is more than 800 m wide. Both examples of SE 2 have a multi-stage, heterolithic fill comprising several cut and fill units.

The lower channel fill is dominated by several upward-fining units consisting of Facies 1, and 2 at the base overlain by Facies 5 near the top. These units gradually amalgamate toward the channel axis and form a thick coarse-grained sandstone fill. In both channels a mudclast-breccia dominated unit near the lower channel margin is observed. The upper fill of the channel is dominated by thin-bedded, fine-grained turbidites intercalated with coarse-grained sandstone lenses. The top of both channels is sharp and planar. The uppermost occurrence of SE 2 is described in detail in Figure 3.3 and illustrates the multi-stage history of erosion and deposition (Units 1-5) observed in this element.

Stratal Element 2 is interpreted to be a feeder channel that supplied a down-flow lobe complex. Its overall dimensions, scour depth and width correspond well with examples described in the literature (e.g. Twitchell *et al*. 1992; Johnson *et al.* 2001; Wynn *et al*. 2002b; Saller *et al*. 2008), and its exclusive occurrence in the upper part of the upper Kaza puts it in the most proximal part of the basin floor. The erosion surfaces and fill of Stratal Element 2 are interpreted to comprise three stages of channel development and fill (see Figure 3.3). Stage 1 comprises the basal scour surface, interpreted to be the master scour surface that was the result of erosion by by-pass flows feeding a down-flow lobe complex, and deposition comprising units 1 and 2, which are characterized by by-pass facies and abundant sediment reworking. Stage 2 is characterized by a period of erosion and full by-pass (erosional surface 3). In this stage the upper part of the channel is widened resulting in a terraced basal scour surface, which is probably the result of increased flow discharge due to upstream channel maturation enhancing transport efficiency to more distal parts of the basin floor. Hereafter the channel entered an aggradational backfilling stage (Units 3 and 4). Stage 3 comprises Unit 5, representing gradual channel

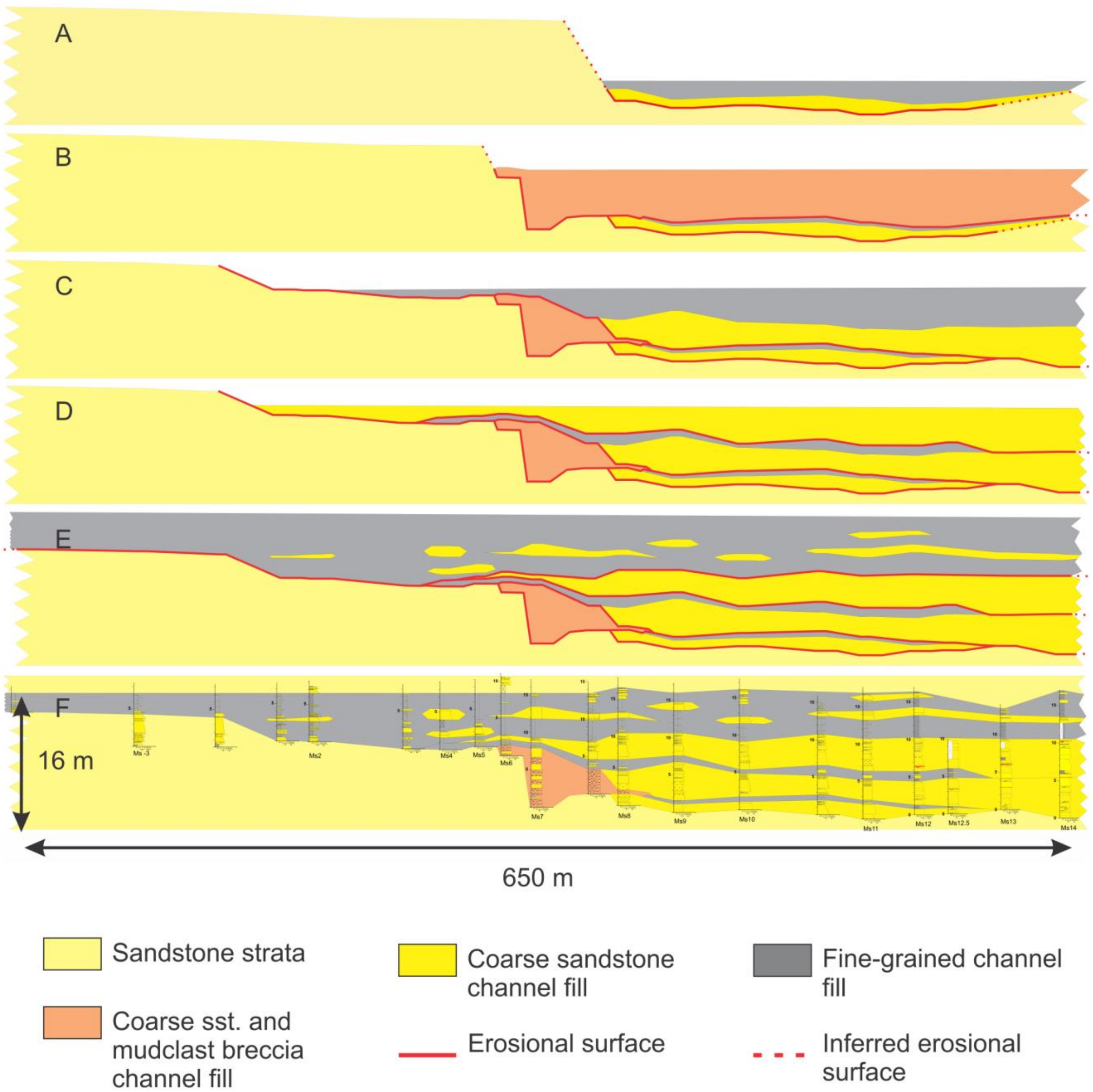

Figure 3.3: Evolution of a deep scour (feeder) channel in the upper Kaza. Note that beds and units are correlated laterally by physically walking them out in the field. A) The original incision (erosional surface 1, or ES1) is approximately 15 m deep, overlain by fill unit 1, an ~3 m thick fining-upward sandstone to siltstone unit. B) ES2 widens the channel by ~20 m and erodes the SE margin of fill unit 1. Fill unit 2 comprises by-pass facies and mud-clast breccia where it is preserved in the SE, and may have extended over much of the width of the channel. C) ES3 widened the top of the channel creating a terrace up to about 3 m high, and additionally deepened the channel towards the NW. Unit 3 then overlies ES3, comprising a basal coarse sandstone fill overlain by fine-grained sandstones and siltstones. D) ES4 eroded the top part of Unit 3 and is overlain by Unit 4, a coarse sandstone fill. E) ES5 eroded Unit 4 towards the SE forming the current base of the channel in the southeasternmost part of the channel, and is, in turn, overlain by Unit 5, fine-grained sandstones and siltstones intercalated with coarse sandstone lenses. F) Correlation diagram including sedimentary logs.

abandonment. The upward-fining trend and decrease in the number of coarse-grained interbeds indicates a gradual shut-down of local sediment supply rather than abrupt abandonment.

3.3.3 Stratal Element 3: Shallow Scour and Heterolithic Channel Fill

Stratal Element 3 comprises shallow (up to 5 m deep) channels with lithologically variable fill (Figure 3.1, Figure 3.4). These elements are not observed in the middle Kaza, but are common in the upper Kaza where they generally become more abundant stratigraphically upward as SE 4 becomes less common (see also Chapter 5). Channel bases form low aspect ratio scours, reaching a maximum depth of several meters over distances of up to several hundred meters laterally. In contrast to the deeply scoured base of feeder channels (SE 2) these basal scours are commonly not terraced, but rather are smooth, gentle sloping surfaces. Strata of SE 3 commonly abruptly overlie or are overlain by laterally continuous sheet-like sandstones of SE 4, but several instances of SE3 are intercalated commonly also. Units of SE 3 are typically 1 – 5 meters thick and uncommonly up to 15 m thick. This suggests local sediment aggradation even after the shallow channel scour was filled. Like SE 2, these channels lack recognizable levees, but commonly pass laterally into progressively finer-grained and thinner-bedded turbidites.

Most channels have a sand-rich fill, although a range exists from sand-rich to more fine-grained turbidite fills. In the thickest part of the fill, interpreted to be the depositional axis of the channel, the basal scour surface is commonly overlain directly by sand-rich beds of Facies 1, 2 and 3 that range from decimeters up to a meter thick. Beds gradually thin and fine to Facies 5 near the top of the channel fill, forming a few to several meter-thick, upward-fining succession.

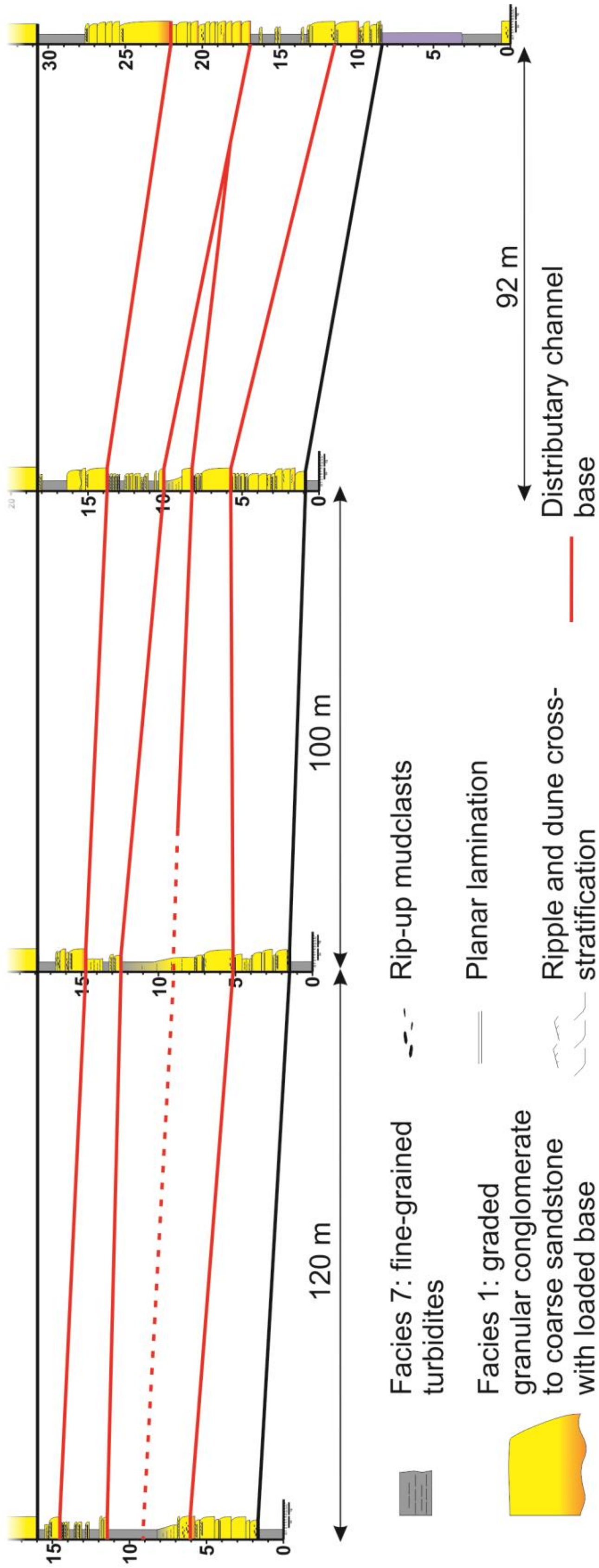

Figure 3.4: Distributary channels in the upper Kaza are a few meters deep and show a distinct lateral facies change. In the channel axis (right side of correlation diagram) strata consist of amalgamated, coarse-grained sandstone capped commonly by dune-cross stratified sandstone. Towards the channel margins (left side of correlation diagram) beds thin and fine, and become progressively more interbedded with fine-grained turbidites of Facies 5. This correlation diagram shows a cross-section of four stacked distributary channels from their axes (right side) to the margins (left side). Bases of channels are shown by red lines; black lines show the base of terminal splays.

A similar facies change is observed laterally, where coarse, amalgamated sandstone beds of Facies 1, 2 and 3 in the channel axis fine and de-amalgamate into strata of Facies 5. Beds are typically continuous from channel axis to the channel margins and into the interpreted overbank area, gradually thinning and fining away from the channel axis. In a small number of cases, however, the axes of two laterally adjacent channel axes merge from opposite directions into an intervening unit of Facies 5 strata. However, much more commonly SE 3 transitions laterally into fine-grained strata of SE 6.

The shallow, broad basal scours of SE 3 indicate that, compared to flows that created the basal erosional surfaces of SE 2, these features were eroded by comparatively low energy flows. The presence of bypass facies at the channel base and axis, in addition to the lateral continuity of beds from channel axis into the overbank area, suggest that while the high-energy cores of depositional turbidity currents were confined to the channel axis, the currents easily and continuously over-spilled their confinement.

Turbidity currents become unconfined down-flow of the upslope channel-levee transition zone (Wynn *et al.*, 2002b), and as a consequence thicken and expand laterally (see Parsons *et al.* (2002) and Alexander *et al*. (2008) for flume study examples, or Hall and Ewing (2007) for a physical examination of turbulent plane wall jets exiting channels). Experiments conducted on wall jets have shown that flows naturally develop slow and fast moving “superstructures” that orient themselves parallel to flow direction (Adrian, 2010; Marusic *et al.*, 2010). It is envisioned that the expanding turbidity currents overrode the entire depositional lobe (Maier *et al*., 2011), while the high-density core of the currents became divided and preferentially diverted through a network of broad and shallow distributary channels that paralleled flow superstructures. Initially flows exploited pre-existing topography, or eroded the basin floor due to increased turbulence near the point of unconfinement (Hogg *et al.*, 1997; Alexander *et al.*, 2008). Later flows may have enhanced these features and over time created a shallow distributary network. Alternatively, the experiments of Yu *et al.*, (2006) report that distributary channels are aggradational with depositional levees; however the channels observed in the upper Kaza lack levees, and have a shallow scoured base. The aggradational nature of these channels however, albeit rare, has been observed in the upper Kaza. These channels have a shallow scour surface, an aggradational fill thicker than the channel's depth, and have architecture similar to the ones described by Yu *et al.* (2006). Stratal Element 3 is interpreted to be the fill of short-lived, shallow distributary channels formed on the surface of a depositional lobe and transferred sediment to downflow terminal splays. These channels were initiated by scouring at the base of flows, which also exploited pre-existing topography. Subsequently channels became infilled, and in some cases aggradational, forming deposits thicker than the depth of the channel's basal scour.

3.3.4 Stratal Element 4: Sheet-like Sandstone

Stratal Element 4 forms amalgamated sheet-like sandstone units 1 to up to 10 m thick (Figure 3.2, Figure 3.5 and Appendix A) that consist almost exclusively of Facies 1, 2 and 3. The basal contact of SE 4 is sharp, and aside from common shallow scours a few cm up to few dm deep, is generally planar. Nevertheless, rare scours up to several meters deep are observed (Figure 3.1). Mudstone rip-ups and sand injections are present locally along the base of these units; most rip-ups and injections are cm- to dm-scale structures, but one mudstone clast observed in the middle Kaza is >3 m long and 40 cm thick, and at one end is still attached to the

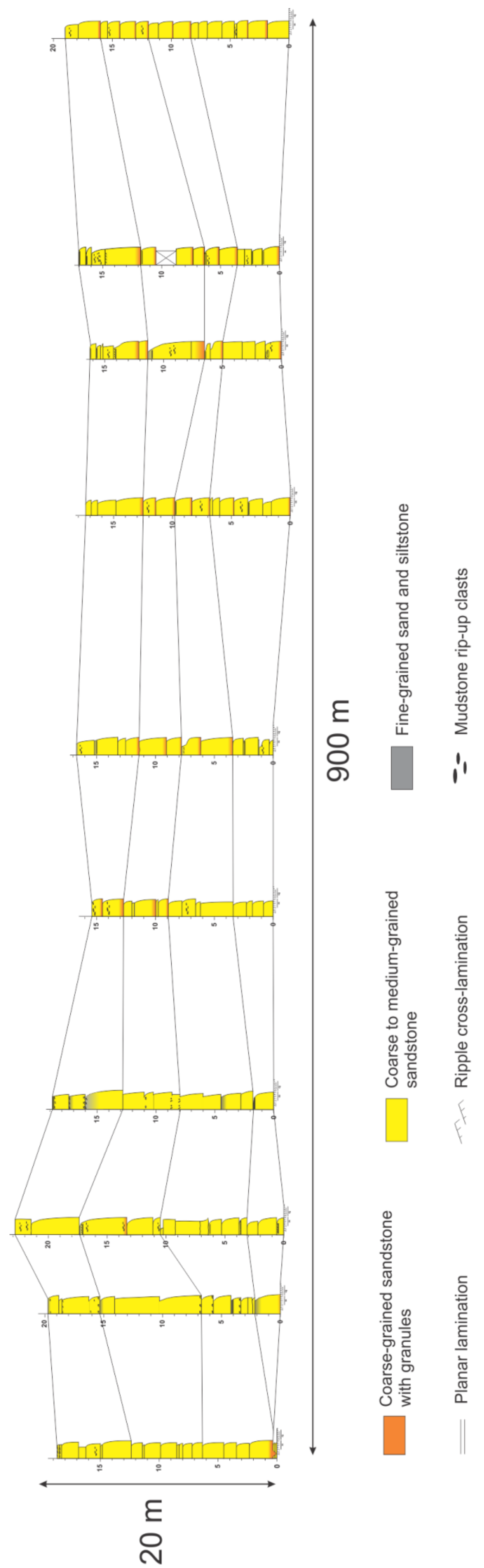

Figure 3.5: Correlation diagram showing the lateral continuity >1 km of four stacked terminal splays (SE 4) in the upper Kaza.

underlying succession of fine-grained medium-bedded turbidites (Figure 3.1). No consistent vertical stacking of facies is observed in SE 4. In the middle Kaza no vertical trends in bed thickness or grain size are observed. In contrast, in the upper Kaza sandstone beds commonly become abruptly interstratified with thin-bedded turbidites in the upper few meters of SE 4. Subtle lateral facies changes over 100's of meters are observed and typically occur as several m-thick massive structureless and amalgamated sandstone (Facies 1) grading laterally to graded sandstone beds with thin and locally eroded Bouma turbidite tops (Facies 3). These facies changes however do not significantly alter the overall sandstone to mudstone ratio of SE 4, which generally is of the order of 90% or more. Nevertheless, although uncommon, rapid lateral changes in sandstone to mudstone ratio are observed in both the upper and middle Kaza. In one example from the middle Kaza, a near-100% sandstone unit changes laterally over 200 m to sandstone interbedded with Facies 5 (fine-grained turbidites), where the sandstone to mudstone ratio is <70% (sandy SE 6b), and then decreases further to ~30% over the next 1 km (muddy SE 6a). Commonly individual units of SE 4 amalgamate and stack to form successions typically ~15 m but up to 50 m thick (Figure 3.5). Less commonly stacked units of SE 4 are separated by thin (few cm to up to 1 m thick) laterally discontinuous (10s to 100s meters) layers of SE 5 and/or SE 6 (Figure 3.2).

Stratal Element 4 is interpreted to be terminal splays formed at the distal ends of distributary channels (SE 3). Here distributary channels gradually become shallower and wider as they pass into terminal splays, and the high-density core of turbidity currents, which are partly confined in the distributary network, progressively overflow their confinement, expand and possibly merge. The uncommon m-scale scours and the m-scale rip-up clasts are interpreted to be the result of erosion caused by locally enhanced turbulence. Such erosion due to flow expansion at the mouths of channels has been observed in both laboratory experiments (e.g. Alexander *et al*,. 2008), and in modern seafloor studies (e.g. Wynn *et al*., 2002b). Deposition is interpreted to be the result of gradual, albeit rapid, flow collapse and capacity-driven deposition immediately downflow.

Stratal Element 4 commonly extends across the width of the upper and middle Kaza outcrops, ~1 km and 2 km, respectively, suggesting that these elements were much more than a few kilometers wide. Moreover, it is important to note that SE 3 and 4 are commonly intercalated in the upper Kaza, suggesting that these two elements have a close temporal and spatial relationship, and together make up a larger depositional element of a submarine fan, termed a depositional lobe. Amalgamated stacks of SE 4 are interpreted to be the distal part of depositional lobes where individual terminal splays amalgamate to form laterally extensive sandstone sheets. The rapid lateral change in sandstone to mudstone ratio observed in a small number of SE 4 units is interpreted to reflect a rapid (over several 100s of meters) lateral facies change near the lateral or downflow margins of terminal splays into fine-grained strata of SE 6 (see below).

3.3.5 Stratal Element 5: Sheet-like Medium-grained Matrix-rich Sandstone

Stratal Element 5 comprises laterally extensive dm to up to ~5 m thick units consisting of at least 50% to 100% matrix-rich strata of Facies 4 (Figure 3.1, Figure 3.2), with beds of Facies 1, 3 and 5 present locally. The base of SE 5 is sharp and commonly non-erosional, and erosion between beds within SE 5 is commonly restricted to narrow (up to several m wide) and shallow, up to 10 cm deep scours. Commonly units of SE 5 are a few beds thick, but thicker and single-bed-thick units are observed also. Stratal Element 5 commonly overlies fine-grained turbidite deposits of SE 6, but also is observed overlying SE 3, and between sand-rich units of SE 4 (Figure 3.2). Most commonly, however, SE 5 occurs lateral to SE 1 (isolated scours; Figure 3.1), and is typically eroded completely over several 10s of meters. Stratal Element 5 can rarely be traced laterally for several 100s of meters, where beds gradually thin and fine until the unit consists almost exclusively of Facies 6 (SE 6a). In both the upper and middle Kaza SE 5 is typically overlain abruptly by sandstone rich strata of SE 3 or 4.

The abundance of fine-grained matrix and common large concentration of mudstone clasts in Facies 4 was likely the result of erosion and entrainment of mud-rich basin-floor sediments at an upstream avulsion node. Such erosional flows are termed Type C flows by Huang *et al.* (2009), and describe flows that have critical densimetric Froude numbers less than unity and experience energetic hydraulic jumps at slope breaks. Here, intense velocity fluctuations result in periodic pressure fluctuations, which are envisioned to cause the disintegration of the seafloor by detachment of large blocks of semi-consolidated sediment, which then are deposited a short distance outboard of the jump. This extensive erosion of the basin floor also supercharges the flows with fine-grained sediment that rapidly mixes into the flow and, as a consequence, abruptly changes the rheology of the suspension outside the jump by increasing its apparent viscosity and dampening turbulence. This, in turn, results in Type B flows outboard of the jump, which have a non-existent critical densimetric Froude number (Huang *et al.*, 2009), and lose their excess energy by rapid capacity-driven sedimentation (Leclair and Arnott, 2003; Arnott, 2007a).

The common occurrence of SE 5 beneath distributary channel and terminal splay deposits (SE 3 and 4 respectively), and its most common occurrence next to isolated scours indicates that they are intimately related, and that deposition of SE 5 immediately precedes (re-) activation of deposition locally. The requisite conditions to create Type C flows are apparently common, and appear to coincide not only with major lobe-switching events that result in abrupt slope-breaks, but also feeder and distributary channel avulsion resulting in relatively shallower slope-breaks. Deposition of SE 5 is interpreted to be related to upstream channel avulsion followed by initiation of deposition down-flow. Importantly, not all distributary channels and terminal splays are underlain by clast- and matrix-rich sandstones, suggesting that their occurrence is not a precondition for the onset of deposition of these elements. If a mature, self-tuned upstream turbidite system is assumed (Straub *et al*,. 2008; Amos *et al.*, 2010), then turbidity currents with a consistent composition can be expected to exit the channel-levee system onto the basin-floor. The observations above suggest that most of these flows did not jump, but rather deposited the bulk of their sediment as Facies 1-3 and built up the sheet-like depositional lobes. In some cases, however, avulsion enhanced slope locally, and the inception of the thick sand-rich sedimentary bodies was preceded by the deposition of matrix- and mud-clast-rich beds of SE 5.

3.3.6 Stratal Element 6: Sheet-like Fine-grained Turbidites

Stratal Element 6 comprises 5 cm- to 35 m-thick sheet-like fine-grained units that are typically thicker in the middle Kaza Group compared to the upper Kaza Group. These units comprise 30% to up to 100% thin- to medium-bedded, fine-grained sandstone to mudstone turbidites (Facies 5), although sandstone interbeds of Facies 1, 2 and 3 are common. The base of SE 6 is sharp and commonly non-erosive, although a few broad, shallow (up to several dm deep) scours are observed. Stratal Element 6 is typically laterally continuous across the entire width of both outcrops, but a few thin units (<5 m thick) are eroded completely; lateral continuity is however greater in the middle Kaza. Stratal Element 6 is divided into two sub-elements termed SE 6a and 6b.

3.3.6.1 Stratal Element 6a.

Stratal Element 6a lacks sandstone interbeds and has the highest gamma-ray counts in strata of the upper and middle Kaza (up to >120 cps), reflective of the highest mudstone content. Geochemically, however, strata resemble those in the rest of the upper and middle Kaza and also slope strata of the Isaac Formation in both major and trace element composition (Marvinney *et al.*, 2009). Stratal Element 6a is less common than SE 6b, and is more common in the middle Kaza. Units of SE 6a are 15-25 m thick (Figure 3.6).

The higher mud content and lack of sandstone interbeds indicates that SE 6a was deposited during episodes of significantly reduced coarse clastic input, possibly related to a highstand of relative sea level (e.g. Vail et al., 1977; Emery and Myers, 1996). Interestingly, the geochemical characteristics of these strata, which suggest typical oxic WSG bottom water conditions, contrasts markedly the interpreted highstand deposits of the Old Fort Point (OFP) Formation (Smith, 2009; Smith et al., 2012), the marker unit that separates the upper and middle Kaza groups. Geochemical attributes of the regionally correlative OFP suggest a single anomalous episode of bottom water anoxia within the Windermere basin related to a eustatic highstand. Deposition of SE 6a is therefore more likely autocyclically controlled, and is interpreted as a distal inter-lobe fine-grained deposit resulting from lobe switching and abandonment.

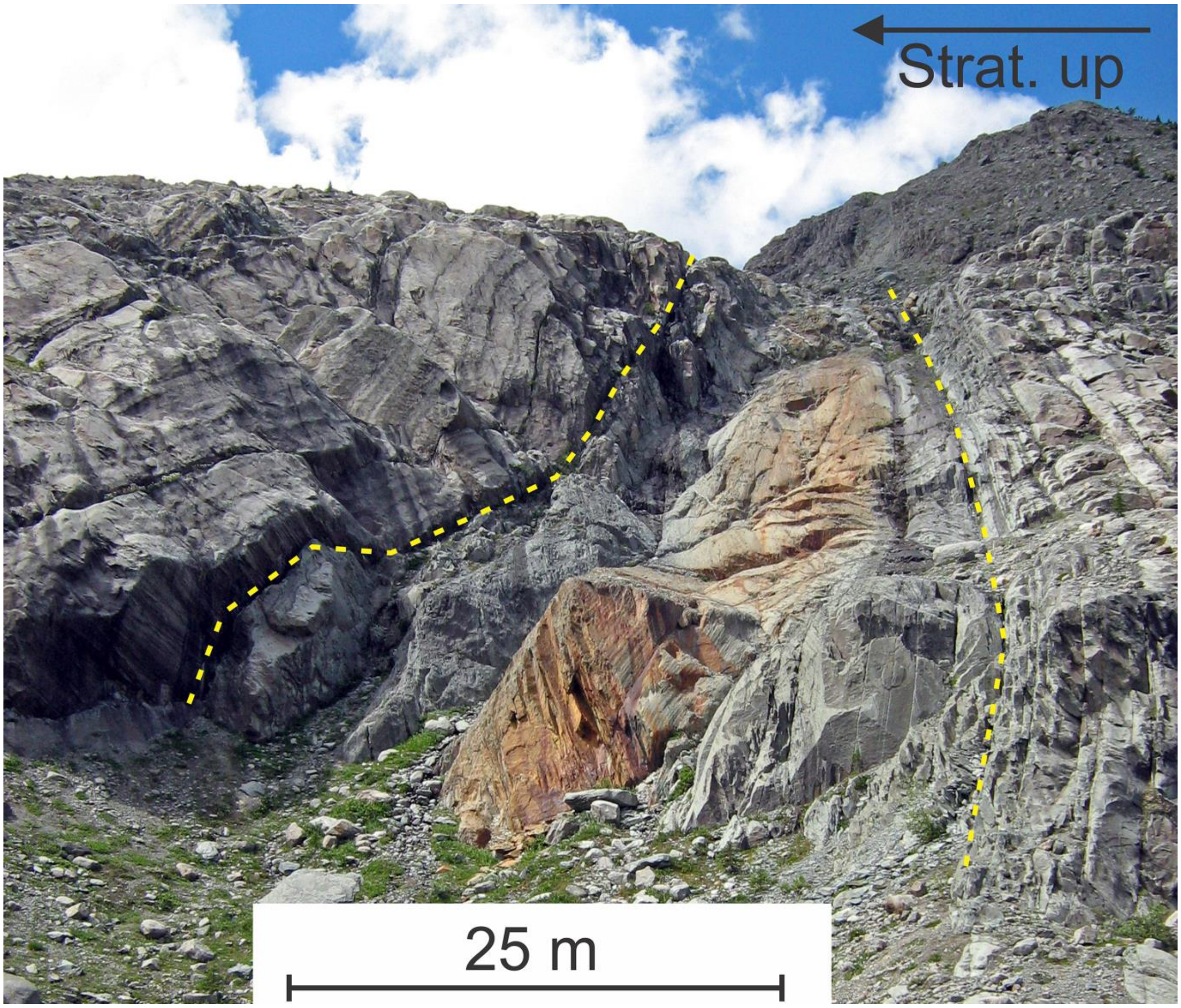

Figure 3.6: Field photograph of a 25 m thick unit comprising fine-grained, thin-bedded turbidites (SE 6a). Yellow lines indicate the lower and upper contacts of the unit. This unit of fine-grained turbidites does not contain any coarse-grained sandstone interbeds.

3.3.6.2 Stratal Element 6b.

Stratal Element 6b differs from SE 6a by the presence of sandstone interbeds, and lower gamma-ray readings, typically 60-80 cps. Units of SE 6b vary greatly in thickness. The thinnest laterally continuous examples are 5 cm thick, and the thickest 35 m. In general, units are thicker in the middle Kaza. The number and abundance of sandstone interbeds also varies, from approximately 5% to 70% of the total thickness of an individual unit (Figure 3.7).

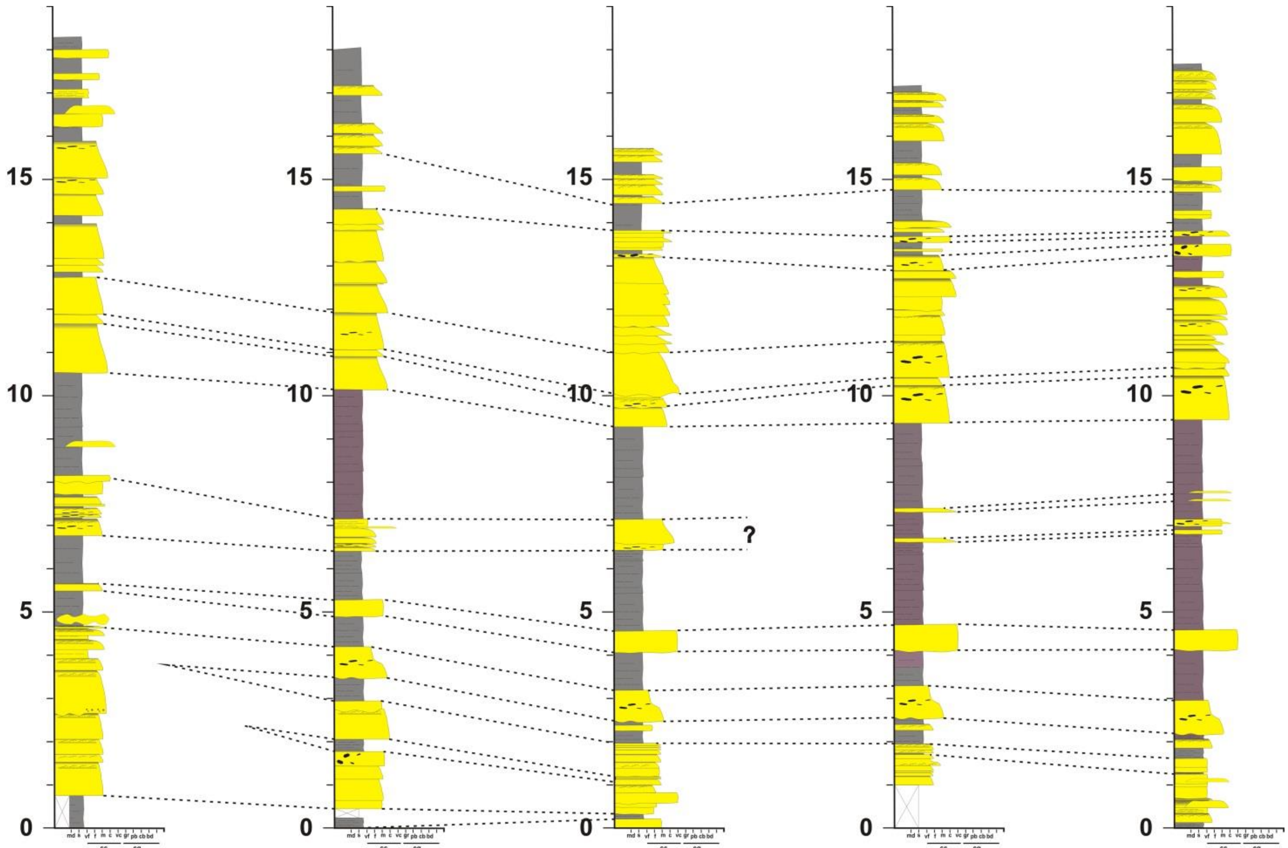

Figure 3.7: Correlation diagram of an up to 18 m thick sheet-like fine-grained turbidite unit from the middle Kaza (between S1 and S2) that contains sandstone interbeds (SE 6b). This unit comprises locally approximately 40% sandstone interbeds, but laterally over distances of several 10s to 100s of meters the sandstone to mudstone ratio varies. Logs are approximately 30 meters apart.

Units of SE 6b are interpreted to be proximal inter-lobe deposits, or intra-lobe deposits that accumulated between active terminal splays and distributary channels. The abundance of sandstone interbeds is interpreted to relate directly to distance from the main axis of deposition, being more abundant closer to a terminal splay or distributary channel. Stratal Element 6b, therefore, is continuous with margins of SE 3 and 4 proximally, and SE 6a in the more distal, laterally and downflow, parts of depositional lobes.

3.3.7 Stratal Element 7: Thick-bedded Chaotic Units

Stratal Element 7 comprises dm to Dm scale (up to several 10s of meters thick), laterally-continuous, mud-rich chaotic beds of Facies 6. These beds are absent in the middle Kaza, and uncommon in the upper Kaza, but become more abundant and thicker towards the top of the upper Kaza. They have been documented as relatively common and thick in base-of-slope deposits of the overlying Isaac Formation (Ross and Arnott ,2007; Arnott *et al.*, 2011). The basal contact of SE 7 is sharp and locally erosive. Beds are commonly laterally continuous and change little in thickness over the width (~ 1 km) of the upper Kaza outcrop. Navarro (pers. comm., 2012) observed an occurrence of SE 7 in her study areas at Castle Creek and Mt. Quanstrom, which based on its stratigraphic position near the Kaza Group – Isaac Formation contact, is potentially correlatable over the ~25 km between Castle Creek and Mt. Quanstrom. Thix suggests that this bed is at least a few 10s of km wide and that it likely covered a large part of the local proximal basin floor. As described in Chapter 2, beds of SE 7 are interpreted to be debrites. The absence of these beds in the middle Kaza and their increase in abundance and thickness stratigraphically upwards may be explained by their relatively short run-out length on the lower slopes of the basin-floor compared to the base-of-slope setting in the overlying Isaac Formation (Ross and Arnott, 2007).

3.3.8 Depositional model

Conceptual models depicting the origin and stratal composition of architectural elements (3D sedimentary bodies) representing Stratal Elements1-6 (2D) are shown in Figure 3.8. The models are based on the full collection of observations from both the middle and upper Kaza. The interpretation of the down-flow (3D dimension) of the elements are based on observations of several elements that are interpreted to be cut by the outcrop in a more proximal vs. more distal location. Isolated scours and avulsion splays are interpreted to have been the first architectural elements formed during lobe deposition. Expanding erosional flows scoured the seafloor locally to create isolated scours, and at the same time deposited avulsion splays at the margins of the flow. As lobe deposition continued, isolated scours were later filled with coarse-grained sandstone.

Subsequent flows exploited pre-existing topography and back-cut a feeder channel. This channel remained in place for the duration of lobe deposition, and experienced several episodes of erosion and fill. The high-energy and dense parts of flows were contained in the channel during this time, but the dilute outer parts of the flows escaped the channel.

Downflow of the feeder channel the high-density core of the flow split into several longitucdinal high- and low-energy structures. The high-energy structures preferentially eroded the seafloor, creating a shallow network of distributary channels. Several channels were active at the same time as the flow blanketed the entire depositional lobe. Coarse-grained sand was preferentially deposited in the shallow channels from the high-energy flow structures, and fine-grained deposition dominated inter-channel areas.

Further downflow the high-engergy structures widened and merged, and consequently the

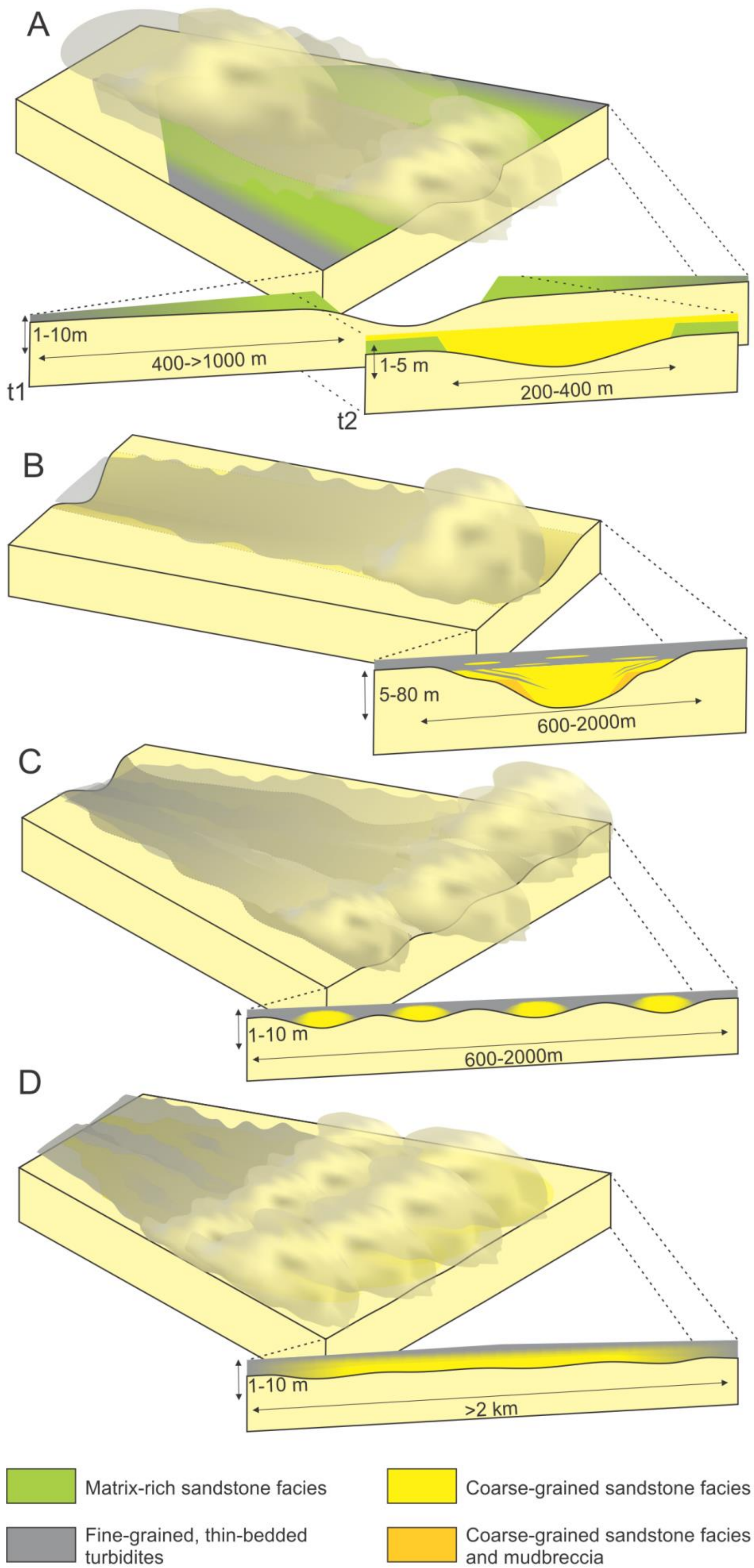
A
1-10m
400->1000 m
t1
1-5 m
200-400 m
t2
B
5-80 m
600-2000m
C
1-10 m
600-2000m
D
1-10 m
>2 km
Matrix-rich sandstone facies
Coarse-grained sandstone facies
Fine-grained, thin-bedded turbidites
Coarse-grained sandstone facies and mudbreccia

Figure 3.8 (previous page): 3D models and interpreted flow structure during deposition of six architectural element types in the Kaza Group. Cross-sections show idealized cross-sections of the resulting stratal elements as seen in the outcrops. A) Following an upstream avulsion energetic jet flows and/or rapidly expanding flows undergoing a submerged hydraulic jump scour the basin floor. Deposition in scours created by hydraulic jumps is minimal, but matrix-rich beds (AE 5) deposit on the margins of these jet flows. Further laterally these strata thin and fine into AE 6. After abandonment (t2) scours are filled with coarse-grained sandstones that near the top of the scour are laterally extensive and form a terminal splay (AE 4). B) Alternatively, subsequent flows may exploit scours to form erosional feeder channels (AE 2) that have a complex history of abandonment and reactivation, resulting in a terraced base and lithologically complex fill. Channel axes comprise coarse-grained sandstone fills intercalated with discontinuous thin-bedded, fine-grained units that thicken towards the channel margins. The lower channel margin is overlain by an intercalated assemblage of mud-clast breccia and coarse-grained sandstone. Following abandonment the channel is filled with fine-grained turbidites intercalated with coarse-grained sandstone lenses. C) Further downflow turbidity currents become unconfined and develop distinct fast and slow moving supercells. Once formed these features become diverted through broad, shallow conduits termed distributary channels (AE 3) that eventually become filled with amalgamated coarse-grained sandstone in their axes. These strata grade laterally and vertically to thinner, finer grained turbidites. Fine-grained strata between widely spaced distributary channels are part of AE 6. D) Down-flow distributary channels gradually become wider and shallower, eventually forming a laterally extensive sheet-like deposit of coarse-grained sandstone (terminal splays; AE 4). After flows become depleted of their coarse-grained load AE rapidly transitions laterally into fine-grained strata of AE 6.

shallow distributary channels also widened and became shallower. Ultimately the flow (and channels) merged and a sheet-like terminal splay consisting of laterally continuous coarse-grained sandstone deposited. On the distal margins of terminal splays the sand-depleted flows deposited fine-grained turbidites.

3.4 Discussion and implications

3.4.1 Limitations

Despite the impressive lateral and vertical scales of periglacially exposed strata at both Castle Creek and Mt. Quanstrom, a number of inherent limitations remain. Firstly, deep-water rocks of the Windermere Supergroup form part of a continental margin turbidite system where spatial scales, for instance the distance from the shelf edge to basin floor, range up to 100s of km (Bell *et al*., 1987; Ross, 1991; Ross *et al*., 1995; Karlstrom *et al*., 2001; Ross and Arnott, 2007). This, in addition to the fact that these rocks crop out in an orogen with its inherent metamorphic and structural complications, makes regional correlation a challenge. Also, the vertically-dipping attitude and two-dimensionality of the exposures in the two study areas makes palaeoflow measurement difficult and third-dimension perspective, beyond several meters, impossible. However by applying Walther's Law to observed general vertical trends in this prograding deep-water system gives clues as to the three-dimensional architecture of the basin-floor depositional system. Comparing the relative abundance, shape and size of architectural (stratal) elements in the Windermere with existing basin-floor models (e.g. Johnson *et al.*, 2001; Mulder and Etienne, 2010, and references within; and many others) the relative proximal and distal relationships between the outcrops can be determined with moderate confidence.

A further cautionary note is that, except for scours and distributary channels, all other elements are larger than the outcrops are wide. This limitation is somewhat alleviated for elements that are sampled multiple times in the vertical dimension of the outcrops, which in turn provides multiple opportunities to observe these elements in different axis or margin positions. For example, terminal splays, whose dimensions greatly exceed those of the outcrop, are common in both the middle and upper Kaza. Multiple exposures of interpreted axial and marginal positions make inferential lateral facies changes possible. Feeder channels, on the other hand, are restricted to only two partly exposed examples, and therefore their interpretation relies heavily on comparisons with similar features described in the literature.

3.4.2 Comparison with Other Ancient and Modern Systems

Studies of deep-water systems commonly describe a hierarchy of depositional units. Despite a plethora of terms used to identify them, units can generally be termed, from largest to smallest: fan, lobe complex, lobe, architectural (or stratal) element, bed. A comparison of lobe dimensions from six depositional systems was compiled by Prélat *et al*. (2010), and a number of studies compared architectural element dimensions and/or their distribution between different systems (e.g. Sullivan *et al.* (2000) compared the Skoorsteenbergen and Ross formations with the western Gulf of Mexico (GOM); Sinclair and Tomasso (2002) compared the Annot Sandstone with the GOM; Pyles (2008) compared the Ross Formation with the GOM; Pyles *et al*. (2011) compared the Lewis Shale, Ross Formation, Brushy Canyon Formation, Pab Formation, Annot Sandstone, Skoorsteenbergen Formation and Ainsa Basin). This study compares stratal elements, with the exception of SE 7, with similar elements in the literature (Table 1). Although SE 7 (debrite) is commonly observed in both seismic and outcrop (e.g. Johnson *et al.*, 2001; Posamentier and Kolla, 2003; Pyles, 2007; Arnott *et al*., 2011), it is not included in Table 1, because in comparison to the other stratal elements observed in this study SE7 is rare. Moreover, debrites do not strictly conform to the definition of an architectural element used in this paper, because they are not building blocks of a lobe, but instead are laterally extensive sheet-like deposits that are on the same hierarchical level as a lobe, and therefore are a fundamental building block of a lobe complex.

With the exception of avulsion splays (SE 5) all the elements presented here have been described and their dimensions reported from previous seismic studies. While a complete listing is beyond the scope of this paper, notable examples are included in Table 1. In most cases, the stratal elements described here are close to or below the resolution of typical industry seismic data.

Accordingly, their size and shape are well known but details of their internal stratigraphy and lithological make up remain uncertain (e.g. see Jaegu *et al*., 2008). Outcrop analogues, on the other hand, resolve well the bed to bed-set scale details of individual architectural elements, but suffer from their limited dimensions, outcrop quality and inherent two-dimensional nature, creating a recognized disconnect between outcrop and seismic datasets (Normark *et al*., 1979). There has been a recent effort to bridge this gap (e.g. Carr and Gardner, 2000; Johnson *et al*., 2001; Hodgson *et al.*, 2006; Pyles, 2007; Prélat *et al*., 2009; this study). From Table 1 it is clear that despite differences in sediment supply and tectonic setting, the overall dimensions of the various architectural elements fall within a relatively narrow range. Also, in studies where multiple elements are described from a single system, the comparative size of the elements is similar to those reported here.

3.4.3 Wider Implications

This study describes the commonly sub-seismic scale stratal elements of basin floor deposits in the WSG, and supports previous research (Sullivan *et al.*, 2000; Sinclare and Tomasso, 2002; Pyles, 2008; Pyles *et al*., 2011) that suggests the dimension and size ratio of basin floor architectural elements is everywhere similar, irrespective of basin size or tectonic setting. Each stratal element (with the exception of debrites) is interpreted to be the 2D manifestation of a 3D architectural element, which is, in turn, a component in a larger scale depositional feature that here is termed a lobe. In their proximal part lobes commonly comprise

Table 1: Comparison of the dimensions of architectural elements reported from this study and other ancient and modern examples.

Fan	Reference	Age	Tectonic Setting	Main grain size	Lobe	Isolated scours	Feeder channel	Distributary channel	Terminal splay	Avulsion Splay	Fine-grained sheets
WSG, Southern Canadian Cordillera	This study	Neoproterozoic	Passive margin	Mixed sand and mud, minor gravel	Several to several 10s km wide, few m up to 50 m thick	100-400 m wide, 1-5 m deep	>600 m (>1 km?) wide, 15 m deep	Several 100s m wide, up to 5 m deep	>1 km to several km wide, up to 10 m thick	Several 100s m wide, few dm to few m thick	~100 m to >2 km (potentially several 10's of km) wide, <1 to ~35 m thick
Lower Brushy Canyon Formation, TX, USA	Carr and Gardner 2000	Permian	Intra cratonic passive margin	Mixed sand and mud				30-150 m wide, 1-3 m deep	200 m wide, 6 m thick		> several km wide, 2-3 m thick
Golo fan system, offshore Corsica, France	Deptuck et al. 2008; Gervais et al. 2010	Pleistocene		Mixed sand and mud, minor gravel	2-14 km long, 1 to >10 km wide, 8-42 m thick	Up to 7 m deep, ~300 m wide		100 m wide, up to 10 m deep	Up to ~10 m thick, several km wide		
Amazon fan, offshore Brazil, South Atlantic	Jegou et al. 2008	Modern	Passive Margin	Mixed sand and mud	21-83 km long, 6-25 km wide			3-5 m deep			
Tanqua area of the Karoo Basin, South Africa	Johnson et al. 2001	Permian	Foreland basin	Mixed sand and mud			300 m - 1 km wide, up to 18 m deep	Overall tabular sheet geometry that is mappable over several kms. Internally lithologically heterogeneous with internal scours and minor channelization	Termed amalgamated to layered sheets, up to ~ 10 m thick		Up to >15 km wide, 1 cm to >10 m thick
Umnak channel mouth, Bering Sea, AK, USA	Kenyon and Millington 1995	Modern		Mixed sand and mud		2.5 km long, 2 km wide, 5 m deep					
Valencia Fan, Northwestern Mediterranean Sea	Morris et al. 1998	Modern	Structure controlled passive margin	Mixed sand and mud		300 m long, 80 m wide, 8 m deep					

Fan	Reference	Age	Tectonic Setting	Main grain size	Lobe	Isolated scours	Feeder channel	Distributary channel	Terminal splay	Avulsion Splay	Fine-grained sheets
Navy Fan, California Borderland, USA	Normark et al. 1979	Modern	Active margin	Sand rich		350 m long, 500 m wide 20 m deep		Up to 0.5 km wide, 5-15 m deep			
Hueneme and Dume fans, Califonia Borderland, USA	Piper et al. 1999	Quaternary	Transpressive	Mixed sand and mud				Termed shallow channel-fill subelement, 100-700 m wide, ~1 m thick, <15 km long	Termed gently lensing subelement 1-2 km wide, <2 m thick		
Skoorsteenbergen Fm., Fan 3, South Africa	Prélat et al. 2009	Permian	Foreland basin	Mixed sand and mud	Several 10s km across, 3-14 m thick				Termed lobe elements, 1-3 m thick		Several 10's of km wide, 0.2-2 m thick
Ross Formation, Ireland	Pyles 2007	Carboniferous	Transtensional	Mixed sand and mud				Termed channels (may include feeder channels), 170 m wide, 4 m thick	Termed lobes 1900 m wide, 2 m thick		>18 km wide, 1-2 m thick
Offshore East Kalimantan, Indonesia	Saller et al. 2008	Pleistocene	Complex extensional and compressional basin	Mixed sand and mud	7.5 km long, 3.5 km wide, 9-40 m thick		392 m wide, 13 m thick	161 m wide, 12.6 m thick, 2.2 km long	500-3000 m long, 400-1200 m wide, 4-13 m thick		
Mississippi Fan, Gulf of Mexico	Twitchell et al. 1992	Modern	Passive margin	Mixed sand and mud	150 km long, 50 km wide, 10-40 m thick		120 km long, 150-300 m wide, 8-10 m high levees that diminish in height downflow	20 km long, <100 m wide, <2 m relief; distal channels <75 m wide, no resolvable relief (identified by low backscatter)			
Agadir Fan, offshore NW Africa	Wynn et al. 2002	Modern	Passive margin	Mixed sand and mud		500 m long, 250-500 m wide, 10.5 m deep; large amalgamated scours are up to 9 km wide					

Fan	Reference	Age	Tectonic Setting	Main grain size	Lobe	Isolated scours	Feeder channel	Distributary channel	Terminal splay	Avulsion Splay	Fine-grained sheets
Lisbon Canyon, offshore Portugal	Wynn et al. 2002	Modern	Passive margin	Mixed sand and mud		Axial part consisting of amalgamated scours 6 km long, 3 km wide; off-axis scours 1 km long and 800 m wide					
Rhone Fan, northwestern Mediterranean	Wynn et al. 2002	Modern	Passive margin	Mixed sand and mud		1 km long, 500 m wide 20 m deep	Along down-stream transect widens from 500 m to 800 m, shallows from 80 m to less than 10 m deep				

scours, scour fills and avulsion splays that herald the onset of local lobe deposition. Further downflow these elements become rare and are replaced by a network of distributary channels that progressively shallow and ultimately merge laterally, forming sheet-like terminal splays. Along their distal and lateral margins, avulsion splays and terminal splays, and distributary channels along their lateral margins, transition rapidly into thin-bedded, fine-grained turbidites. The rare occurrence of feeder channels suggests that most lobes are fed directly by base-of-slope leveed channels, and only rarely by erosional feeder channels that scour previous lobes. Although this study focused on the detailed description of stratal elements in basin floor strata of the WSG only, previous work has shown that they form the basal part of a several km-scale thick, systematically upward-shoaling succession of sandstone-rich basin-floor lobe strata (Meyer and Ross, 2007; this study) overlain progressively by base-of-slope and slope leveed-channel complexes to mudstone-rich upper slope and outer shelf strata (Ross *et al.,* 1995; Arnott, 2007; Navarro *et al*., 2007; Ross and Arnott, 2007; Arnott *et al*., 2011; Khan and Arnott, 2011). This systematic change is interpreted to reflect a Waltherian stratigraphic progression formed by the progradation of the Neoproterozoic continental margin of Laurentia (ancestral North America) into the paleo-Pacific miogeocline (see Figure 1.2, Figure 1.5). Moreover, it is important to note that certain elements are exclusive to different positions in the stratigraphic pile, and by extension along a depositional transect. For example, depositional lobes and leveed channels are documented only in basin floor and base-of-slope/slope strata, respectively.

Recently Pyles *et al*. (2011) reported that while the dimensions of the different architectural elements may vary little between depositional systems, the distribution and abundance of the various architectural elements in 4th-order stratigraphic units do and relates to the “graded” or “out-of-grade” condition of the transport system. Under graded conditions the slope becomes the depocenter and accordingly progrades. In addition, along a depositional transect there is a progressive upward change from mostly lobes to slope channels and levees. During out-of-grade conditions, on the other hand, the slope becomes a zone of bypass causing the depocenter to move onto the basin floor and the system to become highly aggradational. In addition the stratigraphy becomes dominated by broad distributary channel-lobe systems. Strata described here from the WSG are interpreted to be medial to proximal basin floor deposits, and therefore comparable to medial and proximal submarine fan strata of Pyles *et al*. (2011). Basin floor deposits of the passive margin WSG form a stratal package more than 3 km thick, which presumably encompassed a number of 4th (and 3rd) order sedimentary cycles and also some number of graded and out-of-grade stratal conditions. It is important to note that these latter conditions have been reported from slope deposits of the Isaac Formation where mass transport deposits, some up to 135 m thick and dominated by slump, slide and debris flow deposits, episodically interrupt a much more thickly developed sedimentary succession dominated by leveed slope channels formed under generally graded conditions (Arnott *et al*., 2011). Intuitively these changes should be manifest also in the basin floor sedimentary record, and according to Pyles *et al*. (2011), in the abundance of its composite architectural elements. To date no such intercalation has been observed in rocks of the Kaza Group. Instead the sand-rich component of basin floor strata show a consistent km-scale (vertical) change from almost exclusively terminal splays deposited in the medial part of the lobe system to terminal splays with common distributary channel deposits in the more proximal basin floor. The question, then, whether the passive margin WSG, which is generally graded and only temporary out of grade, and therefore different than the passive margin, out-of-grade Pab Sandstone (Pyles *et al*., 2011), is the rule or the exception? Future (seismic) research is needed to describe the temporal and spatial evolution of large, passive margin depositional systems in order to document and link changes between stratigraphic grade and sedimentation patterns on the slope and basin floor.

3.5 Conclusions

Basin-floor deposits are generally one of the least-well understood parts of the submarine turbidite depositional system, especially at the small, architectural or stratal element scale. This study of the middle and upper Kaza groups of the Windermere Supergroup turbidite system adds to the global knowledge base by describing six distinct facies from basin-floor outcrops of the middle and upper Kaza groups. These, then, populate seven stratal elements, which in turn comprise lobes that make up the basin-floor stratigraphy of the middle and upper Kaza. Stratal elements include sand-filled scours, avulsion splays comprising matrix-rich sandstone, small and large channels with mixed sandstone and mudstone fills, sheet-like sandstones, sheet-like fine-grained units and debrites. This study shows that, except for debrites, all elements comprise similar facies, but that it is the overall shape and dimensions of these elements, and more importantly, the internal organization of the constituent lithofacies that uniquely populate each of the different stratal elements.

Comparison of stratal element dimensions between the WSG and architectural elements in other systems reveals a similarity in scale across various fans. This suggests that the detailed lithological data presented in this study can then be extrapolated to other basin-floor studies, and therein provides a robust predictive tool for sediment type and distribution across similarly large, graded, mixed sand-and-mud basin-floor fans, even where lithological data are limited.

Chapter 4: Matrix-rich sandstones: indicators of local sedimentation activation in slope and basin-floor strata

4.1 Introduction

In recent years matrix-rich strata have been increasingly recognized in the deep-marine sedimentary record (Lowe and Guy, 2000; Lowe *et al.*, 2003; Haughton *et al.*, 2003, 2009; Talling *et al*., 2004, 2007, 2012; Barker *et al*., 2008; Hodgson, 2009; Pyles and Jennette, 2009; Kane and Pontén, 2012; Talling, 2013). These deposits bear little resemblance with either classical turbidites (*sensu* Bouma, 1962; Lowe, 1982) or debrites, and are interpreted to have been deposited by flows exhibiting a changing and/or transient flow state. Significantly, matrix-rich beds have most commonly been reported from the distal parts of depositional systems (Talling *et al*., 2012; Talling, 2013). Matrix-rich strata have been termed "slurry beds" by Lowe and Guy (2000), Lowe *et al.* (2003), Sylvester and Lowe (2004), "linked debrites" by Haughton *et al.* (2003), Amy and Talling (2006), Haughton *et al*. (2009), "co-genetic debrite-turbidite beds" by Talling *et al*. (2004), "hybrid event beds" by Haughton *et al*. (2009), Hodgson (2009), Pyles and Jennette (2009), and "transitional flow deposits" by Kane and Pontén (2012). Slurry beds are typically several meters thick with common dewatering structures and (wispy) lamination (Lowe and Guy, 2000; Lowe *et al*., 2003). Co-genetic debrite-turbidite beds, or similarly hybrid event beds, are typically up to about 1 m thick, and made up of a lower, structureless clean sandstone capped by an argillaceous sandstone or sandy mudstone, also termed a linked debrite (Haughton *et al*., 2003, 2009; Talling *et al*., 2004; Barker *et al*., 2008;

Hodgson, 2009), although Pyles and Jennette (2009) report multiple alternating turbidite and debrite intervals. In these studies flow type is inferred from stratal characteristics and ranges from hyperconcentrated and concentrated density (turbidity) flows with significantly suppressed turbulence, and are termed slurry flows (Lowe and Guy, 2000; Lowe *et al*., 2003), transient flows (Kane and Pontén, 2012), or flows that undergo a longitudinal and/or temporal evolution from fully turbulent to a laminar and/or cohesive flow state and deposit composite turbidite-debrite beds (Haughton *et al*., 2003, 2009; Talling *et al*., 2004; Barker *et al.*, 2008; Pyles and Jennette, 2009). Despite on-going efforts to develop an all-encompassing classification scheme for density flows (e.g. Lowe, 1982; Mulder and Alexander, 2001; Talling *et al*., 2012) interpretations based on observed characteristics in the ancient sedimentary record remain problematic and often controversial, particularly in strata interpreted to have been deposited by flows with abundant fine-grained suspended sediment (Baas *et al.*, 2011; Talling *et al*., 2012; Talling, 2013). Recent laboratory experiments (e.g. Best *et al.*., 2001; Baas and Best, 2002, 2008; Sumner *et al*., 2008, 2009; Baas *et al.*, 2009, 2011) have provided important insight into the physical behaviour of fine-grained, sediment-laden flows, and the complex make-up of their matrix-rich deposits, which commonly consist of depositional textures and structures not accounted for in traditional turbidite or debrite models. However the number of laboratory studies to date is limited and many potentially important sedimentological parameters, for example grain size, grain size distribution, grain sorting, rates of sedimentation and their effect(s) on the transport and deposition from fine-sediment enriched flows remain largely unexplored and hence poorly understood. For a comprehensive review of the current state of field and laboratory research on fine-sediment-laden flows and their matrix-rich deposits see also Talling (2013).

Matrix-rich sandstones in deep-water rocks of the Windermere Supergroup (WSG) have been previously recognized and several general observations made (e.g. Leclair and Arnott, 2003; Arnott, 2007b): in the field they are easily identified by their anomalously dark colour, which is a consequence of their high (30 to up to ~50%) fine-grained matrix content; form relatively thin (up to several m thick) laterally continuous bedsets commonly overlain by coarse sandstone; where present they commonly form units composed almost exclusively of matrix-rich sandstone, although locally they are interbedded with upper division turbidites; occur in both slope (Isaac Formation) and basin-floor (upper and middle Kaza groups) strata. In chapters 2.4.8 and 3.3.5 (see also Figure 2.11) matrix-rich strata were briefly introduced; in this chapter these same matrix-rich strata are described further and subdivided into four sub-facies. Additionally, it is shown that these strata often transition abruptly laterally into matrix-poor, coarse-grained sandstones with common large sand- and mudstone clasts. The origin of these matrix-rich sandstones and the basis for their lateral juxtaposition to matrix-poor sandstones is presented.

4.2 Matrix-rich strata in the Windermere Supergroup

Matrix-rich beds typically form units up to several meters thick and are observed throughout the deep-water portion of the WSG. Commonly matrix-rich units transition rapidly laterally into comparatively matrix-poor sandstone (see description below), or are erosionally truncated by overlying beds (Figure 4.1). Each end-member is described in detail below.

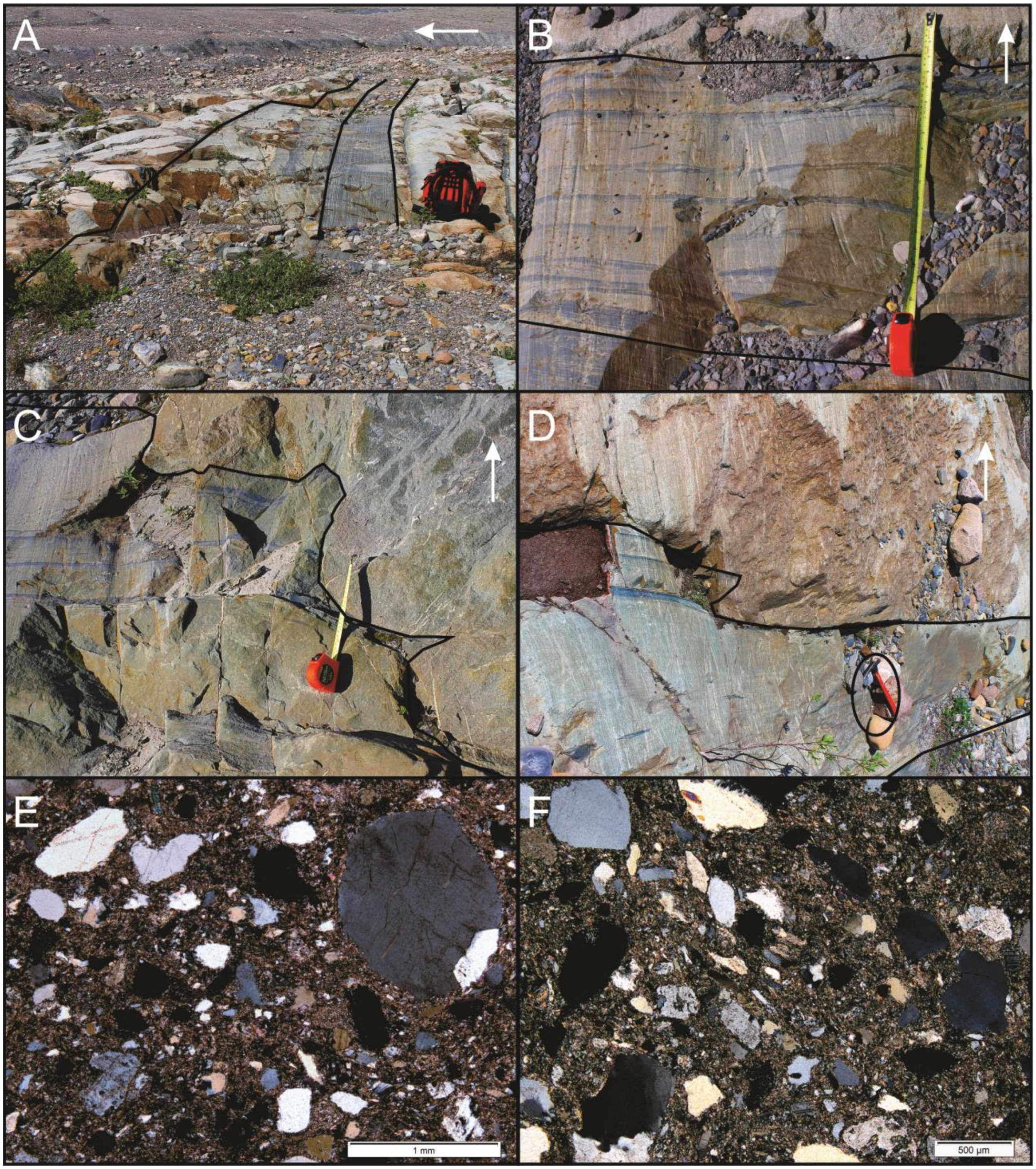

Figure 4.1: (A) A unit of matrix-rich sandstone beds sandwiched between a lower 60 cm thick unit of fine-grained turbidites (dark-grey unit to the left of the backpack) and an overlying up to 18 m thick unit of amalgamated, matrix-poor, coarse-grained sandstone (Fig. 4A coincides with the far right side of the correlation panel in Fig. 9). The abrupt thinning of the matrix-rich unit toward the top of the photo is the result of scour at the base of the matrix-poor sandstone. Black lines indicate unit boundaries. Stratigraphic up is toward the left (arrow). The backpack used for scale is at the top of another coarse-grained matrix-poor sandstone unit. (B) Close-up

photograph of the matrix-rich sandstone unit taken near the top of the photograph in (A) where the matrix-rich unit is thinnest. Black lines indicate unit boundaries. Tape measure is 50 cm long. (C) Close-up photograph of the scour at the base of the sandstone unit. The scour is near-vertical and stepped along bedding surfaces in the matrix-rich unit. Small injections of matrix-poor sandstone into matrix-rich sandstone are visible locally. Tape measure is 25 cm long. (D) Example of a matrix-rich sandstone unit overlain by a coarse-grained, matrix-poor sandstone unit with a steep-walled scour at its base. Geologic hammer is ~50 cm long. (E) and (F) Representative photomicrograph of matrix-rich sandstones in cross-polarized light. Both samples were taken from the middle of a coarse-tail graded, structureless bed. All photos in Fig. 4 are from strata in the upper Kaza.

4.2.1 Description – matrix-rich sandstone facies

All matrix-rich sandstones in deep-water rocks of the WSG are compositionally similar, namely subarkosic sandstone with an abundant (30 to up to ~50%) chlorite and muscovite matrix with minor silt (Figure 4.1). The matrix imparts a distinctive grey-green colour to these strata.

Beds are typically sharp based with flat, planar basal contacts. Nevertheless, locally loaded and undulatory scoured contacts with scour depth of several centimeters are observed. Scours are several 10s cm up to several 10s m long, and result in local bed amalgamation. Beds are several centimeters to ~1 m thick and are massive or coarse-tail graded (measured by a suite of petrographic thin sections taken at multiple ascending stratigraphic levels in the same bed, supplemented with visual observations in the field) with grain size ranging from lower coarse to lower medium sand, and uncommonly upper coarse sand. Typically the top of the bed grades to an up to several cm thick, faintly planar laminated silt-mudstone cap (Figure 4.2). Where matrix-rich strata are overlain and/or erosionally truncated by an overlying coarse sandstone unit (e.g. channel or splay deposits) sandstone injections, flame structures and more rarely pseudonodules are present locally (Figure 2.11d, Figure 4.2). Four sub-facies of matrix-rich sandstones have been identified, three of which add additional characteristics to this basic motif (see Figure 4.3 for summary sedimentary logs):

Subfacies 1: structureless beds as described above (Figure 4.3a and Figure 4.4a). This subfacies represents ~30 % of all matrix-rich sandstones, and typically transitions laterally into subfacies 3;

Subfacies 2: beds with wavy parallel- or planar-laminated fine-grained sandstone tops (Figure 4.3b and Figure 4.4b). Near, or at the top of these beds is an up to several cm thick planar-laminated layer, which in some beds is locally wavy. In addition, laminated strata are comparatively much better sorted (10-20% matrix estimated by thin section analysis) and in some cases carbonate cemented. The wavy parallel- or planar-laminated layer is then typically draped by a several cm thick, faintly planar laminated, sandy mudstone cap. Subfacies 2 represents about 10% of all matrix-rich sandstones;

Subfacies 3: beds with dispersed mudstone clasts (Figure 4.3c, Figure 4.4c, Figure 4.4d). Mudstone clasts are massive, black, rounded and elongated. Sheared and plastically deformed clasts are common. Clasts are typically uniformly distributed throughout the bed, but uncommonly are more abundant towards the top of the bed. Clasts range in size from several cm thick and long to 15 cm thick and ~1 m long, although smaller clasts are more common. The abundance of clasts varies laterally, and may range from abundant to absent over distances of several 10s to 100s of meters. Beds are commonly sharply capped by a several cm thick silt-mudstone cap. This subfacies is common, making up ~70% of all matrix-rich sandstones;

Subfacies 4: beds marked by an abrupt upward change in matrix content (Figure 4.3d, Figure 4.4e, f). These beds comprise a basal layer that is up to about half the bed thickness and has a comparatively lower (30-40%) matrix content. Upward there is an abrupt increase in matrix content (up to 50%) with little change in the size of the dispersed sand grains. Subfacies 4 is relatively uncommon, comprising ~10% of all matrix-rich beds.

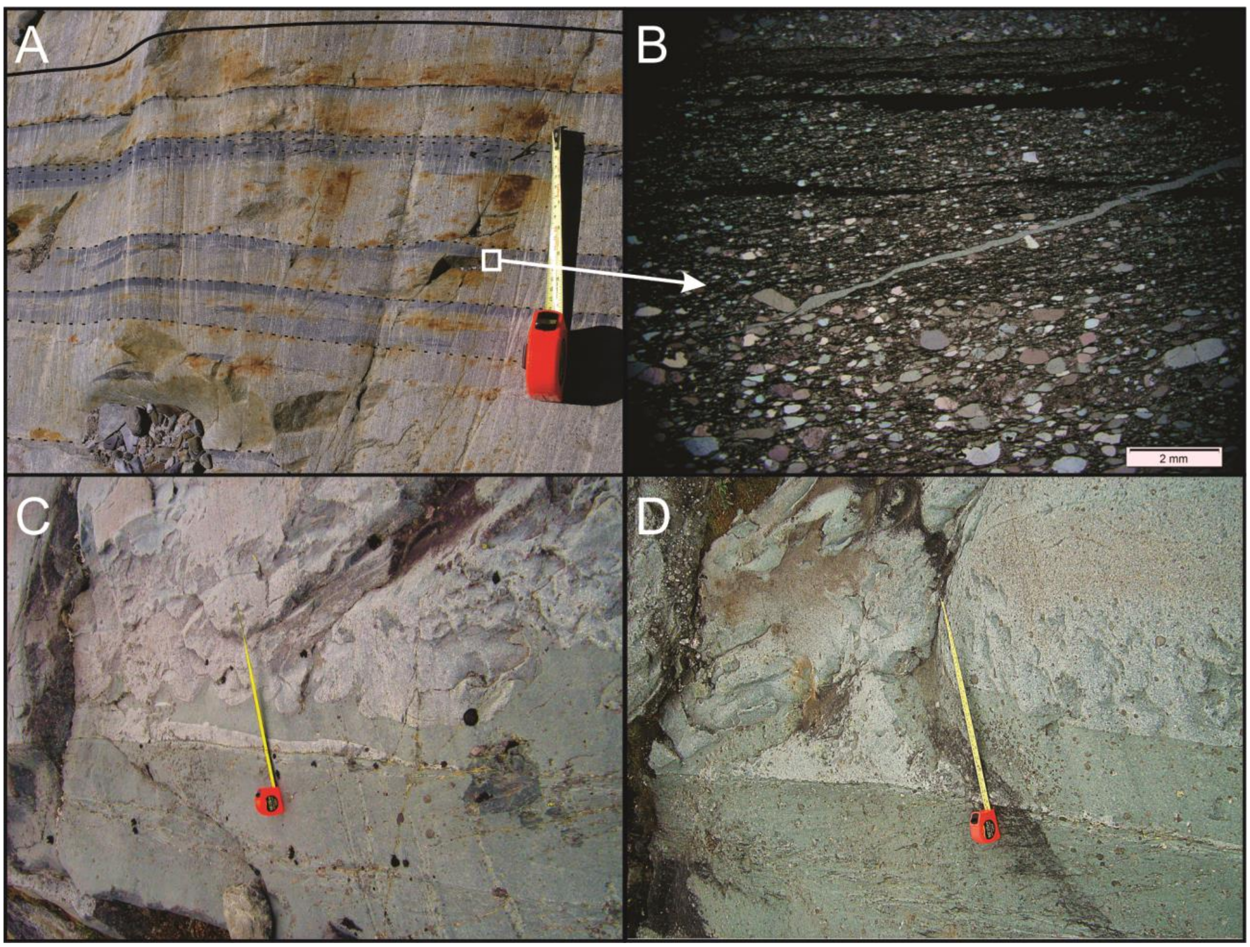

Figure 4.2: (A) Several matrix-rich sandstone beds capped by a thin layer of muddy sandstone. Note the darker colour of the mud caps. Dashed lines highlight bed contacts and the solid line shows the contact with the overlying coarse-grained sandstone terminal splay. Photograph taken in the upper Kaza. Tape measure is 20 cm long. (B) Cross-polarized light photomicrograph of a matrix-rich sandstone bed taken at the contact of the sandstone and its

muddy sandstone cap. The apparent preferential alignment (imbrication) of grains is a consequence of rotation into the plane of tectonic cleavage. (C) and (D) Matrix-rich beds commonly terminate laterally due to scour and/or loading by overlying strata. Rip-up, injection and flame structures are shown in these photographs. Rip-up clasts consisting of matrix-rich sandstone are common in matrix-poor beds that have injections at their bases. Photographs taken in the middle Kaza. Tape measure is 50 cm in both photographs.

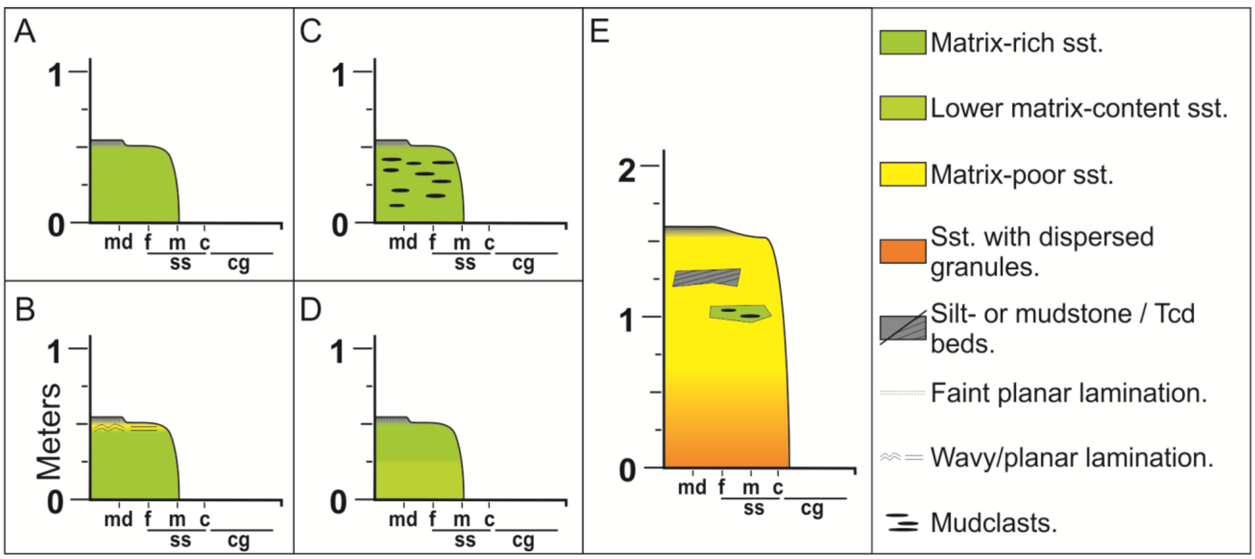

Figure 4.3: Idealized stratigraphic logs of matrix-rich and matrix-poor sandstones. (A) Structureless matrix-rich sandstone (subfacies 1). (B) Matrix-rich sandstone capped by matrix-poor, wavy parallel- or planar-laminated sandstone (subfacies 2). (C) Matrix-rich sandstone with mudclasts (subfacies 3). (D) Matrix-rich sandstone with an abrupt increase in matrix content (subfacies 4). Note that all four subfacies are capped by a thin sandy mudstone drape. (E) Matrix-poor sandstone facies comprising upper very coarse sandstone and dispersed granules in the lower part of the bed. Where present, raft size sand- and mudstone clasts typically occur in the upper half of the bed. Due to common erosional bed contacts sandy mudstone caps are only locally preserved.

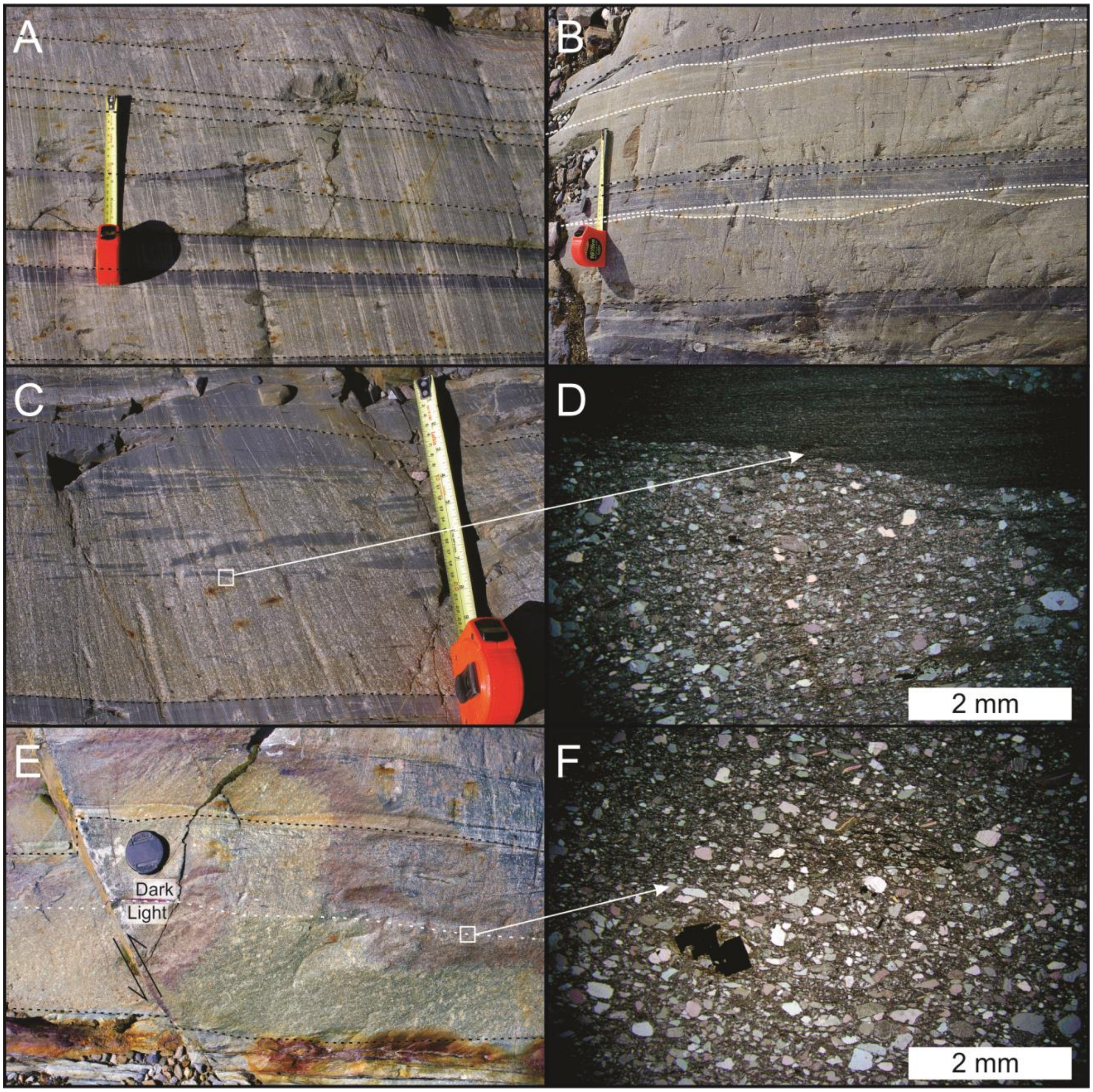

Figure 4.4: (A) Structureless, matrix-rich sandstone beds. Dashed lines highlight bed contacts. The lower three beds have a thin sandy mudstone cap, which is absent in the upper beds. Note the scoured and injected contact between the middle beds that has upturned (to the right) the intruded mudstone layer, and the flame structure (bent to the right by tectonic cleavage) at the uppermost contact. Tape measure is 20 cm long. (B) Matrix-rich sandstone beds capped by wavy parallel and planar laminated sandstone. Black dashed lines highlight bed contacts and white lines delineate the laminated part of the bed. The basal part of the beds comprises an ~20 cm thick coarse-tail graded sandstone with dispersed and elongated mudclasts (note the darker streaks in the photo). This, then, is overlain by an up to 10 cm thick parallel laminated medium sandstone. The beds are capped by a several cm thick mudstone cap. Tape measure is 20 cm long. (C) Close-up of a matrix-rich sandstone bed with small elongated

mudclasts. Dashed lines indicate bed contacts. Tape measure is 25 cm long. (D) Photomicrograph of a thin mudclast in a matrix-rich sandstone bed taken in cross-polarized light. (E) Close-up of a matrix-rich sandstone bed that displays an abrupt upward increase in matrix content at about half the bed's thickness. Black dashed lines highlight bed contacts and the white dashed line marks the abrupt increase in matrix content. Note the lighter colour of the basal, relatively matrix-poor (~40%) layer and the darker colour of the upper, more matrix-rich (up to >50%) layer. Lens cap is 5 cm wide. (F) Cross-polarized photomicrograph at the point of matrix increase. Note the darker, muddier matrix in the upper half of the photograph. All photographs taken in the upper Kaza.

Note that matrix-rich beds can have characteristics of one or more subfacies; for example some beds with mudclasts (subfacies 3) are capped with planar-laminated sandstone (subfacies 2). These beds are counted in both subfacies and thus the total sum of all subfacies is >100%. Matrix-rich sandstone beds occur isolated or intercalated with other commonly sandstone-rich strata (Figure 2.11a, Figure 4.5), but more commonly form laterally discontinuous, up to several meter-thick bedsets that extend laterally for several 10s to 100s of meters with little change in thickness (Figure 4.6). Rarely matrix-rich beds are observed to thin and transition laterally into thin-bedded, fine-grained Bouma T_{cd} and less commonly T_{acd} turbidites. More commonly, though, matrix-rich beds and/or units either transition laterally into the relatively matrix-poor sandstone facies (see below), or are truncated laterally over distances of several to up to 100 meters by scours at the base of channel fills and terminal splays (Figure 3.1, Figure 3.2, Figure 4.5 and Figure 4.6).

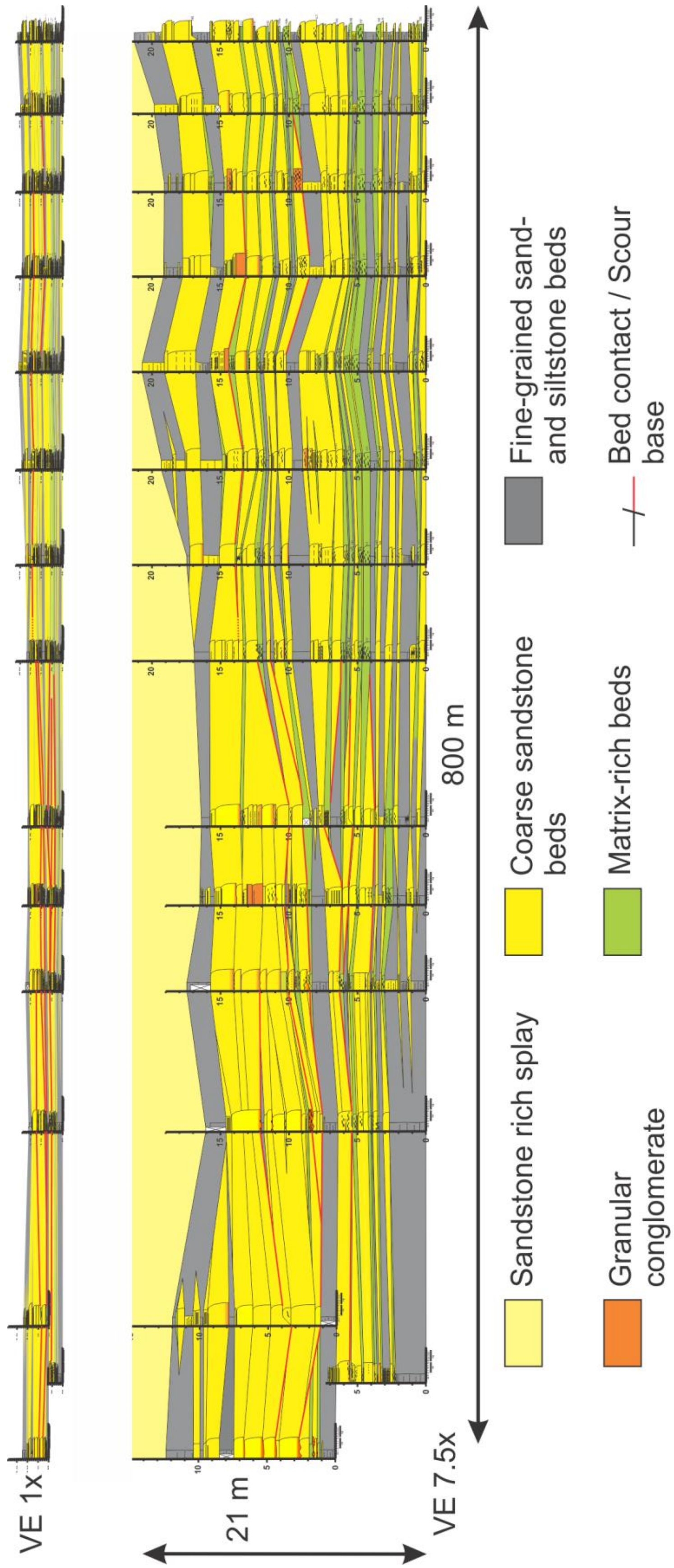

Figure 4.5: Correlation panel shown at VE 1x and VE 7.5x of an ~20 m thick unit comprising intercalated matrix-rich beds (green), clean sandstones (yellow and orange) and thin-bedded, fine-grained turbidites (grey) in the upper Kaza (for location see Fig. 2). Red lines highlight major scour surfaces. The lower ~7 m is dominated by fine-grained turbidites intercalated with medium-bedded, coarse-grained sandstone beds. In this lower part an ~2 m thick unit comprising mostly matrix-rich sandstones (right side of the panel) is laterally adjacent to medium- and thick-bedded, coarse-grained sandstones that have shallow scoured bases locally. The upper ~10 m of the panel comprises intercalated coarse-grained clean sandstones and matrix-rich sandstone beds (right side of the panel), which are laterally adjacent to coarse-grained clean sandstones that fill several meter-deep scours (left side of the panel). Other, shallower scours are also highlighted in the correlation panel. The section is then erosively overlain by an up to 35 m thick sandstone dominated lobe comprising four amalgamated terminal splays. The correlation panel is interpreted to be at a high angle to flow direction.

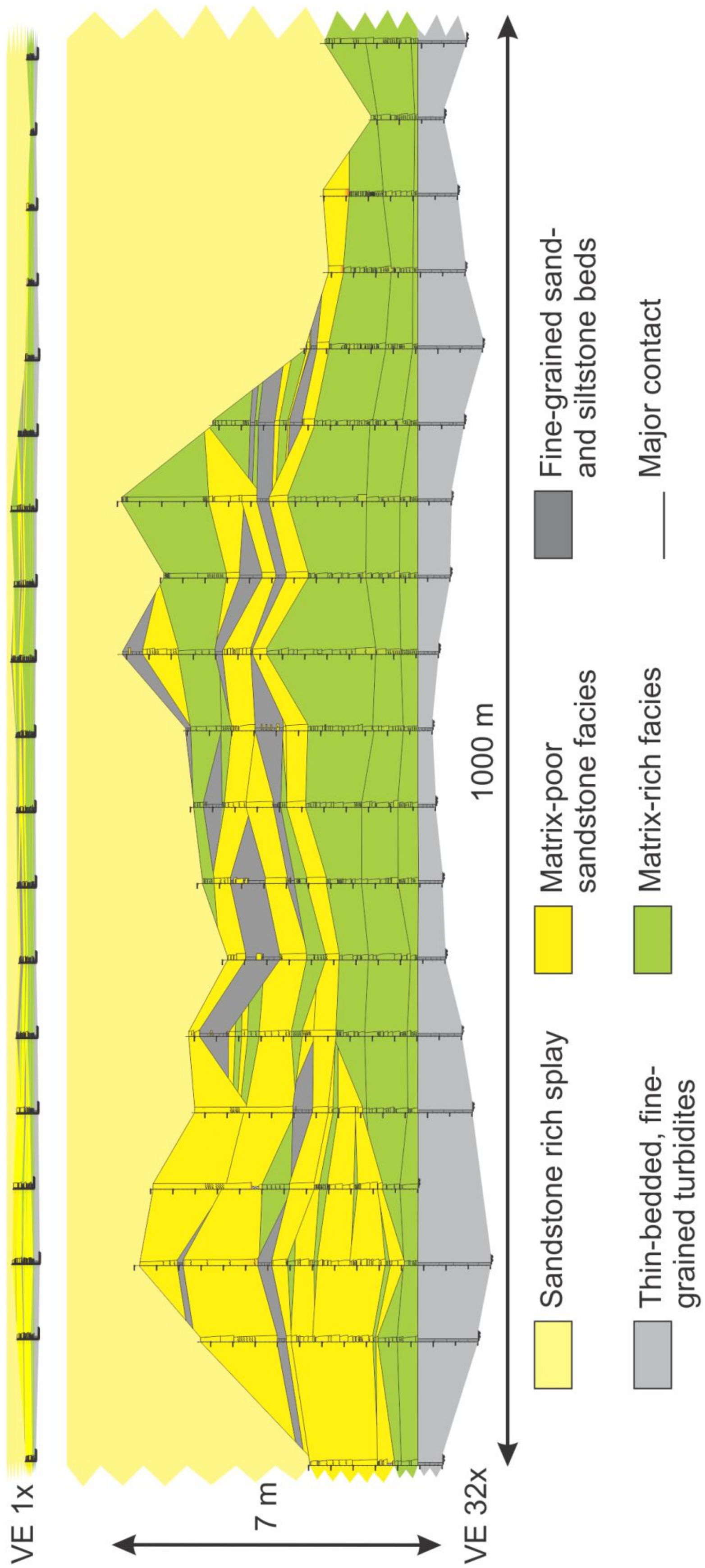

Figure 4.6: Correlation panel shown at VE 1x and VE 32x of an ~7 m thick unit in the upper Kaza (for location see Fig. 2). The unit is divided by a laterally continuous coarse-grained clean sandstone (yellow) bed into a lower and upper sub-unit. In the lower sub-unit matrix-rich beds (green) form an up to 3.5 m thick package comprising mostly non-erosive, laterally continuous beds. These beds, then, are scoured towards the left. The scour reaches a maximum depth of 3 m over ~150 m laterally, and is filled by amalgamated, coarse-grained clean sandstones. Near the margin of the scour matrix-rich and matrix-poor beds are intercalated and matrix-poor beds contain anomalously large, dispersed sand- and mudstone clasts. The upper sub-unit is more heterogeneous with relatively shallow local scours filled by thin-bedded, fine-grained turbidites (grey), clean sandstones and matrix-rich beds. The top of the unit is scoured to a depth of up to 5 m on both sides of the correlation panel. These scours are filled with coarse-grained, amalgamated clean sandstones of the overlying terminal splay, which is part of an up to 18 m thick coarse-grained, amalgamated

sandstone dominated lobe deposit. The correlation panel is interpreted to be at a high angle to flow direction.

4.2.2 Description – matrix-poor sandstone facies

Matrix-poor beds comprise massive to coarse-tail graded subarkose sandstone with 20-30% muscovite-chlorite-silt matrix (Figure 4.7). Grain size typically grades upward from lower very coarse or upper coarse sandstone (1-2 mm) to upper medium or lower medium sandstone (250-500 µm). Within a single bed multiple upward-fining, laterally discontinuous intervals separated by subtle, locally wavy bases can be discerned (Figure 4.7). Rare sub-angular quartz granules are observed also near the base of beds. Beds range from ~10 cm to ~2 m thick. Basal contacts are commonly erosive, with scours up to several dm deep and from several 10s cm to many 10s m wide. Bed tops are only locally preserved and consist of medium-grained structureless or faintly planar laminated sandstone with a thin (up to several cm thick) fine-grained sandstone and siltstone cap. Where beds are amalgamated due to post-depositional erosion, bed contacts are marked by an abrupt increase in grain size and particularly by the presence of quartz granules and can be traced for at least several meters laterally.

Matrix-poor sandstones that are associated laterally with matrix-rich sandstones have similar mineralogical and textural characteristics to coarse-grained sandstones that form terminal splays and channel fills elsewhere in the Windermere Supergroup, but uniquely contain large, tabular sandstone and mudstone clasts (Figure 4.7). Sandstone clasts comprise fragments of matrix-poor, and significantly, matrix-rich sandstone. Mudstone clasts are typically made up of laminated thin-bedded turbidites that commonly are sheared and deformed, although internal structures (e.g. ripple cross-lamination) remain identifiable. Clasts range from several cm thick

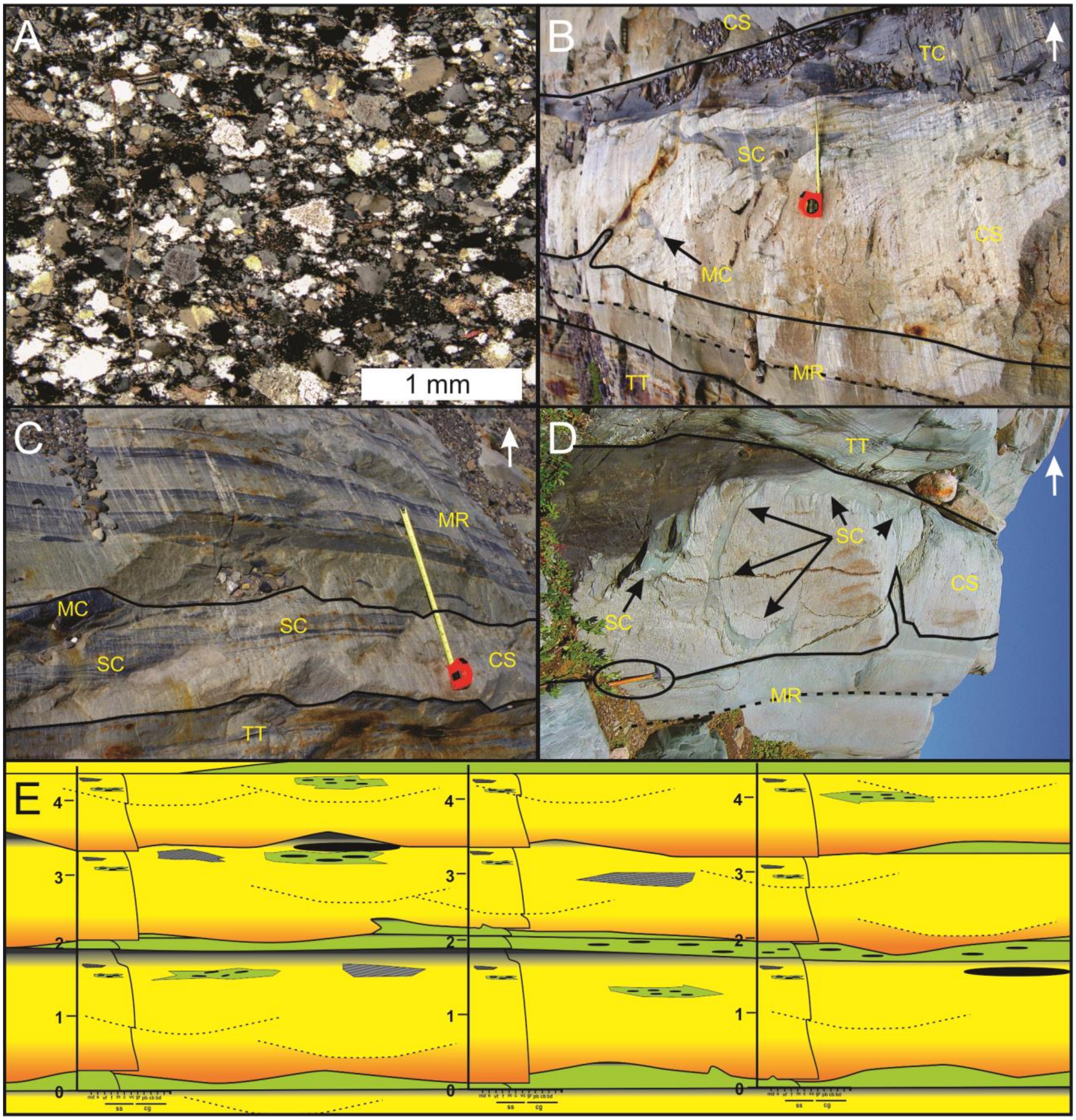

Figure 4.7: (A) Cross-polarized photomicrograph of a matrix-poor sandstone bed. Sample was taken from a bed infilling the 3.5 m deep scour on the left side of Figure 9. (B) Matrix-poor sandstone bed (CS) at the base of the 3.5 m deep scour on the left side of Figure 9. The rust-stained beds at the bottom of the photo (TT) are thin-bedded, fine-grained turbidites (grey in Fig. 9). These turbidites are overlain by two matrix-rich beds (MR), in turn overlain abruptly by the matrix-poor sandstone bed. Note the overall lighter colour of the bed, the erosive base and the large matrix-rich sandstone and mudstone clasts (SC and MC respectively). The bed

is capped by a large internally stratified clast (TC) comprising thin-bedded turbidites that extends beyond the edges of the photograph. Tape measure is 30 cm long. (C) Matrix-poor sandstone bed (base and top indicated by solid lines) sandwiched between matrix-rich sandstone beds. Note the large mud- and sandstone clasts in the matrix-poor sandstone bed. Tape measure is 50 cm. (D) Loading and scouring at the base of a matrix-poor bed (contact and scale indicated by the hammer). Note the large flame structure at the top of the underlying matrix-rich bed. Deformed clasts in the matrix-poor bed comprise matrix-rich sandstone from the underlying bed. Photos A-C from the upper Kaza, photo D from the middle Kaza. (E) Line diagram of intercalated matrix-poor and matrix-rich beds illustrating major lithological features shown also in (B), (C) and (D) (see Fig. 6 for legend). Bed contacts are shown by solid lines. The base of matrix-poor beds is locally erosive and is overlain by coarse-grained sandstone with dispersed granules. Strata then grade typically upward to lower coarse sandstone, but locally grain size increases abruptly within a bed (dotted lines) indicating episodic erosion and subsequent deposition by high-energy turbulent pulses. Anomalously large, dispersed sand- and mudstone clasts, which commonly are internally strtatified, occur locally. Where preserved, beds are then capped by a few-cm-thick sandy mudstone. Matrix-rich beds, on the other hand, comprise medium-grained sandstone capped often by a discontinuous sandy mudstone. Locally matrix-rich beds are steeply eroded; loading and injections are locally present. Three conceptual stratigraphic logs are shown that indicate bed boundaries and grain size changes within beds; vertical scale is in meters, the lateral distance between logs is several 10s of meters.

and long, up to ~15 cm thick and ~1 m long, but uncommon larger sandstone clasts up to several dm thick and several meters long occur also. Along the erosive base of many matrix-poor sandstone beds sandstone sills have intruded locally into older strata and formed what are termed “incipient-clasts” that up to several 10s cm thick, several m long and attached at one end to the parent (Figure 4.2and Figure 4.7). See Figure 4.3for summary sedimentary log.

Matrix-poor sandstones form amalgamated units of comparable thickness to the laterally adjacent matrix-rich unit. Matrix-rich and matrix-poor sandstones are typically intercalated laterally forming a gradual facies transition between adjacent units (Figure 4.5and Figure 4.6).

4.2.3 Stratigraphic occurrence of matrix-rich sandstone units

Matrix-rich sandstones occur, in varying abundance, throughout basin-floor and base-of-slope deposits of the WSG in the study areas. At Mount Quanstrom medial basin-floor deposits of the middle Kaza Group comprise a more than one km thick stack of laterally extensive coarse-sandstone lobe and fine-grained inter-lobe deposits. Here matrix-rich strata are uncommon and only make up <4% of the stratigraphic section, and occur exclusively at the base of terminal splay deposits. They are most common at the base of lobe units, and therefore at the base of the first terminal splay in a larger-scale (up to several 10 m thick) lobe. Also, they occur as up to 1.5 m thick units typically comprising 2-3 beds at the base of individual terminal splays (Figure 3.2). Units of matrix-rich sandstone are commonly eroded by the overlying coarse-grained sandstone splay over distances of several meters to several 10s of meters, and typically have no laterally equivalent matrix-poor sandstones as described above.

In more proximal basin floor strata of the upper Kaza Group at Castle Creek matrix-rich sandstones are more common and make up ~6% of the section. Here too they occur at the base of terminal splays, but also beneath distributary channel fills, and much less commonly are intercalated with fine-grained, thin bedded turbidite deposits and/or individual sandstone beds (see also results of Markov-chain analysis in Section 5.4.2). It is also in the upper Kaza where they are observed to grade laterally into laterally correlative matrix-poor sandstone beds (Figure 4.5, Figure 4.6).

In the base-of-slope channel-levee setting of the Isaac Formation (e.g. Leclair and Arnott, 2003; Arnott, 2007a, b; Khan and Arnott, 2011; Navarro *et al.*, 2007; O’Byrne, 2007; Schwarz and Arnott, 2007) matrix-rich strata are much less common, comprising less than 1% of the stratigraphy. Here they form single and less commonly stacked units up to several m thick that change little in thickness and facies over the width of the outcrop (few 100s m). Moreover, these units are then overlain abruptly by upper medium and coarse-grained sandstone filled channels (Arnott, 2007b).

4.2.4 Interpretation of matrix-rich sandstone facies in the WSG

The maximum grain size observed in matrix-rich beds is lower coarse sand, which can be suspended solely by fluid turbulence (Mulder and Alexander, 2001). High matrix content, however, suggests that cohesive forces, in addition to grain-to-grain interaction, hindered settling and buoyancy most probably also played an important role in grain suspension, in addition to affecting flow behaviour (Mulder and Alexander, 2001; Baas *et al.*, 2009, 2011). The general planar nature of bed bases, scours being uncommon and restricted to a small number of local, few-cm-deep features, suggests turbulence suppression. Coarse-tail grading, on the other hand, indicates that flows were sufficiently dilute and at least minimally turbulent to allow differential grain settling. Alternatively, coarser grains may have settled after deposition through the low-yield strength (fluid saturated) substrate that makes up the bed, resulting in coarse-tail grading. The common mudclasts and abundant matrix in beds suggests that deposition was capacity driven from flows undergoing high rates of sediment fallout (Hiscott, 1994; Leclair and Arnott, 2003). Moreover, the paucity of angular bed forms can also be explained by a high fallout rate that resulted in the rapid burial of incipient bed defects (Arnott and Hand, 1989; Leclair and Arnott, 2005; Sumner et al., 2008, Talling et al., 2012). Alternatively, these characteristics may be a consequence of high near-bed sediment concentration that inhibited particle settling, including tabular, low-density mudclasts, and also suppressed the initiation and/or amplification of bed surface defects that otherwise would have formed angular bed forms (Arnott, 2012). The presence of wavy parallel and planar lamination at the top of some matrix-rich beds, and composed of sand of similar size to that in the underlying, matrix-rich part of the bed, but lacking the high matrix content, suggests that the lamination developed from sediment reworked from the underlying bed during the latter stages of the same sedimentation event. Mudclasts in matrix-rich sandstones comprise relatively small, rounded, massive mudstone. These clasts resemble the silt-mud caps (T_{de} divisions) of fine-grained turbidites that occur throughout the deep-water Windermere Supergroup sedimentary pile, and were sourced upflow from erosion of previously deposited and at least partly consolidated fine-grained sediment. Shearing within the flow was sufficient to deform the clasts, and their even distribution throughout the thickness of the bed indicates that the flows were poorly density or longitudinally stratified, at least in their lower part. Matrix-rich sandstone beds showing no upward change in matrix content (Subfacies 1-3) are interpreted to have been deposited by flows analogous to “quasi-laminar plug flows” (QLPFs) *sensu* Baas *et al*. (2011) or “hyperconcentrated density flows” *sensu* Mulder and Alexander (2001). Conversely, matrix-rich strata with a vertical change in matrix content (Subfacies 4) are interpreted to have been deposited by flows analogous to “upper-transitional plug flows” (UTPFs) or low-concentration QLPFs *sensu* Baas *et al*. (2011), or “concentrated density flows” *sensu* Mulder and Alexander (2001). These flows experience reduced turbulence due to high fine-grained sediment concentration, but even in QLPFs remain turbulent near the bed (Baas *et al*., 2011). Nevertheless, Baas *et al*. strongly emphasize the limitations of direct extrapolation from small-scale laboratory flows with a small number of highly controlled variables to natural flows. The dominant sediment support mechanism in flows that deposited matrix-rich strata described here is interpreted to be hindered settling and not matrix strength, and as a consequence these deposits are not considered debrites *sensu* Middleton and Hampton (1976), Mulder and Alexander (2001), Haughton *et al*. (2009) and Talling *et al.* (2012). The lateral thinning of matrix-rich beds followed by facies change to thin-bedded, fine-grained $T_{(a)cd(e)}$ turbidites with ripple cross-stratification implies a downflow and/or lateral flow evolution that culminated in low-density, low concentration flows analogous to low-density turbidity currents.

4.2.5 Interpretation of matrix-poor sandstone facies in the WSG

Matrix-poor sandstone with grain sizes up to upper very coarse sandstone with rare granules indicate sediment support by a variety of mechanisms, including flow turbulence, grain-to-grain interaction, hindered settling and buoyancy (Mulder and Alexander, 2001). Localized scours along bed contacts indicate that prior to deposition flows were initially energetic and at least locally highly turbulent. Poorly-developed grading, abundance of clasts throughout the bed thickness and absence of traction transport structures indicate that flows were well-mixed vertically and longitudinally, and conditions in the flow changed little during deposition as grains lost to deposition were replenished from higher in the flow (Arnott and Hand, 1989; Kneller and Branney, 1995; Stow and Johansson, 2000; Sumner et al., 2008). These deposits are interpreted to have been emplaced by flows analogous to Lowe (1982) S3 units. Additionally, abrupt intrabed grain size changes and wavy surfaces (Figure 4.7) indicate that during deposition flows became locally erosive and/or non-depositional, which most likely reflects the episodic passage of high- and low-energy turbulent pulses within the flow. The large raft-sized mudstone and sandstone clasts in these beds are distinctly different from clasts elsewhere in Windermere Supergroup stratigraphy; their large size, tabular shape and angularity suggest reduced transport in these energetic flows, and thus are interpreted to have been sourced locally. This is affirmed by the occurrence of “incipient clasts” that are bounded by sandstone injections but remain attached, at least on one end, to the parent strata (Figure 4.2, Figure 4.7). Flows likely “plucked” semi-consolidated blocks of sediment from the seafloor and then deposited them rapidly before they could disintegrate. This “plucking” is interpreted to be related to intense pressure fluctuations within an energetic submerged hydraulic jump that extracted large fragments of the seabed.

4.3 Comparison of matrix-rich strata

Matrix-rich strata described here are distinctly different from debrites described in base-of-slope and basin-floor strata in the Windermere Supergoup (for a comprehensive description and interpretation of debrites in the Windermere Supergroup see Arnott et al., 2011). In the study area debrites are commonly massive, matrix-supported conglomerate that are ~1 m to up several 10s m thick and at least 100s-1000s m wide. Clasts are dispersed in a matrix of silty mudstone and comprise up to several m thick and long, sheared and folded sandstone, mudstone and carbonate fragments and common quartz granules. Matrix-rich sandstones, on the other hand, are notably thinner and much less laterally continuous, and consist typically of medium-grained sandstone with a pervasive matrix of clay (altered to chlorite and muscovite) and minor silt. In addition, clasts are typically smaller and predominantly mudstone (massive or interstratified with siltstone) that resembles local fine-grained strata. Collectively these observations suggest that matrix-rich strata in the study area have a decidedly different origin than their farther-travelled debrite counterparts.

Matrix-rich strata in the Windermere Supergroup superficially resemble “linked debrites”, and the upper debrite part of “co-genetic turbidite-debrite beds” and “hybrid event beds” (e.g. Haughton et al., 2003, 2009; Talling et al., 2004; 2007; 2012; Amy and Talling, 2006;

Hodgson, 2009; Pyles and Jennette, 2009; Talling, 2013) or “slurry beds” and “transitional flow deposits” (Lowe and Guy, 2000; Lowe et al., 2003; Sylvester and Lowe, 2004; Kane and Pontén, 2012), however a number of important differences are noted. A fully developed hybrid event bed has a clean, graded or ungraded, structureless sandstone base (H1 division), followed upward by alternating bands of matrix-rich and matrix-poor sandstone (H2 division), matrix-rich sandstone with mudstone clasts, granules and shear fabrics (H3 division, also termed a linked debrite), parallel- and ripple cross-laminated sandstone (H4 division) and massive mudstone (H5 division). Haughton et al. (2003, 2009) interpreted these divisions to have been deposited from a single flow that underwent a longitudinal transformation from fully turbulent flow with progressive sediment aggradation (H1 division), to transitional flow with intermittent turbulence suppression (H2 division), to laminar flow and en masse freezing of sediment (H3 division), and finally back to turbulent flow (H4 and H5 divisions). Co-genetic debrite-turbidite beds show a similar stratal division with a lower turbidite unit overlain by a debrite (Talling et al., 2004; Hodgson, 2009), although Pyles and Jennette (2009) described co-genetic turbidite-debrite beds in the Ross Formation comprising alternating units of turbidite and debrite during a single depositional event. Transitional flow deposits (Kane and Pontén, 2012) comprise 7 sub-facies, of which “type IV”, “type V” and “type VI” also comprise a lower clean sandstone interval overlain by an argillaceous sandstone interval, but both are interpreted to have been deposited from turbulent and transitional flows. While some matrix-rich beds in the Windermere Supergroup do show an abrupt upward increase in matrix content (see sub-facies 4 above), the basal part of these beds still contains significantly more matrix (30-40%) than “clean” sandstones (up to ~20%) observed elsewhere in deep-water deposits of the Windermere Supergroup (Figure 4.4 and Figure 4.7)., and therefore are unlike sandstones in the H1 division. Moreover, where interbedded (Figure 4.5 and Figure 4.6), matrix-rich and matrix-poor sandstones are commonly separated, except where post-depositionally eroded, by a thin sandy mudstone indicating two discrete episodes of sedimentation (Figure 4.7). The H2 division has not been observed in Windermere Supergroup matrix-rich beds. Subfacies 1, 3 and 4 most closely resemble the H3 division, but in contrast are typically coarse-tail graded (although Haughton et al. (2009) point out that the H3 division may show vertical fractionation of mudclasts, outsized grains and carbonaceous matter), and interpreted to have been deposited, albeit rapidly, grain by grain from turbulent flows that allowed differential grain settling. This, then, differs from the H3 division, which is interpreted to have been deposited from laminar flows and en masse freezing. High-angle ripple cross-stratification (analogous to the H4 division) is not observed at the top of Windermere Supergroup matrix-rich beds, however, the common mud caps are analogous to the H5 division.

Slurry beds are interpreted to have been deposited from turbulent, mud-rich flows that were transitional in character (Lowe and Guy, 2000; Lowe et al., 2003). Distinctive features of slurry beds include abundant dewatering structures and "wispy" lamination (Lowe and Guy, 2000); similar features are also described in Kane and Pontén's (2012) "type I", "type II" and "type III" beds. Both features are absent in the matrix-rich bed of the Windermere Supergroup. Moreover, slurry beds described by Lowe and Guy (2000) are >1 m up to about 15 m thick, and "type I" beds described by Kane and Ponén (2009) are up to 3 m thick. Matrix-rich beds in the Windermere Supergroup, on the other hand, are up to 1 m thick, but generally are centimeters to a few decimeters thick.

In addition to differences in their stratal make-up, the paleogeographic occurrence of matrix-rich beds in the Windermere Supergroup differs also from matrix-rich beds elsewhere.

Linked debrite beds are typically observed “in the lateral and or distal edges of systems otherwise dominated by turbulent flow processes” (Haughton et al., 2009). Pyles and Jennette (2009) describe hybrid beds in basin-margin strata; Hodgson (2009) and Kane and Pontén (2012) also described hybrid event beds and transitional flow deposits to be concentrated near the edges of lobes. Talling et al. (2012) report that low-strength cohesive debrites (Dm-1 in their classification) “are consistently absent in the more proximal parts of systems”, although Talling et al. (2007) report debrite beds on the proximal basin plain in the Agadir Basin. The debrite in the Agadir Basin is, however, much thicker and especially more laterally extensive than typical matrix-rich beds in the Windermere Supergroup, and is probably a better analogue for the debrites described by Arnott et al. (2011). In contrast, matrix-rich sandstones in the Windermere Supergroup are especially common in proximal basin floor strata, but present also in medial basin floor and base-of-slope deposits where they underlie slope channel fills (Arnott, 2007b; O’Byrne *et al*., 2007). This indicates that matrix-rich sandstones described here typically form in more proximal settings compared to previously reported matrix-rich beds, which typically form along the periphery of depositional systems. Moreover, most matrix-rich beds (or matrix-rich parts of beds) have been interpreted to be deposited from flows undergoing a longitudinal change to more cohesive behaviour, whereas matrix-rich beds in the Windermere Supergroup indicate deposition from flows that evolved toward more dilute and fully turbulent conditions at their lateral and/or distal run-out limit.

4.4 Depositional model of matrix-rich strata in the WSG

4.4.1 Summary of observations

Before interpreting the origin of matrix-rich sandstones and explaining their spatial association with matrix-poor sandstones in the Windermere Supergroup, a summary of key observations of matrix-rich strata is presented first:

- consist of massive or coarse-tail graded, medium- to fine-grained sandstone with 30-50% matrix, and capped typically by a few to several cm thick sandy mudstone;
- typically form several meter thick units composed of multiple matrix-rich beds. Less commonly intercalated with coarse-grained sandstones and/or fine-grained turbidites;
- compositionally, texturally and architecturally different from farther-travelled debrites in the Windermere Supergroup;
- matrix-rich sandstone units are commonly adjacent to units of similarly thick but matrix-poor sandstone -- the lateral transition occurring over several 10s to 100s m;
- where interbedded, matrix-rich and matrix-poor sandstones are separated by a typically laterally discontinuous layer of sandy mudstone;
- beds transition laterally over several 10s to 100s meters to fine-grained Tacd and more typically Tcd turbidites;
- matrix-poor sandstones that commonly occur adjacent to matrix-rich sandstones are compositionally similar to coarse-grained sandstone beds that form terminal splay and channel-fill deposits elsewhere in the Windermere Supergroup, but uniquely contain

large sandstone and mudstone clasts. In addition, incipient clasts related to sand injection along the base of beds is common;

- units of matrix-rich sandstone and associated matrix-poor sandstones occur throughout the Middle and upper Kaza (medial and proximal basin-floor fan, respectively) and Isaac Formation (base-of-slope channel-levee systems), but are most common in the upper Kaza (proximal basin-floor setting);

- matrix-rich units typically underlie terminal splays in the middle Kaza, but terminal splays, distributary channels and fine-grained turbidite units in the upper Kaza;

- in the Isaac Formation matrix-rich sandstones underlie slope channels.

4.4.2 Timing of matrix-rich sandstone deposition

Similar to Haughton *et al*. (2009)'s "Type 2" system scale distribution of linked debrites in the Ross Formation (see also their Figure 13B) and Kane and Pontén (2012)'s distribution of transitional flow deposits, matrix-rich beds in the WSG are typically observed at the base of thick coarse-grained sandstone units, and therefore suggestive of the initiation of the local sedimentary system. Haughton *et al.* postulated that these matrix-rich units may be the result of early flows that entered the basin and traveled over "out-of-grade" slopes, which in turn caused erosion and incorporation of fine-grained sediment into the flow. This, then, profoundly modified the rheology and character of the flow, ultimately damping turbulence within the flow. Alternatively, flows with high concentrations of fine-grained sediment may have originated "due to lateral slope failures and/or periods of fan channel incision", which similarly resulted in deposits containing high matrix-content and linked debrites (Haughton *et al*., 2009). A major difference between the distribution of linked debrites in the Ross Formation and matrix-rich strata in the WSG is that in the Ross Formation linked debrites generally only underlie the first major fan deposit. In contrast, matrix-rich beds in the WSG are much more common and are observed throughout the stratigraphy. Here they commonly underlie individual basin floor terminal splays and distributary channels, and base-of-slope sandstone-filled channels. In the WSG, like in the Ross Formation, the abrupt occurrence of matrix-rich strata indicate the large-scale activation of the sedimentary system, but in the WSG also the more common (re-) activation of the smaller-scale, local sedimentary system.

4.4.3 Spatial relation to jet flows and/or hydraulic jumps

From the discussion above it is evident that deposition of matrix-rich beds in the Windermere Supergroup is related to the (local) activation of the sedimentary system, likely due to an upstream avulsion, which implies that flows that deposited these strata underwent a change from relatively confined conditions to unconfined plane-wall jet flow. Direct observation or measurement of natural unconfined turbidity currents on the deep-marine basin floor have to date not been made, but experiments on both submerged and shallow-water unconfined plane-wall jet flows entering a stillwater basin indicate that they can retain their initial speed longitudinally for up to 4 to 6 outlet widths (termed the “zone of flow establishment”, see Rowland et al., 2009 and references within). These flows may or may not be supercritical initially, but can evolve downflow from subcritical to supercritical if, for instance, they were to flow over a locally oversteepened slope (e.g. the margin of a pre-existing lobe). In the zone of flow establishment these super- or subcritical avulsion flows likely scoured the pristine, mud-rich seabed, causing the flow to become rapidly and locally charged with fine-grained sediment (Figure 4.8 and Figure 4.9). Grains that settled through the intensely turbulent sediment dispersion were generally limited to lower coarse sand up to granules and built up a unit of matrix-poor, coarse-grained sandstone immediately adjacent to the high-energy axis of the jet (Figure 4.8 and Figure 4.9). Finer sediment, which consisted of medium sand to clay particles, in addition to rounded mudstone clasts that were unable to settle through the dense sediment suspension, became suspended well above the sea bed and subsequently moved obliquely outward toward the margins of the jet, and it is here that massive or coarse-tail graded, matrix-rich sandstones with common rounded mudclasts accumulated (Figure 4.8 and Figure 4.9). At the same time extensive mixing of ambient fluid within the rapidly expanding current caused it to evolve laterally into a low-concentration turbidity current that then deposited most commonly upper division turbidites (Figure 4.8 and Figure 4.9). Eventually local avulsion related jet flow sedimentation was succeeded by more typical styles of basin-floor sedimentation and the formation, for example, of terminal splay or distributary channels that then buried the avulsion splays.

In the case of supercritical flows that transitioned abruptly downflow to subcritical conditions, intense erosion under the attendant hydraulic jump created the observed several-meter-deep scour (see Figs. Figure 4.5, Figure 4.6, Figure 4.8), and similarly charged the flow with abundant fine-grained sediment. In addition, intense velocity and pressure fluctuations within the jump may have deeply disaggregated the local seabed and allowed large (meters scale), intact fragments of the seabed to be dislodged (Figure 4.8 and Figure 4.9). These large clasts, along with matrix-poor lower coarse sand and coarser sediment, accumulated along the

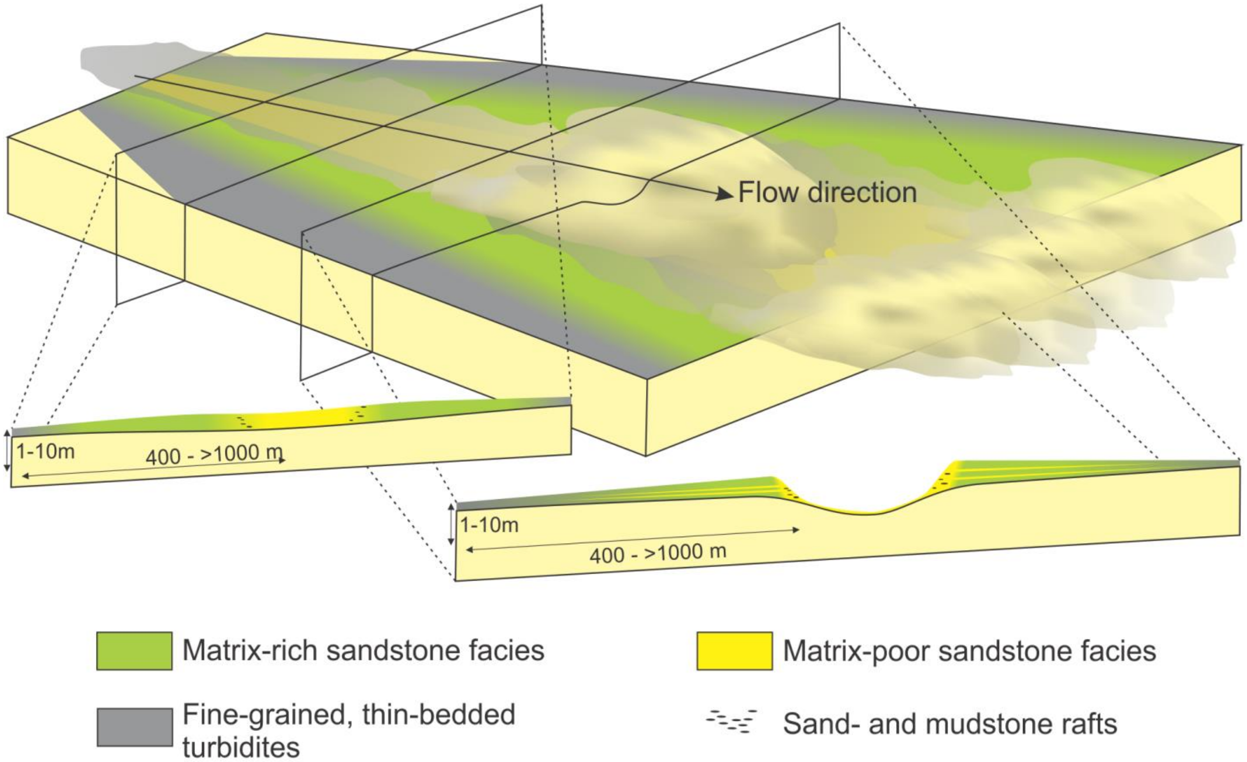

Figure 4.8: Cartoon model of proximal basin-floor matrix-rich bed deposition. Following avulsion plane-wall jets flow over the seabed. Immediately downflow of the avulsion node the flow expands little up to a distance of about 4-6 times the width of the outlet. Here seabed erosion is limited to shallow scours and deposition of matrix-poor sandstone beds that lack large sandstone or mudstone clasts. Matrix-rich beds are deposited further laterally, and then over a distance of several 100 meters laterally transition into thin-bedded, fine-grained turbidites.

If the incoming jet flow is supercritical and undergoes an abrupt flow transition with an associated submerged hydraulic jump, the now rapidly expanding flow deeply scours (up to several m) the seabed and locally excavates meter-scale sand- and mudstone clasts that subsequently accumulate along the margins of the scour. At the same time matrix-rich sandstones formed of sand, but more importantly mud eroded from the central scour, mixed with sediment in the parent flow and deposit along the periphery and possibly downflow of the expanding current. Further laterally these beds thin and transition rapidly into thin-bedded, fine-grained turbidites. Scours are later filled with amalgamated coarse-grained sandstone, which are lithologically similar to those that make-up terminal splays. Additionally, scours and matrix-rich units are commonly overlain by terminal splays. It is therefore likely that after a number of initial avulsion flows more typical basin-floor lobe sedimentation commenced at that location.

margins of the jump. Moreover, the abrupt grain size changes and wavy surfaces within individual matrix-poor beds might represent low-angle scours that formed in a water-saturated by the episodic passage of high and low energy turbulent pulses possibly associated with intense turbulence formed in the jump. Further laterally, like in a simple jet flow, the flow escaping the jump evolved rapidly and deposited matrix-rich sandstones and then fine-grained turbidites. At the same time, but in the jump, the scour remained opened and later became filled during the onset of more typical basin-floor lobe sedimentation.

4.4.4 On the stratigraphic distribution of matrix-rich beds in the WSG

The proposed model of matrix-rich bed deposition as a result of an upflow avulsion, rapid flow expansion and seabed erosion predicts that matrix-rich beds can be deposited anywhere along the transport pathway of a turbidity current, provided there is an upstream avulsion node. Notwithstanding, matrix-rich strata are most common in a proximal basin-floor setting (i.e. the upper Kaza Group in the WSG, Ross and Arnott, 2007), or equivalently channel-lobe transition zone (CLTZ, Wynn *et al*., 2002). Here, flow avulsions result in the lateral shifting of the entire depositional system as lobes switch laterally, and presumably it is here where jet flows and/or hydraulic jumps are most energetic. Accordingly, it is here, that matrix-rich sandstones are most common in deep-marine strata of the WSG, and also where they are clearly associated with large erosive features on the basin-floor. The process of flow avulsion and subsequent flow expansion is, however, not restricted to the CLTZ, and may occur elsewhere in the system. In a base-of-slope channel-levee system, for example, local avulsions might occur at levee breaches, and form downflow crevasse splay deposits adjacent to the parent channel. In the Isaac Formation up to

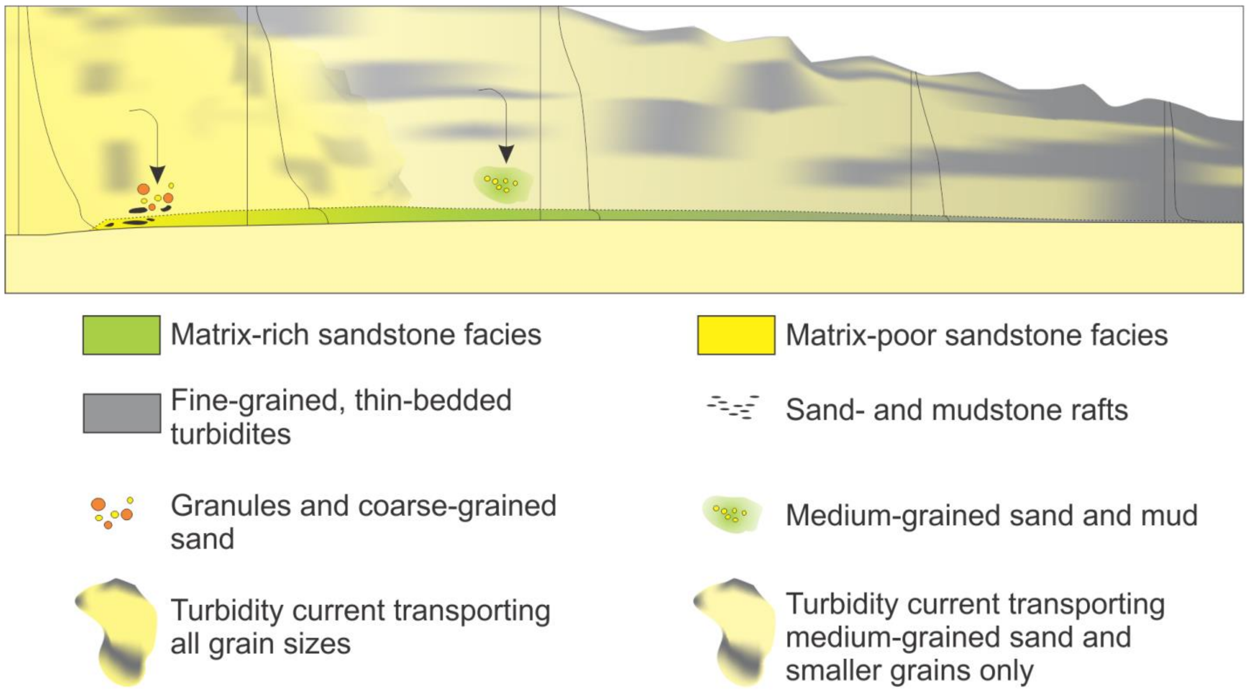

Figure 4.9: Illustration showing the lateral evolution of flow concentration across and lateral to a plane-wall jet and its deposit. In the axial area (left side of the diagram) flow concentration is highest near the bed and rapidly diminishes upward (moderately stratified flow). Intense turbulence at the bed results in local seafloor erosion, which typically is dominated by mud-rich sediment, and the continued transport of coarse-grained sediment. Along the margins of the jet, flow energy rapidly diminishes and the increased sediment concentration in the near-bed region dampens turbulence. This, then, results in rapid deposition of coarse-grained, matrix-poor sandstone, and, if present, large mud- and sandstone clasts. Further laterally the flow becomes rapidly depleted in coarse-grained sediment, especially coarse sand and coarser, and relatively enriched in fine-grained sediment. The flow now becomes plug-like with a significantly reduced vertical sediment concentration gradient. It is under these conditions that matrix-rich sandstones are deposited. Still further laterally, the loss of sediment by earlier deposition, in addition to the continuous entrainment of ambient fluid, causes the now low sediment concentration flow to become fully turbulent, and accordingly, the deposition of fine-grained, thin-bedded turbidites.

several-meter-thick matrix-rich units overlain by sandstone-filled channels in the Isaac Formation have been interpreted to be crevasse splays (Arnott, 2007b; O'Byrne *et al*., 2007) that according to Arnott (2007b) are equivalent to seismically-resolved stratal features termed "high amplitude reflection packages", or HARPs. In a more distal basin-floor setting setting dominated by terminal splay deposition upflow avulsion results in deposition of matrix-rich units that are significantly thinner and less common than in more proximal settings.

4.4.5 On the paucity of matrix-rich beds in more distal settings (middle Kaza Group) in the WSG

To date all studies that describe matrix-rich sandstones have shown them to occur in lobe, fan, or basin fringes, and most attribute their formation to flow transformation from turbulent to transitional or laminar flow (e.g. Haughton et al., 2009; Pyles and Jennette, 2009; Kane and Pontén, 2012), although Talling et al. (2007; 2010; 2012) describe debrites that originated on the continental slope and are far-traveled. In contrast matrix-rich sandstones, while present in more distal deposits in the Windermere Supergroup (middle Kaza Group), are most common in proximal basin-floor deposits (upper Kaza Group). This disparity in spatial occurrence begs the question whether the most distal fringes of the deep-water fan and/or lobes of the Windermere Supergroup are not exposed (or not yet studied), or there is a different explanation for their paucity in more distal settings.

The middle Kaza Group has been interpreted to represent a medial basin-floor setting, and is to date the most distal part of the Windermere Supergroup that has been studied in detail. This means that the most distal part of the fan has indeed not been studied, and that matrix-rich beds could theoretically be more abundant in fan-fringe settings. However, several instances of lobe fringes are exposed in both the middle and upper Kaza, and do not contain matrix-rich beds, but rather consist of matrix-poor sandstone transitioning rapidly laterally into thin-bedded, fine-grained, upper division turbidites. This, then, implies that flows on the basin floor in the

Windermere Supergroup did not transform into transitional or laminar type flows on their lateral or distal run-out margins, and that matrix-rich beds in the Windermere Supergroup generally formed downflow of an avulsion node. Here an alternative explanation for the paucity of matrix-rich beds is proposed.

As stated above, long-traveled mud-rich flows or debrites are unlikely the origin of matrix-rich beds described in this study; the debrites described by Arnott et al. (2007) are probably long traveled debrites. In many models proposed for the origin of matrix-rich sandstone beds (including this study) formative flows were initially sandy turbidity currents with relatively low mud content. The mud component, then, was sourced locally by erosion of either the lower slope or basin floor (e.g. Haughton et al., 2009, Pyles and Jennette, 2009). This implies a pre-condition for the formation of matrix-rich beds: the local presence of erodible mud on the seafloor. In the Windermere Supergroup this condition was met following avulsion, which shifted the path of turbidity currents to flow over previously off-axis (fine-grained) deposits. Downflow of the avulsion node, however, sandstone-dominated architectural elements (distributary channels and terminal splays) blanketed the fine-grained strata rapidly. In the Windermere Supergroup these elements comprise very coarse sandstone and locally granular conglomerate beds up to several meters thick (Meyer and Ross, 2007), which would have protected the underlying fine-grained strata from erosion by subsequent flows. Most flows that reached the medial basin-floor, then, lacked access to an erodible muddy substrate, and as a consequence lacked the requisite mud for matrix-rich sandstone deposition. Previous studies that described matrix-rich sandstones on the margins of fans or lobes are relatively finer-grained (fine to medium sand) systems: e.g. the Britannia Sandstone (Lowe and Guy, 2000), Brae-Miller and Magnus fans (Haughton, 2003), Ross Formation (Pyles and Jennette, 2009), Tanqua depocentre, Karoo Basin (Hodgson, 2009). This, then, raises the question: is the distribution of matrix-rich beds in Windermere Supergroup unique among the published examples because of the comparatively coarse-grained nature of the depositional system? Future research will no doubt describe matrix-rich sandstones in many more depositional systems and thereby provide further insight into the origin of these enigmatic deposits.

4.5 Conclusions

Matrix-rich sandstones in the deep-water deposits of the WSG comprise massive to coarse-tail graded sandstones with 30% to up to ~50% matrix content, rarely matrix content increases abruptly in the upper half of the bed. Beds commonly contain small, rounded mudstone clasts and rarely are capped by ripple cross-stratified sandstone. Although seemingly similar to "slurry beds" (e.g. Lowe and Guy, 2000), "linked debrites" (e.g. Haughton *et al*., 2009), "hybrid beds" (e.g. Hodgson, 2009) and "co-genetic debrite-turbidites" (e.g. Talling *et al*., 2004), a number of important differences are noted.

Matrix-rich strata are related directly with their lateral equivalent deposits, which include erosive coarse-grained sandstone beds that contain large, tabular mudstone and sandstone clasts and interfinger with matrix-rich beds, and up to several meter deep coarse-sandstone filled scours. Based on these observations it is inferred that matrix-rich strata in the WSG were deposited as a direct result of upflow avulsion. In some cases the resulting plane-wall jet underwent a hydraulic jump some distance from the avulsion node that locally enhanced seabed erosion and supercharged the flow with fine-grained sediment. Within the jump the flow rapidly mixed its sediment load and then downflow and laterally collapsed rapidly. Along the proximal margins of the jet flow and hydraulic jump coarse-grained, matrix-poor sandstones containing large sand- and mudstone rafts were deposited. Further downflow energy was dissipated by rapid deposition of matrix-rich beds, which then transition rapidly into fine-grained thin-bedded upper division turbidites.

Matrix-rich beds are most common in proximal basin-floor strata (channel-lobe transition zone). Here avulsions result in energetic plane-wall jets and/or hydraulic jumps, and accordingly matrix-rich strata are observed most commonly lateral to coarse-grained sandstones that filled jet or hydraulic jump scours. Matrix-rich beds are also observed in more distal basin-floor strata underlying terminal splays and distributary channels, indicating that smaller-scale avulsions of feeder and distributary channels result also in seafloor erosion of fine-grained sediment. In base-of-slope channel-levee settings matrix-rich sandstone units are adjacent to slope channels, and are interpreted to be crevasse splays. This, therefore, indicates that matrix-rich strata are not location specific, but instead are the result of a suite of sedimentological conditions commonly associated with channel avulsion.

Chapter 5: Spatial organization and temporal evolution of the stratal elements that make-up deep-marine, basin-floor lobes and fans – insights from the Neoproterozoic Kaza Group, Windermere Supergroup, southern Canadian Cordillera.

5.1 Introduction

Chapters two, three and four in this thesis described and interpreted the sedimentary facies (small scale) and stratal elements (meso scale) in deep-water, basin-floor strata of the Winderemere Supergroup. This chapter begins with a brief overview of the largest scale depositional systems on the basin floor, namely submarine lobes and fans, and then:

1. populates basin-floor lobes with their composite meso-scale stratal elements based on their spatial and stratigraphic relationships, and then proposes an evolutionary depositional model that forms basin-floor lobes;
2. populates the composite basin-floor fan with the component lobes;
3. describes the long-term evolution of the basin-floor fan system in the WSG based on changes in the vertical and lateral stacking of stratal elements in the large, km scale stratigraphy;
4. creates realistic artificial 1D stratigraphic logs of proximal basin-floor strata using Microsoft Excel™.

5.2 Submarine fans and lobes

5.2.1 History of submarine fan models

Submarine gravity flows are the principal mechanisms that transport coarse-grained sediment from the continental shelf and slope onto the deep marine basin floor (Menard, 1955; Mutti and Normark, 1987, 1991; Shanmugam *et al*., 1994). These flows derive their energy from gravity that acts on suspended sediment, propelling them down the continental slope, and in many cases onto the basin floor (Shanmugam *et al*,, 1994). There, a dramatic reduction in slope causes flows to become depletive and deposit much of their sediment load in large-scale depositional features termed submarine fans (Menard, 1955; Mutti and Normark, 1987, 1991; Posamentier and Kolla, 2003; Posamentier and Walker, 2007; Mulder and Etienne, 2010). In the modern oceans submarine fans exhibit a variety of shapes and sizes, with a length and width ranging from a few tens to more than a thousand kilometers (Figure 5.1). As a consequence, even the smallest examples are typically much larger than even the largest single outcrop analogue, an important dimensional disparity that has been recognized for the past several decades (e.g. Normark, 1978; Walker, 1992). Furthermore, fans can form deposits that range up to many kilometers thick, especially in actively subsiding basins. Accordingly, the study of these large depositional systems has typically been conducted using geophysical (mainly seismic) methods, with most early stratigraphic models were based on geophysical data (e.g. Normark, 1970; Vail *et al*., 1977; Bouma *et al*.., 1985; Posamentier *et al.*, 1988, 1991; Reading and Richards, 1994). In early works it was recognized that several factors, including sediment supply, tectonic regime and sea level, played a major role in the delivery of sediment into the deep ocean, and in turn controlled the characteristics of the submarine fan (Vail *et al*., 1977; Bouma *et al*.., 1985; Posamentier *et al.*, 1988, 1991; Reading and Richards, 1994; Reading, 1996). Interactions of these factors are complex, and a single fan model or classification scheme is unable to capture the myriad depositional scenarios in a satisfying manner. Notwithstanding, general fan models are a useful tool for communicating key process-response relationships and predicting the large-scale morphology of basin-floor fans (e.g. Reading and Richards, 1994).

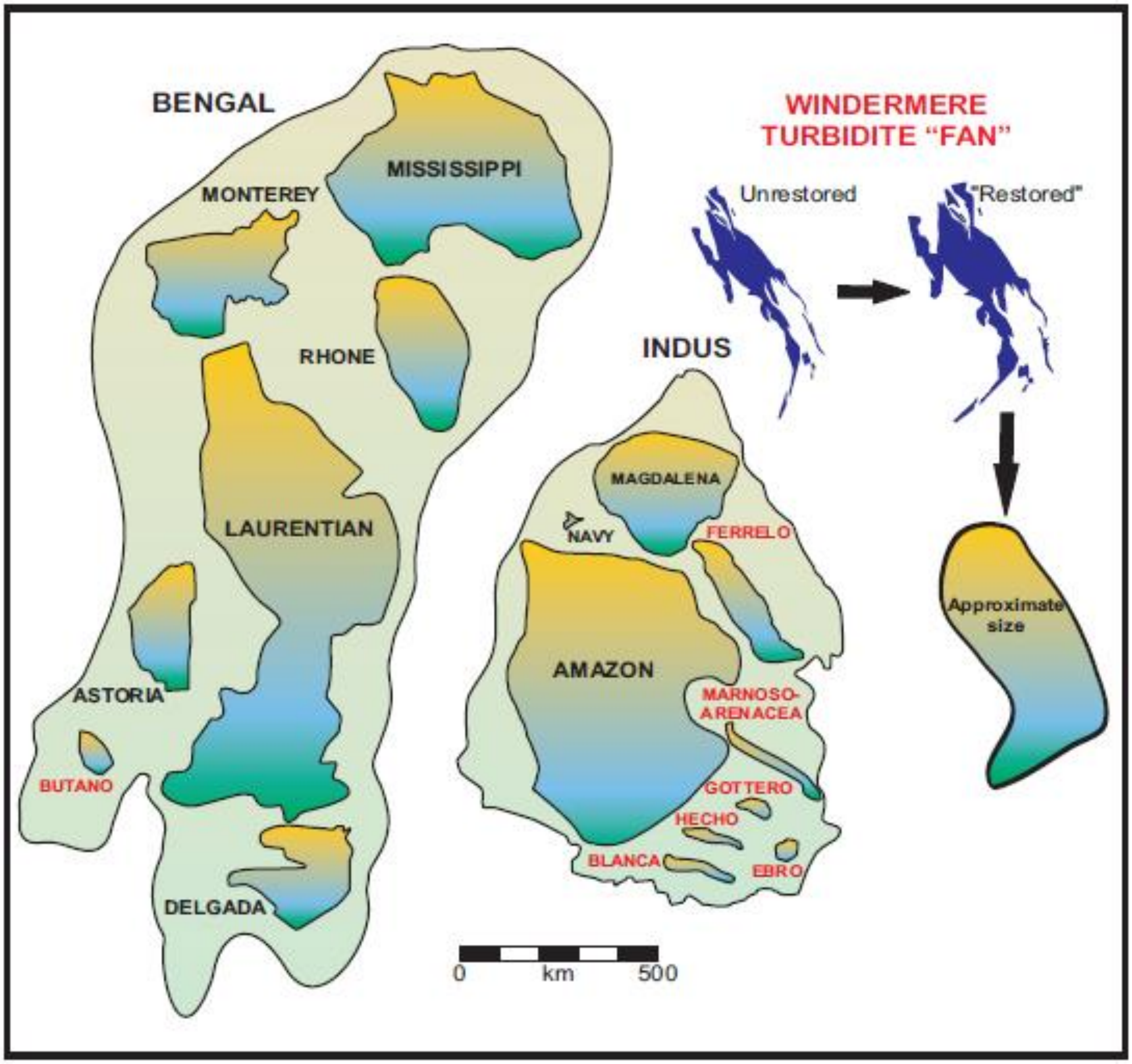

Figure 5.1: Comparison of fan sizes in modern (black text) and ancient (red text) turbidite systems. Palinspastic restoration of the Neoproterozoic Windermere turbidite system is included for dimensional comparison (redrawn by Khan (2012), inset map of the WSG from Ross, 2001, modified from Barnes and Normark, 1985).

The first submarine fan model was proposed by Normark (1970) and in a down-flow direction consisted of an upper fan, mid- or suprafan and lower fan (Figure 5.2). The upper fan was characterized by large leveed fan-valleys that down-flow formed a network of smaller distributary channels on the suprafan, and ultimately sheet deposits in the lower fan region (Normark, 1970). Since this original publication submarine fan models have used the same, or similar terminology to describe the various parts of a fan beyond the slope-break (e.g. Mutti and Ghibaudo, 1972; Damuth and Kumar, 1975; Moore *et al*., 1978; Walker, 1978; Mutti, 1985). These early models, however, did not address several key variables that subsequently have been shown to profoundly influence fan morphology, including sea-level fluctuation, tectonics and sediment calibre (Reading and Richards, 1994; Stow and Mayall, 2000). Since then, scientific and maybe more profoundly economic interest in these systems has grown significantly, and accordingly, various workers have proposed more refined and complete models.

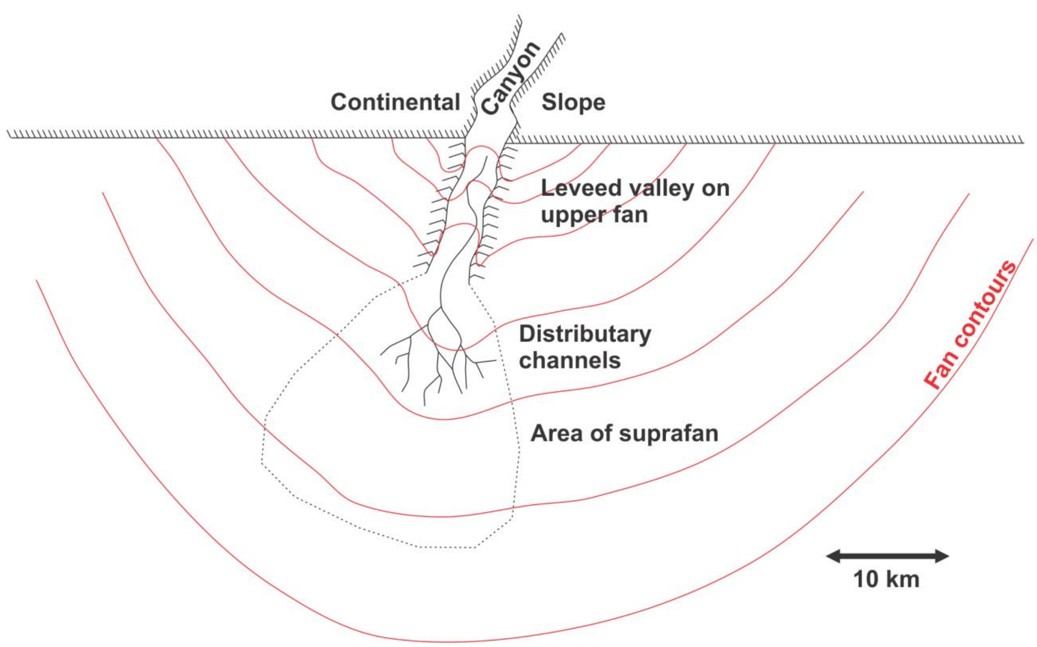

Figure 5.2: Fan growth model of Normark (1970) comprising an upper-, middle- (supra-) and lower fan. The upper fan is characterized by a leveed channel valley, the middle fan contains many smaller distributary channels, which are absent from the sheet-like morphology of the lower fan (redrawn from Normark, 1970).

Mutti (1985) proposed a model that took into account the volume of the input gravity currents; Shanmugam and Moiola (1988) focused on models that described fan morphology from various tectonic settings; Mutti and Normark (1987, 1991) introduced for the first time a hierarchical system where smaller scale architectural elements populate larger composite sedimentary bodies, in total forming five scale orders. To date, however, arguably the most comprehensive classification scheme for submarine fans was proposed by Reading and Richards (1994), which subsequently was updated by Stow and Mayall (2000) (Figure 5.3). This classification categorizes submarine fans based on their input sediment calibre (mud-, sand- and gravel-rich systems) and nature of the input source (point source, multiple source ramps and slope apron linear source). In virtually all submarine fan models, including Stow and Mayall's, the most distal part of the depositional system consists of unconfined, lobate features termed depositional lobes, and it is these features that are of particular interest in this study of the middle and upper Kaza Group, and are examined in more detail below.

5.2.2 Depositional lobes

The term "lobe" is commonly used to describe a morphological unit in deep-water turbidite systems with an ovoid planform shape and positive topography. However, the term "lobe" has been used variously to describe a variety of depositional structures or features since its introduction by Normark (1970), and accordingly resulted in considerable confusion and a need to define how the term is used in each context. For example, Bouma (1985) used the term

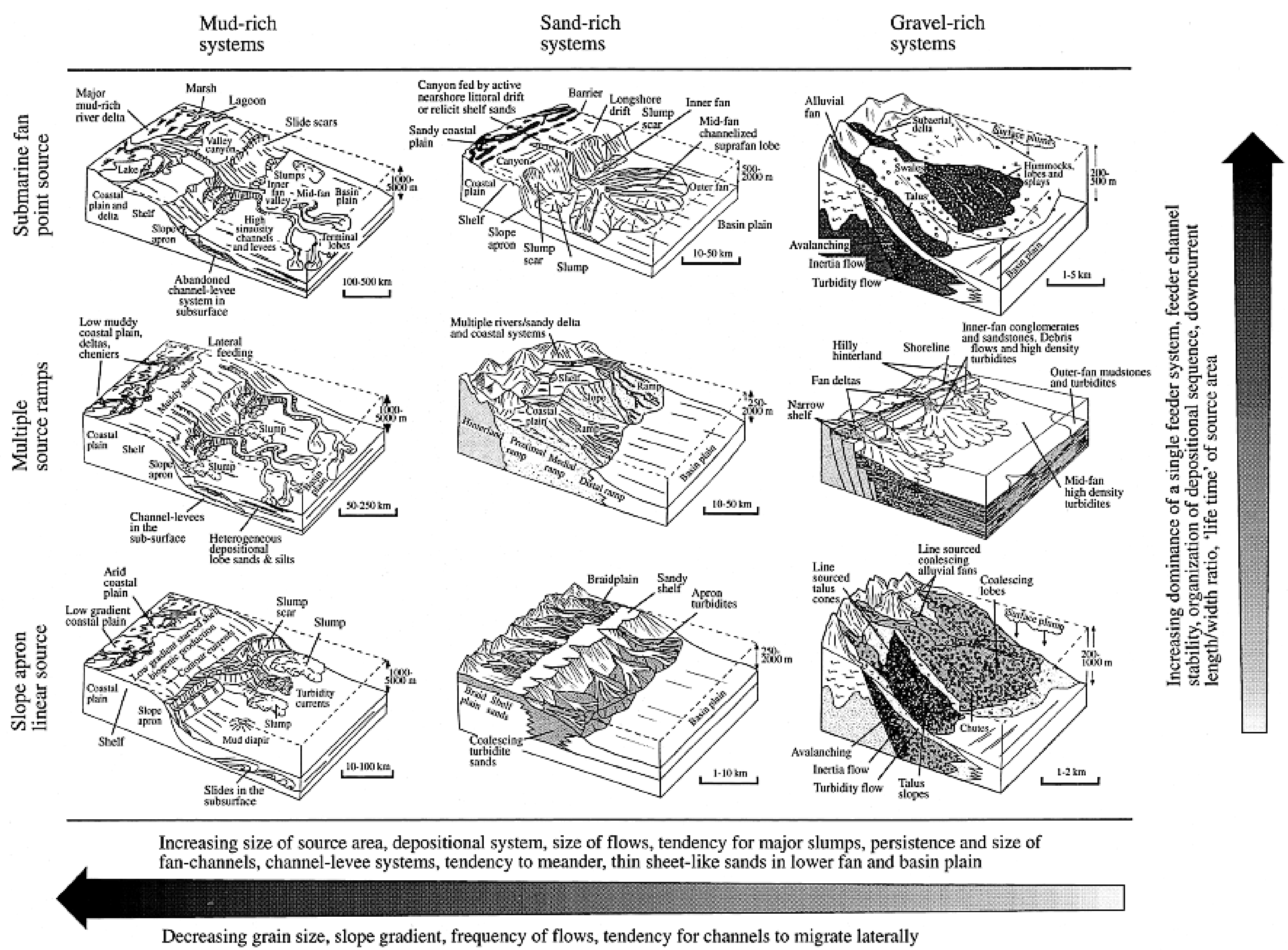
Mud-rich systems
Sand-rich systems
Gravel-rich systems
Submarine fan point source
Multiple source ramps
Slope apron linear source
Major mud-rich river delta
Marsh
Lagoon
Slide scars
Valley canyon
Lake
Coastal plain and delta
Shelf
Slope apron
Slumps
Inner fan valley
Mid-fan
Basin plain
High sinuosity channels and levees
Terminal lobes
Abandoned channel-levee system in subsurface
1000-5000 m
100-500 km
Canyon fed by active nearshore littoral drift or relicit shelf sands
Sandy coastal plain
Barrier
Longshore drift
Slump scar
Inner fan
Mid-fan channelized suprafan lobe
Canyon
Coastal plain
Outer fan
Basin plain
Slump
500-2000 m
10-50 km
Alluvial fan
Subaerial delta
Surface plume
Swale
Talus
Hummocks, lobes and splays
200-500 m
Avalanching
Inertia flow
Turbidity flow
1-5 km
Low muddy coastal plain, deltas, cheniers
Lateral feeding
Coastal plain
Channel-levees in the sub-surface
Heterogeneous depositional lobe sands & silts
50-250 km
Multiple rivers/sandy delta and coastal systems
Hinterland
Proximal ramp
Medial ramp
Distal ramp
Ramp
250-2000 m
Hilly hinterland
Shoreline
Inner-fan conglomerates and sandstones. Debris flows and high density turbidites
Fan deltas
Narrow shelf
Outer-fan mudstones and turbidites
Mid-fan high density turbidites
Arid coastal plain
Low gradient coastal plain
Slump scar
Turbidity currents
Mud diapir
Slides in the subsurface
10-100 km
Braidplain
Sandy shelf
Apron turbidites
Braid plain
Shelf sands
Coalescing turbidite sands
1-10 km
Line sourced talus cones
Line sourced coalescing alluvial fans
Coalescing lobes
Chutes
Talus slopes
200-1000 m
1-2 km
Increasing dominance of a single feeder system, feeder channel stability, organization of depositional sequence, downcurrent length/width ratio, 'life time' of source area
Increasing size of source area, depositional system, size of flows, tendency for major slumps, persistence and size of fan-channels, channel-levee systems, tendency to meander, thin sheet-like sands in lower fan and basin plain
Decreasing grain size, slope gradient, frequency of flows, tendency for channels to migrate laterally

Figure 5.3 (previous page): Classification of deep-water systems based on grain size and nature of sediment supply: single point (submarine fan), multiple sources (ramp), or linear source (slope apron) (from Stow and Mayall, 2000; after Reading and Richards, 1994).

“fan lobe” to describe the most recent channel-levee complex of the Mississippi turbidite system. However, many authors use the term “lobe” or “depositional lobe” to refer to the distal, unconfined and unchannelized part of an active or abandoned channel-levee system (Mutti and Ricci Lucci 1972; Normark, 1978; Mutti and Normark, 1987). The most recent definition of a “depositional lobe” describes a sedimentary body with low positive topography and lobate shape that forms on the distal end of channel-levee systems (Mulder and Etienne, 2010). In this study the definition is expanded to include all stratal elements that were created by flows sourced from a single upstream leveed-channel complex between major avulsion events.

Lobes at the ends of channel-levee systems are either attached or detached. In systems with a high sand/clay ratio (e.g. Valencia Fan, Morris *et al*., 1998; Laurentian Fan, Normark *et al*., 1983) lobes are detached from the channel mouth. The intervening zone is termed the Channel-Lobe Transition Zone (CLTZ) and characterized by by-pass and/or erosion (Wynn *et al*., 2002). In systems with low sand/clay ratio (e.g. Zaire Fan, Savoye *et al*., 2000; Mississippi Fan, Twitchell *et al*., 1992), however, the CLTZ is absent. High-resolution seismic has shown also that lobes can be connected to the main channel-levee system by smaller feeder channels that lack levees (Saller *et al*., 2008). Several lobes that are associated with the same main leveed channel form lobe complexes of the order of several tens of km long/wide, and several 10s of m thick. Three main styles of lobe stacking are recognized: aggradational, shingled or compensational (Bouma, 2000). These complexes, in turn, stack to form the distal part of a submarine fan.

The planform shape of lobes varies based on sediment input (Reading and Richards, 1994; Stow and Mayall, 2000) and spatial confinement (Jegou, 2008; Jegou *et al*., 2008). Lobes have a typical length and width of 10-20 km and are typically 5-40 m thick (Jegou, 2008; Prélat *et al*., 2010). In cross-section lobes typically have a flat planar upper surface with steeper slopes along the sides (Mulder and Etienne, 2010). Due to the preferential loss of a significant part of the fine sediment fraction during transport through the channel-levee system, flows entering the basin-floor sedimentary system are typically relatively enriched in sand, and lobes therefore comprise typically sand-rich deposits, although the initial sediment input can remain little changed in short (length) systems (Mulder and Etienne, 2010). With more recent advances in high-resolution seismic and detailed outcrop studies it has been increasingly recognized that lobes are composed of smaller scale elements with a length and width of few 100 m to few km and several m thick (termed lobe elements by Saller *et al*., 2008; Prélat *et al.* 2009; Mulder and Etienne 2010, lobe units by Gervais, 2002; Gervais *et al*., 2006; Deptuck *et al*., 2008; stratal elements in this study; see also section 3.2). Stratal elements, in turn, are composed of beds (i.e. single event beds). The internal architecture of lobes, and by extension the composite submarine fan, is more complex than that proposed in the early stratigraphic models.

This study adopts the following stratigraphic hierarchy, from smallest to largest: event bed, stratal element, lobe, lobe complex (not observed in the stratigraphy at the scale of the outcrops) and submarine fan. Chapter 1 focuses on event bed scale description and interpretation, which then are used to populate and aid in interpreting the formative processes of stratal elements in Chapters 2 and 3. The following sections (Section 5.3 and 5.4) describe the distribution of these stratal elements in the middle and upper Kaza Group and build a model for internal lobe architecture (Section 5.5). The large (km) scale stratigraphy of the WSG has been interpreted to represent a prograding continental margin wedge (Ross and Arnott, 2007), and by extension the long-term stratigraphic trends in the middle and upper Kaza provide insight into the WSG's prograding submarine fan architecture (Section 5.5.1).

5.3 Stratal element distribution in the middle and upper Kaza Group

The middle and upper Kaza Group comprise seven stratal elements: isolated scours, avulsion splays, feeder channels, distributary channels, terminal splays, fine-grained turbidite deposits and debrites. The shapes, sizes and internal facies arrangement of these elements were described in chapters three and four and are summarized in Table 1. Here, these same elements are assembled into a larger spatial and stratigraphic context. First, in sections 5.3.1 and 5.3.2, general observations are presented that describe the lateral and vertical relationships between stratal elements, followed by a Markov Chain analysis (section 5.4) on the lower ~100 m thick part of the upper Kaza outcrop that quantitatively describes the natural vertical relationships between stratal elements. These data, then, are used in conjunction with existing basin-floor lobe models to propose a model for internal lobe architecture, and ultimately a model for the prograding basin floor fan of the WSG (see section 5.5).

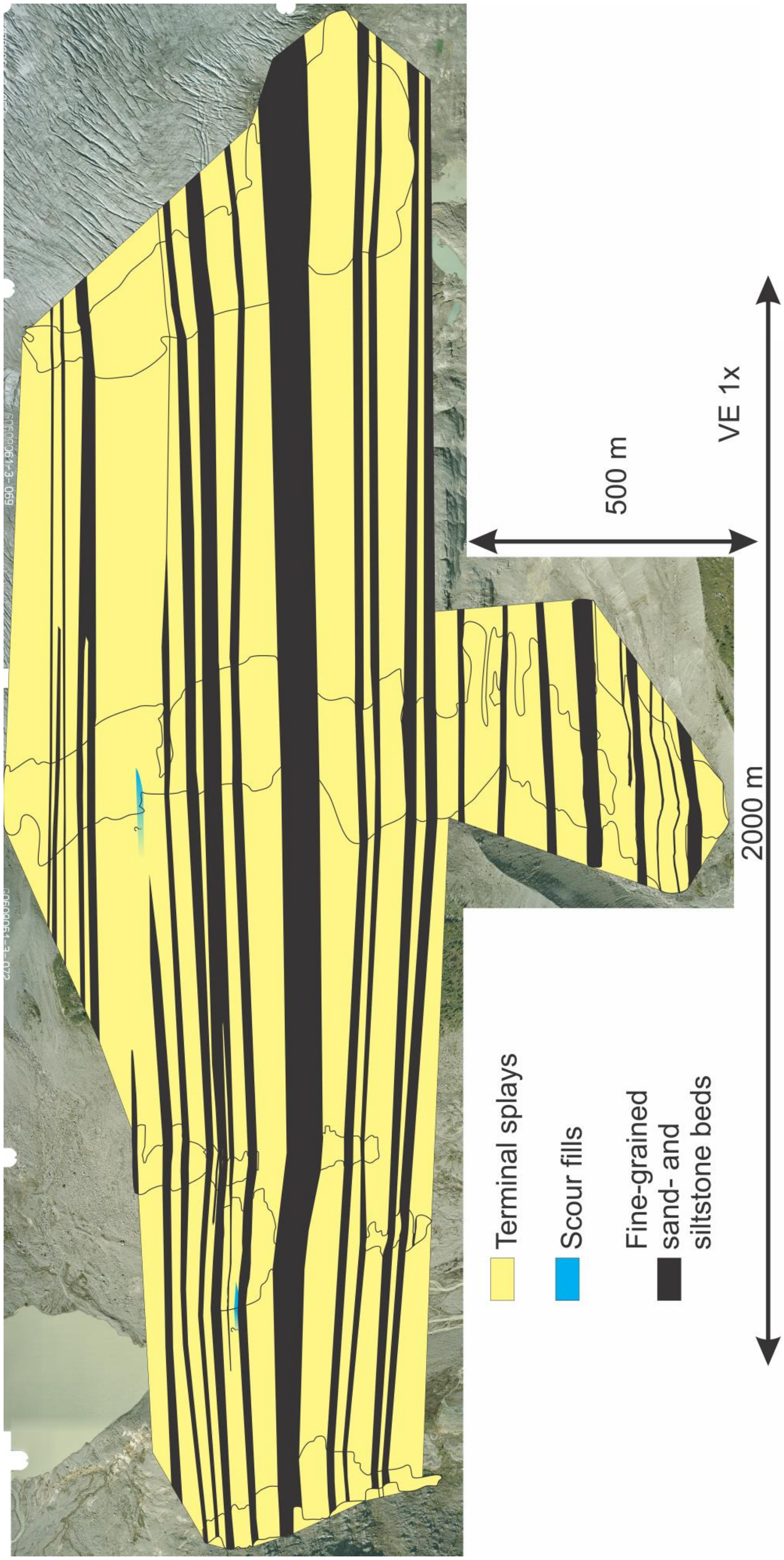

Figure 5.4: Correlation panel of the middle Kaza outcrop at Mt. Quanstrom. Note the simple stratal architecture composed almost exclusiverly of terminal splays and fine-grained turbidite units. Avulsion splays form laterally discontinuous units commonly <1 m thick, and because of their thinnes are not shown in this diagram. Thin black lines delineate the accessible and mapped outcrops.

5.3.1 Stratal element distribution in the middle Kaza Group

At Mt. Quanstrom the middle Kaza comprises four stratal elements: terminal splays, isolated scours, avulsion splays and fine-grained turbidite units (Figure 5.4). Terminal splays are comprised of 75-100% amalgamated coarse-grained sandstone, and are up to ~10 m thick. These stratal elements most commonly stack vertically to form amalgamated sandstone units up to several Dm thick (Figure 5.4) that typically are continuous across the two km wide outcrop without significant lateral change in the sandstone to mudstone ratio. Stacked terminal splays are typically amalgamated, which commonly makes it difficult or impossible to discern bounding surfaces within the larger-scale sandstone units. As a result their stacking arrangement (aggradational, shingled or compensational) cannot be determined. Terminal splays are rarely observed adjacent to other stratal elements, which is interpreted to reflect their large lateral extent that greatly exceeds the width of the outcrop. In the middle Kaza, terminal splays are uncommonly terminated laterally by isolated scours, or transition gradually, although rapidly (over several 10s to 100s of meters) into coarse-grained, medium-bedded sandstone interbeded with fine-grained turbidites.

Only two isolated scours are identified in the middle Kaza, and both are only partly exposed (Figure 5.4), therefore their lateral extent is not known. They occur near the base of two several Dm thick sandstone units. Scours are up to 5 m deep and truncate coarse-grained sandstone beds of a terminal splay (Figure 3.2 and Figure 5.5). The fill of the upper scour comprises amalgamated coarse-grained sandstone that drapes the basal surface (Figure 5.5), whereas beds near the base of the lower scour onlap the erosional surface (Figure 3.2), but towards the top progressively follow the contour of the scour and are continuous outside the scour, where they form the base of the overlying terminal splay.

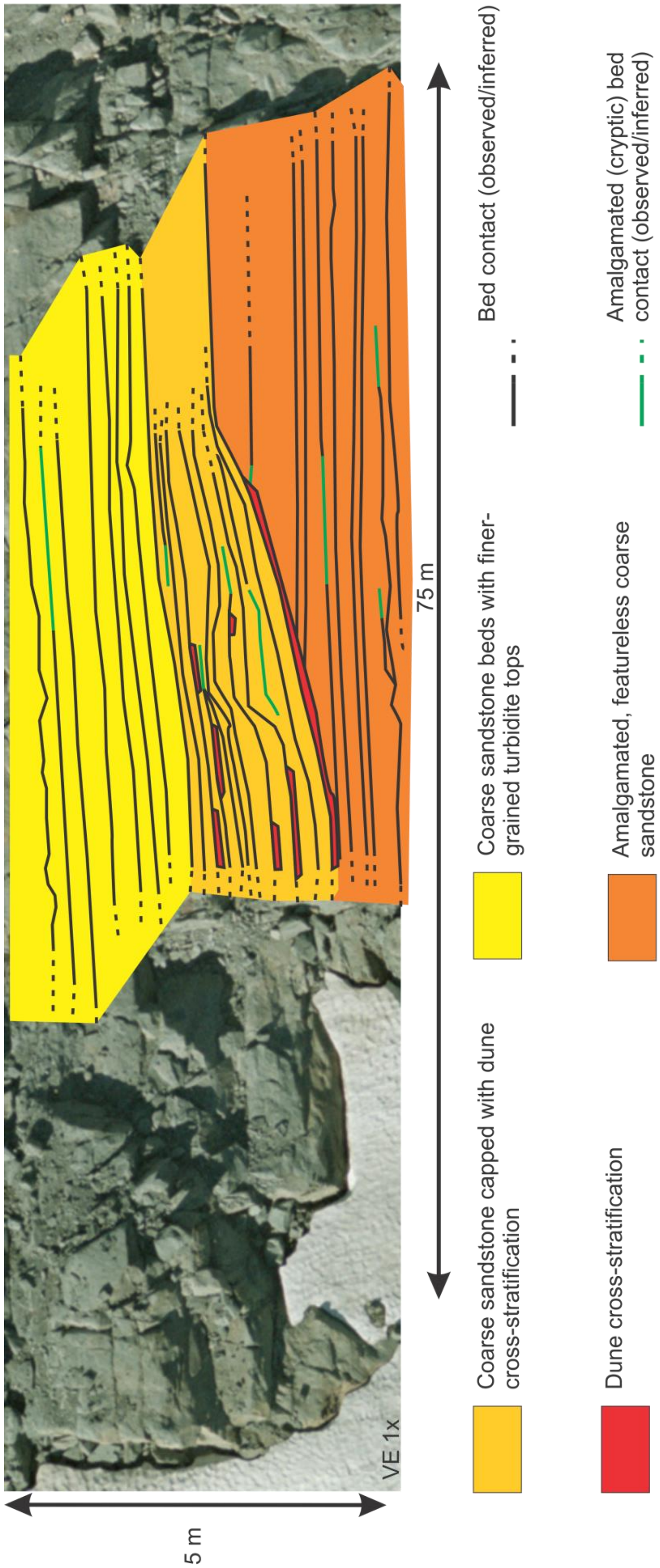

Figure 5.5: Detailed bed-scale map of the upper isolated scour in the middle Kaza.

Avulsion splays typically form up to ~1 m thick units made up of 1-5 beds and generally occur at the base of coarse-grained sandstone units (i.e. the base of the lowermost terminal splay in Dm thick sandstone units comprising multiple stacked terminal splays), but occur also between terminal splays (Figure 3.2 and Appendix A). Avulsion splays in the middle Kaza typically are truncated laterally over 10s of meters by overlying coarse-grained sandstone of terminal splays, and here pseudonodules, flame structures and injections are common (Figure 2.11d).

Stratal elements comprising fine-grained turbidites with 0-50% sandstone interbeds are <1 m to up to 35 m thick and form laterally continuous units that change little in thickness or lithological character across the Mt. Quanstrom outcrop. In a small number of cases, however, fine-grained turbidite units transition laterally into terminal splays (Figure 5.4).

The intercalataion of amalgamated terminal splays and fine-grained turbidites dominate the stratigraphy in the middle Kaza, collectively making up >95% of the outcrop at Mt. Quanstrom. These two stratal elements, at least at the scale of the outcrop, form a relatively simple "layer cake" stratigraphy (Figure 5.4), that is observed also in middle Kaza strata at Eagle Valley, located ~ 25 km north- northwest (i.e. slightly oblique to depositional dip) of Mt. Quanstrom (Appendix D).

5.3.2 Stratal element distribution in the upper Kaza Group

The upper Kaza outcrop at Castle Creek comprises seven stratal elements: isolated scours, avulsion splays, feeder channels, distributary channels, terminal splays, fine-grained turbidite units and debrites. Not only is there a more diverse assemblage of different stratal elements in the upper Kaza, but their arrangement is more complex than in the middle Kaza (Figure 5.6 and Figure 5.7).

Compared to the middle Kaza, isolated scours and avulsions splays are significantly more abundant, and commonly laterally adjacent to one other in the upper Kaza (see discussion in chapters 3 and 4). Nevertheless, compared to the other stratal elements, isolated scours are rare in the upper Kaza, and are typically up to several 100 m wide and have a coarse-grained, amalgamated sandstone fill. Avulsion splays typically comprise several matrix-rich sandstone beds that form units up to several m thick. Laterally, avulsion splays are associated with matrix-poor sandstones containing uncommon, but anomalously large sandstone and mudstone clasts (see chapters 3 and 4). Isolated scours and avulsions splays are predominantly overlain by terminal splays and/or distributary channels, and less commonly fine-grained turbidite units.

Two feeder channels are partially exposed near the stratigraphic top of the upper Kaza at Castle Creek (Figure 5.6). Both channels have a complex, terraced basal scour surface that truncates underlying terminal splays, and comprises a multi-stage fill made-up of coarse-grained sandstones and mudstones (Figure 3.3). The upper part of the fill consists mostly of thin- and medium-bedded turbidites suggesting local abandonment of the channel (see also Chapter 3), and the channels are overlain by avulsion and terminal splays. Neither channel has a recognizable levee.

Distributary channels are commonly overlain by terminal splays, and typically transition laterally into fine-grained turbidites. Clustering of distributary channels is common in the upper

Figure 5.6: Correlation panel of the upper Kaza at the Castle Creek outcrop at Castle Creek. The basal ~120 m of the outcrop was mapped in high detail (see also Figure 5.7). The colours represent the locally dominant stratal element in the stratigraphy.

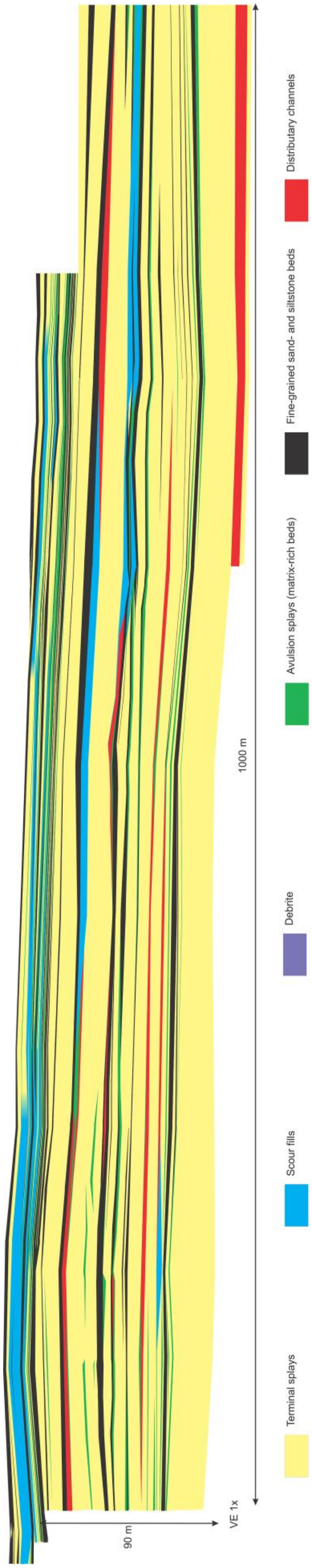

Figure 5.7: Detailed correlation diagram of the lower 120 m of the upper Kaza at the Castle Creek outcrop.

Kaza: typically several distributary channels are stacked vertically (Figure 3.4, Figure 5.7), and in few instances laterally adjacent distributary channels are separated by a fine-grained turbidite unit (Figure 5.7).

In contrast to the middle Kaza, where terminal splays typically stack to form several Dm thick amalgamated sandstone units (Figure 5.4), terminal splays in the upper Kaza more commonly occur as single stratal elements that are much thinner, generally of the order of few meters, up to ~5 m thick and are often intercalated with other stratal elements (Figure 5.6 and Figure 5.7). Nevertheless, uncommon examples of a few Dm-thick stacked terminal splay units do occur in the upper Kaza (Figure 5.6 and Figure 5.7, see also Figure 3.5). However, in spite of their thinner, non-amalgamated nature, terminal splays in the upper Kaza, like in the middle Kaza, are the most common stratal element (>50% of stratal elements, see also section 5.4.2), resulting in a high overall sandstone to mudstone ratio (75:25) in the upper Kaza. Similar to the middle Kaza, in the upper Kaza a small number of terminal splays transition rapidly laterally into fine-grained turbidite units, but more commonly are laterally continuous across the outcrop with little change in thickness or facies.

Fine-grained units in the upper Kaza are thinner and less laterally extensive (Figure 5.6 and Figure 5.7) than in the middle Kaza. In addition, fine-grained units more commonly transition laterally into sandstone-rich stratal elements (terminal splays, avulsion splays and distributary channels), and more often are erosionally truncated along the base of channels and isolated scours (see for example Figure 4.5). An important result of their comparative thinness and partial to complete erosion by younger sandstone-rich stratal elements, is that these latter elements commonly amalgamate locally, generally improving vertical sandstone connectivity.

Debrites are absent in the lower ~200 m thick part of the upper Kaza outcrop, but become more abundant and thicker stratigraphically upward, where they form several-meter-thick beds that extend across the width of the upper Kaza outcrop (Figure 5.6, see also Figure 4 in Meyer and Ross, 2007). Moreover, debrites, but also slides and slumps, become increasingly more common further upward in the transition zone and base-of-slope deposits of the Isaac Formation (Meyer, 2004, Meyer and Ross, 2007; Arnott *et al*., 2011; Navarro, pers. comm.).

5.4 Markov chain analysis in the upper Kaza

5.4.1 Introduction to Markov chain analysis

A Markov chain is a mathematical model that describes the sequential change of a system between discrete states (Everitt and Skrondal, 2010). This model assumes that a finite number of states exists, and that the change from one state to the next depends only on the current state of the system (memoryless system, termed also a first-order Markov chain, Everitt and Skrondal, 2010). Each state is assumed to be discrete (either in time, space or any other discrete measurement). The change from one state to another in the system is termed a transition. The probabilities associated with various state-changes are called transition probabilities (Everitt and Skrondal, 2010).

The system is assumed to change randomly from one state to another based on the transition probabilities between states. Therefore it is impossible to predict with certainty the state of a Markov chain at a given point in the future. The transition matrix describes the transition probabilities from one state to another, with which the statistical properties of the system can be predicted. For example the steady state of the system can be calculated, which describes the statistical distribution of states in a theoretical infinite Markov chain.

In sedimentological and stratigraphic studies Markov chains are commonly used to describe the vertical succession of facies types, stratal elements and/or stratigraphic sequences (e.g. Kane and Pontén, 2012), and statistical analysis of Markov chains is used to test if the vertical succession of these discrete elements within a stratigraphic section exhibits non-random behaviour (e.g. Gingerich, 1969; Krumbein and Dacey, 1969; Carr, 1982; Powers and Easterling, 1982; Davis, 1986; Lehrmann and Goldhammer, 1999).

5.4.2 Results

The upper Kaza was selected for Markov chain analysis because it has a more complex stratigraphy compared to the middle Kaza, and a more rigorous numerical description of this part of the system is likely to benefit from statistical modeling. The lower ~90 m thick part of the upper Kaza (Figure 5.7) was selected because this section was logged and mapped in the most detail, and thus provides the most accurate input data for analysis. The input for the Markov chain consisted of the vertical stacking of stratal elements observed in each of the ~ 90 m long stratigraphic logs (K1 – K10), in total comprising 369 observations (i.e. individual occurrences of the stratal elements in the logs). This part of the outcrop comprises five stratal element types (in the Markov chain referred to as states), namely isolated scours, avulsion splays, terminal splays, distributary channels and fine-grained deposits (Figure 5.7). First a transition counts matrix was compiled from the observations, from which the transition probability matrix and steady state distribution of stratal elements was calculated (Figure 5.8). These data, then, were converted into a graphical state diagram (Figure 5.8). The transition matrix and state diagram support the general observations described in Section 5.3.2 regarding the vertical stratal stacking patterns in the upper Kaza, but also show trends not readily identified in the field or upon visual inspection of the correlation diagrams.

Isolated scours are rare, comprising only 2% of the stratal elements in the measured sections, which is indicated also by the low percentage of transition probabilities toward isolated scours. The Markov chain indicates that scours are most commonly overlain by fine-grained turbidites, and less commonly terminal splays and rarely avulsion splays.

Avulsion splays comprise 11% of the total number of stratal elements and most commonly overlie terminal splays, less commonly distributary channels, isolated scours and fine-grained turbidites. In turn, avulsion splays are most commonly overlain by terminal splays, less so by fine-grained turbidites and distributary channels, and rarely by isolated scours.

Distributary channels comprise 7% of the stratal elements. Distributary channels are one of two stratal elements that cluster vertically: 14% of the time one distributary channels overlies another. Distributary channels also overlie avulsion splays and less commonly terminal splays and rarely fine-grained turbidites. In turn, distributary channels are often overlain by terminal splays, and less so by fine-grained turbidites and avulsion splays.

Terminal splays are the most common stratal element, comprising 53% of all observations. Terminal splays typically overlie fine-grained deposits and avulsion splays, and

A

Observed transition matrix - counts						
From/To	sc	as	dc	ts	f	SUM
sc	0	1	0	4	6	11
as	1	0	8	37	13	59
dc	0	3	4	13	8	28
ts	4	49	15	65	55	188
f	6	6	1	69	0	82

B

Observed transition matrix - probabilities						
From/To	sc	as	dc	ts	f	SUM
sc	0.00	0.09	0.00	0.36	0.55	1
as	0.02	0.00	0.14	0.63	0.22	1
dc	0.00	0.11	0.14	0.46	0.29	1
ts	0.02	0.26	0.08	0.35	0.29	1
f	0.07	0.07	0.01	0.84	0.00	1
SUM	0.11	0.53	0.37	2.64	1.34	5
Steady state	0.02	0.11	0.07	0.53	0.27	1

C

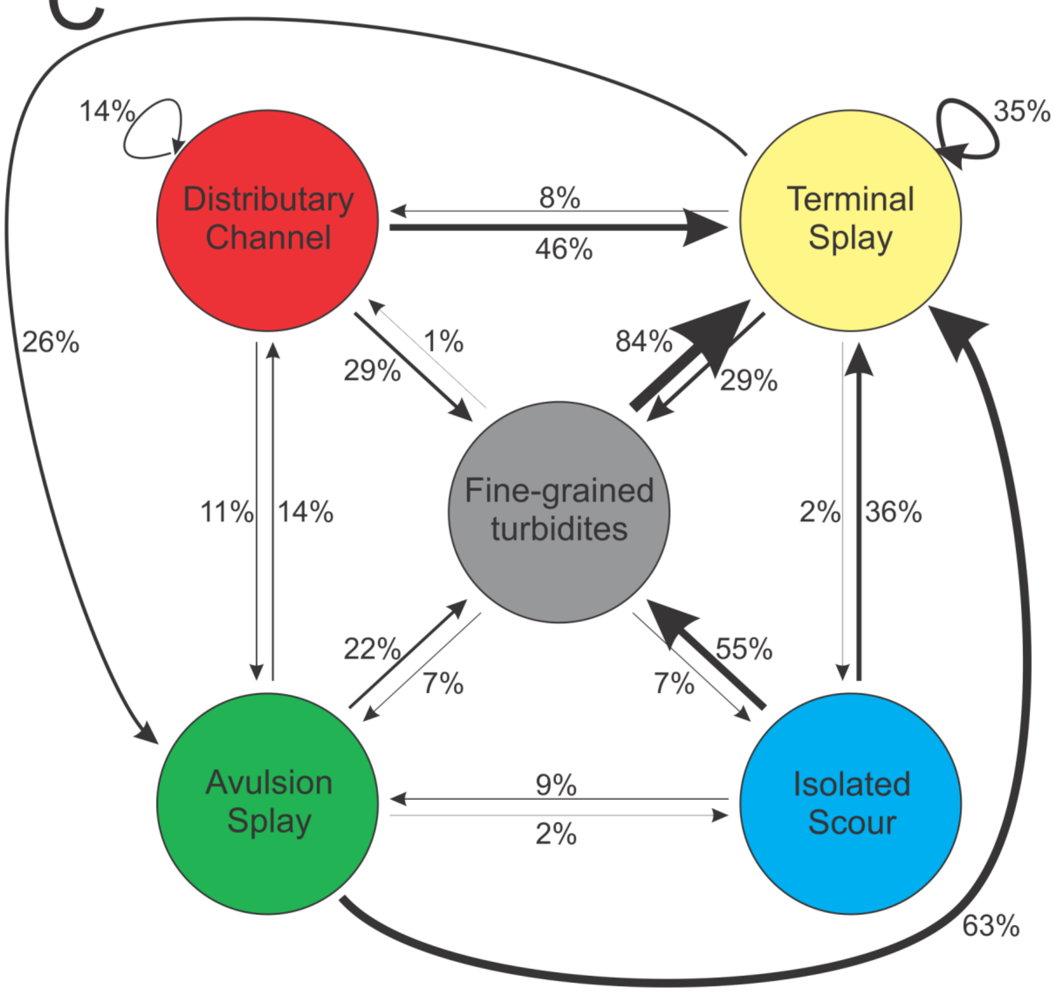

Figure 5.8 (previous page): Results of Markov chain analysis in the lower 90 m of the upper Kaza exposed at Castle Creek. The input data is derived from ten ~90 m long stratigraphic logs. In total 369 stratal elements are included in the analysis. A) Transition counts matrix; sc = isolated scours, as = avulsion splays, dc = distributary channels, ts = terminal splays, f = fine-grained turbidites. B) Transition probability matrix and steady state of the system. C) State diagram, higher transition probabilities are indicated by thicker arrows.

less commonly distributary channels and isolated scours. Terminal splays stack to form amalgamated sandstone units, and also are overlain commonly by fine-grained turbidites and avulsion splays. More rarely terminal splays are overlain by distributary channels and scours.

Fine-grained turbidites comprise 27% of the stratal elements and predominantly overlie isolated scours and less commonly terminal splays, distributary channels and avulsion splays. In turn, fine-grained turbidites are most commonly overlain by terminal splays, less commonly by isolated scours and avulsion splays, and rarely by distributary channels.

5.5 Interpretation

The stratigraphy of the Middle and upper Kaza groups exhibit obvious and significant differences, which most likely is a result of their different location on the basin floor with respect to the distance from the channel-lobe transition zone. The middle Kaza is dominated by laterally extensive, non-channelized, sheet-like terminal splay and fine-grained deposits that change little in character over the width of the outcrop at Mt. Quanstrom (>2 km). Moreover, observations in time-equivalent strata ~25 km slightly oblique to depositional dip at Eagle Valley show similar stratigraphyic characteristics (see also Appendix D), indicating that the length/width scale of the depositional system was at least on the order of 10s of kms. Erosion in the middle Kaza is restricted to rare several meter deep scours and minor erosion at bed bases; channels and debrites are absent. The middle Kaza is interpreted to represent deposition in an unconfined mid- to lower fan setting. The common several Dm thick sandstone units consisting of one or more amalgamated terminal splays are interpreted to be the distal parts of depositional lobes and the equally thick fine-grained units are interpreted to be off-axis and distal fine-grained strata deposited following an avulsion and lateral shift of the sand-rich depositional axis. Similar observations and interpretation were reported by Saller *et al*. (2008) from a relatively small deep-marine basin in offshore southeast Indonesia, where lateral avulsive displacement of the depocenter was measured in the order of 10s of kms. Upstream avulsion results in the alternating activation/deactivation of the sedimentary system downflow, and combined with the observed general lack of significant erosion in these distal settings, results in the observed “layer cake” stacking pattern of thick sedimentary units. Avulsion splays and isolated scours, although rare, are observed in the middle Kaza, and are interpreted to be the result of either anomalously energetic flows that eroded the seafloor in more distal locations, or represent local progradation of lobes.

The upper Kaza consists of a more diverse assemblage of stratal elements compared to the middle Kaza. In addition, erosional features (isolated scours and channels) are common and debrites are present, suggesting a more proximal depositional setting. Isolated scours and avulsion splays are interpreted to form immediately downflow of an avulsion node and at the onset of local sedimentation (see also Chapter 4). These features are most common in the upper Kaza, and together with the observed distributary channels in the upper Kaza, collectively indicate a mid-fan position. The overall high sandstone to mudstone ratio in the upper Kaza indicates that the main input location of coarse-grained sediment and the axis of sedimentation was always relatively close, which is likely the result of a fixed location of the upflow canyon and/or leveed-channel complex. Terminal splays and fine-grained turbidite units are generally thin in the upper Kaza and additionally less likely stack vertically, indicating an avulsion dominated depositional system. Feeder channels, although rare, erode underlying terminal splays. These large channels are interpreted to be the result of erosion by a (locally) out-of-grade system, which after an upstream avulsion adjusts to its new base level by eroding and back-cutting through the pre-existing seafloor. Collectively these observations indicate a proximal basin-floor (middle fan to "distal" upper fan) location of the upper Kaza. Sediment was likely sourced from a relatively fixed sediment input location (point source type input, see Figure 5.3) resulting in rapid avulsion in response to the filling of local accommodation, and temporary out-of-grade conditions.

5.5.1 Idealized basin-floor lobe and fan model

5.5.1.1 Idealized 2D cross-sections

In this study a lobe is defined as a three-dimensional sedimentary body with a generally lobate planform shape that includes all stratal elements formed downflow of the channel-levee complex between major avulsion events (avulsions at the mouth of the channel-levee system or of the feeder channel). Note, however, that the Mt. Quanstrom and Castle Creek outcrops only provide a 2D cross-sectional view of basin-floor strata. Figure 5.9 shows idealized 2D stacking patterns of stratal elements and stratigraphic cross sections, which are based on descriptions of

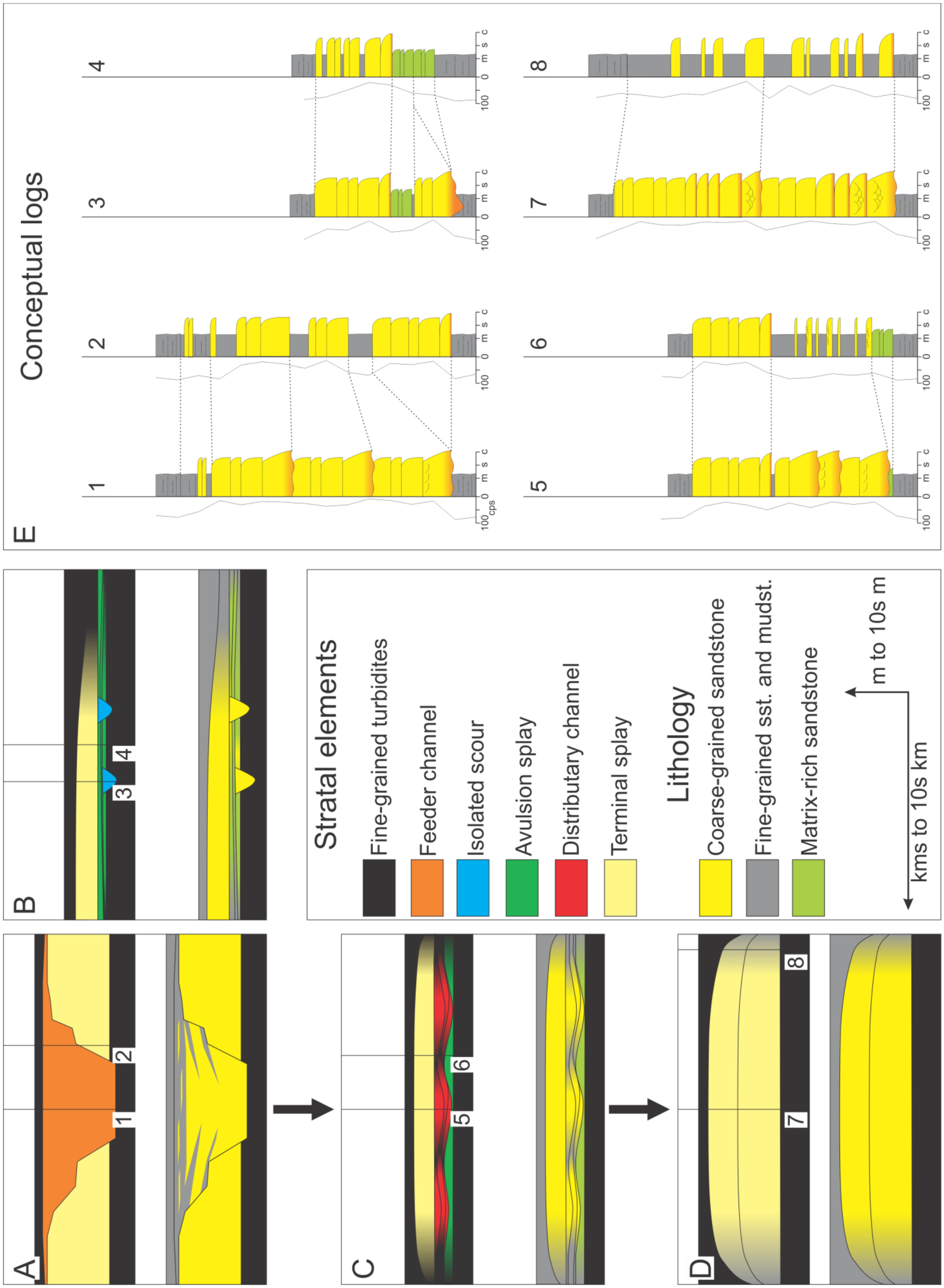
A
B
C
D
E
Conceptual logs
1
2
3
4
5
6
7
8
100
cps
0
m
s
c
Stratal elements
Fine-grained turbidites
Feeder channel
Isolated scour
Avulsion splay
Distributary channel
Terminal splay
Lithology
Coarse-grained sandstone
Fine-grained sst. and mudst.
Matrix-rich sandstone
kms to 10s km
m to 10s m

Figure 5.9 (previous page): Idealized stracking pattern and transverse cross-sections of stratal elements. A-D follow observations from the top of the upper Kaza to the middle Kaza (corresponding to a proximal to distal transect) A) Cross-section of a feeder channel based on Figure 3.3. Feeder channels are observed only in the most proximal (upper) part of the upper Kaza (Figure 5.6). These relatively long-lived channels have a terraced erosional scour base that terminates terminal splays and a complex, multi-stage fill (see section 3.3.2). B) Isolated scours are most common in the proximal part of the upper Kaza. Here they are latearlly associated with avulsion splays (see Figure 4.5 and Figure 4.6). Units comprising isolated scours and avulsion splays are commonly overlain by terminal splays. C) Throughout the stratigraphy of the upper Kaza avulsion splays are commonly overlain by distributary channels and terminal splays. Distributary channels, in turn, commonly overlie one another (Figure 3.4). D) In the middle Kaza terminal splays are typically thicker and stack to form several Dm thick sandstone units (Figure 5.4, Figure 3.2 and Appendix A). Similar stacking of terminal splays is less common, but observed also in the upper Kaza (Figure 3.5). E) Idealized stratigraphic and scintillometer logs. Numbers indicate the location of the logs in figures A-D; dotted lines show correlations between adjacent logs.

stratal element stacking in sections 5.3 and 5.4 and facies distribution within stratal elements in Chapter 3. Applying Walther's Law these cross-sections, then, are used to populate an idealized 3D lobe (see section 5.5.1.2).

5.5.1.2 Idealized lobe

An ideal lobe starts its development at the time of an avulsion and spatially immediately downflow of the avulsion node (Figure 5.10). First unconfined jet flows erode the muddy seafloor and create isolated scours. At the same time sand containing large mud- and sandstone clasts accumulates along the margins of the jet. Deposition laterally and downflow of the jet consists of avulsion splays and/or coarse-grained sandstone, which further laterally and distally fine and thin rapidly into thin-bedded, fine-grained turbidites (Figure 5.10). If avulsion events have a short recurrence interval, then flows will be redirected elsewhere on the fan and isolated scours and avulsions splays will be blanketed with off-axis fine-grained turbidites. Conversely, if

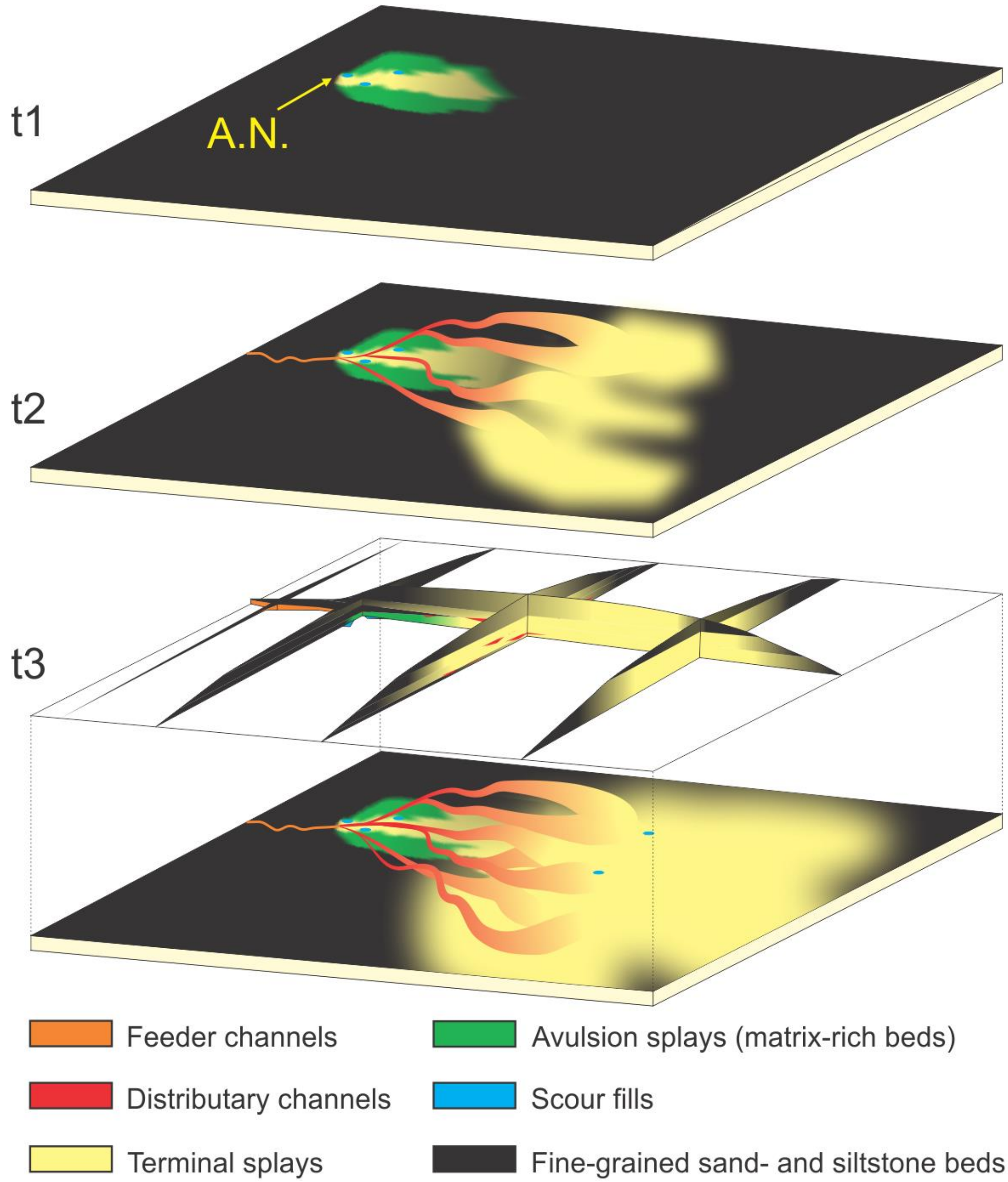

Figure 5.10: Idealized evolution of a depositional lobe. t1) The lobe is initiated by an upstream avulsion event at the avulsion node (A.N.). Immediately downflow the initial unconfined jet flows erode the sea floor creating scours and depositing sandstones and avulsion splays. t2) Later flows organize themselves into a network of discrete distributary channels that downflow merge laterally into a terminal splay. At the same time, but further upflow, erosion creates a feeder channel. t3) During the lifetime of a lobe multiple distributary channel avulsions result in the vertical stacking of distributary channels and terminal splays. The fence diagram shows the conceptual internal stratigraphy of a lobe. Lobe length and width dimensions are of the order of 10s to 100s of km.

the system becomes stabilized in a single location, then after some time flows become focused through channels. Pre-existing topography of the seafloor determines the creation of feeder channels: if the initial slope of the seabed is out-of-grade in relation to general transport conditions, then an incised feeder channel develops. The feeder channel, in turn, bifurcates downflow and a distributive network of shallow channels is created (Figure 5.10). If a feeder channel does not develop, then the distributary channels are attached directly to the upflow channel-levee system. Shallow distributary channels are relatively short-lived features that avulse shortly after their formation and commonly stack vertically. Distributary channels become progressively shallower and wider downflow, until they finally merge laterally at their distal ends to form a non-channelized sheet-like terminal splay (Figure 5.10). If the system is stable for a prolonged period of time, then terminal splays stack to form amalgamated sand units up to several Dm thick (Figure 5.10). Finally, after local accommodation is filled the depositional system avulses and lobe creation repeats, but elsewhere.

5.5.1.3 Idealized fan

Multiple episodes of avulsion followed by lobe deposition results in the formation of lobe complexes, and ultimately the submarine fan (Figure 5.11). Basin-floor fan deposits of the middle and upper Kaza Group form an up to ~2 km thick sedimentary succession (Figure 1.5). The upward changing sedimentary trend in the Kaza Group, namely a “layer cake” arrangement of terminal splays and fine-grained turbidites (middle Kaza) to a more complex arrangement of a larger variety of elements (upper Kaza), is interpreted to represent the progradation of the basin-

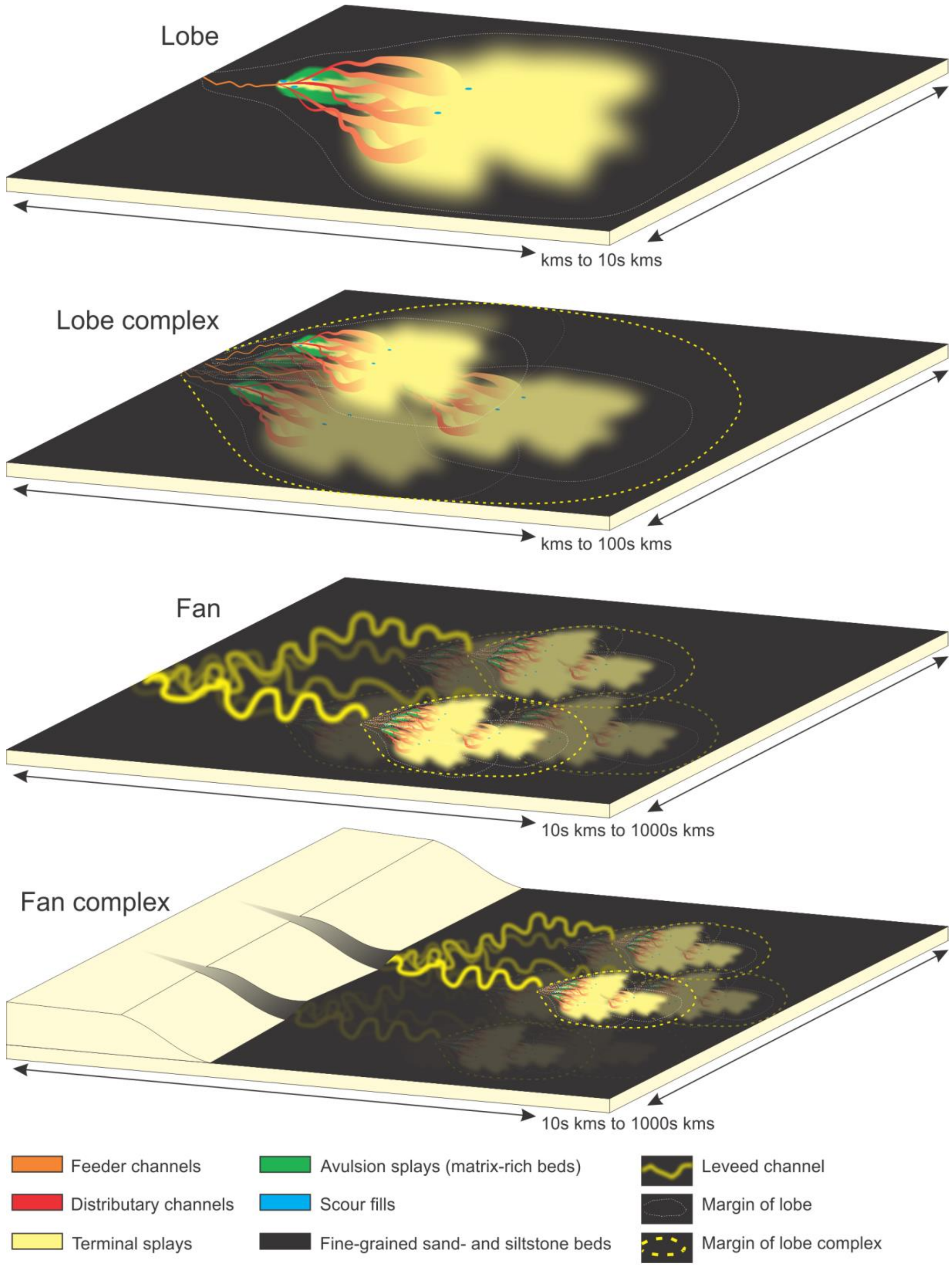

Figure 5.11: Schematic of an ideallized submarine fan complex and its constituent components – note the progressive change in horizontal scale from lobe to fan complex. At the smallest scale an individual lobe is created by the process outlined in section 5.5.1.2 and Figure 5.10. Avulsion of the feeder channel results in spatial shifting of the depositional axis, and a new lobe forms on the seafloor. Several lobes fed by the same channel-levee, but different feeder channels, then, form a lobe complex. Avulsion of the channel-levee system results in shifts in the position of lobe complexes, which, in turn stack to form the submarine fan. Avulsion of the upflow canyon results in the deposition of fan complexes, each fan fed by a different canyon.

floor fan; an idealized block diagram of the fan is shown in Figure 5.12 with the locations of the middle and upper Kaza outcrops indicated by red rectangles. The middle Kaza outcrop at Mt. Quanstrom exposes a more distal location, where upstream avulsions cause large lateral lobe shifts, resulting in a monotonous stratigraphy of alternating coarse-grained distal lobe (terminal splay) and off-axis fine-grained units (Figure 5.12). The overlying upper Kaza outcrop at Castle Creek, on the other hand, exposes a more proximal location that is close to the mouth of the channel-levee complex. Here flows are more energetic and form a wider variety of stratal elements. A relatively fixed input point and more frequent avulsions results in comparatively thinner stratal elements, yet a higher overall sandstone to mudstone ratio with much more local sandstone amalgamation (Figure 5.12).

Alternatively, differences in the stratigraphy and architecture between the middle and upper Kaza Group could be the result of upflow canyon avulsion and deposition in two different submarine fans, collectively forming a fan complex (Figure 5.11). Due to the size of the depositional system and structural deformation related to later Mesozoic orogenesis, basin-floor strata of the WSG in the Cariboo Mountains cannot be linked directly to the feeder canyons located in the Lake Louise area, a distance of several 100 kms. It is, therefore, not possible to confirm whether the deposits formed in a single or multiple fans.

5.6 Modelling 1D stratigraphic logs

Depletion of shallow water reservoirs has increasingly shifted the focus of oil companies towards ultra-deep offshore prospects (e.g. Mulder and Etienne, 2010). In these deep-water

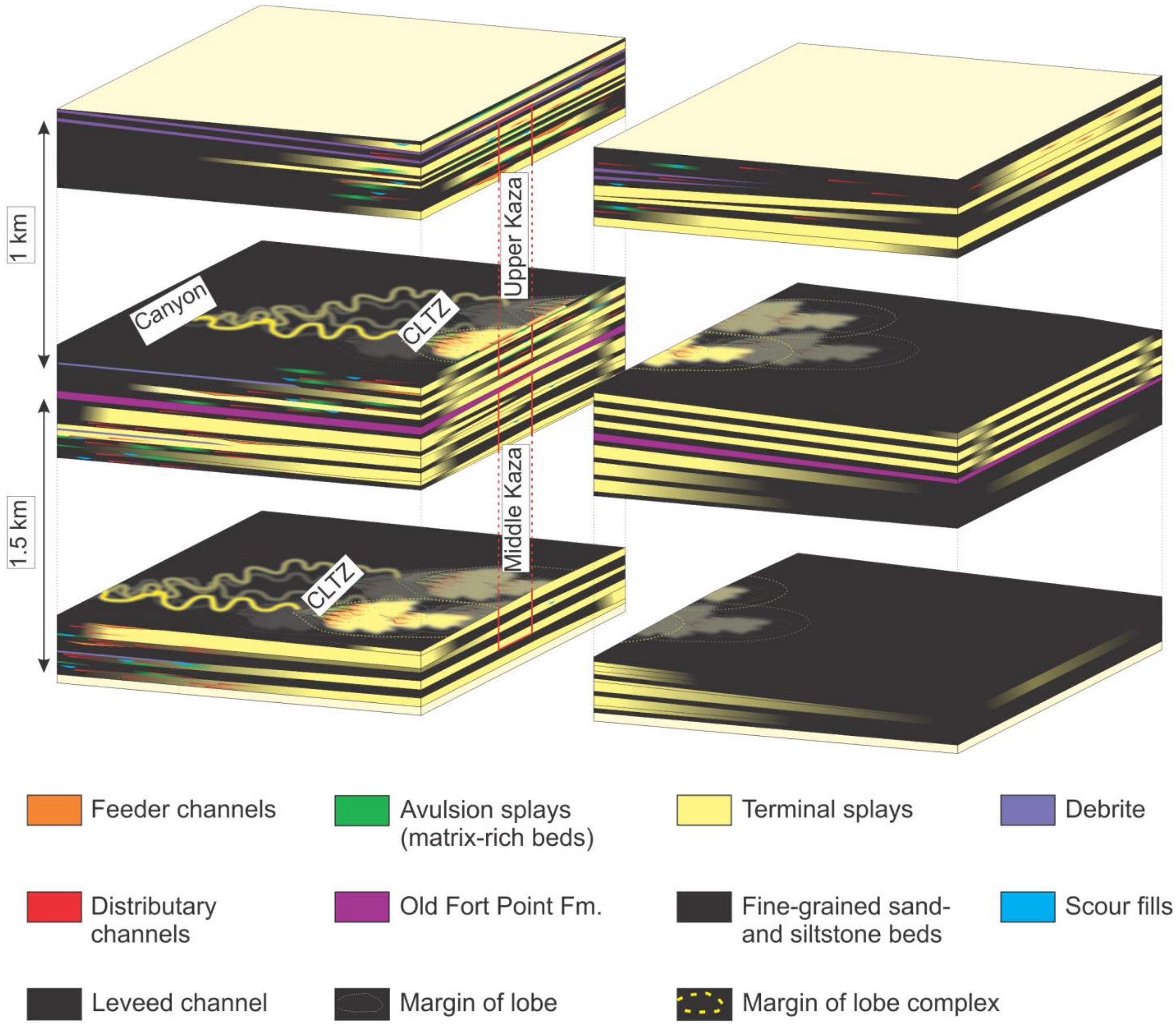

Figure 5.12: Depositional model of basin-floor fan strata of the Kaza Group. The middle Kaza comprises laterally extensive distal sheet-like lobe deposits, which in outcrop form alternating Dm thick sandstone rich terminal splay and fine-grained turbidite units. The upper Kaza comprises more proximal deposits, plus a wider variety and more complex stacking of stratal elements. The middle and upper Kaza are stratigraphically separated by the regionally extensive Old Fort Point marker unit (see Chapter 1.2). Collectively these strata are interpreted to be the deposits of a prograding basin-floor fan. General flow direction in the diagram is from left to right; the cut in the middle indicates the location of the outcrops with relation to the channel-levee system, the left block shows more proximal deposits and the right side shows coeval but more distal strata.

settings oil companies rely heavily on relatively low resolution seismic imagery to determine the architecture of target reservoirs. These data may in some cases resolve the large-scale architecture of fans and lobes, but only poorly their internal stratigraphy. Reservoir geometry predictions are, then, commonly assessed by modelling of strata based on spatially sparse core data and statistical models. Another method is to create synthetic core data that can be used as input for reservoir models. In this section the results of the Markov Chain analysis (section 5.4) and the widely available Microsoft Excel™ spreadsheet program are used to propose a technique for creating 1D stratigraphic logs. The proposed technique comprises two parts: a freeware Markov Chain simulator add-in for Microsoft Excel™ (see section 5.6.1) developed by Dr. Paul A. Jensen (University of Texas, downloadable at: http://www.me.utexas.edu/~jensen/ORMM/excel/markov.html), and a spreadsheet that automatically calculates a thickness for each stratal element in the series output by the Markov Chain simulator (see section 5.6.2).

5.6.1 Markov Chain simulator add-in

The input of the Markov Chain simulator add-in for Excel consists of the probability matrix calculated in section 5.4.2 (Figure 5.8b). In addition, the operator needs to specify the initial "state" of the system (i.e., which stratal element the program uses as a starting point) and how many steps to calculate (i.e. total number of stratal elements in the simulated stratigraphic column). Based on the input matrix and the specified variables the add-in automatically calculates a new series of stratal elements (Figure 5.13). Additionally, the add-in automatically

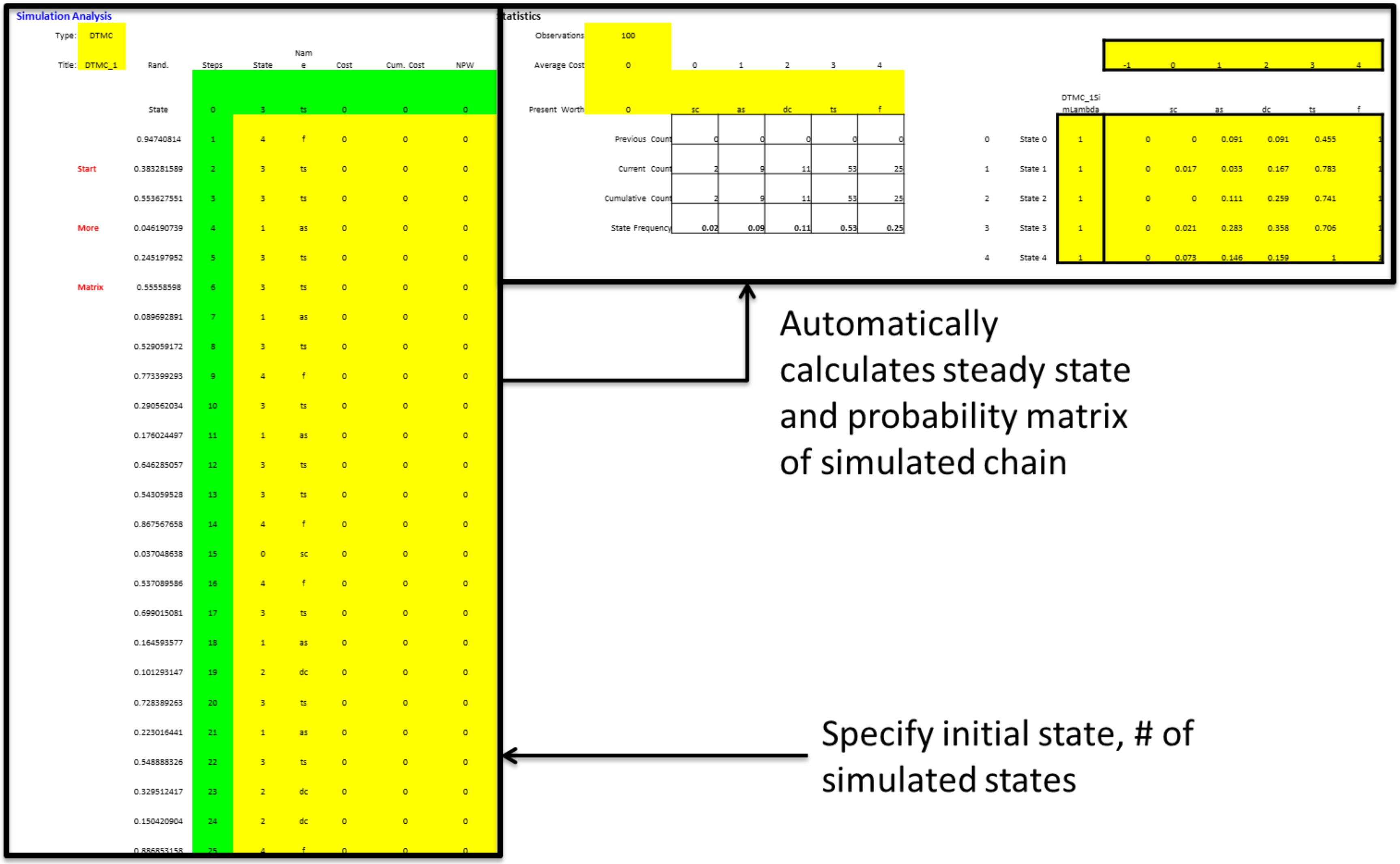

Simulation Analysis
Statistics
Automatically calculates steady state and probability matrix of simulated chain
Specify initial state, # of simulated states

Figure 5.13 (previous page): Screenshot of the Markov chain simulator Excel spreadsheet. The input for the simulator is a probability matrix. The user has to specify an initial state and the number of consecutive states to calculate. The simulator automatically calculates the steady state and probability matrix of the simulated sequence for easy comparison with the input matrix.

calculates the probability matrix and theoretical steady state of the output series, which are useful data for comparing the output with the input data (Figure 5.13). A new simulation can be started simply with a push of the “start” button, each time producing a new series of stratal elements.

5.6.2 Creating stratigraphic logs

The output of the Markov Chain simulator is a series of stratal elements based on the probability matrix. However, these elements cannot be converted directly to a stratigraphic log because the stratal elements lack thickness. In order to determine their thickness, it is first assumed that the thickness of each stratal element in the upper Kaza is normally distributed about the mean thickness of that element in the outcrop (Figure 5.14). In order to create the most realistic simulated stratigraphic logs an Excel™ spreadsheet is used, which takes the input from the Markov Chain simulator and outputs thickness values for each stratal element reflecting the observed thickness data.

The spreadsheet that calculates a thickness value for stratal elements comprises several columns (Figure 5.15). Column A reads the output series form the Markov Chain simulator (Figure 5.13). Column D creates random thickness values for each stratal element based on the element type in Colum A using Excels “NORM.INV” and “RAND” functions. The formula used in the Excel™ software follows an “IF” type statement, which first determines which stratal element is present in Column A. Then, the program looks up the mean thickness and standard deviation of the thickness for that element (Figure 5.14), and calculates a thickness for the stratal element in Column A with function: NORM.INV(RAND(), μ, σ). This function returns the thickness value based on probability RAND() (a random number between 0 and 1), mean thickness of the given stratal element (μ) and standard deviation of the thickness (σ). These values are based on a normal distribution, and therefore nonrealistic thickness values are occasionally calculated (i.e. values of 0 or less). Unrealistic values, then, are set to 0.1 (0.1 m is the cutoff value of stratal element thickness), and all values are rounded to one decimal in Column B. Column C calculates a cumulative thickness for the stratigraphic column.

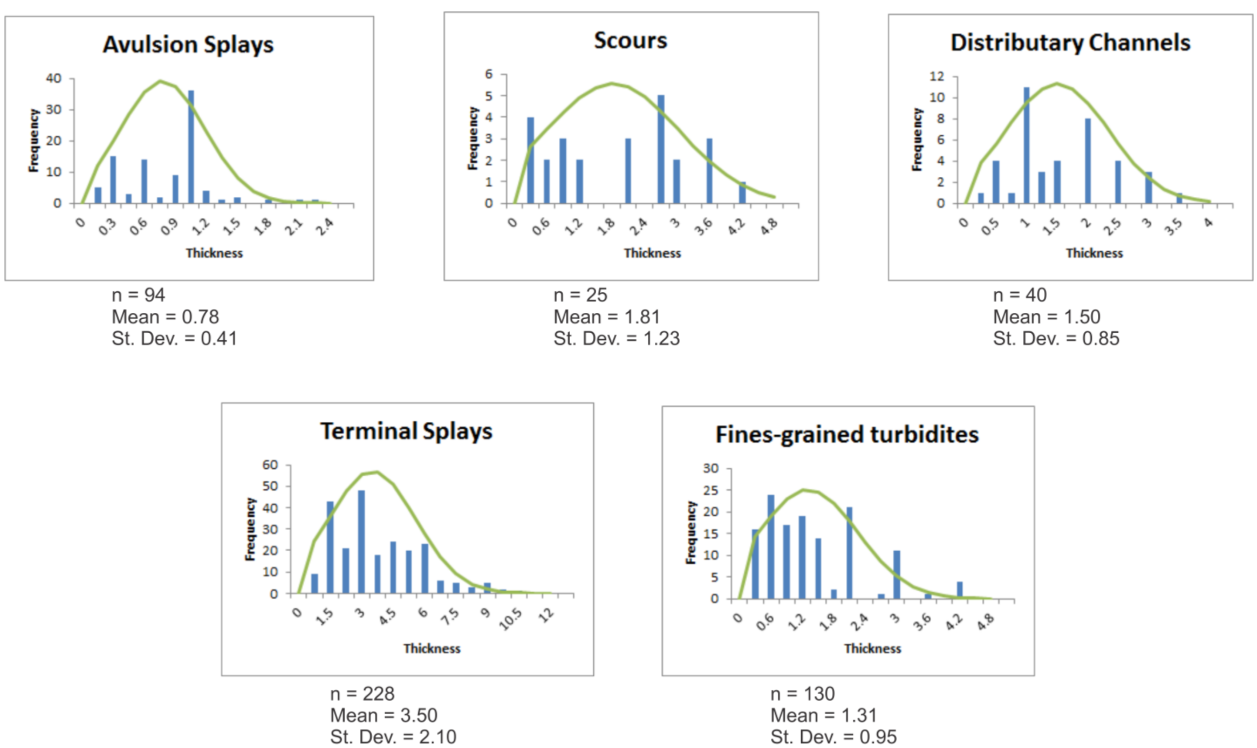

Figure 5.14: Thickness distribution of stratal elements in the upper Kaza. Observation counts are represented by the blue histogram and the calculated normal distribution is shown by the green curve. Because a negative thickness is unrealistic the normal distribution is forced to be 0 for a theoretical thickness of 0 or less.

A	B	C		D
Element	Thickness	Cumulative thickness		Random thickness values
sc	1.9	1.9	Create random numbers	1.913094898
f	0.4	2.3		0.431293492
ts	4.2	6.5		4.15983555
ts	6.6	13.1		6.564978678
ts	6.6	19.7		6.616184626
ts	4.5	24.2		4.538689411
as	1.0	25.2		0.987905956
ts	4.4	29.6		4.362839306
as	0.1	29.7		-0.145910119

Figure 5.15: Example of the spreadsheet that calculates thicknesses for the simulated series of stratal elements.

The final output of this Excel spreadsheet technique is a series of stratal elements that is based on the input probability matrix, and each stratal element has a unique thickness value that is based on the normal distribution of thickness of stratal elements observed in the upper Kaza. These data, then, are plotted in order to visually inspect the output and compare the simulated stratigraphic logs to the upper Kaza stratigraphic logs. Four simulated logs are shown in Figure 5.16 and show a remarkable visual similarity in both distribution and thickness of stratal elements to the measured section from the upper Kaza at Castle Creek. Such artificial logs could potentially be useful input for more sophisticated geologic software that create geocellular, reservoir and synthetic seismic models.

Log from the Upper Kaza.

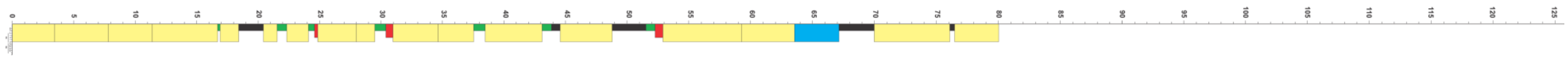

Simulated logs.

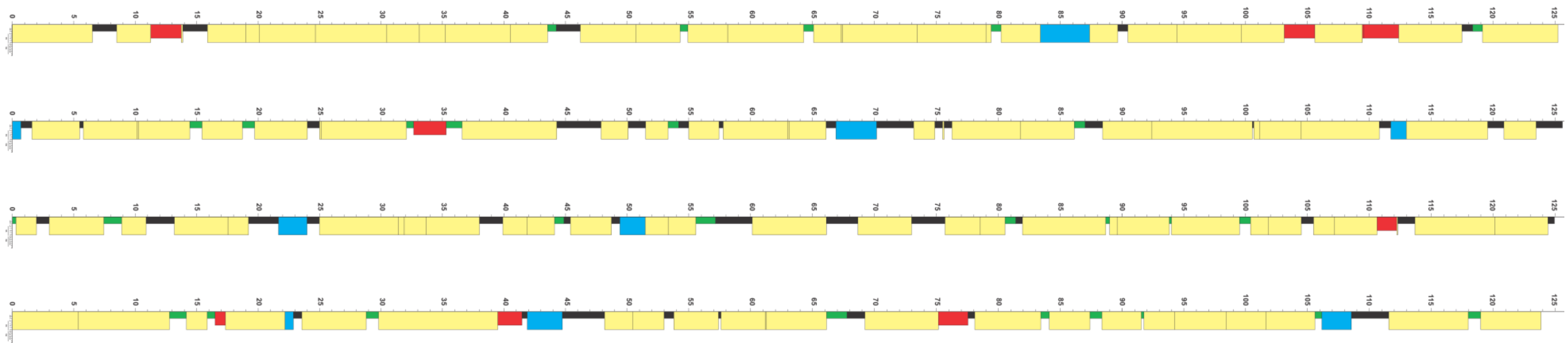

Figure 5.16 (Previous page): Comparison of a log of stratal elements in the upper Kaza and four simulated logs. Visually the simulated logs appear to represent the input data well.

5.7 Conclusion

In this chapter the stratigraphic distribution of stratal elements in the middle and upper Kaza were described. The middle Kaza has a relatively monotonous stratigraphy consisting of alternating Dm thick coarse-grained sandstone and fine-grained turbidite units. These strata are interpreted to be distal lobe deposits corresponding to the middle and lower fan. The layer-cake stratigraphy is interpreted to be the result of upstream avulsion and the lateral shifting on lobes over distances of several 10s of km, and accordingly activates or deactivates the local sedimentary system.

The upper Kaza comprises a wider variety and more complex arrangement of stratal elements. Debrites and common erosional features suggest a proximal location. The high sandstone to mudstone ratio and relatively thin stratal elements indicate that the sediment source was close by and that the system was avulsion dominated. Markov chain analysis is used to quantify the vertical transitions between stratal elements, the result of which confirm the visual and field observations. These strata are interpreted to be more proximal deposits corresponding to the upper and middle fan.

These data are then used to propose an evolutionary development of a depositional lobe. Lobes are initiated by an upstream avulsion event. Scours, avulsion splays and sandstones containing large rip-up clasts comprise the first stratal element of a lobe. Subsequent flows create a distributary network, which downflow transition into terminal splays. However in cases where following avulsion the seafloor is initially out-of-grade, extensive scouring forms an incised feeder channel that downflow transitions successively into distributary channels and then terminal splays. This feeder channel, then, is active for the lifetime of the lobe, while the downflow distributary channels and terminal splays avulse, creating stacked units of these stratal elements.

In the last section of this chapter a process is proposed for creating artificial sedimentary logs. This method consists of two parts: simulating a sequence of stratal elements based on the observed transition matrix, and calculating a thickness for each stratal element. The output stratigraphic logs based on this method show a good fit with the input stratigraphic logs of the upper Kaza.

Chapter 6: Thesis conclusions, contribution and areas for future research

6.1 Conclusion

The final repository of coarse-grained clastic sediment is the deep-water basin-floor fan. These sedimentary systems are, despite their large size, one of the least understood on Earth. Submarine fans on and under the modern seafloor are typically investigated with seismic, sonar and core, which typically lack the vertical and lateral resolution, respectively, to effectively identify and characterize small-scale stratal elements that make-up submarine fans. Outcrops of ancient submarine fans, on the other hand, are typically hampered by lateral and/or vertical exposure limitations, and worldwide only a small number of exceptional outcrops provide the crucial link between the mm- and meter scale (lamina to bed) observations and cm to km-scale (lobe to fan) elements. One such system is the deep-water turbidite system of the Windermere Supergroup. In this thesis two well-exposed occurrences of the more proximal upper Kaza Group and more distal middle Kaza Group are described and interpreted to document, at various scales, submarine fan deposits of the Windermere turbidite system. The narrative of the thesis follows a logical scalar progression, starting with the description and interpretation of strata at the lamina to bed scale, then stratal element scale and finally the lobe and fan scale. Each scale forms part of a stratigraphical hierarchy, where smaller scale features populate the sedimentary bodies of progressively larger scale features.

At the lowest hierarchical level seven sedimentary facies make up the stratigraphy of the middle and upper Kaza Group, including:

1. Coarse-grained massive and graded sandstone deposited by concentrated and hyperconcentrated turbidity currents;
2. Coarse-grained graded sandstone capped by dune cross-stratified and/or planar stratified sandstone. The basal part of the bed was deposited by concentrated and hyperconcentrated turbidity currents; the tails of the currents reworked the underlying bed to create dunes and/or upper stage plane bed;
3. Coarse-grained graded sandstone with finer grained Bouma turbidite (T_{b-d}) tops. The basal part of the bed was deposited by concentrated turbidity currents; the upper part of the bed was deposited by the dilute tail part of flows;
4. Medium- to coarse-grained, massive to coarse-tail graded, matrix-rich sandstone capped by a sandy silt-mud layer deposited rapidly by "transitional" flows containing a high concentration of fine-grained sediment;
    4.1. Like Facies 4, but with ripple cross-stratification between the featureless basal part of the bed and the sandy silt-mud cap;
    4.2. Like Facies 4, but containing small, elongated and commonly sheared mudstone clasts.
    4.3. Beds with an abrupt upward increase in matrix content;
5. Coarse-grained massive and graded sandstone containing anomalously large sand- and mudstone clasts deposited by concentrated and hypercontentrated turbidity currents. The sand- and mudstone clasts are interpreted to have been sourced locally and deposited rapidly;
6. Fine-grained, thin-bedded turbidites deposited by dilute turbidity currents;

7. Chaotic fine-grained deposits containing abundant deformed sandstone and mudstone clasts interpreted to be debrites.

Collectively these seven facies make up larger, meso-scale stratal elements in the middle and upper Kaza Group, including:

1. Isolated scours comprising scours up to several 100 m wide and few m deep with sharp erosive bases and typically a coarse-grained sandstone fill. Beds of the fill are amalgamated and near the base onlap the basal scour surface, beds near the top of the scour are continuous across and beyond the scour margins;
2. Avulsion splays consisting of matrix-rich sandstones and matrix-poor sandstones that contain large sand- and mudstone clasts. Avulsion splays form units up to several m thick and several 100 m wide. Laterally and distally matrix-rich beds typically thin and fine;
3. Feeder channels that have an up to 15 m deep terraced erosional basal surface and a complex, multi-stage channel fill comprising amalgamated coarse-grained sandstone in the channel axis and stratified sandstone and fine-grained turbidites towards the margins. The upper part of the channel fill comprises abandonment facies (thin-bedded, fine-grained turbidites);
4. Distributary channels are up to few meters deep and several 100 m wide. The low aspect basal scour surface is overlain by amalgamated coarse-grained sandstone near the channel axis, which fine and thin both upward and laterally. Beds of the channel fill drape the basal scour surface and in many cases are continuous from the channel's axis onto its margins;

5. Terminal splays comprise typically >90% amalgamated coarse-grained sandstone bodies that are up to 10 m thick and typically are laterally extensive showing little change in facies or thickness across the outcrops;
6. Fine-grained turbidite units are up to 35 m thick and comprise thin-bedded, fine-grained T_{cd} turbidites with coarse-grained sandstone interbeds. These units are typically laterally extensive, but in the upper Kaza are locally eroded.

These stratal elements are systematically and predictably arranged, both spatially (along a single depositional transect) and temporally (stratigraphically upward) and form the sedimentary bodies of depositional lobes. Lobes typically became initiated by channel avulsion, and hence deactivation of an older lobe. In the proximal part of the system scours up to several meters deep and several tens to hundreds of meters wide are interpreted to have formed by erosion within a hydraulic jump downflow of an avulsion node. Erosion also formed the common large, tabular mudstone clasts, some up to 9 m long and 40 cm thick, and charged the flow with fine-grained sediment. Laterally and further downflow rapid expansion and consequent deposition from successive flows built-up dm- to several meter-thick units consisting of distinctively matrix- and mudstone-clast-rich beds, termed avulsion splays. Avulsion splays are significantly more common in the proximal basin floor, and commonly are observed beneath distributary channel and terminal splay deposits, and indicate activation of sedimentation, at least locally.

Successive flows then exploited the basin-floor topography and on the proximal basin-floor carved an up to 15 m-deep feeder channel. It then expanded and bifurcated downflow forming a network of shallow (several m deep) distributary channels, which eventually terminate in sandstone-rich terminal splays, each a few up to about 10 m thick. Both these elements commonly overlie the earlier deposited matrix-rich beds of an avulsion splay. During the lifetime of a single lobe the feeder channel remains fixed, but the downflow distributary channel network and its associated terminal splays wander, causing them to stack vertically. Eventually an upstream avulsion shuts off local sediment supply, causing a new lobe to be initiated elsewhere on the fan, and the processes outlined above repeats.

Stacking of lobes, in turn, builds the largest scale sedimentary body, the basin-floor fan. The architecture of the fan is inferred from the long-term (km-scale) trends in stratigraphy. In the more distal middle Kaza, alternating Dm-thick sandstone and fine-grained units are interpreted to be the distal parts of sandy lobes and inter-lobe deposits, respectively. The sheet-like arrangement of these units and their thickness indicates that upstream avulsions resulted in significant lateral displacement of lobes in this distal location, which in turn activated and deactiveated the local sedimentary system for long periods of time. In the upper Kaza, on the other hand, its more complex stratigraphy, more common erosional features and higher overall sandstone to mudstone ratio indicates that a point-source input located not too far upflow fed the system, and compared to the middle Kaza was much more avulsive in response to the more rapid filling of local accommodation space.

Modelling 1D stratigraphic logs is a potential first step towards 2D and 3D basin-floor fan models, including geocellular, reservoir and seismic models. In this thesis a method to create synthetic 1D stratigraphic logs is presented, which is based entirely on the universally available Microsoft Excel™ program. The only input needed for this modelling is the original measured stratigraphic logs, which are then used in a Markov chain analysis to calculate the transition matrix between stratal elements and basic statistics of their thicknesses. The final output of the model consists of simulated logs, which upon visual inspection show good similarity with the original (field measured) input logs.

6.2 Contributions

Motivation to study basin-floor fan deposits is both academic and economic. These deposits house some of the largest hydrocarbon reserves in the world, and a detailed knowledge of their internal stratigraphy aids in the assessment of drilling risk and help to improve overall hydrocarbon recovery. Petroleum companies rely heavily on models to predict the value of hydrocarbon assets, and commonly use forward modelling based on limited datasets. Collectively the observations in this thesis support existing lobe and fan models, but also provide some conceptual refinement and some important new sedimentological insights. Main contributions of this thesis include:

- The WSG is, to date, the only ancient continental scale passive margin system with a mixed grainsize distribution that has been described in detail. As such, the basic facies descriptions and interpretations provide valuable information about how these systems are formed and the flows that create them.
- With the advance of high-resolution seismic some architectural (stratal) elements have been identified in the subsurface, and outcrop studies have also contributed significantly to our knowledge of these meso-scale elements. In subsurface studies, however, the internal facies and facies distribution are inferred from seismic reflectors or widely spaced drill cores, and as a result are generally not well known. Outcrop studies, therefore, provide the key information to fill the knowledge gap between these datasets and seismic. This study contributes by describing the internal stratigraphy of all stratal elements in the WSG.

- Matrix-rich sandstones have been described from various other modern and ancient systems, but only on the margins of the sedimentary system. In the WSG units of matrix-rich sandstone are, in contrast, most common on the proximal basin floor. Here these deposits are termed avulsion splays, and a novel model for their emplacement is proposed.
- Based on the spatial arrangement of stratal elements in the upper and Kaza groups a model for lobe evolution is proposed. Although this model follows existing models that describe the spatial arrangement of stratal elements closely, it adds to them by proposing a complete evolutionary model of lobe deposition from initiation by an upstream avulsion to shut-down. Additionally, existing lobe models typically include distributary channels, terminal splays and fine-grained deposits only, and rarely feeder channels. The lobe model proposed here also includes isolated scours and avulsion splays.

6.3 Areas for future research

6.3.1 General

- This study focused on the middle and upper Kaza Group, which are interpreted to be middle and upper fan deposits, respectively. Previous studies have interpreted the lower Kaza to be distal (lower) fan deposits, but to date no detailed work has been conducted to document its sedimentology or stratigraphy. This work is essential in order to complete the basin-floor fan model of the WSG.
- Observations at a regional scale indicate that the general stratigraphy of the middle Kaza is similar to that described here, at least on a scale of 10s of kilometers. A more detailed

regional study of the middle Kaza, including several known outcrops, would provide a better overall picture of the large-scale stratigraphy and spatial changes in the more distal but still sand-rich part of the WSG basin-floor fans.

6.3.2 Chapter 2

- Petrographic analysis in this study consisted principally of visual inspection of the rocks in the field, supplemented by thin section analysis of representative samples of each sedimentary facies. A more systematic petrographic thin section analysis that consistently samples individual beds both vertically and along strike would provide further insight into flow characteristics at the time of deposition.
- Investigating in detail the post-depositional diagenetic and metamorphic processes that have affected these rocks was beyond the scope of this thesis, but a more detailed petrographic and geochemical study may reveal interesting clues regarding these post-depositional processes. This additional study would be helpful in better understanding, for example, if fine-grained and coarse-grained strata were affected unevenly by deformational (tectonic) stress, and whether observations reported here need to be adjusted in any way to better interpret primary depositional conditions.

6.3.3 Chapter 3

- Most stratal elements were walked out in the field to aid stratigraphic correlation and allow general observations to be made regarding facies and bedding trends. However, only two sand units were mapped in bed-by-bed detail in the middle Kaza (Figure 3.2 and Appendix A). Such high-resolution mapping provides valuable information regarding the internal bed-scale architecture of stratal elements that cannot be captured even by closely spaced logs. In the best exposed areas of the upper Kaza outcrop at Castle Creek several stratal elements could be mapped in similar detail to provide more information of their internal make-up.

6.3.4 Chapter 4

- In this chapter matrix-rich sandstones were subdivided into four subfacies. Future research (ongoing in 2013 as part of Natasa Povovic's M.Sc. thesis work) will map the lateral trends and changes of subfacies in matrix-rich beds. Of particular interest is the lateral extent of ripples that cap some beds and their spatial relationship to the matrix-poor sandstone facies. These observations, then, will provide additional insight into the spatial evolution of fine-grain sediment laden flows.
- This study described what is interpreted to be a lateral progression of deposits in and adjacent to a plane wall jet flow with or without a hydraulic jump. Natasa Popovic's thesis work includes several additional units comprising matrix-rich sandstones. Preliminary work in 2012 indicates that at least one section includes a more longitudinal or oblique profile, which will add to the depositional model proposed in this thesis.
- Similar to the point made regarding Chapter 2, additional detailed petrography of matrix-rich sandstones would add valuable data and aid in the interpretation of the formative depositional flows of these strata.

6.3.5 Chapter 5

- In this study only the lower ~120 m of the upper Kaza at Castle Creek was mapped in detail (Figure 5.7). A similarly detailed map of the upper part of the upper Kaza exposure would provide not only a more complete picture of these deposits, but also provide additional raw data as input for statistical analysis and modelling.
- The Markov chain analysis in this study can be expanded with statistical testing to verify whether the observed transition matrix can be explained by a random process, or if the vertical trend of stratal element succession is guided by some underlying process.
- Modelling of the proximal basin floor is restricted to 1D stratigraphic logs in this study. Future work may include 2D and 3D stratigraphic modelling, including geocellular, synthetic seismic and reservoir models.

References

Aalto, K.R., 1971, Glacial marine sedimentation and stratigraphy of the Toby conglomerate (upper Proterozoic), southeastern British Columbia, northwestern Idaho and northeastern Washington: Canadian Journal of Earth Sciences - Revue Canadienne des Sciences de la Terre, v. 8, p. 753–787.

Adrian, R.J., 2010, Closing in on models of wall turbulence: Science, v. 329, p. 155-156.

Aitken, J. D., 1969, Documentation of a sub-Cambrian unconformity, Rocky Mountain Ranges, Alberta: Canadian Journal of Earth Sciences, v. 6, p. 193–200.

Aitken, J. D., and D. M. R. McDonough, (compilers), 1990, Late Proterozoic glaciation, rifting and eustacy, as illustrated by the Windermere Supergroup: Geological Association of Canada, Nuna Research Conference, Invermere and Valemount, British Columbia, Field Trip Guidebook, p. 1.1–10.27.

Alexander. J., McLelland, S.J., Gray, T.E., Vincent, C.E., Leeder, M.R., and Ellett, S., 2008, Laboratory sustained turbidity currents form elongate ridges at channel mouths: Sedimentology, v. 55, p. 845-868.

Allen, J.R.L., 1991, The Bouma division A and the possible duration of turbidity currents: Journal of Sedimentary Petrology, v. 61, no. 2, p. 291-295.

Amos, K.J., Peakall, J., Bradbury, P.W., Roberts, M., Keevil, G., and Gupta, S., 2010, The influence of bend amplitude and planform morphology on flow and sedimentation in submarine channels: Marine and Petroleum Geology, v. 27, p. 1431–1447.

Amy, L., and Talling, P.J., 2006, Anatomy of turbidite and debrite sandstones based on long distance (120 x 35 km) bed correlation, Marnoso-arenacea Formation, Northern Apennines, Italy: Sedimentology, v. 53, p. 161-212.

Arnott, R.W.C., 2007a, Stratal architecture and origin of lateral accretion deposits (LADs) and conterminuous inner-bank levee deposits in a base-of-slope sinuous channel, lower Isaac Formation (Neoproterozoic), East-Central British Columbia, Canada: Marine and Petroleum Geology, v. 24, p. 515-528.

Arnott, R.W.C., 2007b, Stratigraphic architecture and depositional processes of a proximal crevasse splay and genetically related, sinuous channel fill, Isaac Formation, British Columbia, Canada: *in* T. H. Nilsen, R. D. Shew, G. S. Steffens, and J. R. J. Studlick, eds., Atlas of deep-water outcrops: AAPG Studies in Geology 56.

Arnott, R.W.C., 2012, Turbidites, and the case of the missing dunes: Journal of Sedimentary Research, v. 82, p. 1-6.

Arnott, R. W., and F. J. Hein, 1986, Submarine canyon fills of the Hector Formation, Lake Louise, Alberta: Late Precambrian syn-rift deposits of the proto-Pacific miogeocline: Bulletin of Canadian Petroleum Geology, v. 34, p. 395–407.

Arnott, R.W.C., and Hand, B.M., 1989, Bedforms, primary structures and grain fabric in the presence of suspended sediment rain: Journal of Sedimentary Petrology, v. 59, no. 6, p. 1062-1069.

Arnott, R. W., and G. M. Ross, 2007, Overview: outcrop analysis of an ancient, passive margin, turbidite system: Windermere Supergroup, British Columbia, Canada, in T. H. Nilsen, R. D. Shew, G. S. Steffens, and J. R. J. Studlik, eds., Atlas of deep-water outcrops: AAPG Studies in Geology 56, p. 81–84.

Arnott, R.W.C., Wallace, K., and Laurin, J., 2011, Stratal architecture and temporal evolution of a passive margin mass-transport deposit, Neoproterozoic Isaac Formation, Cariboo Mountains, British Columbia, Canada, In: Mass-transport deposits in deepwater settings (Eds. Shipp, R.C., Weimer, P., Posamentier, H.W.), SEPM Special Publication no. 96, 532 pp.

Baas, J.H., and Best, J.L., 2002, Turbulence modulation in clay-rich sediment-laden flows and some implications for sediment deposition: Journal of Sedimentary Research, v. 72, p. 336-340.

Baas, J.H. and Best, J.L. 2008, The dynamics of turbulent, transitional and laminar clay-laden flow over a fixed current ripple: Sedimentology, v. 55, p. 635–666.

Baas, J.H., Best, J.L., Peakall, J., and Wang, M., 2009, A phase diagram for turbulent, transitional and laminar clay suspension flows: Journal of Sedimentary Research, v. 79, p. 162–183,

Baas, J.H., Best, J.L., Peakall, J., 2011, Depositional processes, bedform development and hybrid bed formation in rapidly decelerated cohesive (mud-sand) sediment flows: Sedimentology, v. 58, p. 1953-1987.

Bagnold, R.A., 1954, Experiments on a gravity-free dispersion of large solid spheres in a Newtonian fluid under shear: Proceedings of the Royal Society of London, v. 225, p. 49-63.

Bagnold, R.A., 1962, Auto-suspension of transported sediment: turbidity currents: Proceedings of the Royal Society of London, v. 265, p. 315-319.

Barker, S.P., Haughton, P.D.W., McCaffrey, W.D., Archer, S.G., and Hakes, B., 2008, Development of rheological heterogeneity in clay-rich high-density turbidity currents: Aptian Britannia Sandstone Member, U.K., continental shelf: Journal of Sedimentary Research, v. 78, p. 45–68.

Barnes, N. E., and W. R. Normark, 1985, Diagnostic parameters for comparing modern submarine fans and ancient turbidite systems, in A. H. Bouma, W. R. Normark, and N. E.

Barnes, eds., Submarine fans and related turbidite systems: New York, Springer-Verlag, p. 13–14 and back-pocket wall chart.

Beaubouef, R.T., Rossen, C., Zelt, F.B., Sullivan, M.D., Mohig, D.C., and Jennette, D.C., 1999, Deep-water sandstones, Brushy Canyon formation, West Texas. *In*: Field Guide for AAPG Hedberg Field Research Conference. AAPG Continuing Education Course Note Series, vol. 40, p. 48.

Beaubouef, R.T., Van Wagoner, J.C., and Adair, N.L., 2003, Ultra-high resolution 3-D characterization of deep-water deposits-II: Insignts into the evolution of a submarine fan and comparisons with river deltas: AAPG Search and Discovery Article #90013.

Bell, R.T., Jefferson, C.W., and Brennan, E., 1987, An hypothesis for an Australian- Canadian connection in the late Proterozoic and the birth of the Pacific Ocean: Australian Institute of Mining and Metallurgy, Pacific Rim Congress '87, Parksville, Victoria, p. 39–50.

Bernhardt, A., Jobe, Z.R., and Lowe, D.R., 2011, Stratigraphic evolution of a submarine channel-lobe complex system in a narrow fairway within the Magallanes foreland basin: Cerro Toro Formation, southern Chile: Marine and Petroleum Geology, v. 28, p. 785-806.

Best, J.L., Kirkbride, A.D., and Peakall, J., 2001, Mean flow and turbulence structure of sediment-laden gravity currents: new insights using ultrasonic Doppler velocity profiling. In: Particulate Gravity Currents (Ids. W.D. McCaffrey, B.C. Kneller and J. Peakall), IAS Spec Publ., 31, p.159-172.

Bouma, A.H., 1962, Sedimentology of some Flysch deposits: A graphic approach to facies interpretation: Elsevier, 168 pp.

Bouma, A.H., 2000, Fine-grained, mud-rich turbidite systems: model and comparison with coarse-grained, sand-rich systems, in A. H. Bouma, and C. G. Stone, eds., Finegrained turbidite systems: AAPG Memoir 72/SEPM Special Publication No. 68, p. 9– 20.

Bouma, A.H., Normark, W.R., Barnes, N.E., eds., 1985, Submarine Fans and Related Turbidite Systems: New York, Springer-Verlag, 351 p.

Buckley, S., E. Schwarz, V. Terlaky, J. Howell, and R.W.C. Arnott, 2010, Combining aerial photogrammetry and terrestrial lidar for reservoir analog modeling: Photogrammetric Engineering & Remote Sensing, v. 76, p. 953–963.

Campbell, R.B., Mountjoy, E.W., and Young, F.G,. 1973, Geology of McBride map-area, British Columbia: Geological Survey of Canada, Paper 72–35, 104 p.

Cantero, M.I., Cantelli, A., Pirmez, C., Balachandar, S., Mohring, D., Hickson, T.A., Yeh, T., Naruse, H., Parker, G., 2012, Emplacement of massive trubidites linked to extinction of turbulence in turbidity currents: Nature Geoscience, v. 5, p. 42-45.

Carr, T.R., 1982, Log linear models Markov chains and cyclic sedimentation: Journal of Sedimentary Petrology, v. 52, p. 905-912.

Carr, M., and Gardner, M.H., 2000, Portrait of a basin- floor fan for sandy deep-water systems, Permian lower Brushy Canyon Formation, west Texas, *in* A. H. Bouma and C. G. Stone, eds., Fine-grained turbidite systems: AAPG Memoir 72/SEPM Special Publication 68, p. 215–232.

Charlesworth, H. A. K., J. L. Weiner, A. J. Akehurst, H. U. Bielenstein, C. R. Evans, R. E. Griffiths, D. B. Remington, M. R. Stauffer, and J. Steiner, 1967, Precambrian geology of the Jasper region, Alberta: Research Council of Alberta, Bulletin, v. 23, p. 74.

Coleman, J., and D. B. Prior, 1982, Deltaic environments, in P. A. Scholle, and D. Spearing, eds., Sandstone depositional environments, v. 139–178: AAPG Memoirs 31.

Colpron, M., Logan, J.M., and Mortensen, J.K., 2002, U-Pb zircon age constraint for late Neoproterozoic rifting and initiation of the lower Paleozoic passive margin of western Laurentia: Canadian Journal of Earth Sciences = Revue Canadienne des Sciences de la Terre, v. 39, p. 133–143.

Damuth, J. E., and N. Kumar, 1975, Amazon Cone: morphology, sediments, age, and growth pattern: Geological Society of America Bulletin, v. 86, p. 863–878.

Davis. J.C., 1986, Statistics and Data Analysis in Geology: New York. John Wiley and Sons, 646 p.

Davis, L., 2010, Architecture of deep-marine interchannel deposits: Isaac Formation, Windermere Supergroup (Neoproterozoic), Southern Canadian Cordillera. M. Sc. Thesis, University of Ottawa.

Deptuck, M.E., Piper, D.J.W., Savoye, B., and Gervais, A., 2008, Dimensions and architecture of late Pleistocene submarine lobes off the northern margin of East Corsica: Sedimentology, v. 55, p. 869-898.

Devlin, W. J., H. K. Brueckner, and G. C. Bond, 1988, New isotopic data and a preliminary age for volcanics near the base of the Windermere Supergroup, northeastern Washington, U.S.A: Canadian Journal of Earth Sciences = Revue Canadienne des Sciences de la Terre, v. 25, p. 1906–1911.

Dill, R. F., 1964, Sedimentation and erosion in Scripps submarine canyon head., *In*: R. L. Miller (Ed.), Marine Geology: London, Macmillan, p. 23–41.

Drinkwater, N.J., and Pickering, K.T., 2001, Architectural elements in a high-continuity sand-prone turbidite system, late Precambrian Kongsfjord Formation, northern Norway: Application to hycrocarbon reservoir characterization: American Association of Petroleum Geologists Bulletin, v. 85, no. 10, p. 1731-1757.

Elliott, T., 2000, Depositional architecture of a sand-rich, channelized turbidite system: the upper Carboniferous Ross Sandstone Formation, western Ireland. *In*: Weimer, P., Slatt, R.M., Coleman, J., Rossen, N.C., Nelson, H., Bouma, A.H., Styzen, M.J., Lawrence, D.T. (Eds.), Deep-water Reservoirs of the World. GCSSEPM, p. 342-373.

Emery, D., and Myers, K.J., 1996, Sequence stratigraphy: Oxford, Blackwell Science, 297 p.

Evenchick, C. A., R. R. Parrish, and H. Gabrielse, 1984, Precambrian gneiss and late Proterozoic sedimentation in north-central British Columbia: Geology, v. 12, p. 233–237.

Everitt, B.S., and Skrondal, A., 2010, The Cambridge Dictionary of Statistics. Cambridge University Press, 4th ed., 478 p.

Fanning, C. M., and P. K. Link, 2004, U-Pb SHRIMP ages of Neoproterozoic (Sturtian) glaciogenic Pocatello Formation, southeastern Idaho: Geology, v. 32, p. 881–884.

Ferguson, C. F., 1994, Structural geology and stratigraphy of the northern Cariboo Mountains between Isaac Lake and Fraser River, British Columbia, Ph.D. thesis, University of Calgary, Calgary, 331 p.

Ferri, F., T. Hoy, and R. M. Friedman, 1999, Description, U-Pb age and tectonic setting of the Quesnel Lake Gneiss, east-central British Columbia: British Columbia Geological Survey Branch, Geological Fieldwork, Paper 1999–1, p. 69–80.

Fildani, A., Normark, W.R., Kostic, S., and Parker, G., 2006, Channel formation by flow stripping: large-scale scour features along the Monterey East Channel and their relation to sediment waves: Sedimentology, v. 53, p. 1265-1287.

Fildani, A., Shultz, M.R., Graham, S.A., and Leier, A., 2007, A deep-water amalgamated sheet system, Punta Barrosa Formation, Marina's Cliff, Chile. *In*: Nilsen, T., Shew, R., Steffens, G., Studlick, J. (Eds.), Deep-water Outcrops of the World Atlas: American Association of Petroleum Geologists Studies in Geology, 56, pp. 125-127.

Fildani, A., Hubbard, S.M., and Romans, B.W., 2009. Stratigraphic Evolution of Deepwater Architecture: Examples of Controls and Depositional Styles from the Magallanes Basin, Chile. *In*: Society of Sedimentary Geology, Fieldtrip Guidebook 10, p. 73.

Flint, S.S., Hodgson, D.M., Sprague, A.R., Brunt, R.L., Van der Merwe, W.C., Figueiredo, J., Prelat, A., Box, D., Di Celma, C., and Kavanagh, J.P., 2011. Depositional architecture and sequence stratigraphy of the Karoo basin floor to shelf edge succession, Laingsburg depocentre, South Africa: Marine and Petroleum Geology, v. 28, p. 658-674.

Frenz, M., Wynn, R.B., Georgiopoulou, A., Bender, V.B., Hough, G., Masson, D.G., Talling, P.J., and Cronin, B.T., 2008, Unravelling turbidite basin fill complexity: a case study from the Late Quaternary turbidite fill of the Agadir Basin, offshore Atlantic Morocco: International Journal of Earth Sciences, v. 98, p. 721-733.

Gabrielse, H., and R. B. Campbell, 1991, Upper Proterozoic assemblages, in H. Gabrielse, and C. J. Yorath, eds., Geology of the Cordilleran orogen in Canada: Geological Society of America, Geology of North America, v. G-2, p. 125–150.

Gammon, P. R., R. W. C. Arnott, and G. M. Ross, 2007, Architectural relationship between channels, levees, and debris flows: Isaac Channel 6, Castle Creek South, lower Isaac Formation, Windermere Supergroup, British Columbia, Canada, in T. H. Nilsen, R. D. Shew, G. S. Steffens, and J. R. J. Studlik, eds., Atlas of deep-water outcrops AAPG Studies in Geology 56, p. 102–105.

Gardner, M.H., and Borer, J.M., 2000, Submarine channel architecture along a slope to basin profile, Brushy Canyon Formation, west Texas. *In*: Bouma, A.H., Stone, C.G. (Eds.), Fine-grained Turbidite Systems. American Association of Petroleum Geologists Memoir 72 195e214. SEPM Special Publication, vol. 68.

Gardner, J.V., Bohannon, R.G., Field, M.E., and Masson, D.G., 1996, The morphology, processes, and evolution of Monterey Fan: a revisit. *In*: Gardner, J.V., Field, M.E., Twichell, D.C. (Eds.), Geology of the United States' Seafloor: The view from GLORIA. Cambridge Univ. Press, New York, NY, p. 193–220.

Gardner, M.H., Borer, J.M., Melick, J.J., Mavilla, N., and Wagerle, R.N., 2003, Stratigraphic process-response model for submarine channels and related features from studies of Permian Brushy Canyon outcrops, west Texas: Marine and Petroleum Geology 20, 757-787.

Gerasimoff, M. D., 1988, The hobson lake pluton, Cariboo Mountains, British Columbia, and its significance to mesozoic and early Cenozoic Cordilleran tectonics: Master thesis, Queen's University, Kingston.

Gervais, A., 2002, Analyse multi-échelles de la morphologie, de la géométrie et de l'architecture d'un système turbiditique sableux profond (système du Golo, marge est-Corse, mer Méditerranée). Unpubl. Ph.D. thesis, Univ. Bordeaux 1, 288 p.

Gervais, A., Savoye, B., Mulder, T., and Gonthier, E., 2006, Sandy modern turbidite lobes: a new insight from high resolution seismic data: Marine and Petroleum Geology, v. 23, p. 485–502.

Gingerich, P.D., 1969, Markov analysis of cyclic alluvial sediments: Journal of Sedimentary Petrology, v. 39, p. 330-332.

Google Earth, 2005, Castle Creek and Mt. Quanstrom exposure locations. 10U 690462.73mE and 5876480.73mN. ©Cnes/Spot 2012, ©Province of British Columbia 2010, ©Google 2012. http://www.earth.google.com [December 16 2012]

Groenenberg, R.M., Hodgson, D.M., Prélat, A., Luthi, S.M., and Flint, S.S., 2010, Flow-deposit interaction in submarine lobes: insights from outcrop observations and process-based numerical model realisations: Journal of Sedimentary Research, v. 80, p. 252–267.

Guibaudo, G., 1992, Subaqueous sediment gravity flow deposits: practical criteria for their field description and classification: Sedimentology, v. 39, p. 423-454.

Gutenberg, B. A., 1939, Tsunamis and earthquakes: Sismological Society of America Bulletin, v. 29, p. 517–526.

Hall, J.W., and Ewing, D., 2007, Three-dimensional turbulent wall jets issuing from moderate-aspect-ratio rectangular channels: AIAA Journal, v. 45, no. 6, p. 1177-1186.

Haughton, P.D.W., Barker, S.P., McCaffrey, W.D., 2003, 'Linked' debrites in sand-rich turbidite systems – origin and significance: Sedimentology, v. 50, p. 459-482.

Haughton, P.D.W., Davis, C., McCaffrey, W., Barker, S., 2009, Hybrid sediment gravity flow deposits – Classification, origin and significance: Marine and Petroleum Geology, v. 26, p. 1900-1918.

Heezen, B. C., 1956, Corrientes de turbidez del Rio Magdelena: Sociedad Geografica de Columbia Bulletin, v. 51–52, p. 135–143.

Heezen, B.C., and Ewing, M., 1952, Turbidity currents and submarine slumps and the 1929 Grand Banks earthquake: American Journal of Science, v. 250, p. 849–873.

Hein, F. J., and M. E. McMechan, 1994, Proterozoic- Lower Cambrian strata of the Western Canada Sedimentary Basin, in G. D. Mossop and I. Shetsen, eds., Geological Atlas of the Western Canada Sedimentary Basin: Canadian Society of Petroleum Geologists and Alberta Geological Survey, Calgary, Alberta, p. 57–68.

Henkel, D. J., 1970, The role of waves in causing submarine landslides: Geotechnique, v. 20, p. 75–80.

Hiscott, R.N., 1994, Loss of capacity, not competence, as the fundamental process governing turbidity currents: Journal of Sedimentary Research, v. 64, p. 209-214.

Hodgson, D.M., 2009, Distribution and origin of hybrid beds in sand-rich submarine fans of the Tanqua depocentre, Karoo Basin, South Africa: Marine and Petroleum Geology, v. 26, p. 1940-1956.

Hodgson, D.M., Flint, S.S., Hodgetts, D., Drinkwater, N.J., Johannessen, E.J., and Luthi, S.M., 2006, Stratigraphic evolution of fine-grained submarine fan systems, Tanqua depocenter, Karoo Basin South Africa. Journal of Sedimentary Research, v. 76, p. 19-39.

Hogg, A.J., Huppert, H.E., and Dade, W.B., 1997, Erosion by planar turbulent wall jets: Journal of Fluid Mechanics, v. 338, p. 317-340.

Hsu, S.K., Kuo, J., Lo, C.L., Tsai, C.H., Doo, W.B., Ku, C.Y., and Sibuet, J.C., 2008, Turbidity currents, submarine landslides and the 2006 Pingtung Earthquake off SW Taiwan: Terr. Atmos. Ocean Sci., v. 19, p. 767-772.

Huang, H., Imran, J., Pirmez, C., Zhang, Q., and Chen, G., 2009, The critical densiometric Froude number of subaqueous gravity currents can be non-unity or non-exitent: Journal of Sedimentary Research, v. 79, p. 479-485.

Hubbard, S.M., Romans, B.W., Graham, S.A., 2008. Deep-water foreland basin deposits of the Cerro Toro Formation, Magallanes Basin, Chile: architectural elements of a sinuous basin axial channel belt: Sedimentology, v. 55, p. 1333-1359.

Jaeger, H.M., Nagel, S.R., and Behringer, R.O., 1996, The physics of granular materials: Physics Today, v. 49, p. 32-36.

Jegou I., 2008. Etude de la transition chenal-levées/lobes dans les systèmes turbiditiques récents. Application à un système intra-pente du Delta du Niger, à l'éventail turbiditique de l'Amazone et au Néofan du Petit-Rhône. Unpubl. Ph.D. thesis, Univ. Bretagne Occidentale, 350 p.

Jegou, I., Savoye, B., Pirmez, C., and Droz, L., 2008, Channel–mouth lobe complex of the recent Amazon Fan: the missing piece: Marine Geology, v. 252, p. 62–77.

Johnson, S.D., Flint, S., Hinds, D., and De Ville Wickens, H., 2001, Anatomy, geometry and sequence stratigraphy of basin floor to slope turbidite systems, Tanqua Karoo, South Africa: Sedimentology, v. 48, p. 987-1023.

Kane, I.A., Pontén, A.S.M., 2012, Submarine transitional flow deposits in the Paleogene Gulf of Mexico: Geology, v. 40, no. 12, p. 1119-1122.

Karlstrom, K. E., Ahall, K.-I., Harlan, S. S., Williams, M. L., McLelland, J. and Geissman, J. W., 2001, Long-lived (1.8–1.0 Ga) convergent orogen in southern Laurentia, its extensions to Australia and Baltica, and implications for refining Rodinia: Precambrian Research, v. 111, p. 5–30.

Kendall, B. S., Creasar, R.A., Ross, G.M., and Selby, D.S., 2004, Constraints on the timing of Marinoan “Snowball Earth” glaciation by 187Re–187Os dating of a Neoproterozoic, post-glacial black shale in western Canada: Earth and Planetary Science Letters, v. 222, p. 729–740.

Kenyon, N. H., and Millington, J., 1995, Contrasting deep-sea depositional systems in the Bering Sea, *in* K. T. Pickering, R. N. Hiscott, N. H. Kenyon, F. Ricci Lucchi, and R. D. A. Smith, eds., Atlas of deep water environments: architectural style in turbidite systems: London, Chapman and Hall, p. 196–202.

Khan, Z., and Arnott, R.W.C., 2010, Experimental modelling of multiple non-climbing ripple set beds from suspended particle fallout: American Association of Petroleum Geologists 2010 Annual Convention and Exhibition, Abstracts Volume 19, p. 131.

Khan, Z.A., and Arnott, R.W.C., 2011, Stratal attributes and evolution of asymmetric inner- and outer-bend levee deposits associated with an ancient deep-water channel-levee complex within the Isaac Formation, southern Canada: Marine and Petroleum Geology, v. 28, p. 824-842.

Khan, Z.A., Arnott, R.W.C., and Pugin, A., 2011, An alternative model of producing topography in the crest region of deep-water levees: AAPG Bulletin, v. 95, n. 12, p. 2085-2106.

Khripounoff, A., Vangriesheim, A., Babonneau, N., Crassous, P., Dennielou, B., and Savoye, B., 2003, Direct observation of intense turbidity current activity in the Zaire submarine valley at 4000 m water depth: Marine Geology, v. 194, p. 151–158.

Kneller, B., and Branney, M.J., 1995, Sustained high-density turbidity currents and deposition of thick massive sands: Sedimentology, v. 42, p. 607-616.

Kostic, S., Sequeiros, O., Spinewine, B., Parker, G., 2010, Cyclic steps: A phenomenon of supercritical shallow flow from the high mountains to the bottom of the ocean: Journal of Hydro-environmental Research, v. 3, p. 167-172.

Krumbein, W.C., and Dacey, M.F., 1969, Markov chains and embedded Markov chains in geology: International Association of Mathematical Geology Journal, v. 1, p. 79-96.

Kubli, T. H., 1990, Geology of the Dogtooth Range, northern Purcell Mountains, British Columbia, Ph.D. thesis, University of Calgary, Calgary, 324 p.

Laurin, J., K. Wallace, R. W. C. Arnott, and E. Schwarz, 2007, Stratigraphic anatomy and depositional history of a mass-transport complex, Isaac Formation, Windermere Supergroup, British Columbia, Canada, in T. H. Nilsen, R. D. Shew, G. S. Steffens, and J. R. J. Studlik, eds., Atlas of deep-water outcrops: AAPG Studies in Geology 56, p. 119–122.

Leclair, S.F., and Arnott, R.W.C., 2003, Coarse-tail graded, structureless strata: indicators of an internal hydraulic jump: *in* Roberts, H.H., Rosen, N.C., Filion, R.H., and Anderson, J.B., eds., Shelf Margin Deltas and Linked Down Slope Petroleum Systems: Global Significance and Future Exploration Potential: SEPM, Gulf Coast Section, Houston, p. 817–836.

Leclair, S.F., and Arnott, R.W.C., 2005, Parallel lamination formed by high-density turbidity currents: Journal of Sedimentary Research, v. 75, p. 1–5.

Leeder, M.R., 1982, Sedimentology; Process and Product: London, Unwin Hyman, 344 p.

Lehrmann, D.J., and Goldhammer, R.K., 1999, Secular variation in parasequence and facies stacking patterns of planform carbonates: a guide to application of stacking-patterns analysis in strata of diverse ages and settings: *in* Advances in Carbonate Sequence Stratigraphy: Application to Reservoirs, Outcrops and Models. SEPM Special publication no. 63, p. 187-225.

Link, P.K., 1993, Middle and late Proterozoic stratified rocks in the western U.S. Cordillera, Colorado Plateau, and Basin and Range Province, *in* J.C. Reed, Jr. M.E. Bickford, R.S. Houston, P.K. Link, D.W. Rankin, P.K. Sims, and W.R. Van Schmus, eds., Precambrian: Conterminous U.S., The Geology of North America: Geological Society of America Decade of North American Geology Series, v. c-3, p. 474-690.

Lowe, D.R., 1975, Water escape structures in coarse-grained sediments: Sedimentology, v. 22, p. 157-204.

Lowe, D.R., 1979, Sediment gravity flows: their classification and some problems of application to natural flows and deposits: Soc. Econ. Paleontologists Mineralogists Spec. Pub. 27, p. 75-82.

Lowe, D.R., 1982, Sediment gravity flows: II. Depositional models with special reference to the deposits of high-density turbidity currents: Journal of Sedimentary Petrology, v. 52, p. 279-297.

Lowe, D.R., Guy, M., 2000, Slurry-flow deposits in the Britannia Formation (Lower Cretaceous), North Sea: a new perspective on the turbidity current and debris flow problem: Sedimentology, v. 47, p. 31-70.

Lowe, D.R., Guy, M., Palfrey, A., 2003, Facies of slurry-flow deposits, Britannia Formation (Lower Cretaceous), North Sea: implications for flow evolution and deposit geometry: Sedimentology, v. 50, p. 45-80.

Lund, K., Aleinikoff, J.N., Evans, K.V., and Fanning, C.M., 2003, SHRIMP U-Pb geochronology of Neoproterozoic Windermere Supergroup, central Idaho: Implications for rifting of western Laurentia and synchroneity of Sturtian glacial deposits: Geological Society of America Bulletin, v. 115, p. 349–372.

Maier, K.L., Fildani, A., Paull, C.K., Graham, S.A., McHargue, T.R., Caress, D.W., and McGann, M., 2011, The elusive character of discontinuous deep-water channels: New insights from Lucia Chica channel system, offshore California: Geology, v. 39, p. 327-330.

Martinsen, O.J., Lien, T., and Walker, R.G., 2000, Upper Carboniferous deep water sediments, western Ireland: analogues for passive margin turbidite plays. *In*: Weimer, P., Slatt, R.M., Coleman, J., Rossen, N.C., Nelson, H., Bouma, A.H., Styzen, M.J., Lawrence, D.T. (Eds.), Deep-water Reservoirs of the World. Gulf Coast Section-SEPM, p. 533-555.

Martinsen, O.J., Lien, T., Walker, R.G., and Collinson, J.D., 2003, Facies and sequential organization of a mudstone-dominated slope and basin floor succession: the Gull Island Formation, Shannon basin, western Ireland: Marine and Petroleum Geology, v. 20, p. 789-807.

Marusic, I., Mathis, R., and Hutchins, N., 2010, Predictive model for wall-bounded turbulent flow: Science, v. 329, p. 193-196.

Marvinney, K.L., Hoskinson, K.N., Smith, M., Terlaky, V., Arnott, R.W.C., and Chiarenzelli, J.R., 2009, Geochemistry of Neoproterozoic Mudrocks from the Windermere Supergroup: Geological Society of America Northeastern Section 44th Annual Meeting March 22-24 2009. Poster Presentation.

McDonough, M. R., 1989, Stratigraphy and structure of the Late Proterozoic Miette Group, northern Selwyn Range, Rocky Mountains, British Columbia, Ph.D. thesis, University of Calgary, Calgary, 290 p.

McKee, E.D., and Weir, G.W., 1953, Terminology for stratification and cross-stratification in sedimentary rocks: Geological Society of America Bulletin, v. 64, p. 381-390.

Menard, H. W., 1955, Deep-sea channels, topography, and sedimentation: AAPG Bulletin, v. 39, p. 236–255.

Meyer, L., 2004, Internal architecture of an ancient deep-water, passive margin, basin-floor fan system, Upper Kaza Group, Windermere Supergroup, Castle Creek, British Columbia: M.Sc. thesis, University of Calgary, Calgary, 175 p.

Meyer, L., and Ross, G.M., 2007, Channelized lobe and sheet sandstones of the Upper Kaza Group basin-floor turbidite system (Windermere Supergroup), British Columbia, Canada:

in T. H. Nilsen, R. D. Shew, G. S. Steffens, and J. R. J. Studlick, eds., Atlas of deep-water outcrops: AAPG Studies in Geology 56.

Miall, A.D., 1985, Architectural-element analysis: A new method of facies analysis applied to fluvial deposits: Earth-Science Reviews, v. 22, p. 261–308.

Middleton, G.V., and Hampton, M.A., 1973, Sediment gravity flows: mechanics of flow and deposition. In: Turbidity and Deep Water Sedimentation (Eds G.V. Middleton and A.H. Bouma), SEPM, Pacific Section, Short Course Lecture Notes, 1-38.

Middleton, G.V., Hampton, M.A., 1976, Subaqueous sediment transport and deposition by sediment gravity flows: In: Marine Sediment Transport and Environmental Management (Eds D.J. Stanley and D.J.P. Swift), p. 197-218, Wiley, New York.

Mills, P.C., 1983, Genesis and disgnostic value of soft-sediment deformation structures – a review: Sedimentary Geology, v. 35, p83-104.

Moore, G. T., G. W. Starke, L. C. Bonham, and H. O. Woodbury, 1978, Mississippi Fan, Gulf of Mexico – Physiography, stratigraphy, and sedimentological patterns, in A. H. Bouma, G. T. Moore, and J. M. Coleman, eds., Framework, Facies, and Oil-trapping Characteristics of the Upper Continental Margin: AAPG Studies in Geology 7, p. 155–192.

Morris, S. A., Kenyon, N.H., Limonov, A.H., and Alexander, J., 1998, Downstream changes of large-scale bedforms in turbidites around the Valencia channel mouth, north-west Mediterranean: implications for palaeoflow reconstruction: Sedimentology, v. 45, p. 365–377.

Mosher, D. C., D. J. W. Piper, D. C. Campbell, and K. A. Jenner, 2004, Near-surface geology and sedimentfailure geohazards of the central Scotian slope: AAPG Bulletin, v. 88, p. 703–723.

Mountjoy, E. W., 1980, Mount Robson, Alberta-British Columbia: Geological Survey of Canada Map 1499A, scale 1:250,000, 1 sheet.

Mulder, T., and Alexander, J., 2001, The physical character of subaqueous density flows and their deposits: Sedimentology, v. 48, no. 2, p. 269-299.

Mulder, T., and Etienne, S., 2010, Lobes in deep-sea turbidite systmems: State of the art: Sedimentary Geology, v. 229, p. 75-80.

Murphy, D. C., 1987a, Suprastructure/infrastructure transition, east-central Cariboo Mountains, British Columbia; geometry, kinematics and tectonic implications: Journal of Structural Geology, v. 9, p. 13–29.

Murphy, D. C., 1987b, Kaza Group, eastern Wells Gray Park, British Columbia: Geological Survey of Canada Paper 87–1A, p. 735–742.

Murphy, D. C., and C. J. Rees, 1983, Structural transition and stratigraphy in the Cariboo Mountains, British Columbia: Geological Survey of Canada Paper 83–1A, p. 245–252.

Mussa-Caleca, M., 2008, Architecture and depositional history of a Neoproterozoic deepwater slope channel complex in a passive margin setting: Isaac Formation, Windermere Supergroup, southern Canadian Cordillera: M.Sc. thesis, University of Ottawa, Ottawa, 128 p.

Mutti, E., 1985, turbidite systems and their relations to depositional sequences, *in* G. G. Zuffa, ed., Provenance of Arenites: NATO-ASI Series: Dordrecht, Reidel, p. 65–93.

Mutti, E., and G. Ghibaudo, 1972, Un esempio di torbiditi di conoide sottomarina esterna: le Arenario di San Salvatore (formazione di Bobbio, Miocene) nell'Appennino di Piacenza: Memorie dell'Accademia delle Scienze di Torino, Classe di Scienze Fisiche, Matematiche e Naturale, Serie 4a, no. 16, p. 1–41.

Mutti, E., and W. R. Normark, 1987, Comparing examples of modern and ancient turbidite systems: problems and concepts, in J. R. Leggett, and G. G. Zuffa, eds., Marine Clastic Sedimentology: Concepts and Case Studies: London, Graham and Trotman, p. 1–37.

Mutti, E., and W. R. Normark, 1991, An integrated approach to the study of turbidite systems, in P. Weimer, and M. H. Link, eds., Seismic facies and sedimentary processes of submarine fans and turbidite systems: New York, Springer-Verlag, p. 75–106.

Mutti, E., and Ricci Lucchi, F., 1972, Turbidites of the northern Apennines: Introduction to facies analysis (English translation by T.H. Nilsen, 1978): International Geology Review, v. 20, p. 125-166.

Navarro, L., 2006, Depositional architecture and evolution of deep-water base-of-slope and slope channel complexes in a passive margin setting: Isaac Formation, Windermere Supergroup (Neoproterozoic) southern Canadian Cordillera: M.Sc. thesis, University of Ottawa, Ottawa, 272 p.

Navarro, L., Khan Z., and Arnott, R.W.C., 2007, Architecture of a deep-water channel levee complex: Channel 3, Castle Creek South, Isaac Formation, Windermere Supergroup, Bristish Columbia, Canada, in T. H. Nilsen, R. D. Shew, G. S. Steffens, and J. R. J. Studlik, eds., Atlas of deep-water outcrops: AAPG Studies in Geology 56, p. 93–96.

Normark, W. R., 1970, Growth Patterns of Deep-Sea Fans: AAPG Bulletin, v. 54, p. 2170–2195.

Normark, W.R., 1978, Fan valleys, channels, and depositional lobes on modern, submarine fans: characters for recognition of sandy turbidite environments, American Association of Petroleum Geologists Bulletin, v. 62, p. 912-931.

Normark, W.R., Piper, D.J.W., and Hess, G.R., 1979, Distributary channels, sand lobes, and mesotopography of Navy submarine fan, California borderland, with applications to ancient fan sediments: Sedimentology, v. 26, p. 749–774.

Normark, W.R., Piper, D.J.W., and Stow, D.A.V., 1983, Quaternary development of channels, levees, and lobes on milddle Laurentian Fan: AAPG Bulletin, v. 67, no. 9, p. 1400–1409.

O'Byrne, C.J., Barton, M.D., Steffens, G.S., Pirmez, C., and Buergisser, H., 2007, Architecture of a laterally migrating channel complex: Channel 4, Isaac Formation, Windermere

Supergroup, Castle Creek north, British Columbia, Canada, in T. H. Nilsen, R. D. Shew, G. S. Steffens, and J. R. J. Studlick, eds., Atlas of deep-water outcrops: AAPG Studies in Geology 56, p. 115–118.

Parrish, R., and R. L. Armstrong, 1983, U-pb zircon age and tectonic significance of gneisses in structural culminations of the Omineca crystalline belt, British Columbia; the Geological Society of America, Rocky Mountain section, 36th annual meeting; cordilleran section, 79th annual meeting. Abstracts with Programs – Geological Society of America, v. 15, p. 324.

Parrish, R. R., R. J. Scammell, and J. K. Mortensen, 1988, The age of the Mount Copeland syenite gneiss and its metamorphic zircons, Monashee Complex, southeastern British Columbia: Geological Survey of Canada Paper 88–2, p. 21–28.

Parsons, J.D., Schweller, W.J., Stelting, C.W., Southard, J.B., Lyons, W.J., and Grotzinger, J.P., 2002, A preliminary experimental study of turbidite fan deposits: Journal of Sedimentary Research, v. 72, no. 5, p. 619-628.

Pigage, L.C., 1977, Rb-sr dates for granodiorite intrusions on the northeast margin of the Shuswap metamorphic complex, Cariboo Mountains, British Columbia: Canadian Journal of Earth Sciences = Revue Canadienne Des Sciences De La Terre, v. 14.

Piper, D.J.W., Cochonat, P., and Morrison, M.L., 1999a. The sequence of events around the epicenter of the 1929 Grand Banks earth- quake: initiation of debris flows and turbidity current inferred from sidescan sonar: Sedimentology, v. 46, p.79–97.

Piper, D.J.W., Hiscott, R.N., and Normark, W.R., 1999b, Outcrop- scale acoustic facies analysis and latest Quaternary development of Hueneme and Dume submarine fans, offshore California: Sedimentology, v. 46, p. 47-78.

Piper, D.J.W., Normark, W.R., 2001, Sandy fans – from Amazon to Huemene and beyond: American Association of Petroleum Geologists Bulletin, v. 85, no. 8, p. 1407-1438.

Pickering, K.T., and Clark, J.D., 1996, Architectural elements and growth patterns of submarine channels: application to hydrocarbon exploration: American Association of Petroleum Geologists Bulletin, v. 80, no. 2, p. 194–221.

Pickering, K.T., Hiscott, R.N. and Hein, F.J., 1989, Deep Marine Environments: Clastic Sedimentation and Tectonics. Unwin Hyman, London, 416 pp.

Price, R. A., 2000, The southern Canadian Rockies: evolution of a foreland thrust and fold belt: GeoCanada 2000, Field Trip Guidebook 13, 244 p.

Posamentier, H.W., and Kolla, V., 2003, Seismic geomorphology and stratigraphy of depositional elements in deep-water settings: Journal of Sedimentary Research, v. 73, no. 3, p. 367-388.

Posamentier, H.W., and Walker, R.G., 2007. Deep water turbidites and submarine fans. In Posamentier, H.W., and Walker, R.G., eds., Facies Models Revisited, SEPM Special Publication No. 84, p. 399-520.

Posamentier, H.W., Erskine, R.D., and Mitchum, R.M., JR., 1991, Models for submarine fan deposition within a sequence stratigraphic framework, *in* Weimer, P., and Link, M.H., eds., Seismic Facies and Sedimentary Processes of Submarine Fans and Turbidite Systems: New York, Springer-Verlag, p. 127–136.

Posamentier, H.W., Jervey, M.T., and Vail, P.R., 1988, Eustatic controls on clastic deposition I—conceptual framework, *in* Wilgus, C.K., Hastings, B.S., Kendall, C.G.St.C., Posamentier, H.W., Ross, C.A., and Van Wagoner, J.C., eds., Sea Level Changes: An Integrated Approach: SEPM, Special Publication 42, p. 109–124.

Postma, G., Nemec, W., and Kleinspehn, K.L., 1988, Large floating clasts in turbidites: a mechanism for their emplacement: Sedimentary Geology, v. 58, p. 47-61.

Powers, D.W., and Easterling, R.G., 1982, Improved methodology for using embedded Markov chains to describe cyclical sediments: Journal of Sedimentary Petrology, v. 52, p. 913-923.

Prélat, A., Hodgson, D.M., and Flint, S.S., 2009, Evolution, architecture and hierarchy of distributary deep-water deposits: a high-resolution outcrop investigation from the Permian Karoo Basin, South Africa: Sedimentology, v. 56, p. 2132-2154.

Prélat, A., Covault, J.A., Hodgson, D.M., Fildani, A., and Flint, S.S., 2010, Intrinsic controls on the range of volumes, morphologies, and dimensions of submarine lobes: Sedimentary Geology, v. 232, p. 66-76.

Privett, K., 2008, Architecture and depositional history of a Neoproterozoic depositional lobe in a passive margin setting, Lower Kaza Group, Windermere Supergroup, southern Canadian Cordillera, 68 p. + CD. B. Sc. Honours Thesis, University of Ottawa.

Pyles, D.R., 2007, Architectural elements in a ponded submarine fan, Carboniferous Ross Sandstone, western Ireland. *In*: Nilsen, T.H., Shew, R.D., Steffens, G.S., Studlick, J.R.J. (Eds.), Atlas of Deepwater Outcrops. American Association of Petroleum Geologists Studies in Geology, v. 56, p. 19.

Pyles, D.R., 2008, Multiscale stratigraphic analysis of a structurally confined submarine fan: Carboniferous Ross Sandstone, Ireland: AAPG Bulletin, v. 92, p. 557–587.

Pyles, D.R., and Jennette, D.C., 2009, Geometry and architectural associations of co-genetic debrite–turbidite beds in basin-margin strata, Carboniferous Ross Sandstone (Ireland): Applications to reservoirs located on the margins of structurally confined submarine fans: Marine and Petroleum Geology, v. 62, p. 1974-1996.

Pyles, D.R., Syvitski, J.P.M., and Slatt, R.M., 2011, Defining the concept of stratigraphic grade and applying it to stratal (reservoir) architecture and evolution of the slope-to-basin profile: An outcrop perspective: Marine and Petroleum Geology, v. 28, p. 675-697.

Reading, H. G., 1996, Sedimentary Environments: process, facies and stratigraphy: Cambridge, Blackwell Science, 688 p.

Reading, H. G., and M. Richards, 1994, Turbidite systems in deep-water basin margins classified by grain size and feeder system: AAPG Bulletin, v. 78, p. 792–822.

Reesor, J. E., 1973, Geology of the Lardeau map-area, east-half, British Columbia: Geological Survey of Canada Memoir 369, 129 p.

Reid, L.F., 2003, Stratigraphy, structure, petrology, geochronology and geochemistry of the Hobson Lake area (Cariboo Mountains, British Columbia) in relation to the tectonic evolution of the southern Canadian Cordillera: Doctoral thesis, University of Calgary, Calgary, 221 p.

Reid, L.F., P.S. Simony, and G.M. Ross, 2002, Dextral strike-slip faulting in the Cariboo Mountains, British Columbia: a natural example of wrench tectonics in relation to Cordilleran tectonics: Canadian Journal of Earth Sciences = Revue Canadienne des Sciences de la Terre, v. 39, p. 953–970.

Rocheleau, J., 2011, Depositional architecture of a near-slope turbidite succession: Upper Kaza Group, Windermerer Supergroup, Castle Creek, British Columbia, Canada: Masters thesis, University of Ottawa, Ottawa, 94 p.

Romans, B.W., Fildani, A., Hubbard, S.M., Covault, J.A., Fosdick, J.C., and Graham, S.A., 2011, Evolution of deep-water stratigraphic architecture, Magallanes Basin, Chile: Marine and Petroleum Geology, v 28, no. 3, p. 612-628.

Ross, G.M., 1991, Tectonic setting of the Windermere Supergroup revisited: Geology, v. 19, p. 1125-1128.

Ross, G.M., 2001, The Neoproterozoic Windermere Supergroup: An on-land continental margin turbidite system: Geological Survey of Canada Open File 3932, 2 sheets.

Ross, G.M., and D.C. Murphy, 1988, Transgressive stratigraphy, anoxia, and regional correlations within the late Precambrian Windermere grit of the southern Canadian Cordillera: Geology, v. 16, p. 139–143.

Ross, G.M., and S.A. Bowring, 1990, Detrital zircon geochronology of the Windermere Supergroup and the tectonic assembly of the southern Canadian Cordillera: Journal of Geology, v. 98, p. 879–893.

Ross, G.M., and R.R. Parrish, 1991, Detrital zircon geochronology of metasedimentary rocks in the southern Omineca Belt, Canadian Cordillera: Canadian Journal of Earth Sciences = Revue Canadienne des Sciences de la Terre, v. 28, p. 1254–1270.

Ross, G.M., and Ferguson, C.A., 2003, Geology and structure cross-sections, Eddy, British Columbia; Geological Survey of Canada, “A” Series Map, 1967A, scale 1:50,000, 1 sheet.

Ross, G.M., and Arnott, R.W.C., 2007, Regional Geology of the Windermere Supergroup, Southern Canadian Cordillera and Stratigraphic Setting of the Castle Creek Study Area, in T. H. Nilsen, R. D. Shew, G. S. Steffens, and J. R. J. Studlick, eds., Atlas of Deep-Water Outcrops: AAPG Studies in Geology 56.

Ross, G.M., McMechan, M.E., and Hein, F.J., 1989, Proterozoic history: birth of the miogeocline, in B. D. Ricketts, ed., The western Canada sedimentary basin: Canadian Society of Petroleum Geologists, p. 79–104.

Ross, G.M., Bloch, J.D., Krouse, H.R., 1995, Neoproterozoic strata of the southern Canadian Cordillera and the isotopic evolution of seawater sulfate: Precambrian Research, v. 73, p. 71-99.

Rothwell, R.G., Thomson, J., and Kahler, G., 1998, Low-sealevel emplacement of a very lare Late Pleistocene 'megaturbidite' in the western Mediterranean Sea: Nature, v. 392, p. 377-380.

Rowland, J.C., Stacey, M.T., and Dietrich, W.E., 2009, Turbulent characteristics of a shallow wall-bounded plane jet: experimental implications for river mouth hydrodynamics: Journal of Fluid Mechanics, v. 627, p. 423-449.

Saller, A., Werner, K., Sugiaman, F., Cebastiant, A., May, R., Glenn, D., and Barker, C., 2008, Characteristics of Pleistocene deep-water fan lobes and their application to an upper Miocene reservoir model, offshore East Kalimantan, Indonesia: AAPG Bulletin, v. 92, no. 7, p. 919-949.

Savoye, B., Cochonat P, Apprioual R, Bain O, Baltzer A, Bellec V, Beuzart P, Bourillet J.-F, Cagna R, Cremer M, Crusson A, Dennielou B, Diebler D, Droz L, Ennes J.-C, Floch G, Guiomar M, Harmegnies F, Kerbrat R, Klein B, Kuhn H, Landure J.-Y, Lasnier C, Le Drezen E, Le Formal J.-P, Lopez M, Loubrieu B, Marsset T, Migeon S, Normand A, Nouze H, Ondreas H, Pelleau P, Saget P, Seranne M, Sibuet J.-C, Tofani R, Voisset M, 2000, Structure and recent evolution of the Zaire deep-sea fan: preliminary results of the Zaïango 1 & 2 cruises (Angola-Congo margin). C. R. Acad. Sci., Ser. IIA 331 (3), 211–220.

Schwarz, E., and R. W. C. Arnott, 2007a, Anatomy and evolution of a slope channelcomplex set (Neoproterozoic Isaac Formation, Windermere Supergroup, southern Canadian Cordillera): implications for reservoir characterization: Journal of Sedimentary Research, v. 77, p. 89–109.

Schwarz, E., and Arnott, R.W.C., 2007b, Anatomy and evolution of a slope channelcomplex set (Neoproterozoic Isaac Formation, Windermere Supergroup, southern Canadian Cordillera): implications for reservoir characterization: Journal of Sedimentary Research, v. 77, p. 89–109.

Shanmugam, G., 2006, Deep-water processes and facies models: Implications for sandstone petroleum reservoirs: New York, Elsevier, 476 p.

Shanmugam, G., and R. J. Moiola, 1988, Submarine fans: characteristics, models, classification, and reservoir potential: Earth-Science Reviews, v. 24, p. 383–428.

Shanmugam, G., L. R. Lehtonen, T. Straume, S. E. Syversten, R. J. Hodgkinson, and M. Skibeli, 1994, Slump and debris flow dominated upper slope facies in the Cretaceous of the

Norwegian and Northern North Seas (61–67 N): implications for sand distribution: AAPG Bulletin, v. 78, p. 910–937.

Sinclair, H.D., and Tomasso, M., 2002, Depositional evolution of confined turbidite basins: Journal of Sedimentary Research, v. 72, p. 451-456.

Sixsmith, P.J., Flint, S.S., Wickens, H.deV., and Johnson, S.D., 2004, Anatomy and stratigraphic development of a Basin floor turbidite system in the Laingsburg Formation, Main Karoo Basin, South Africa. Journal of Sedimentary Research, v. 74, p. 239-254.

Smith, M.D., 2009, Stratigraphic and geochemical evolution of the Old Fort Point Fm., southern Canadian Cordillera: the deep-marine perspective of Ediacaran post-glacial environmental change. Ph. D. Thesis, University of Ottawa.

Smith, M.D., Arnaud, E., Arnott, R.W.C., and Ross, G.M., 2012, The record of Neoproterozoic glaciations in the Windermere Supergroup, southern Canadian Cordillera, In: The Geological Record of Neoproterozoic Glaciations (eds. Arnaud, E., Halverson, G.P., Shields-Zhou, G.), Geological Society Memoir no. 36., 752 pp.

Sprague, A.R., Sullivan, M.D., Campion, K.M., Jensen, G.N., Goulding, F.J., Garfield, T.R., Sickafoose, D.K., Rossen, C., Jennette, D.C., Beaubouef, R.T., Abreu, V., Ardill, J., Porter, M.L., and Zelt, F.B., 2002, The physical stratigraphy of deep-water strata: A hierarchical approach to the analysis of genetically related stratigraphic elements for improved reservoir prediction (abs.): AAPG Annual Meeting Program, p. A167.

Stow, D.A.V., and Johansson, M., 2000, Deep-water massive sands: nature, origin and hydrocarbon implications: Marine and Petroleum Geology, v. 17, p. 145-174.

Stow, D.A.V., and M. Mayall, 2000, Deep-water sedimentary systems: new models for the 21st century: Marine and Petroleum Geology, v. 17, p. 125–135.

Straub, K.M., Mohrig, D.C., Buttles, J., McElroy, B., and Pirmez, C., 2008, Interactions between turbidity currents and topography in aggrading sinuous submarine channels: A laboratory study: Geological Society of America Bulletin, v. 120, p. 368–385.

Sullivan, M., Jensen, G., Goulding, F., Jennette, D., Foreman, L., and Stern, D., 2000, Architectural analysis of deep-water outcrops: implications for exploration and development of the Diana sub-basin, western Gulf of Mexico. *In*: Weimer, P., Slatt, R.M., Coleman, J., Rossen, N.C., Nelson, H., Bouma, A.H., Styzen, M.J., Lawrence, D.T. (Eds.), Deep-water Reservoirs of the World. GCS-SEPM, p. 1010-1031.

Sumner, E., Amy, L., and Talling, P.J., 2008, Deposit structure and processes of sand deposition from a decelerating sediment suspension: Journal of Sedimentary Research, v. 78, p. 529 - 547.

Sumner, E.J., Talling, P.J., and Amy, L.A., 2009, Deposits of flows transitional between turbidity current and debris flow: Geology, v. 37, p. 991–994.

Sylvester, Z., Lowe, D.R., 2004, Textural trends in turbidites and slurry beds from the Oligocene flysch of the East Carpathians, Romania: Sedimentology, v. 51, p. 945-972.

Talling, P.J., 2013, Hybrid submarine flows comprising turbidity current and cohesive debris flow: Deposits, theoretical and experimental analyses, and generalized models: Geosphere, v. 9, p. 460-488

Talling, P.J., Amy, L.A., Wynn, R.B., Peakall, J., and Robinson, M., 2004, Beds comprising debrite sandwiched within cogenetic turbidite: origin and widespread occurrence in distal depositional environments, Sedimentology, v. 51, p163-194.

Talling, P.J., Wynn, R.B., Masson, D.G., Frenz, M., Cronin, B.T., Schiebel, R., Akhmetzhanov, A.M., Dallmeier-Tiessen, S., Benetti, S., Weaver, P.P.E., Georgiopoilou, A., Zuhlsdorff, C., and Amy, L.A., 2007, Onset of submarine debris flow deposition far from original giant landslide: Nature, v. 450, p. 541-544.

Talling, P.J., Masson, D.G., Sumner, E.J., and Malgesini, G., 2012, Subaqueous sediment density flows: Depositional processes and deposit types: Sedimentology, v. 59, p. 1937-2003.

Tripsanas, E. K., W. R. Bryant, and B. A. Phaneuf, 2004, Slope-instability processes caused by salt movements in a complex deep-water environment, Bryant Canyon area, northwest Gulf of Mexico: AAPG Bulletin, v. 88, p. 801–823.

Twitchell, D.C., Schwab, W.C., Nelson, C.H., Kenyon, N.H., and Lee, H.J., 1992, Characteristics of a sandy depositional lobe on the outer Mississippi fan from SeaMARC IA sidescan sonar images: Geology, v. 20, p. 689-692.

Vail, P.R., Mitchum, R.M., and Thompson, S., 1977, Seismic stratigraphy and global changes of sea level, part 3: Relative changes of sea level from coastal onlap, in C.E. Clayton, ed., Seismic stratigraphy - applications to hydrocarbon exploration: Tulsa, Oklahoma, American Association of Petroleum Geologists Memoir 26, p. 63-81.

Walker, R.G., 1978, Deep-water sandstone facies and ancient submarine fans: models for exploration for stratigraphic traps: AAPG Bulletin, v. 62, p. 932–966.

Walker, R.G., 1992, Turbidites and submarine fans: *in* Facies models, response to sea level change (eds. R.G. Walker, N.P. James), Geological Association of Canada.

Warme, J.E., R.A. Slater, and R.A. Cooper, 1978, Bioerosion in submarine canyons, in D. J. Stanley, and G. K. Kelling, eds., Sedimentation in Submarine Canyons, Fans, and Trenches: Stroudsburg, Dowden, Hutchinson & Ross, p. 65–70.

Wheeler, J.O., and P. McFeely, 1991, Tectonic Assemblage Map of the Canadian Cordillera and adjacent parts of the United States of America: Geological Survey of Canada, "A" series Map, 1712A, scale 1:2,000,000, 2 sheets.

Wynn, R.B., Kenyon, N.H., Masson, D.G., Stow, D.A.V., and Weaver, P.P.E., 2002a, Characterization and recognition of deep-water channel-lobe transition zones: AAPG Bulletin, V. 86, no. 8, p. 1441-1462

Wynn, R.B., Weaver, P.P.E., Masson, D.G., and Stow, D.A.V., 2002b, Turbidite depositional architecture across three inter-connected deep-water basins on the Northwest African Margin: Sedimentology, v. 49, p. 669-695.

Xu, J.P., Noble, M.A., and Rosenfeld, L.K., 2004, In-situ measurements of velocity structure within turbidity currents: Geophysical Research Letters, v. 31, Art. No. L09311.

Xu, J.P., Swarzenski, P.W., Noble, M., and Li, A.C., 2010, Event-driven sediment flux in Huemene and Mugu submarine canyons, southern California: Marine Geology, v. 269, p. 74-88.

Yu, B., Cantelli, A., Marr, J., Pirmez, C., O'Byrne, C., and Parker, G., 2006, Experiments on self-channelized subaqueous fans emplaced by turbidity currents and dilute mudflows: Journal of Sedimentary Research, v. 76, p. 889-902.

Appendix A: Detailed map of S1 in the Middle Kaza.

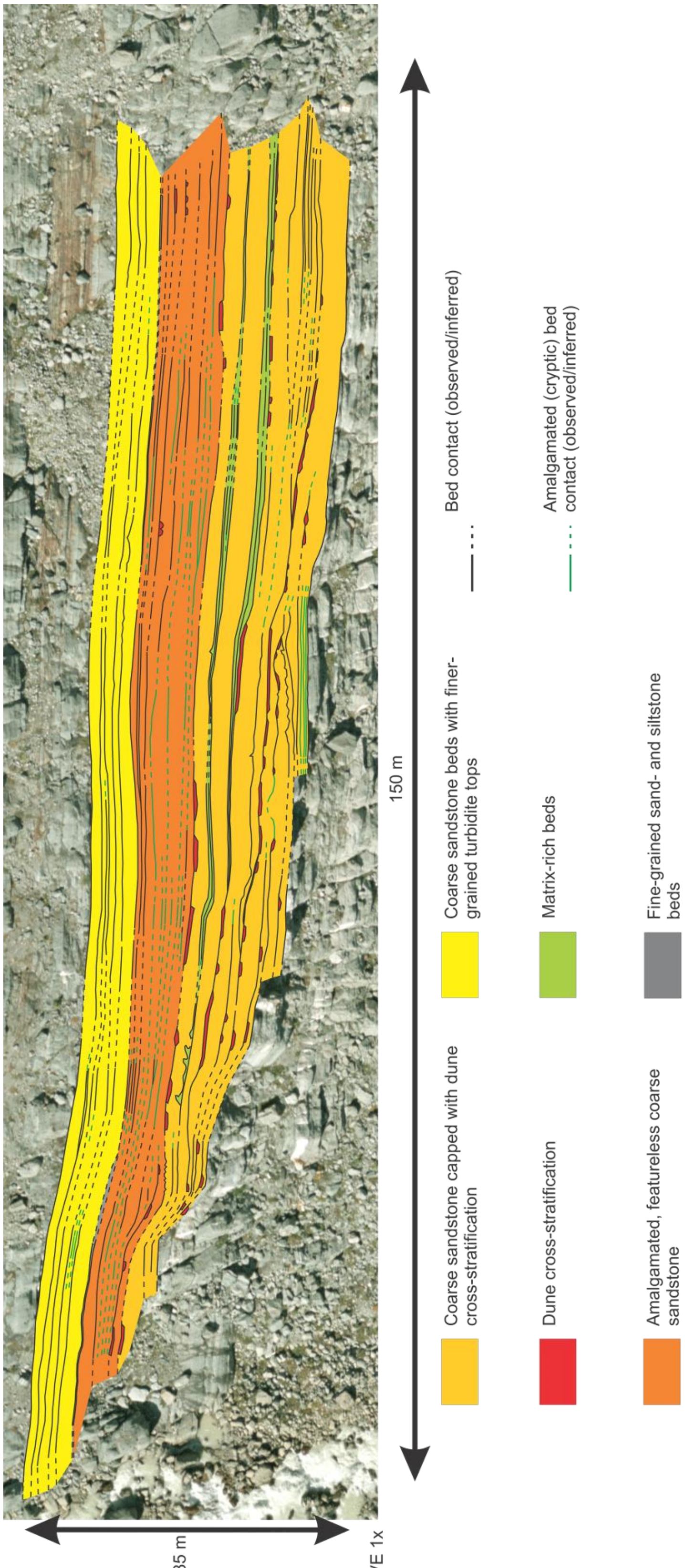

Detailed map of S1.

Appendix B: Description and interpretation of the six facies identified in basin-floor strata of the Windermere Supergroup.

Facies	Description		Interpretation		
	Lithology	Stratigraphic attributes	Sediment support and transport mechanism	Depositional process	Type of flow
1	Massive to normally coarse-tail graded, upper very coarse to lower very coarse sub-arkose sandstone with locally dispersed sub-angular granules and pebbles up to 8 mm in diameter Matrix content is ~20-30% and consists of silt with minor chlorite and muscovite. Rounded to sub-angular mudclasts are present locally. Scintillometer measurements are between 40-60 counts per second (cps).	Beds range from several decimeters to >3 m thick. Basal contacts commonly undulate with scours up to 30-40 cm deep. Beds are commonly amalgamated. Pipe, dish, ball-and-pillow and flame structures are abundant locally.	Near the bed and front of the sediment-charged turbidity current grain-to-grain interaction and hindered settling are probably the primary support mechanisms, but near the top and towards the tail where the flow is less dense and grain size smaller, turbulence most probably dominates (Bagnold 1954, 1962; Middleton and Hampton 1973; Jaeger *et al*. 1996).	Structureless massive or graded beds indicate deposition from the base of the flow by gradual although rapid aggradation (Arnott and Hand 1989; Stow and Johansson 2000, Sumner *et al*. 2008). Here sediment concentration exceeded flow capacity (Allen 1991) and sediment was deposited rapidly from collapsing laminar sheared layers, preventing the initiation of traction current bed forms (Arnott and Hand 1989, Kneller and Branney 1995; Sumner *et al*. 2008). Sediment was replenished by downward settling from areas higher in the flow (Kneller and Branney 1995; Stow and Johansson 2000; Sumner *et al*. 2008). Mudclasts may have been transported in such flows along a density interface separating the lower, dense part of the current from the upper, more dilute part (Postma *et al*. 1988).	Poorly stratified concentrated density flows *sensu* Mulder and Alexander 2001 or high density turbidity current *sensu* Lowe 1982. The presence of dewatering and loading structures in coarse sandstone indicates rapid deposition of sand and short recurrence interval between depositional events (Lowe 1975; Stow and Johansson 2000).
2	Coarse-tail graded sandstone. Matrix is generally absent in the upper part of the bed and pores are filled with ferroan calcite cement. Scintillometer measurements range from 30-50 cps in the lower, graded sandstone part of the bed, and decrease to 20-30 cps in the well-sorted layer at the top.	Beds are typically ~1-2 m thick; bases are commonly erosional with shallow (<20 cm deep) scours. Beds are capped commonly with medium- to large-scale (5 cm to >1 meter) cross-stratified or planar-laminated sandstone.	Similar to Facies 1.	Basal graded part of bed is similar to deposition of Facies 1. Medium- and large-scale cross-stratification at the tops of beds are interpreted to be dunes whereas planar stratified sandstone is interpreted to represent plane bed transport in high or low concentration flows. Both formed of sediment reworked from the underlying structureless part of the bed.	Type of flow depositing the basal part of the bed is similar to Facies 1. The presence of dunes indicates that the formative flows were sufficiently dilute to permit the initiation, amplification and development of dune bed forms (Arnott 2012; Talling *et al*. 2012), whereas, if flows were faster and/or the sediment

					concentration too high, traction-transported sediment formed plane bed (Arnott 2012).
3	The basal part of the bed comprises coarse-tail graded sandstone similar to Facies 1. This, then, is overlain abruptly by distinctly darker grey-coloured, fine and very fine sandstone. Small, rounded mudclasts are typically concentrated near abrupt grain size change within the bed. Scintillometer measurements range from 40-60 cps in the lower, graded sandstone part of the bed, and increase to 60-75 cps in the well-sorted layer at the top.	Beds are ~1 m thick. Grain-size change is abrupt between the lower and upper part of the bed. The upper part comprises common planar and ripple cross-lamination, capped locally by a thin layer of siltstone.	The sediment support mechanism for the lower part of the bed is similar to Facies 1. The upper fine-grained part of the bed most probably indicate fully turbulent conditions in a low concentration flow (Mulder and Alexander 2001; Talling *et al*. 2012).	Depositional process of the graded basal part of beds is similar to Facies 1. In the upper part of the bed, high matrix content in the planar-laminated sandstone indicates capacity driven deposition that prevented formation of angular bed forms (Leclair and Arnott 2005; Sumner *et al*. 2008; Arnott 2012; Talling *et al*. 2012). The overlying unit of single-set, non-climbing ripple cross-stratification is analogous to the Bouma Tc division (Bouma 1962) formed under low rates of sediment fallout (Khan and Arnott 2010). The uppermost siltstone drape indicates deposition from the low energy tail part of flows and is analogous to the Bouma Td division (Bouma 1962).	The type of flow depositing the basal part of the bed is similar to Facies 1. The upper part of the bed was deposited from a decelerating and longitudinally stratified flow with a high-concentration body depositing the relatively matrix-rich planar laminated unit, followed by a dilute tail that formed the ripple cross-stratified and then silt layers.
4	Massive to coarse-tail graded subarkose sandstone with a grain size ranging from lower medium to lower coarse sand, and commonly with abundant (30-50%) chlorite and muscovite matrix with minor silt, giving the rocks a distinctive dark grey-green colour. Rounded and elongated sandstone and mudstone clasts are locally common, and are typically sheared and highly plastically deformed; their abundance varies laterally over 10's to 100's of meters, but are vertically uniformly distributed within the bed. Scintillometer readings range from 50-70 cps.	Basal contacts are typically non-erosive. Bed thickness ranges from 10 cm to 1 m. Small-scale (<5cm thick) cross-stratification (i.e. ripple) is rare, but where present occurs at the top of the bed and contains notably less matrix.	The grain size and high matrix content indicate that turbulence, grain-to-grain interaction, buoyancy and hindered settling played important roles in suspending sediment (Mulder and Alexander 2001).	Distinctively poorly-sorted, matrix-rich, massive to subtly graded beds with abundant mudclasts represent capacity-driven deposition from flows undergoing extreme rates of sediment fallout (Hiscott 1994; Leclair and Arnott 2005). Such high rates of fallout completely suppressed the development of tractional bed forms (Arnott and Hand 1989; Leclair and Arnott 2005; Sumner *et al*. 2008). The ripple cross-stratified layer at the top of some beds is notably better sorted and finer grained, indicating deposition of new sediment sourced from the low energy, dilute tail part of flows (analogous to the Bouma Tc division; Bouma (1962)).	The poorly-sorted, matrix-rich nature of beds and the even distribution of dispersed mudclasts indicates that these flows were likely poorly stratified, and may have been transitional in nature between cohesive and non-cohesive flow (Talling *et al*. 2004, 2012; Baas and Best 2002, 2008). However most beds are coarse-tail graded suggesting that grain mobility was not entirely restricted and that some differential grain settling occurred.
5	Graded fine-grained sandstone to siltstone and mudstone. Scintillometer readings range from 60-65 cps in sandier intervals to over 120 cps in mud rich intervals.	Beds range from 1 cm to 20 cm thick. Beds typically composed of a thin structureless unit overlain by planar and/or cross-laminated sandstone, and topped by a thin silty cap.	Sediment was fully supported by fluid turbulence.	These beds are analogous to Bouma Tabcd(e) turbidites (Bouma 1962).	Relatively dilute, well stratified and fully turbulent flows.
6	Matrix-supported, ungraded conglomerate composed of a mud-rich matrix and chaotically dispersed sand- and mudstone clasts. Dispersed quartz pebbles are	Beds are ~1 to several 10's of m thick. Clasts are typically sheared and deformed, but commonly	Matrix strength provides the main sediment support.	Deformed clasts indicate that they were consolidated but not lithified at the time of transport. The occurrence of large meter-scale clasts indicates that turbulence, which most likely would disintegrate unlithified clasts,	Cohesive debris flow with high (up to >90%) sediment concentration (Leeder 1982).

	present also and locally abundant. Scintillometer readings tend to be highly variable, but generally are of the order of 50-70 cps.	preserve original stratification.		was damped (Postma *et al*. 1988). The flow deposited by "en-masse" freezing (Mulder and Alexander 2001; Talling *et al*. 2012).	

Appendix C: Location of cross-sections in the Upper Kaza.

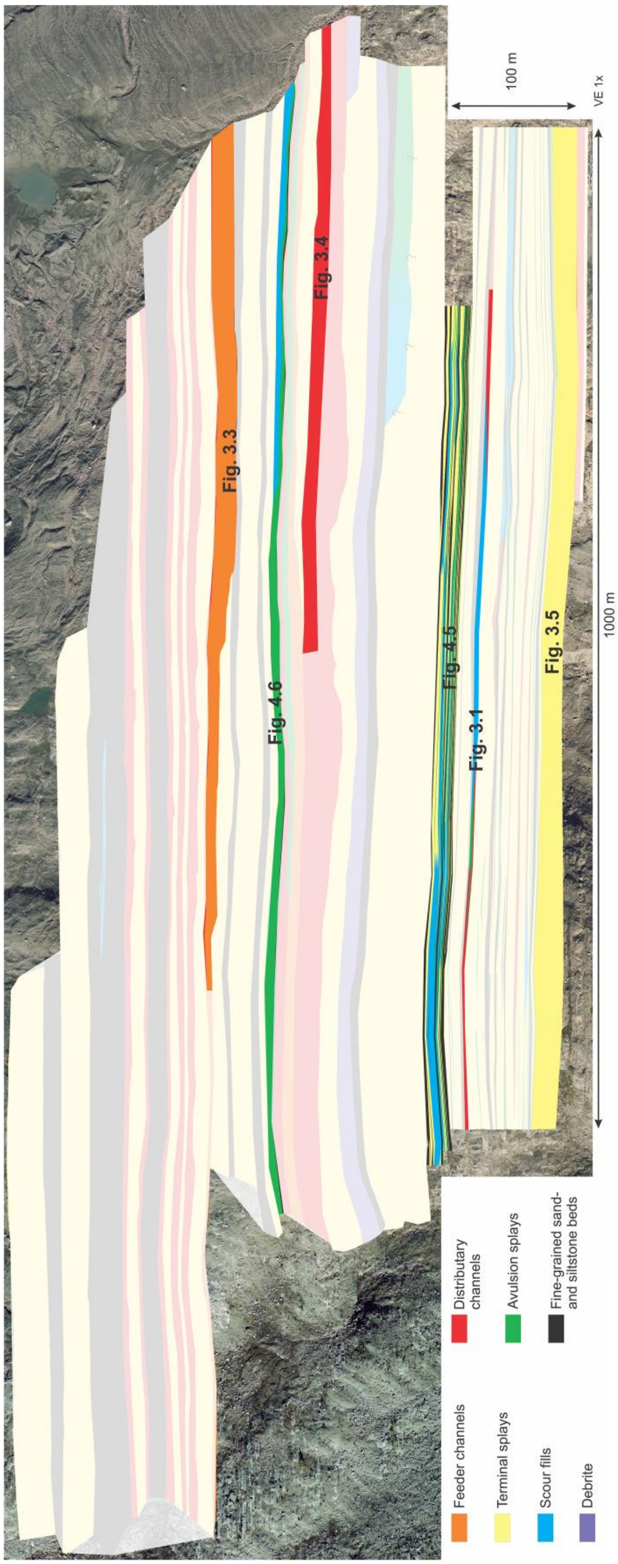

Image showing the location of figures in chapters 3 and 4.

Appendix D: Stratigraphic correlation of the Middle Kaza at the Eagle Valley outcrop.

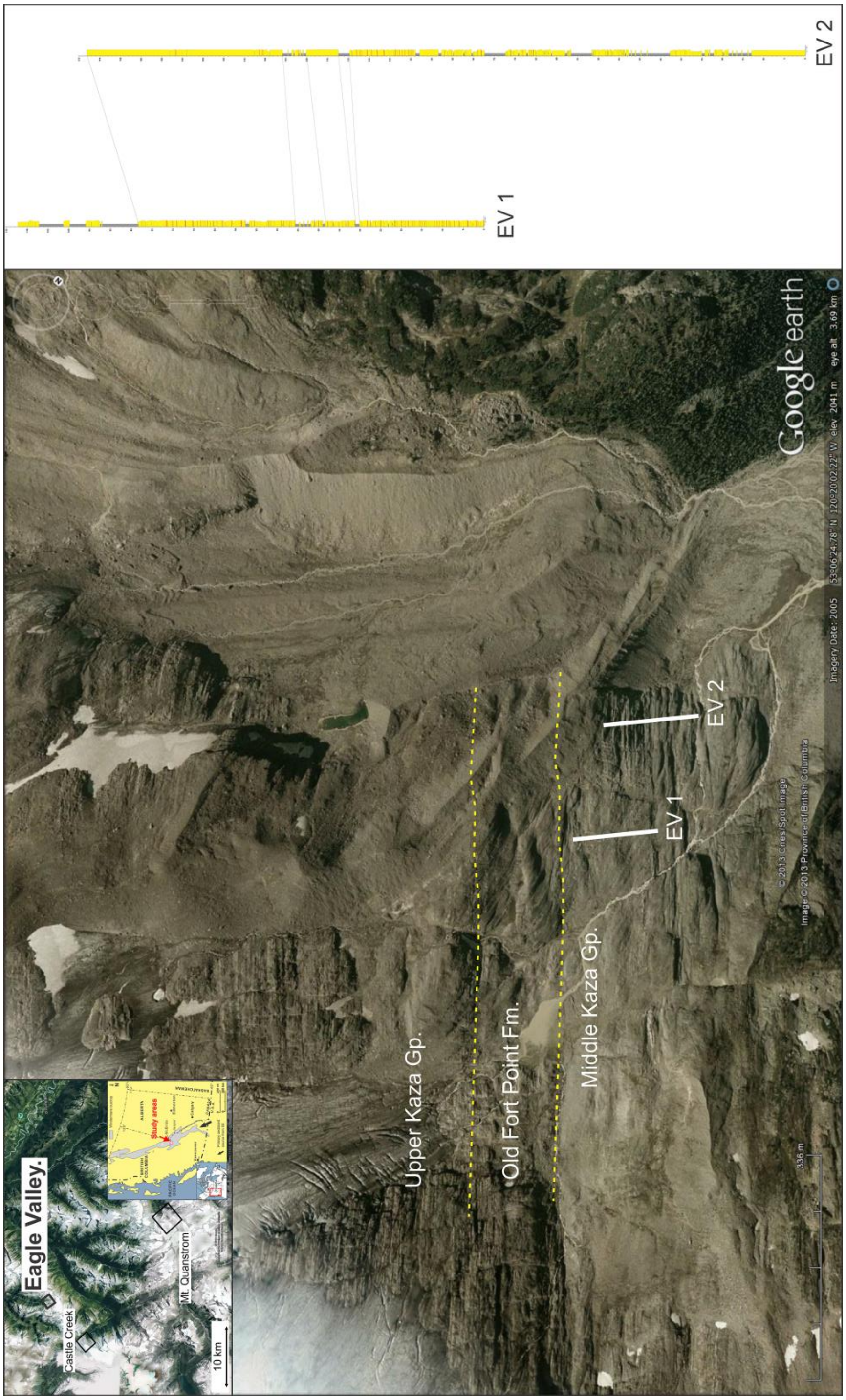

Inset image shows location of the Eagle Valley outcrop. Background images © Cnes/Spot 2012, © Province of British Columbia 2010, © Google 2012.

Appendix E: Combining aerial photogrammetry and terrestrial lidar for reservoir analog modeling

Combining Aerial Photogrammetry and Terrestrial Lidar for Reservoir Analog Modeling

Simon J. Buckley, Ernesto Schwarz, Viktor Terlaky, John A. Howell, and R.W. (Bill) Arnott

Abstract

High-resolution aerial photography was captured covering a geological outcrop at Castle Creek, British Columbia, Canada. Here, for the purposes of hydrocarbon analog modeling, the outcrop was required to be accurately surveyed, so that key stratigraphic surfaces could be mapped in three dimensions. Because the outcrop strata were vertically orientated, these surfaces could be tracked over a wide area; however, to provide a true reconstruction of the geology, it was necessary to also model localized vertical cliffs providing a cross-section through the stratigraphy. Terrestrial lidar was utilized to cover these cliff sections which were poorly represented in the 2.5D aerial data. The integrated outcrop surface was textured with metric aerial and terrestrial imagery providing a photorealistic model that could be used for interpretation by geologists. This formed the basis for building a geocellular model of the geological volume, which was used to assist in the understanding of subsurface reservoirs where data are often limited.

Introduction

The use of digital spatial data collection techniques is becoming common within the geology discipline. In particular, studies of hydrocarbon outcrop analogs have recently begun to embrace techniques such as digital photogrammetry, the global positioning system (GPS), and laser scanning (Pringle *et al.*, 2004; Bellian *et al.*, 2005; Lebel *et al.*, 2007; Buckley *et al.*, 2008). Outcrop analogs give geologists first-hand experience of the depositional environments and geometric configurations of subsurface oil and gas producing reservoirs, and aquifers. Because the subsurface is normally inaccessible for study, except for disparate drilled well bores and geophysical measurements, outcrop analogs are used to improve the statistical modeling required when planning an extraction strategy for hydrocarbon production (Pringle *et al.*, 2006). Typically, a geocellular model is used to represent the reservoir or reservoir analog volume. Such a model integrates geometrical, geophysical, and geological interpretation into a computer-based realization of the subsurface. The geometry of geological features (for example, stratigraphic surfaces and faults) constrains the model in space, while grid cells (voxels) are assigned properties relating to the geology, porosity, permeability, and fluid saturations. Fluid flow simulation can then be used to assess the production potential of the geological volume and the impact of different heterogeneities and well distributions upon the recovery from the oil field. In recent years, geocellular models of reservoir analogs have been generated combining geometrical configurations and sedimentological attributes extracted from outcrop data and petrophysics from reservoirs (e.g., Enge *et al.*, 2007). The contribution of geomatics techniques within this scenario is by providing high-resolution and accurate geometry for constraining the geocellular model. In addition, the creation of virtual outcrop models gives a three-dimensional environment for interpretation, analysis and education which, combined with traditional field data, is of extreme value for the geologist (Lebel and Da Roza, 1999; Banerjee and Mitra, 2004). Higher resolution spatial data allows more detailed studies to be carried out at a variety of scales, and in a more quantitative manner than possible using traditional field techniques alone (Enge *et al.*, 2007).

Criteria for outcrop selection are based on the similarity of the analog processes and geology within the subsurface reservoir, the degree of exposure, and the "three-dimensionality" of the outcrop, as well as more practical issues, such as vegetation cover and accessibility. The amount of three-dimensional exposure is critical for being able to recreate the geological volume (Bryant *et al.*, 2000; Pringle *et al.*, 2004; Enge *et al.*, 2007), and the outcrop must have surfaces exposing the geology along the dip direction (Groshong, 1999). Without this, it may not be possible to determine the geometry of key stratigraphic surfaces behind the outcrop face, increasing uncertainty in the resultant model. For subsurface reservoirs, where 3D seismic data are available, surfaces may be tracked over large distances in all directions; however, for outcrop data where surfaces disappear below, or are eroded above, the ground, recreating surface geometry is more challenging. In this case, the available

Simon J. Buckley and John A. Howell are with the Centre for Integrated Petroleum Research, University of Bergen, Postboks 7800, N-5020 Bergen, Norway (simon.buckley@cipr.uib.no).

Ernesto Schwarz is with Centro de Investigaciones Geológicas (CONICET), National University of La Plata, 1 #644, B1900TAC La Plata, Buenos Aires, Argentina.

Viktor Terlaky and R.W. (Bill) Arnott are with the Department of Earth Sciences, University of Ottawa, 140 Louis Pasteur, K1N 6N5 Ottawa, Canada.

Photogrammetric Engineering & Remote Sensing
Vol. 76, No. 8, August 2010, pp. 953–963.

0099-1112/10/7608–0953/$3.00/0

three-dimensionality is used to constrain the modeled geological volume, using lines and points digitized on the outcrop to act as guides for extrapolating surfaces behind the outcrop faces. Coupled with this is an extensive conceptual geological model of the system, developed using traditional fieldwork, which is used to assist with surface recreation.

The introduction of terrestrial laser scanning (lidar) has had a large impact on the study of outcrops, as the rapid, precise data acquisition of the active laser sensor allows topography to be captured without the relatively complex and time consuming processing workflow of close-range digital photogrammetry. The associated uncertainties in automated terrain extraction, caused by a complicated surface or low image texture, are also removed, making the procedure attractive for non-specialists. This has been seen in the recent growth of applications and literature related to laser scanning in geology (Bellian *et al.*, 2005; Sagy *et al.*, 2007; Buckley *et al.*, 2008).

This paper reports on research combining two techniques, digital aerial photogrammetry and terrestrial laser scanning, for creating a high-resolution photo-realistic model of a large outcrop occurring at Castle Creek, east-central British Columbia, Canada. The site is characterized by vertically-dipping layers, a result of compression and uplift during the building of the mountain belt within the southern Canadian Cordillera, where the study area is located. The integration of the two methods was therefore required: aerial photogrammetry to model the overall outcrop surface, and terrestrial lidar to develop the third dimension at localized cliff sections providing a cross-section through the stratigraphy. The model was then used as the basis for interpretation and digitization of geological surfaces, allowing the recreation of the geology within a geocellular model.

Background to the Castle Creek Study Area

The Castle Creek study area is situated in the Cariboo Mountains, east-central British Columbia, Canada. These mountains form part of the southern Canadian Cordillera, an extensive orogenic belt that borders the western margin of Canada and was built mainly during the Mesozoic (Ross *et al.*, 1995). At Castle Creek, a 2 km-thick succession of sandstones and mudstones belonging to the Neoproterozoic Windermere Supergroup crops out (Figure 1). The present day strata dip near-vertically, as they have been rotated approximately 95° during uplift from the near-horizontal setting in which they were originally deposited (Ross and Arnott, 2008). Additionally, due to the relatively recent retreat of the Castle Creek glacier, the outcrop surface is polished and largely free of vegetation. This allows geologists to track key stratigraphic surfaces and bed packages laterally for hundreds of meters, while the stratigraphy can be followed up uninterrupted for over two kilometers (Figure 1). This is in sharp contrast to many analog studies, which may be limited in terms of stratigraphic thickness by the height of cliffs or depth of quarrying, as well as areal extension provided by outcrop exposure.

The succession exposed at Castle Creek is interpreted to represent deep-marine sediments deposited mainly by turbidity currents in a passive (continental) margin, and is collectively known as the Windermere Turbidite System (Ross

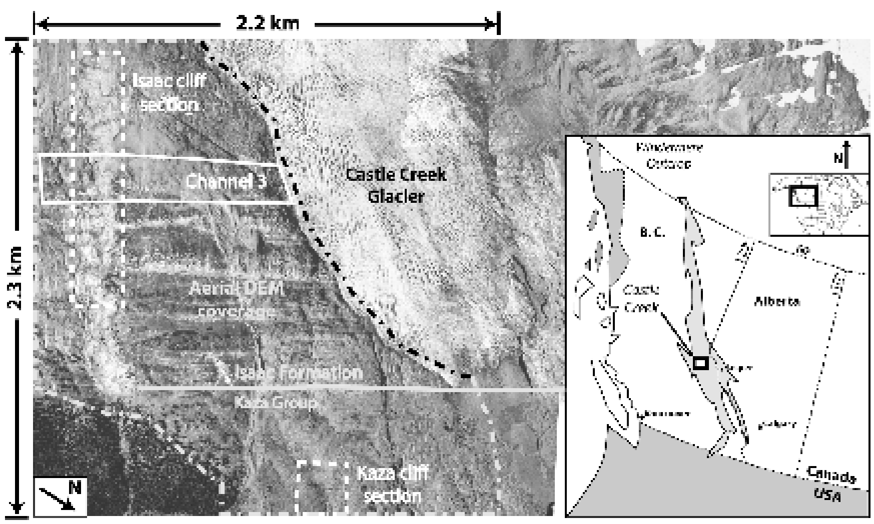

Figure 1. Aerial photograph mosaic of Castle Creek, British Columbia, Canada, showing extents of the geological area, the stratigraphic units of the Windermere Turbidite System and the location of the Isaac Channel 3 section. Also shown is the coverage of the DEM created from the stereo aerial photography (dashed-dotted line) and the location of cliff sections scanned using terrestrial lidar (dashed lines). Inset: location map showing the extent of the Windermere Turbidite System (after Ross, 1991).

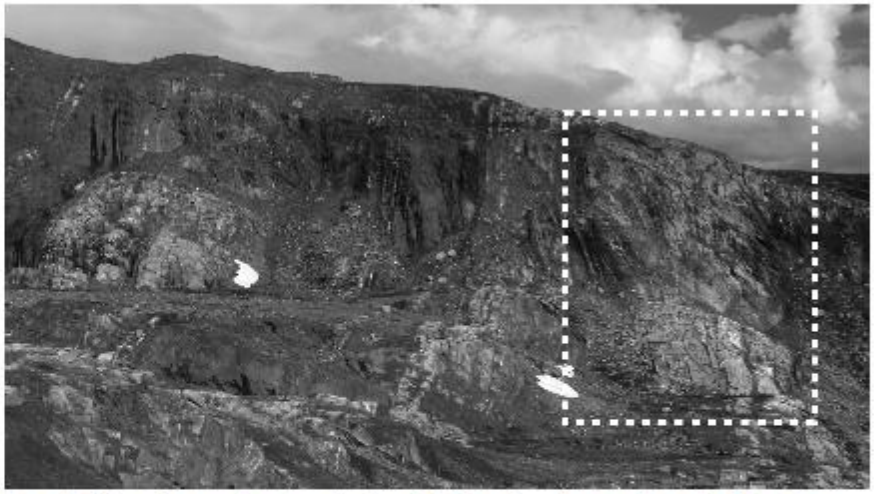

Figure 2. Cliff section exposing channel bodies of the Isaac Formation, as photographed from the ground (cliff height: approximately 90 m). The Isaac Channel 3 study area is highlighted.

and Arnott, 2008). The Kaza Group at the bottom of the section is composed of sandstone-dominated, sheet-like to poorly-channelized deposits interpreted to represent a basin floor setting (Ross and Arnott, 2008). The overlying Isaac Formation comprises six major, laterally extensive (kilometer-scale), sandstone-rich units surrounded by thin-bedded, mudstone-rich strata and debris-flow/slide complexes, interpreted to represent slope deposition (Schwarz and Arnott, 2007; Ross and Arnott, 2008). These deep-marine deposits are relevant because of current hydrocarbon exploration and development being conducted in similar continental-margin basins, such as offshore Brazil, West Africa and the Gulf of Mexico (Schwarz and Arnott, 2007).

This particular study focused on a detailed subset of the Castle Creek area, with the aim of modeling part of a single large channel body as a geocellular volume. This area (marked on Figure 1; Figure 2) was termed Isaac Channel 3 and represents one of six major sandstone-rich channel units present within the Isaac Formation at Castle Creek (Navarro *et al.*, 2008). This unit provides geologists with the opportunity to study well-exposed channelized deposits and laterally adjacent levee and overbank deposits, as well as acting as an analog for modern turbidite settings (Navarro *et al.*, 2008). The size of the Isaac Channel 3 area was approximately 1,100 m by 100 m and, like the Castle Creek area as a whole, consisted of a well-exposed 2D section. For this study, it was aimed to be able to map the relative position of key geological surfaces with a precision of around 0.3 m over the outcrop extent.

Technique Selection

The near-vertical orientation of the layers means that the outcrop stratigraphy is exposed effectively as a two-dimensional cross-section. Because of the lack of vegetation on the outcrop surface, a method such as digital aerial photogrammetry or airborne laser scanning would have been suitable for acquiring topographic data. However, the relatively smooth outcrop surface, and the requirement for high-resolution imagery for geological mapping meant that aerial stereo-photography was the preferred method for terrain modeling. In addition, as part of earlier work on the Castle Creek outcrop, high-resolution aerial photography had already been captured and was available for photogrammetric processing (Schwarz and Arnott, 2007).

For the Isaac Channel 3 study area, a certain amount of three-dimensionality was present in the topographic undulation of the outcrop surface. However, near-vertical cliffs (up to 100 m high) occurring in the Castle Creek area, and across the study section (Figure 2), offered the opportunity to model more detailed profiles through the outcrop. Although the aerial photogrammetric data gave excellent coverage of the outcrop surface, little 3D information was present for the modeling of the volume. Vertical aerial photography allows only a 2.5D representation of the terrain, which was insufficient for this study, where extra detail in the cliffs was required. Therefore, a terrestrial laser scanner equipped with a digital camera was used to acquire higher resolution terrain data covering selected cliffs, which allowed the continuation of the geological surfaces in the dip direction into the outcrop (Figure 3) to be retrieved. In this way, the two techniques were complementary, with the aerial data giving more 2D coverage of the whole area where less accuracy was required in mapping the various layers, and the laser data gave increased accuracy and allowed the interpretation of more subtle details of the 3D geometry.

Data Collection Methodology

Aerial photography had been flown in summer 2001 using a calibrated Zeiss RMK TOP30 camera equipped with a 300 mm lens (calibrated $f = 304.953$ mm). With a flying height of

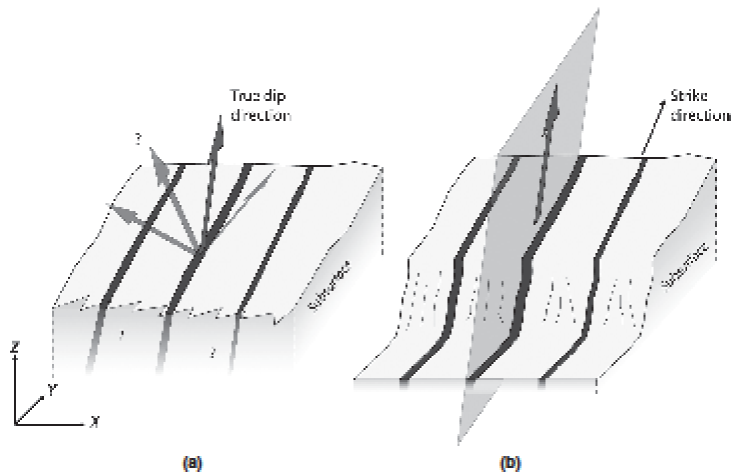

Figure 3. Diagram showing the requirement for three-dimensional exposure when attempting to model a geological outcrop: (a) Terrain surface with low relief, and (b) Additional relief creates a cross section through the geology in the dip direction, allowing the orientation of layers to be measured.

around 3,300 m (10,827 ft) ASL and an average ground height of 2,000 m (6,562 ft) AMT, this configuration resulted in a photo scale of approximately 1:4000. The overlap between adjacent photographs was 70 percent and sidelap of 10 percent. The area highlighted in Figure 1 was chosen for digital elevation model (DEM) extraction, equivalent to the main geological study area in Castle Creek South (approx. 2.2 km × 2.3 km). Within this area were two cliffs where geologists carried out detailed sedimentological fieldwork, i.e., the Kaza section at the base of the stratigraphy and the Isaac section that contained the Isaac Channel 3 area. The DEM extraction area was covered by 12 photographs in three strips. Prints of the aerial photography had previously been used by geologists for assisting with field correlation and mapping of the various layers across the outcrop (Schwarz and Arnott, 2007; Navarro *et al.*, 2008). On commencement of this stage of the project, the set of photography was scanned at 13 μm resolution, resulting in a ground pixel spacing of approximately 0.1 m.

Terrestrial laser scanning was carried out in August 2006, for collection of topographic data covering the Kaza and Isaac cliff sections. A Riegl LMS-Z420i laser scanner was used for this work (Riegl, 2009). With a maximum range (based on the reflectance of natural rock targets) of around 650 m, quoted point accuracy of 0.01 m, and point acquisition rate of up to 12,000 points per second, this scanner was ideal for capturing the Castle Creek cliff sections. The Isaac section (containing four large sandstone-dominated channel units, including Isaac Channel 3) was 900 m long, 200 m deep, and up to 90 m high (Figure 2). The smaller Kaza cliff section was 450 m long, 170 m deep and up to 50 m high. A calibrated Nikon D100 six-megapixel camera was mounted on the laser scanner, providing high-resolution digital images that were registered to the scanner coordinate system by means of a calibrated rigid mounting transformation (Jansa *et al.*, 2004). Nikkor 85 mm and 50 mm lenses were used for the Isaac and Kaza sections respectively.

The Isaac section required six scan positions to cover the length of the cliff, while the shorter Kaza section required four, including at least 20 percent overlap between adjoining scans. The average point spacing was 0.1 m for both areas. At each position, imagery was also taken with the digital camera for use later on for building a textured 3D model of the outcrop, and for assistance with geological interpretation. The camera was also operated handheld so that images could be taken from an optimal angle to the cliff, as best results for the texturing were obtained when the camera orientation was closest to normal to the outcrop (e.g., Debevec *et al.*, 1996). These images were registered to the project coordinate system by space resection, using manually identified tie-points between corresponding natural features in the image and laser data. The average standard deviation for the resection was around 1.5 pixels.

The terrestrial scan data were registered with GPS using an antenna mounted on top of the laser scanner recording data for the duration of the scan position setup. Data were post-processed relative to a base station operating within the confines of the study area. The base station coordinates were determined using precise point positioning from three days of observation. This GPS configuration provided the Universal Transverse Mercator (UTM) Zone 10 positions of the scanner centers, with standard deviations of the processed baselines better than 0.1 m in the horizontal and vertical directions.

Surface Modeling and Data Registration

A limited number of natural ground control points (GCPs) had been previously collected using real-time kinematic GPS, though because of the remoteness of the field area and problems with accessibility caused by the difficult terrain, the number and distribution was not optimal for performing an accurate aerial triangulation for the whole block of 12 photos (Wolf and Dewitt, 2000). An alternative approach to integrating the two datasets was therefore adopted, using the GCPS to give an initial block orientation, which was then refined using a surface matching approach. This initial orientation resulted in the correct relative orientation, but with an error in the external orientation corresponding to the limited quality of the photo-control points. Comparison between the initial aerial DEM position and the lidar data revealed up to 5 m of difference in areas of overlap corresponding to the cliff sections. A triangular irregular network (TIN) DEM was extracted from the orientated image data, with additional breaklines manually measured along sharp changes in surface gradient. The processed photogrammetric DEM consisted of close to 460,000 triangles, with an average point spacing of 3 m, which was sufficient to represent the relatively smooth outcrop surface.

The raw lidar point clouds were registered using a surface matching approach in the PolyWorks® software by InnovMetric Software, Inc. Overlap between the scans was minimized in a least squares adjustment to recover the transformations relative to a fixed scan in the center of the cliff section (see e.g., Besl and McKay, 1992, for details on surface matching). The main advantage of this approach over the more conventional use of control points sited on the outcrop face is the reduction of expensive field time. Additional advantages are found in the redundancy of using all available data, especially on this outcrop where there was almost no vegetation; and the ability to quantify mismatch between the overlap areas, indicating the success of the solution (Buckley and Mitchell, 2004). Once all scans were matched to a common coordinate system, the scan centers were transformed to the UTM coordinate system using the GPS scanner center positions and 3D conformal transformation (with Root Mean Square Error of 0.060 m).

The raw point clouds were merged and filtered to reduce the point density in overlap areas (Buckley and Mitchell, 2004). However, further reduction was necessary before a triangle mesh could be created, as with 3.5 million points, this was still too many to be easily meshed and visualized without specialized hardware. An advantage of laser scanning is the collection of point clouds that may be of a higher density than required by the current application, but may be useful for posterity to allow the data to be revisited for further, unanticipated purposes. The merged point clouds were reduced by calculating the normal distance between each point to a plane formed by the neighboring points, where a distance lower than a tolerance of 0.05 m signaled insignificant contribution to the topography. The flagged points were eliminated and the remainder triangulated to form 3D meshes. The resulting meshes contained 1.1 million triangles for the Isaac section and 500,000 triangles for the Kaza section, with average point spacing of 0.4 m.

Once triangle surfaces had been defined for both the aerial and ground-based datasets, surface matching was again employed to recover the transformation that would minimize the differences between the two datasets. The two meshes derived from the laser scanning data (Isaac and Kaza sections) were used as large control patches, held fixed while the aerial DEM was allowed to move. Requirements for a successful solution are for gradients to exist in different directions on conjugate surfaces, and for there to be enough similarity between the surfaces to ensure good correspondence, even when removing outliers (Besl and McKay, 1992). Too much noise or difference between the datasets would strongly influence the least squares procedure, resulting in poor solutions being found. In this case, surface gradients were provided by the relief in the general outcrop topography, especially in the steeper cliff sections. Because of the glacier-scoured outcrop surface, little difference in sampling between the aerial and ground-based terrain models was expected. In particular, only small amounts of localized change would have occurred, despite the five year gap between the two datasets being captured. This was anticipated to have been limited to small differences in vegetation and distribution of snow patches. The surface matching problem is ill-posed (Besl and McKay, 1992); therefore reasonably close initial approximations are a requirement for the solution to converge. In this case the exterior orientation of the photogrammetric block provided by the GCPS was sufficiently close to act as an initial approximation.

A potential problem in matching may have arisen due to the different sampling strategies of the two measurement systems. Because the aerial photogrammetry measured a 2.5D surface, flat areas would be well covered and cliff sections poorly recorded; in contrast, the terrestrial laser scanner recorded cliff sections well, but was limited in coverage of the surrounding topography due to the deflection angle to horizontal surfaces brought about by the low field of view of the instrument. However, examination of the terrestrial models showed that a sufficient amount of data was present below and above the cliff faces in the two areas (e.g., Figure 4a).

Convergence of the matching algorithm was achieved, with the resolved transformation parameters improving the integration of the two datasets. Differences between the two surfaces were found by calculating the normal distance between each triangle centre in the lidar DEM to the aerial DEM (Figure 4b). This revealed a mean error of −0.0018 m and a standard deviation of 0.3919 m, with errors following a normal distribution. This was around the level of error expected, as the more sparsely sampled aerial surface was prone to interpolation error during comparison with the lidar surface, especially in areas of sudden topographic change where some larger errors existed. In addition, features too small to be sampled by the aerial DEM (less than the point density), but of significance in the lidar model, such as surface debris, are apparent in the difference map (Figure 4b). Although the distribution of the two control patches relative to the whole DEM was relatively poor compared to conventional GCPS, the results of the matching showed good agreement between the two models. Results for the Isaac section are shown in Figure 4, with similar results obtained for the Kaza section.

Texture Mapping

Once surface matching was performed, the aerial and lidar models could be directly utilized in a single coordinate system. However, for being able to visualize, interpret and perform quantitative analysis on the geology, it was necessary to first integrate the DEM data with the aerial and terrestrial imagery (e.g., Forkuo and King, 2004). Because of the glacier-polished rock surface, the outcrop surface contained much geology that could not be distinguished by changes in topography. Hence, texture mapping was performed to add geologic information to the dataset. The models from the Isaac and Kaza sections were merged with the aerial DEM to create a single 3D mesh, with the higher accuracy lidar triangles replacing the aerial data in areas of overlap. Rectification of the aerial and ground-based imagery was carried out to remove the effects of lens distortion prior to texture mapping. Because the camera orientation and position was known for each image, triangle vertices could be projected into the imagery to determine image coordinates of the texture patches (Wolf and Dewitt, 2000). Where multiple images were available for a single triangle, parame-

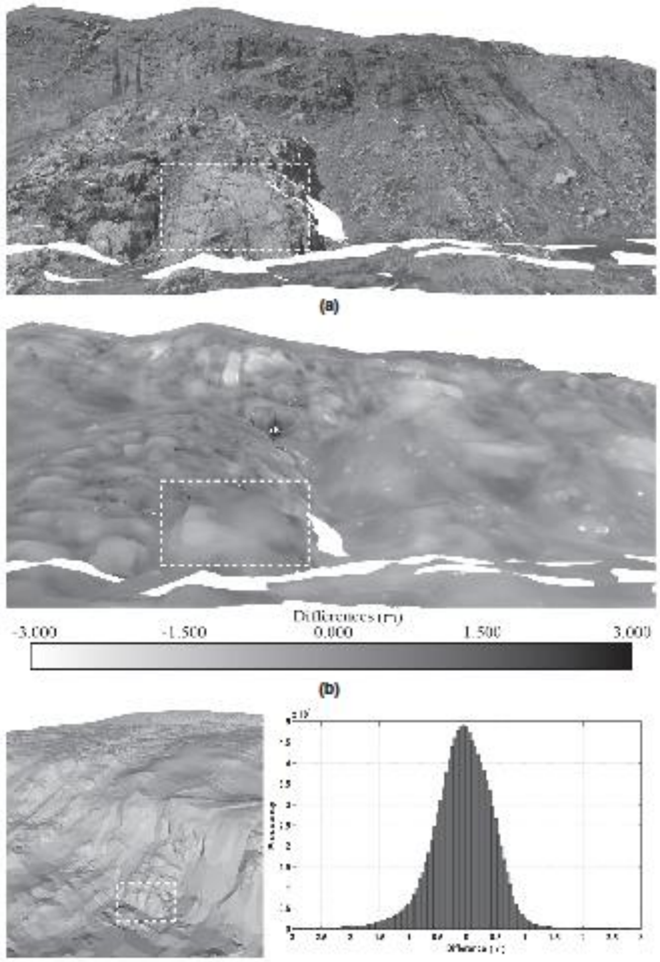

Figure 4. Post-registration differences between the terrestrial lidar and aerial photogrammetric surfaces for the Isaac cliff section: (a) Textured lidar model, (b) Lidar model colored with difference map, (c) Oblique view of aerial photogrammetric DEM, showing the low triangle resolution in steep areas of the cliff (corresponding areas are marked in (a), (b) and (c)). Height of section is approximately 90 m, and (d) Histogram of differences.

ters based on the angle between the triangle normal and the image ray, the area of the triangle in the image, and the distance between the camera and the triangle were used to select the most suitable image to use (Debevec *et al.*, 1996; El-Hakim *et al.*, 1998). A second adjustment of the triangle-image map was then performed to ensure that where possible adjacent triangles were mapped using the same image (e.g., El-Hakim *et al.*, 1998). For interpretation, it is distracting to have regions of single or few triangles mapped with different images, as radiometric and geometric distortions can detract from the geology.

Because of the different view directions of the aerial and terrestrial imagery, the texture mapping parameters described above ensured that most triangles on the cliff sections were textured with images from the ground, while the remainder of the merged model was textured using the aerial photos. The result was a single model of the Castle Creek outcrop comprising the two data collection methods (Figure 5). The

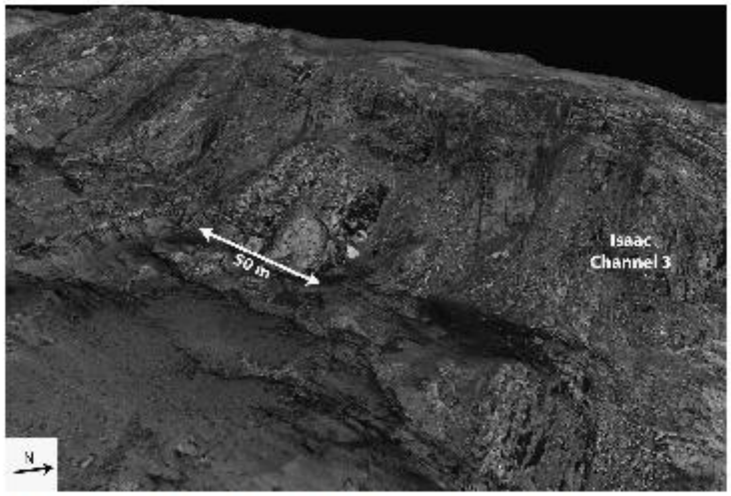

Figure 5. Final outcrop model of part of the Isaac cliff section comprising merged photogrammetric and lidar terrain data, and texture-mapped with aerial and terrestrial photographs.

use of lidar and close-range imagery adds high resolution to the cliff sections, enabling more detailed study of the outcrop in the depth direction, as it enters the subsurface. This result, combined with the extensive aerial coverage of the 2D outcrop stratigraphy, enhanced geological interpretation.

Geological Modeling of the Isaac Channel 3 Section

The virtual outcrop model for the Castle Creek area provided a base for integration of project data, including field measurements and sedimentary logs, i.e., *cross-sections* through the outcrop where the geologist records rock attributes bed-by-bed along a measured line. Particularly important was that it was possible for geologists to visualize the data using 3D viewing software and a stereo display, allowing new angles of view, and an appreciation of the area as a whole, i.e., interpretations not possible in the field or with aerial photo prints. In addition, the combined model could be simultaneously viewed at various scales: the aerial data used for the wider area, while more details could be gained in the cliff sections (where much conventional geological fieldwork had been carried out) by zooming-in to these areas. Using this virtual outcrop model, a geo-model was built for the Isaac Channel 3 detailed study area using the methodology outlined in Enge *et al.* (2007).

First, the area of interest was cut out of the overall model, to save on computer hardware resources during visualization. Then, 3D lines corresponding to the key bounding stratigraphic surfaces from the deep-marine channel fill and overbank/levee units were interpreted and digitized directly on the virtual outcrop model (Figure 6).

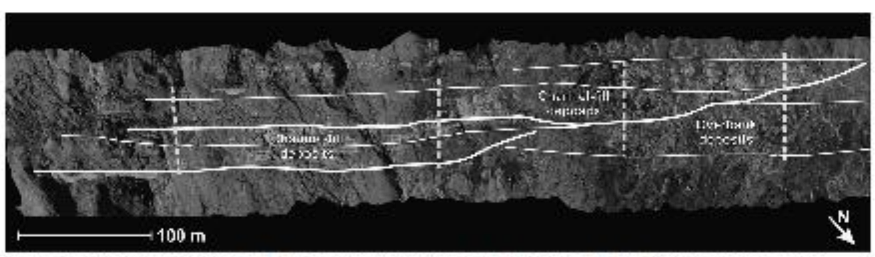

Figure 6. Plan view showing selected lines interpreted and digitized onto the virtual outcrop model. Dashed lines are locations of the sedimentary logs where rock attributes are measured bed-by-bed in the field. Note the cross-sectional channel shapes (marked by thicker lines). D-1 to D-4 indicate four main depositional stages from oldest overbank deposits to youngest channel-fill deposits.

These lines formed the spatial constraints for the geological volume, which were combined with the geologists' conceptual model (Navarro *et al.*, 2008) for extrapolating geological surfaces. Geo-models from outcrop data are typically used to examine the effects of different geological heterogeneities on numerically simulated fluid flow. These heterogeneities may include the lateral and vertical stacking of deep marine channels, in which the material in the channel-fill deposits is typically permeable while the clays that were deposited outside the channel are typically not, and provide barriers to hydrocarbons moving through the reservoir. In most reservoir cases the beds are sub-horizontal or gently tilted; however as the Castle Creek outcrops had been uplifted during mountain building it was necessary to remove the tilt of the outcrop. A simple rotation of 95° around an axis parallel to the strike of strata was applied using structural restoration software (3DMove; Midland Valley Exploration).

The structurally-restored lines were imported to a reservoir modeling package (Irap RMS; Roxar ASA), software which is used primarily by the petroleum industry for modeling subsurface reservoirs, using data such as seismic and well cores, and planning strategies for hydrocarbon extraction. The software allows the integration of many forms of spatially-referenced geological data in a common environment. The lines were used as guides to assist in the creation of 2.5D grid surfaces representing the key geological layers, using a b-spline algorithm to extrapolate the data away from the actual outcrop face (Figure 7). There is potential during this procedure for large amounts of error to be introduced, both from the choice of extrapolation technique, as well as the limited amount of input data used. This is where geological understanding is critical, as well as the accuracy of the spatial data. In this case, lines mapped using the virtual outcrop data were of high enough accuracy to recreate the subtle dips between the layers. Quality control of the generated surfaces was carried out by removing the structural rotation to the surfaces and displaying them simultaneously with the 3D textured model (Figure 8). In this way, the intersection of the surfaces with the digitized lines on the outcrop model revealed the success of the surface gridding, at least where an exact match should have existed. In addition, the overall trend of the surfaces away from the outcrop face could be checked.

The generated surfaces define the geological volume that bound different channel and levee units within the model. The terraced, composite surfaces at the base of the channel-fill units (Figures 6 and 7) would have been very difficult to recreate without the aid of the 3D data. The space between two surfaces represented modeling zones, which were gridded in 3D and populated with a stochastic representation of the lithofacies (Figure 9). Facies modeling was heavily constrained by sedimentary log data imported as "wells" in the geomodel. Such a geocellular model may be examined statistically to determine connectivity between packages, as well as by running flow simulation experiments. Consequently, the geocellular model based on outcrop data can assist geologists' understanding of the processes and geometry occurring in the reservoir analog and may provide insights and input variables to build more realistic and accurate subsurface models of deep-marine turbidite-dominated reservoirs.

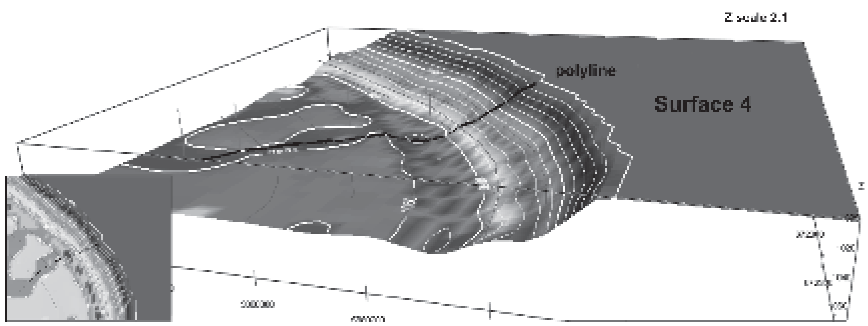

(a)

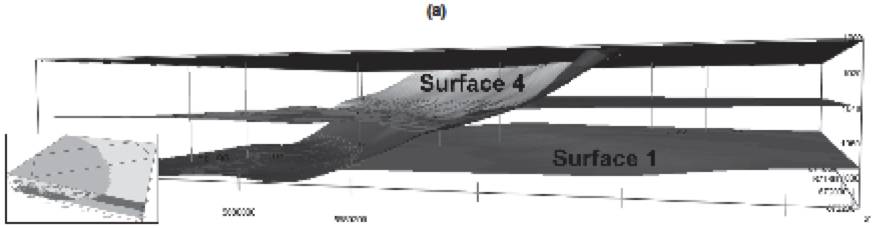

(b)

Figure 7. Key stratigraphic surfaces in reservoir modeling environment, with structural restoration applied: (a) Example surface created from digitized lines and geological knowledge. (b) Side view showing relative position of surfaces defining the modeling volume. Size of model is approximately 1200 m × 1,000 m, and the vertical exaggeration is 2:1.

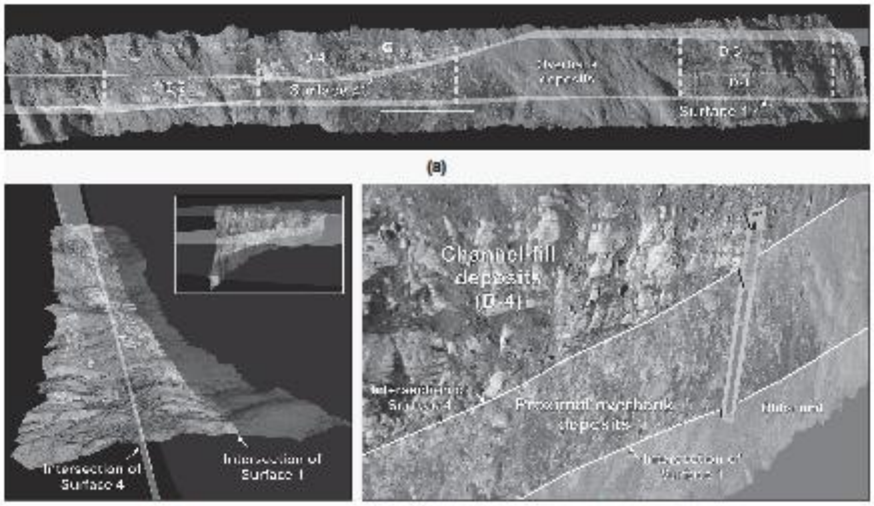

(a)

(b) (c)

Figure 8. Digital surfaces representing geological layers created in reservoir modeling software from digitized lines, and with structural rotation removed so that they can be visualized simultaneously with the textured outcrop model (surfaces visualized with 50 percent transparency): (a) Plan view showing selected surfaces: a relatively flat basal surface (Surface 1) and a channel-cut surface (Surface 4). Compare with lines in Figure 6 (Outcrop section approximately 1,100 m × 100 m); (b) Perspective view (from west to east) of outcrop with same surfaces intersecting; inset shows outcrop section in structurally-restored view, and (c) Detailed view showing intersection of surfaces with outcrop and sedimentary log, viewed as if structural rotation existed.

Conclusions

The potential for digital spatial data collection techniques to contribute to and enhance geological outcrop modeling research is high, and has been demonstrated in this paper using an integrated data collection approach for modeling a large outcrop at Castle Creek, Canada. Because of the limited three-dimensionality of the outcrop, terrestrial laser scanning was used to augment a DEM derived from aerial photogrammetry, so that geological layers could be interpreted with high enough precision to extend the outcrop surfaces in the dip direction within a reservoir modeling package. The study shows that the presence of a high-resolution digital outcrop model serves as a framework for detailed interpretation and geological field data integration within a project, and is a valuable teaching asset. For the Castle Creek outcrop, this enabled a new appreciation of the spatial relationships between the channel bodies to be gained. The employment of geomatics techniques offers a more quantitative approach to outcrop geology, an area that is anticipated to grow in the future.

Acknowledgments

This research is funded by industry members of the Windermere Consortium (Anadarko Petroleum, Canadian Natural Resources, Ltd., Devon Petroleum, Ltd., Husky Energy, Encana Corp., Nexen, Inc., and Shell) and an NSERC Collaborative Research and Development Grant. The Research Council of Norway and StatoilHydro ASA are acknowledged for supporting the Virtual Outcrop Geology group at the University of Bergen (Petromaks, Project 163264). Thanks to Roxar ASA, Riegl Laser Measurement Systems GmbH and Midland Valley Exploration for providing their software to the authors' institutions. Lilian Navarro and Shan Khan collected the sedimentological data, and Tor Even Aas is acknowledged for assistance in structural restoration.

References

Banerjee, S., and S. Mitra, 2004. Remote surface mapping using orthophotos and geologic maps draped over digital elevation models: Application to the Sheep Mountain anticline, Wyoming, *American Association of Petroleum Geologists Bulletin*, 88(9):1227–1237.

Bellian, J.A., C. Kerans, and D.C. Jennette, 2005. Digital outcrop models: Applications of terrestrial scanning lidar technology in stratigraphic modelling, *Journal of Sedimentary Research*, 75(2):166–176.

Besl, P.J., and N.D. McKay, 1992. A method for registration of 3-D shapes, *IEEE Transactions on Pattern Analysis and Machine Intelligence*, 14(2):239–256.

Bryant, I., D. Carr, P. Cirilli, N. Drinkwater, D. McCormick, P. Tilke, and J. Thurmond, 2000. Use of 3D digital analogues as templates in reservoir modelling, *Petroleum Geoscience*, 6(3):195–201.

Buckley, S.J., and H.L. Mitchell, 2004. Integration, validation and point spacing optimisation of digital elevation models, *The Photogrammetric Record*, 19(108):277–295.

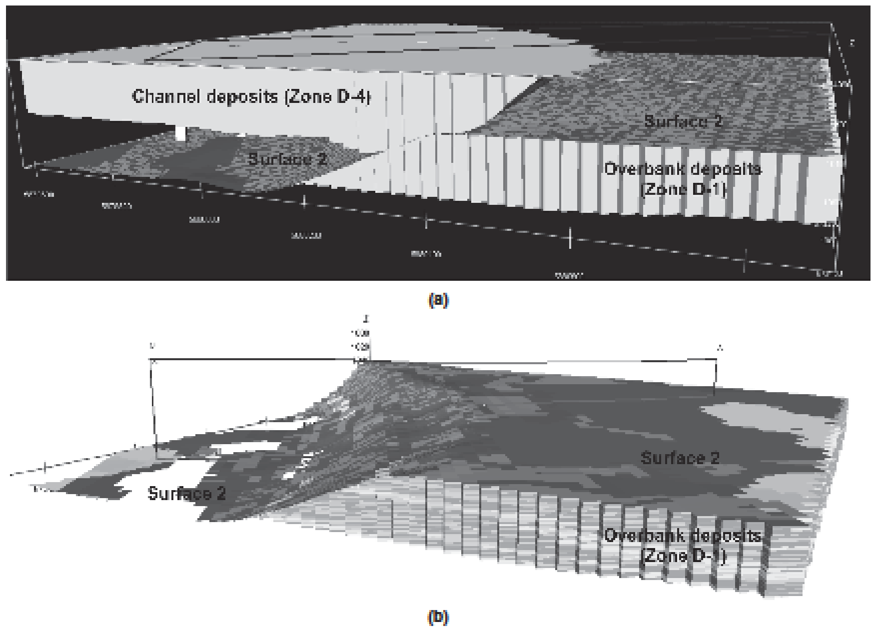

Figure 9. Geocellular model of Isaac Channel 3: (a) The volume between input surfaces is gridded, (b) Each cell is populated with representative rock types (facies), according to outcrop data and the geological interpretation (dark grey: thin-bedded turbidites; mid grey: medium-bedded turbidites; light grey: thick-bedded turbidites). Overbank deposits overlying Surface 1 and channel-fill deposits overlying Surface 4 are shown for illustration. Size of model is approximately 1200 m × 1000 m, and the vertical exaggeration is 2:1.

Buckley, S.J., J.A. Howell, H.D. Enge, and T.H. Kurz, 2008. Terrestrial laser scanning in geology: Data acquisition, processing and accuracy considerations, *Journal of the Geological Society*, 165(3):625–638.

Debevec, P.E., C.J. Taylor, J. Malik, 1996. Modeling and rendering architecture from photographs: A hybrid geometry- and image-based approach, *Proceedings of SIGGRAPH 96*, 04–09 August, New Orleans, Louisiana, pp. 11–20.

El-Hakim, S.F., C. Brenner, and G. Roth, 1998. A multi-sensor approach to creating virtual environments, *ISPRS Journal of Photogrammetry and Remote Sensing*, 53(6):379–391.

Enge, H.D., S.J. Buckley, A. Rotevatn, and J.A. Howell, 2007. From outcrop to reservoir simulation model: Workflow and procedures, *Geosphere*, 3(6):469–490.

Forkuo, E.K., and B. King, 2004. Automatic fusion of photogrammetric imagery and laser scanner point clouds, *International Archives of the Photogrammetry, Remote Sensing and Spatial Information Sciences*, 35(B4):921–926.

Groshong, R.H., 1999. *3-D Structural Geology: A Practical Guide to Surface and Subsurface Map Interpretation*, Springer, Berlin, 324 p.

Jansa, J., N. Studnicka, G. Forkert, A. Haring, and H. Kager, 2007. Terrestrial laser scanning and photogrammetry - Acquisition techniques complementing one another, *International Archives of the Photogrammetry, Remote Sensing and Spatial Information Sciences*, 35(B5).

Lebel, D., and R. Da Roza, 1999. An innovative approach using digital photogrammetry to map geology in the Porcupine Hills, Southern Alberta, Canada, *Photogrammetric Engineering & Remote Sensing*, 65(3):281–288.

Lebel, D., G. Kenny, D. Kirkwood, P. Pouliot, J.-S. Marcil, C. Deblonde, and P. Molard, 2007. Imagery integration methods for precise geological mapping of rugged terrain, Alberta, Canada, *Photogrammetric Engineering & Remote Sensing*, 73(5):585–593.

Navarro, U.L., Z. Khan, and R.W.C. Arnott, 2008. Depositional architecture and evolution of a deep-marine channel-levee complex: Isaac formation (Windermere Supergroup), Southern Canadian Cordillera, *Atlas of Deep-Water Outcrops: AAPG Studies in Geology 56* (T.H. Nilsen, R.D. Shew, G.S. Steffens, and J.R.J. Studlick, editors), CD-ROM, Chapter 127, 22 p. DOI:10.1306/12401041St563288.

Pringle, J.K., A.R. Westerman, J.D. Clark, N.J. Drinkwater, and A.R. Gardiner, 2004. 3D high-resolution digital models of outcrop analogue study sites to constrain reservoir model uncertainty: An example from Alport Castles, Derbyshire, UK, *Petroleum Geoscience*, 10(4):343–352.

Pringle, J.K., J.A. Howell, D. Hodgetts, A.R. Westerman, and D.M. Hodgson, 2006. Virtual outcrop models of petroleum reservoir analogues: A review of the current state-of-the-art, *First Break*, 24(3):33–42.

Riegl, 2009. Terrestrial Scanning, URL: *http://www.riegl.com/products/terrestrial-scanning/*, Riegl Laser Measurement Systems GmbH, Horn, Austria (last date accessed: 08 June 2010).

Ross, G.M., 1991. Tectonic setting of the Windermere Supergroup revisited, *Geology*, 19(11):1125–1128.

Ross, G.M., J.D. Bloch, and H.R. Krouse, 1995. Neoproterozoic strata of the southern Canadian Cordillera and the evolution of seawater sulfate, *Precambrian Research*, 73(1–4):71–99.

Ross, G.M., and R.W. Arnott, 2008. Regional Geology of the Windermere Supergroup, Southern Canadian Cordillera and Stratigraphic Setting of the Castle Creek Study Area, *Atlas of Deep-Water Outcrops: AAPG Studies in Geology 56* (T.H. Nilsen, R.D. Shew, G.S. Steffens, and J.R.J. Studlick, editors), CD-ROM, Chapter 124, 16 p., DOI:10.1306/12401038St563286.

Sagy, A., E.E. Brodsky, and G.J. Axen, 2007. Evolution of fault-surface roughness with slip, *Geology*, 35(3):283–286.

Schwarz, E., and R.W.C. Arnott, 2007. Anatomy and evolution of a slope channel-complex set (Neoproterozoic Isaac Formation, Windermere Supergroup, southern Canadian Cordillera): Implications for reservoir characterization, *Journal of Sedimentary Research*, 77(2):89–109.

Wolf, P.R., and B.A. Dewitt, 2000. *Elements of Photogrammetry with Applications in GIS)*, Third edition, McGraw-Hill, New York, 624 p.

(Received 20 March 2009; accepted 17 August 2009; final version 11 December 2009)